

**GRAVITY WAVE GENERATION  
BY VORTICAL FLOWS  
IN A ROTATING FRAME**

**Rupert Ford**

Churchill College  
Cambridge

A dissertation submitted for  
the degree of Doctor of Philosophy  
at the University of Cambridge

October, 1993

To my grandparents

Margaret and Ted

## Preface

This thesis is the result of my own work, and includes nothing which is the outcome of work done in collaboration. Except where stated otherwise, the research reported in this thesis is original. No part of it has been submitted for a degree or any similar qualification at any other university.

This thesis would not have been possible without the enthusiasm, suggestions and encouragement of my supervisor, Professor Michael E. McIntyre. His enduring love of fluid dynamics will remain an inspiration to me for the rest of my life. All members of the atmospheric dynamics group have, at some time, made a valued contribution to my academic life in DAMTP. I would particularly like to thank Peter Haynes for discussions about instability theory, David Dritschel for discussions about vortex dynamics and conformal mappings, and Saravanan for suggestions about numerical modelling. Stephen Cowley generously allowed me use of his computational resources to enable me to complete the simulations in chapter 4 quickly. I would also like to thank the people who have given so generously of their time over the last few months in reading the manuscript and suggesting improvements to it. They are Ben Edgington, Stefan Llewellyn-Smith, Gudrun Magnusdottir, John Scinocca and David Tan — my deepest thanks to you all. I would also like to thank all other members of DAMTP, research staff, computer officers and secretaries, who have helped me in any way.

Throughout my thesis work I have profited from discussions with many scientists at other institutions. Particular thanks go to Glenn Flierl, Joe Keller, Bernard Legras, Lorenzo Polvani, Rich Rotunno, Ted Shepherd and Joe Tribbia. During the summer of 1992 I was a fellow at the Woods Hole Summer School in Geophysical Fluid Dynamics. I thank the organisers and participants for an enjoyable and rewarding summer.

For financial and travel support I thank the Natural Environment Research Council, and for travel support I thank additionally Churchill College and the European Geophysical Society. Finally, I would like to thank my parents for getting me this far, and for their unending love.

# Contents

<b>1</b>	<b>Introduction</b>	<b>1</b>
1.1	Balance and Imbalance . . . . .	2
1.2	Potential vorticity inversion . . . . .	6
1.3	Slow manifold hypothesis . . . . .	14
1.4	Approach of this thesis . . . . .	18
<b>2</b>	<b>Asymptotic analysis at low Froude number</b>	<b>21</b>
2.1	Introduction . . . . .	22
2.2	Gravity wave generation as a singular perturbation problem . . . . .	28
2.2.1	Perturbation expansion for the vortical flow . . . . .	30
2.2.2	Dynamics of the wave zone resulting from the vortical flow . . . . .	39
2.2.3	The effect of wave radiation on the vortical flow . . . . .	42
2.3	Implications for balance and potential vorticity inversion . . . . .	44
2.4	The effect of gravity wave radiation upon a rotating elliptical patch of uniform potential vorticity – an explicit example of generalized adjustment . . . . .	48
2.4.1	Evolution of the vortex boundary . . . . .	49
2.4.2	The solution at leading order in $F$ . . . . .	51
2.4.3	The solution to $O(F^2)$ . . . . .	53
2.4.4	V-states for weakly divergent flow . . . . .	57

2.4.5	The effect of gravity wave radiation . . . . .	61
2.5	Discussion . . . . .	66
2.6	Appendix A . . . . .	68
2.6.1	Region I . . . . .	70
2.6.2	Region II . . . . .	72
2.6.3	Region III . . . . .	72
2.7	Appendix B . . . . .	73
<b>3</b>	<b>Instability of vortices and jets</b>	<b>75</b>
3.1	Introduction . . . . .	76
3.2	Instability of a circular vortex with discontinuous potential vorticity . . . . .	81
3.2.1	The basic state . . . . .	81
3.2.2	The disturbance equations . . . . .	82
3.2.3	The limit $F \ll 1$ . . . . .	83
3.2.4	Numerical eigenvalue calculations . . . . .	89
3.2.5	The limit of large mode number . . . . .	118
3.2.6	The Sozou modes . . . . .	129
3.3	Instability of a circular vortex with smooth potential vorticity . . . . .	133
3.3.1	Disturbance equations . . . . .	133
3.4	Relevance to the existence or non-existence of a slow manifold . . . . .	143
3.5	Instability of a parallel jet . . . . .	148
3.5.1	The basic state . . . . .	149
3.5.2	Ripa's theorem . . . . .	149
3.5.3	The disturbance equations . . . . .	151
3.5.4	Numerical technique . . . . .	152

3.5.5	Results of the eigenvalue calculations . . . . .	153
3.5.6	The limit of large wavenumber . . . . .	155
3.5.7	The limit $q \rightarrow \infty$ . . . . .	157
3.5.8	Eigenvalue calculations for large $q$ . . . . .	164
3.5.9	Remarks . . . . .	166
3.6	Discussion . . . . .	166
<b>4</b>	<b>Nonlinear simulation of gravity wave generation</b>	<b>169</b>
4.1	Introduction . . . . .	170
4.2	A “Lighthill” theory of gravity wave generation for a periodic parallel flow . . . . .	177
4.3	Pseudoenergy and pseudomomentum for the shallow water equations . . . . .	180
4.4	The numerical model . . . . .	183
4.5	Overview of numerical simulations . . . . .	186
4.6	Jets with moderate Rossby number and variable Froude number . . . . .	191
4.7	Cyclonic strips at large Rossby number . . . . .	210
4.8	Anticyclonic strips with non-negative potential vorticity . . . . .	223
4.9	Anticyclonic strips with negative potential vorticity . . . . .	234
4.10	Discussion . . . . .	248
<b>5</b>	<b>Discussion</b>	<b>253</b>
5.1	Review of aims and objectives of this thesis . . . . .	254
5.2	Suggestions for further research . . . . .	256
<b>6</b>	<b>References</b>	<b>258</b>

# Chapter 1

## Introduction

## 1.1 Balance and Imbalance

*“The striking errors in the ‘forecast’, which has been obtained by computing forms, may be traced back to the large apparent convergence of wind. It may be asked whether this spurious convergence arises from the errors of observations with balloons, or from the finite horizontal differences being too large, or thirdly from the process by which winds at points, arranged in a rectangular pattern, are interpolated between the observing stations . . .”*

Thus Richardson (1922) first gave prominence to the idea that inaccuracies in the data used to initialize his pioneering numerical forecast could have given rise to the failure of that forecast. The failure consisted of large spurious variations in the computed pressure field over a 6 hour forecast interval. In fact, Richardson had forecast a pressure variation in one location of 145mb in 6 hours, whereas the actual change in pressure over that period had been of the order of 1mb.

The phenomenon that Richardson had come upon is well known today both to theoreticians and to practitioners of numerical weather prediction - that large scale atmospheric flow away from the equator is, to a good first approximation, in a state of geostrophic balance, in which the Coriolis and pressure gradient terms constitute the principal balance in the horizontal momentum equation.

It now seems almost certain (Platzman 1967, 1968) that Richardson developed some appreciation of this fact in the following twenty years, and that the difficulty had even been foreseen by Margules (1904). Eventually, however, it was when Charney (1951) applied his recently-developed “quasi-geostrophic” theory (Charney 1947, 1948, 1949) to numerical forecasting that forecasts were able to predict an evolution of fields at least qualitatively in line with observations. Even more remarkable in Charney’s (1948) paper is his far-sighted remark that the conservation of potential temperature and potential vorticity on fluid particles may alone be sufficient to determine the nature of large scale atmospheric motions. In his words

*“The motion of large-scale atmospheric disturbances is governed by the laws of conservation of potential temperature and potential vorticity, and by the conditions that the horizontal velocity be quasi-geostrophic and the pressure be quasi-*

*hydrostatic.”*

In present day terminology, adopted in this thesis, the quasi-geostrophic and quasi-hydrostatic conditions are “balance” conditions, which enable one to determine the velocity and temperature fields knowing only the mass under each isentropic surface, and the distribution of potential vorticity on each isentropic surface. The resulting system of equations is referred to as a balanced model.

Some appreciation of the importance of potential vorticity had already been developed in the ten years preceeding Charney’s work. Rossby (1936), Rossby *et al.* (1939) and Ertel (1942) had been independently developing some fundamental understanding of the dynamical implications of the conservation of potential vorticity on fluid particles, although they did not postulate that it could be “inverted” to give other dynamical information, as Charney (1948) had noted in his “quasi-geostrophic” approximation. The first explicit application of potential vorticity inversion was made by Kleinschmidt (1950a,b;1951,1955,1957), who used an exact form of potential vorticity inversion for axisymmetric structures in his studies of upper level cyclones.

The potential vorticity  $Q$  is defined by

$$Q = \rho^{-1}(2\Omega + \nabla \times \mathbf{u}) \cdot \nabla \theta, \quad (1.1)$$

where  $\rho$  is the air density,  $\Omega$  is the Earth’s angular rotation vector,  $\mathbf{u}$  is the fluid velocity in coordinate axes fixed on the Earth, and  $\theta$  is the potential temperature (or any function of it). In the absence of friction or diabatic processes,  $Q$  is a materially conserved quantity:

$$\frac{DQ}{Dt} = 0. \quad (1.2)$$

Although the hydrostatic approximation is valid for large scale motion throughout the atmosphere, the quasi-geostrophic approximation is seldom sufficiently accurate to render it of practical use in numerical weather prediction. On the other hand, the absence of any balancing procedure is known to give rise to large errors of the type encountered by Richardson. Consequently, balanced equations have been developed for atmospheric modelling which are more accurate than the quasi-geostrophic equations, while still retaining the robustness of a balanced system of equations, being insensitive to errors in the initial data. Indeed, although the “quasi-

geostrophic” approximation remains the best known example of a balanced system, many others have been proposed, each with varying degrees of analytical tractability and practical accuracy.

At this point, it is essential to be clear as to exactly what is required of a balanced model. Following Hoskins *et al.* (1985), we may define a balanced model by prescribing a method for determining the velocity field everywhere given only the mass under each isentrope ( $\theta$ -surface), the potential vorticity distribution on each isentrope, and the  $\theta$  distribution on the boundary of the domain. The proposed “inversion” procedure should not depend on knowledge of the PV distribution at any time other than the current time. The integration forward in time proceeds in principle by advecting the potential vorticity according to (1.2).

Before proceeding, in §1.2, to a discussion of how one might set about inverting the potential vorticity to obtain the other dynamical fields, it is instructive to consider the features of the flow which no balanced model, however accurate, can capture.

To fix ideas, let us consider the shallow water equations on an  $f$ -plane:

$$\frac{D\mathbf{u}}{Dt} + f\mathbf{k} \times \mathbf{u} + g\nabla h = 0 \quad (1.3)$$

$$\frac{Dh}{Dt} + h\nabla \cdot \mathbf{u} = 0, \quad (1.4)$$

Firstly, we consider the dispersion relation for the linearized system corresponding to (1.3,1.4):

$$\omega(\omega^2 - f^2 - c_0^2(k^2 + l^2)) = 0, \quad (1.5)$$

where  $\omega$  is the wave frequency and  $c_0 = (gH)^{1/2}$  is the gravity wave phase speed. There are three roots. One root,  $\omega = 0$ , corresponds to “slow” waves, which are the analogue of Rossby waves in this system. Their frequency would be modified in the presence of a background planetary vorticity gradient. The other two roots correspond to propagating waves only if  $\omega > f$ . These correspond to “fast” surface inertio-gravity waves, which owe their existence to the restoring effect of gravity on the free surface, and whose frequency is modified by background rotation.

In a balanced model, however, there is only one time derivative, resulting from the advection of potential vorticity. The resulting dispersion relation will therefore have only one root, which must, by symmetry, correspond to some appropriate generalization of the slow Rossby wave. A balanced model is therefore a model which filters from the equations of motion gravity waves, which are generally of much greater phase speed than typical fluid velocities.

Moreover, since a balanced model contains two fewer time derivatives than the full system, the inversion procedures required by a balanced model to obtain the velocity and height fields from the potential vorticity can in general be defined by imposing two constraints on the full shallow water system. The selection of the two constraints must be made carefully, however, if the model is still to possess analogues of potential vorticity, which should be conserved on fluid particles, and analogues of total mass, energy, and enstrophy, which should be conserved globally. Indeed, several popular balanced models, such as the Balance Equations (Lorenz, 1960) in the form in which they are usually integrated, do not possess a full set of conservation laws. However, from a theoretical viewpoint, it nonetheless seems clear that the unifying concept in any discussion of balanced dynamics must be that of advection of potential vorticity on fluid particles, together with the specification of sufficient constraints that the potential vorticity can be inverted to give all the other dynamical information necessary to proceed with the integration.

A second thought experiment which one can conduct, and which also illustrates that there cannot be freely propagating gravity waves in a balanced model, is to consider the classical “Rossby adjustment” problem (see, e.g., Gill, 1982). In this thought experiment we consider a rotating shallow water fluid consisting of two semi-infinite regions of uniform potential vorticity of different values, which intersect along a straight line of infinite length. If we suppose that initially there is no motion then, by considering the potential vorticity, there must be a discontinuity in surface elevation along the line of intersection. Now suppose that ultimately the fluid evolves to remove the surface discontinuity. By symmetry, the final state must also be one of two semi-infinite regions of uniform potential vorticity intersecting along a straight line of infinite length, but the energy associated with this final state is always less than the energy associated with the initial state.

Now, since the potential vorticity is uniform everywhere in the fluid away from the interface, its conservation on fluid particles reduces the number of independent time derivatives away from the interface from three to two in the fluid away from the interface. The resulting waves in these regions are therefore gravity waves, which can propagate away from the interface to infinity, and account for the loss of energy. To a balanced model, however, which depends only upon knowledge of the potential vorticity field, both initial and final states look exactly the same, and would possess the same velocity and height fields. There is no Rossby adjustment, and no

gravity wave radiation.

## 1.2 Potential vorticity inversion

Over the years, many balanced models have been proposed for use in different circumstances. In this section, we start by deriving two very simple balanced models via scaling arguments, and proceed to discuss different ways in which balanced models can be constructed.

To begin, let us return briefly to the shallow water equations, this time on a  $\beta$ -plane:

$$\frac{D\mathbf{u}}{Dt} + f\mathbf{k} \times \mathbf{u} + g\nabla h = 0 \quad (1.6)$$

$$\frac{Dh}{Dt} + h\nabla \cdot \mathbf{u} = 0, \quad (1.7)$$

in which the Coriolis parameter  $f$  represents  $f_0 + \beta y$ , where  $f_0$  and  $\beta$  are constants. Let us further assume that  $\beta y \ll f_0$  (in a sense to be defined), so that the Coriolis parameter does not change much over the range of latitudes which we are considering (these assumptions are made here to facilitate a pedagogical development of a “potential vorticity view” of quasi-geostrophy, and will be removed in subsequent discussions of balance). The potential vorticity is defined as

$$Q = \frac{f + \zeta}{H + h}, \quad (1.8)$$

where  $H$  is the mean layer depth and  $h$  represents departures of the total layer depth from the mean; and  $\zeta$  is the relative vorticity. Let us now assume, as is implicit in the scalings of Charney (1948), that  $Q$  has only small departures from its background value  $f_0/H$ . This requires that the Rossby number  $Ro = U/fL \ll 1$ , so that

$$Q \sim \frac{f_0}{H} + \frac{\zeta + \beta y}{H} - \frac{f_0 h}{H^2}. \quad (1.9)$$

Then the advective timescales  $D/Dt$  must be long compared with the inertial timescale  $f_0^{-1}$ , so the shallow water momentum equation (1.6) gives

$$f_0 \mathbf{k} \times \mathbf{u} + g\nabla h = 0 \quad (1.10)$$

at leading order. Taking the curl of this equation implies  $\nabla \cdot \mathbf{u} = 0$ . Therefore we can introduce a streamfunction  $\psi$  such that  $\mathbf{u} = \mathbf{k} \times \nabla \psi$ , and from (1.10) we have  $h = (f_0/g)\psi$ . The

approximation (1.9) to the potential vorticity becomes

$$Q \sim \frac{1}{H} \left( f_0 + \beta y + \nabla^2 \psi - \frac{f_0^2}{gH} \psi \right). \quad (1.11)$$

Scaling arguments show that  $f_0$  is an order of  $Ro^{-1}$  larger than either of the terms involving  $\psi$  in (1.11), which are themselves of the same order of magnitude, and hence the effects of local potential vorticity anomalies and the background planetary vorticity gradient enter at the same order in the quasi-geostrophic scaling if  $\beta y/f_0 = O(Ro)$ .

It follows that, knowing  $Q$ , one can in principle invert (1.11) with evanescence or no normal flow boundary conditions to give  $\psi$ , and hence  $\mathbf{u}$  and  $h$ .

An alternative, but equally valid, balance condition is to relax the assumption that potential vorticity perturbations are small compared with the background value  $f_0/H$ , but to continue to assume, as is implicit in the quasi-geostrophic scaling, that the Froude number  $F = U/(gH)^{1/2} \ll 1$ . The implication of this assumption (see chapter 2 for details of the scaling analysis) is that  $h/H = O(F^2)$ . This means that height perturbations are small, the flow is approximately non-divergent, and the potential vorticity perturbations are dominated by the relative vorticity  $\zeta$  and variations in the planetary vorticity  $\beta y$ , which is not now required to be small compared with  $f_0$ . Once again we may introduce a streamfunction  $\psi$ , but now the potential vorticity becomes

$$Q \sim \frac{1}{H} \left( f_0 + \beta y + \nabla^2 \psi \right). \quad (1.12)$$

The result is the Euler equations for a two-dimensional incompressible perfect fluid. Again, decay of velocity to infinity or no normal flow boundary conditions can be used to invert (1.12) to give velocity and height fields.

The quasi-geostrophic and Euler equations have been widely used for both analytical and numerical work. Analytically, and from the perspective of the ‘‘contour dynamics’’ algorithm (Dritschel, 1989, 1993; Pullin 1992; Dritschel & Saravanan 1993) they are attractive because a linear operator (Laplacian or Helmholtzian) must be inverted to obtain the other dynamical fields from the potential vorticity. Along with the Planetary Geostrophic or ‘‘thermocline’’ equations (Robinson & Stommel, 1959), in which the effects of inertia are neglected entirely, they are the only balanced models to have been proposed in which only linear operators need be inverted. From the perspective of numerical methods other than contour dynamics, their

advantage also derives from their simplicity. Indeed, few other balanced models can be integrated as quickly as the full shallow water equations, provided the latter are integrated using a large implicit time-step (Allen, personal communication).

The disadvantage of these simple balanced models lies in that they are only leading order approximations, and it is quite possible that one could proceed to higher order in Rossby or Froude number before nonlinear coupling between vortical motions and gravity waves led inevitably to the appearance of freely propagating gravity waves in the solution, and made any further improvements fundamentally impossible.

Indeed, the quasi-geostrophic approximation places two additional constraints upon the flow: the Coriolis parameter can vary only by an amount of order Rossby number throughout the entire domain of interest, and the surface elevation must have a gradient of the order of the Rossby number. These restrictions can be lifted by using the semi-geostrophic approximation (Salmon, 1985), which is also a low Rossby number approximations, formally valid to the same order in Rossby number as the quasi-geostrophic approximation. An interesting derivation of the semi-geostrophic system with variable Coriolis parameter and order-one surface gradients was given by Salmon (1988a), in which he showed that the semi-geostrophic equations can be derived from the shallow water system by making an approximation to the symplectic tensor in a constrained Hamiltonian, whereas an equivalent derivation of the quasi-geostrophic equations required the arbitrary introduction of a reference state and a metric tensor. The Euler equations were also derived via the constrained Hamiltonian approach, making approximations in the symplectic tensor. This method ensures that any balanced equations which are derived possess a full set of conserved quantities.

The essential point is that, although in principle the quasi-geostrophic system had solved the basic problem of unbalanced fields which Richardson had encountered, by the mid-1950s it was becoming clear that something more accurate was needed for practical purposes. A significant development in balanced models occurred when Charney (1955) proposed a balanced system with a higher order of approximation than the quasi-geostrophic system.

For his new system, he assumed that the flow was non-divergent ( $\nabla \cdot \mathbf{u} = 0$ ). Taking the divergence of the momentum equation (1.6), and applying  $\nabla \cdot \mathbf{u} = 0$ , one obtains a second

constraint:

$$\nabla \cdot (f \nabla \psi) + 2 \left( \frac{\partial^2 \psi}{\partial x^2} \frac{\partial^2 \psi}{\partial y^2} - \left( \frac{\partial^2 \psi}{\partial x \partial y} \right)^2 \right) = \nabla^2 h. \quad (1.13)$$

The two constraints, (1.13) and  $\nabla \cdot \mathbf{u} = 0$ , thus constitute a balanced model.

Condition (1.13) was also one of the balance constraints used by Lorenz (1960) in his derivation of what have now become known as the Balance Equations. However, although he used only the rotational component of the velocity in his balance constraint (1.13), some divergence remains in his system. The divergence is obtained via a diagnostic relation, and is used in the prognostic equation for the vorticity. The system constitutes a balanced model, since there is one prognostic equation and two constraints, although vorticity, rather than potential vorticity, has typically been used as the prognostic variable of integration in numerical work (Norton *et al.*, 1986).

McWilliams (1992) presents a scaling analysis to show that (1.13) is formally valid when  $F^2 \ll 1$  and  $F^2/Ro \ll 1$ . At high Rossby number, the condition is simply one of small divergence, and at leading order (1.13) reduces to the barotropic vorticity equation. At small Rossby number one recovers the quasigeostrophic scaling, and (1.13) reduces to quasigeostrophic balance.

The Balance Equations have been the focus of several numerical studies over the last decade. Norton *et al.* (1986) show how the balance equations may be implemented in a numerical scheme, and McWilliams *et al.* (1986) present a numerical study of oceanic vortices on a  $\beta$  plane, in which there is practically no discernable difference between the potential vorticity fields of the Balance Equation integrations and the shallow water integrations. In their cases, Rossby numbers are of order one, but they consider vortices which are either barotropic or have at most two baroclinic modes. The structures are thus rather deep, and their Froude numbers are consequently rather small, so explaining the good agreement between Balance Equation and shallow water integrations.

An extensive numerical and analytical investigation of the properties of a large number of different balanced models has been presented by Allen *et al.* (1990a,b) and Barth *et al.* (1990). In addition to considering existing balanced models, they also present some models of their own. In interpreting their results, however, it should be noted that their models impose only one, not two, constraints, on the dynamics, and two fields must be integrated in the subsequent

evolution (albeit that one is integrated using an implicit time step). Their models should not therefore be regarded as balanced models in the sense described above, although their dynamics are certainly constrained in some way. For the purposes of this discussion, I shall refer to these as “semi-balanced” models.

The first paper (Allen *et al.*, 1990a), presents the models they considered, and investigates properties of their stationary solutions and coastal Kelvin waves. Following Gent & McWilliams (1983a), they use boundary conditions in such a form that coastally trapped Kelvin waves are retained in all balanced models except the quasi-geostrophic model. In the subsequent analysis of the performance of the different models, presented in the second and third papers, they take as a measure of model accuracy the root mean square departure of the surface height from that of the corresponding shallow water integration.

The second paper (Barth *et al.*, 1990) investigates the evolution when the models are initialized with sinusoidal flow over a Gaussian topography in a doubly periodic geometry. The main conclusion is that the classical Balance Equations perform best - almost as well as the shallow water equations. One of the “semi-balanced” models constructed by Allen *et al.* (1990a) performs about equally well though, for reasons described above, should probably not be regarded as a balanced model. The quasigeostrophic model invariably performs the worst, all the more so when the topography is of order one height.

The third paper (Allen *et al.*, 1990b) is similar in spirit to the second, but the geometry is now a confined channel, which makes desirable the inclusion of coastal waves in as many balanced models as will support them. To satisfy the channel wall boundary conditions, the initial flow is uniform, rather than sinusoidal. Similar results on the relative accuracy of the various balanced models are found here when compared with those presented in the second paper, although in this case one of the “semi-balanced” systems performs better than the Balance Equations, and even better than the shallow water equations with a large implicit time step.

Spall & McWilliams (1992) addressed the question of whether there might be significantly more accurate balance schemes than the Balance Equations by comparing integrations of the Balance Equations and of a higher order balance scheme with integrations of the shallow water equations initialized with the same (balanced) fields in a doubly-periodic domain. They define the “unbalanced” amplitude for any field as the difference between the balanced model inte-

gration and the shallow water integration with the same balanced initial fields. In their study, they find that, at very low Rossby numbers, the higher order balance scheme initially gives rise to less energy in the unbalanced motions than the Balance Equations, but in time both orders of balance lead to the same (very small) degree of energy in the unbalanced flow. At higher Rossby number, agreement between the two different orders of balance is even closer for earlier times, and remains good for the whole integration, but both model integrations depart significantly further from the corresponding shallow water integrations than was the case at low Rossby number.

They present two different scaling analysis to investigate the nature of the “unbalanced” flow, which predict how its amplitude should scale with Froude and Rossby numbers. At low Rossby numbers, the unbalanced flow is consistent with a single scale analysis, which assumes that it has length and time scales of the same order as the balanced flow. The so-called unbalanced flow therefore has characteristics very similar to the balanced flow, and it seems plausible that it might be possible to obtain it as a higher order correction to balance in a more accurate balanced model. At high Rossby numbers, however, the amplitude of the unbalanced flow is consistent with a multiple scale analysis. The multiple scale analysis assumes that the unbalanced flow is dominated by free gravity waves, which appear to inherit the length scale of the balanced motions, but possess significantly higher frequencies. They conclude that at low Rossby numbers further corrections may be possible to their balance schemes, since the dynamics which is not captured by the balanced models seems nonetheless similar in character to the balanced dynamics. On the other hand, at high Rossby numbers the principal component of the unbalanced flow is similar for both balanced models, but is essentially different from the balanced dynamics. The principal unbalanced flow in this case corresponds to freely propagating gravity waves. Such motions are, for reasons described in §1.1, essentially unbalanced, and can almost certainly not be slaved to the potential vorticity evolution, as is required for a balanced model.

Charney balance (condition (1.13) with  $\nabla \cdot \mathbf{u} = 0$ ) was the basis for a study of a series of balanced models by Norton (1988), and McIntyre & Norton (1993). Their hierarchy of balanced models was constructed by successively eliminating higher order Eulerian or Lagrangian time derivatives of the divergence field. Their “first order” balance sets the divergence field and its first Eulerian time derivative to zero, and is therefore equivalent to Charney’s (1955) balance

scheme. Their “second order” balance sets the first and second time derivatives of the divergence field to zero, their “third order” the second and third time derivatives to zero, and so on. With two constraints now supplied, they use the advection of potential vorticity as their temporal evolution equation, and at every time-step the velocity fields required to advect the potential vorticity are obtained through instantaneous nonlinear elliptic inversion operators acting on the potential vorticity field.

They present integrations of a forced polar vortex in a single layer of shallow water on a hemisphere, with balanced initial conditions. They compare their integrations using successive order of balanced models with integrations of the full shallow water equations, and find that successive models up to the third order of their balanced models achieve improvements over lower orders in the hierarchy, but that their fourth order model seldom achieved noticeable improvements over their third order one. Boundary conditions imposed at the equator are equivalent to imposing antisymmetry. The simulations do not therefore have physical boundaries at the equator, and any equatorial Kelvin waves which develop must be regarded as part of the unbalanced flow (for a discussion of equatorial Kelvin waves in balanced models, see Gent & McWilliams, 1983b).

Comparing the divergence field from the shallow water and balanced integrations, they find that, aside from small differences in the magnitude of features which are common to both integrations, the most significant difference between balanced and shallow water simulations is a long equatorial Kelvin wave, trapped at the hemispherical “boundary”, but apparently propagating freely around the equator, with a group velocity consistent with the dispersion relation for equatorial Kelvin waves, and not apparently slaved to the vortical motions. This Kelvin wave is not present in any of their balanced integrations, but is present in almost all the corresponding shallow water integrations. This fact should not be surprising in view of the discussion of the inadmissibility of inertio-gravity waves in balanced models at the end of §1.1. What might be regarded as surprising, however, is that the wave has exceptionally low amplitude (at most about 10% of the maximum divergence in the flow), even when the Rossby numbers are of order one throughout a large region of the domain, and the Froude number reaches a maximum value of 0.7. It seems that the coupling between vortical motions and free gravity waves tends to be rather weak, even when there are no obvious small parameters in the flow, and hence, for systems without a large initial amount of free gravity wave activity, free

gravity waves develop in the flow only to very low amplitude. On the other hand, the fact that the fourth order inversion scheme does not perform significantly better than the third, and the ubiquitous emergence of a well-defined Kelvin wave in the shallow water simulations, suggest, but do not prove, that there is some ultimate limitation to potential vorticity inversion and balanced dynamics. We shall return to this point in §1.3, and again in chapter 3.

A somewhat different framework of balance was also considered by Norton (1988), following on the ideas of Non Linear Normal Mode Initialization, developed independently by Machenhauer (1977) and Baer & Tribbia (1977). The technique consists of first decomposing the equations into linear normal modes. The full equations are then cast in the framework of the normal mode decomposition, and a slaving relation derived to bound the gravity modes to the Rossby modes, on the assumption that the natural frequencies of the gravity modes are large compared with typical inverse time scales for the flow. A succession of balance inversion operators can be derived by this procedure. The zeroth order normal mode inversion consists in setting the amplitudes of the gravity wave mode amplitudes to zero. The first order inversion sets the time derivative of the gravity modes to zero. The second order inversion, obtained by Tribbia (1984), effectively sets the second time derivative of the gravity modes to zero. Like McIntyre & Norton's (1993) primitive equation inversions, this procedure can proceed indefinitely although, also like McIntyre & Norton's procedure, it will quickly become impractical as its complexity increases.

It has occasionally been suggested that the generation of gravity waves by vortical motions could be thought of as a generalization of the Rossby adjustment process discussed in §1.1, and that construction of an accurate balanced model might require the adjustment to be parametrized in some way. Although there are some difficulties with the idea, which will become clear as the thesis develops, two interesting proposals have developed from it.

In a recent paper, Vallis (1992) suggested that the production of gravity waves by vortical motions might be parametrized as a form of generalized Rossby adjustment. Following this idea, he proposed a balanced model in which the total energy of the system is minimized, subject to the condition that the potential vorticity field remain unchanged. Two constraints can be derived from the associated Euler-Lagrange equations, which can be used to define a balance system. Curiously, however, the method does not reconstruct steady axisymmetric solutions of the shallow water equations, which is perhaps related to the fact that it does not respect the

Casimir invariants of the shallow water system.

Another proposal (T. G. Shepherd, personal communication), is to divide the system into fast and slow components, very much like the normal mode decomposition. In the case of a canonical Hamiltonian system, in which fast variables have only fast conjugate variables, and slow variables have only slow conjugate variables, it is clear that, regarding the slow variables as fixed, the fast variables on their own constitute a reduced Hamiltonian system. To parametrize the adjustment process one might think of extremizing the “fast” Hamiltonian with respect to the fast variables, holding the slow variables fixed, since they are not supposed to change appreciably while the adjustment process is taking place. This procedure provides a slaving relation for the fast variables to the slow variables.

In truncated models of the atmosphere, there are typically twice as many gravity modes as Rossby modes. The reason for this is the presence of a Casimir density - the potential vorticity - which makes the full system non-canonical and, in the case of the shallow water system, reduces its order from 4 to 3. The canonical description involves either particle positions and momenta (two of each), or three Clebsh potentials and height (Salmon, 1988b). Truncated models of the atmosphere tend to inherit the non-canonical structure of their infinite dimensional counterpart (Bokhove, personal communication), and it is no longer clear whether the fast variables constitute a Hamiltonian system by themselves, since the existence of a Hamiltonian for the fast variables, which could be extremized to parametrize an adjustment process, is not assured if the full system is non-canonical. If Darboux’ theorem is invoked to make the system canonical, it is not clear that the canonical variables will separate into canonically conjugate fast variables and canonically conjugate slow variables.

### 1.3 Slow manifold hypothesis

In assessing different schemes for potential vorticity inversion, with different properties with respect to accuracy, analytical tractability and attempts to parametrize gravity wave generation in a physically motivated way, one is constantly left to wonder whether there might not be some more fundamental property of the shallow water equations involved – whether they might not possess a true “slow manifold”, on which the entire flow is determined exactly by the potential vorticity field, and which, once on, the solution will remain on for all time.

The origination of the “slow manifold” hypothesis originated in a paper of Leith (1980), in which he postulates the existence of a manifold  $\mathcal{M}$  with a phase space one third the dimension of the phase space of a full normal mode decomposition of the shallow water equations, for which, in his words

*“any state vector in  $\mathcal{M}$  would continue to move slowly in it, while any state vector not in  $\mathcal{M}$  would oscillate about it”.*

The implication of the existence of a slow manifold for any finite dimensional system is that the gravity wave modes can be slaved exactly to the Rossby wave modes. Similarly, for an infinite dimensional system, there would exist elliptic inversion operators acting on the instantaneous potential vorticity field such that, if the velocity and height fields associated with a given potential vorticity field were consistent with the inversion operators at an initial instant in time, then they would remain consistent with the given inversion operators for all subsequent times under evolution of the full (shallow water) system. A slow manifold can then be regarded as an exact balance, to which all known balanced models are approximations.

Questions regarding the existence or non-existence of a slow manifold have almost always been posed within the context of low order models. There are obvious conceptual simplifications in doing so. In particular, the fields are typically broken down into  $3 \times N$  normal modes of the system. One third of the modes are “Rossby” modes ( $\mathcal{R}_i$ ), and two thirds are gravity modes ( $\mathcal{G}_i$ ). The evolution of the  $\mathcal{R}_i$  and the  $\mathcal{G}_i$  is given by

$$\frac{d\mathcal{R}_i}{dt} + \Omega_i \mathcal{R}_i = \mathcal{N}^{\mathcal{R}_i}(\mathcal{R}, \mathcal{G}) \quad (1.14)$$

$$\frac{d\mathcal{G}_i}{dt} + \omega_i \mathcal{G}_i = \mathcal{N}^{\mathcal{G}_i}(\mathcal{R}, \mathcal{G}) \quad (1.15)$$

where the  $\mathcal{N}_{\mathcal{R}_i}$  and  $\mathcal{N}_{\mathcal{G}_i}$  are nonlinear functions required to account for the nonlinear interaction of Rossby modes  $\mathcal{R}_i$  and gravity modes  $\mathcal{G}_i$ , and no summation over repeated indices is intended.

The existence of a slow manifold for this system is equivalent to the existence of functions  $\mathcal{F}_i$  for  $i = 1, \dots, 2N$ , such that, given suitable initial conditions, the gravity wave modes can be slaved exactly to the Rossby wave modes by the functional relationship

$$\mathcal{G}_i = \mathcal{F}_i(\mathcal{R}_1, \dots, \mathcal{R}_N). \quad (1.16)$$

On the slow manifold, we would have

$$\frac{d\mathcal{G}_i}{dt} \equiv \frac{d\mathcal{F}_i}{d\mathcal{R}_j} \frac{d\mathcal{R}_j}{dt}, \quad (1.17)$$

where summation is understood for  $j = 1, \dots, N$ , and hence for a slow manifold to exist there would equivalently have to exist a solution to the nonlinear slaving relation

$$\sum_{j=1}^N \frac{d\mathcal{F}_i}{d\mathcal{R}_j} \left( \mathcal{N}^{\mathcal{R}_j}(\mathcal{R}, \mathcal{F}) - \Omega_j \mathcal{R}_j \right) + \omega_i \mathcal{F}_i = \mathcal{N}^{\mathcal{G}_i}(\mathcal{R}, \mathcal{F}) \quad (1.18)$$

for  $i = 1, \dots, 2N$ .

The suitable boundary conditions are that the amplitudes of the gravity wave modes  $\mathcal{G}_i$  should tend to zero as the amplitudes of the Rossby wave modes  $\mathcal{R}_j$  tend to zero. The leading order of the solution should then be equivalent to a quasi-geostrophic normal mode expansion. If this is not assured, then any invariant manifold found could not really be thought of as a slow manifold, since it would be dominated by gravity wave activity in the low Rossby number limit.

A further subtlety is that the the slow manifold, if it exists, might not exist over the whole range of  $\mathcal{R}$ -space, but rather might only exist in some region  $\mathbf{M}$  of Rossby mode phase space. The important point is that, if this is so, any trajectory initially in  $\mathbf{M}$  must remain in  $\mathbf{M}$ . It is not sufficient, for example, to be able to define a slow manifold in the neighbourhood of the origin if trajectories can then depart from that neighbourhood, perhaps to re-enter it not on the slow manifold.

Lorenz (1980) considered a 9 component model based on the shallow water equations on the  $f$ -plane. He found that for sufficiently small Rossby numbers the system appeared evolve towards a three-dimensional attractor, which corresponded approximately to quasi-geostrophic balance. Subsequently, he showed (Lorenz, 1986) that an unforced 5-component system, with three Rossby wave components and two gravity wave components, possessed a slow manifold. The proof, however, relied on an additional symmetry of the equations, in part an artifact of the small number of gravity wave components in the system, and it was not clear that the nine-component model used in Lorenz (1980), or a continuous fluid model, would possess sufficient symmetries to allow similar construction of a slow manifold..

Experiments with 9 component systems by Errico (1982), Warn & Menard (1986), and Vautard & Legras (1986) have suggested that gravity wave generation is an almost universal

property of models with the appropriate ratio of gravity wave modes to Rossby wave modes, and the result of Lorenz (1986) should be regarded as somewhat atypical of low order models.

There are various other ways in which simple models can be made to have slow manifolds. Tribbia (personal communication) has investigated a model in which the Rossby wave modes force the gravity wave modes, but the gravity wave modes do not react back upon the Rossby wave modes. It follows at once that the Rossby modes can be integrated on their own, and the gravity modes can then be integrated *a posteriori*. Imposing the condition that the gravity mode amplitudes tend to zero as the Rossby mode amplitudes tend to zero determines the gravity modes uniquely, and the model thus possesses a slow manifold, on which the gravity modes can be diagnosed from the Rossby modes, and are not required for the temporal integration of the model. One might in some sense regard the model as a description of how gravity waves are generated by vortical motions, but not including the effect describing how the vortical motions are affected by gravity wave generation. This philosophy has strong parallels with the Lighthill theory of aerodynamic sound generation (Lighthill, 1952), which we shall discuss in chapter 2 but is almost certainly fundamentally different from a realistic model of Rossby wave – gravity wave interaction.

When forcing and dissipation are introduced into simple models, additional difficulties may arise. Lorenz & Krishnamurthy (1987) demonstrated numerically that the 5 component model of Lorenz (1986) did not possess a slow manifold when forcing was introduced and was sufficiently strong. Some doubt has recently been cast on their result by Jacobs (1991), who shows for the same model how to obtain the slow manifold in the neighbourhood of fixed points of the system. His proof, however, relies on constructing analytic solutions by Taylor series, whose radius of convergence vanishes when the forcing and dissipation are turned off, and may be quite small otherwise. The Rossby numbers required for the slow manifold to exist thus depend on the amplitudes of forcing and dissipation. Moreover, phase space trajectories are guaranteed to remain in the region where the slow manifold exists only when the dissipation dominates over forcing and nonlinear evolution, in which case the entire system evolves towards a fixed point. The problem in all other cases is exactly that which was discussed earlier – the trajectories are not assured to remain in the region in which the slow manifold is defined, and may leave the region, perhaps to subsequently re-enter it not on the slow manifold. The study of Lorenz & Krishnamurthy (*op. cit.*) was not confined to the limited regime where all trajectories approach

the fixed point, so explaining the apparent discrepancy between the two papers. This has been discussed in the literature by Lorenz (1992).

## 1.4 Approach of this thesis

The aims of this thesis are three-fold:

- To investigate the generation of gravity waves in the shallow water system, and the dependence of their amplitudes and character on the Froude and Rossby numbers of the basic flow;
- To quantify the effect of the generation of gravity waves in the shallow water system on the potential vorticity distributions which generate them;
- To establish whether, without additional regard to flow geometry, there can or cannot exist a slow manifold for the shallow water equations in any region of Froude and Rossby number space.

The approach adopted to these questions in this thesis is as follows:

In chapter 2, we analyse the nature of interaction between vortical motions and gravity waves in the limit of low Froude number  $F$  and order-one Rossby number  $Ro$ . We begin by developing a theory of gravity wave generation by vortical motions. It is straightforward to show that there is a formal equivalence between two-dimensional compressible gas dynamics and the non-rotating shallow water system, in the case where the adiabatic gas exponent  $\gamma$  in the former is taken equal to two. The theory is thus an extension of the existing theory of aerodynamic sound generation, first proposed by Lighthill (1952), in which a compact vortical source generates acoustic waves having the same frequency as the vortical motions, but a wavelength which is greater than the vortical length scale by the order of  $F^{-1}$ .

The analysis proceeds via a singular perturbation expansion in  $F$ , generalizing the analysis of Crow (1970) to include the effect of background rotation upon both the high order Froude number corrections to the vortical source motion and gravity waves it generates. Within this framework we can also investigate the effect which the radiated waves have on the vortical motions, which is inaccessible via Lighthill's (1952) analysis. The chapter ends with a specific

example of the effect of gravity wave radiation on a rotating ellipse of uniform potential vorticity, which is a consistent leading order solution to the low Froude number dynamics (Kida, 1981; Lamb; 1932), generalizing a study by Zeitlin (1988, 1991).

Chapter 3 is motivated by the observation that when a small disturbance is made to the boundary of an axisymmetric vortex of uniform potential vorticity in the shallow water equations, the low Froude number analysis of chapter 2 predicts that, provided the frequency of the disturbance exceeds the inertial frequency in magnitude, the disturbance at a rate of order  $F^{2m}$ , where  $m$  is the mode number of the disturbance (Broadbent & Moore 1979; Kop'ev & Leont'ev, 1983, 1985, 1986).

We note that the instability may be regarded as a mixed Rossby-gravity instability in the sense of Sakai (1989), and investigate its growth rates over a range of  $F$ — $Ro$  space. In the spirit of Knessel & Keller (1992), we develop a WKBJ analysis to show that the instability persists for all Froude and Rossby numbers of the basic vortex, and can be generalized in a limited fashion to vortices with a continuous and monotonic potential vorticity profile. The implications for the existence of a slow manifold for the shallow water system are discussed.

The analysis for the axisymmetric vortex is compared with a similar analysis for parallel flow, with a single discontinuity of potential vorticity. Ripa's (1983) theorem states that the parallel flow will be stable if the ratio of the potential vorticities in the two layers is less than 4:1. In the final part of chapter 3, I show that the stability boundary provided by Ripa's theorem is indeed the stability boundary of the flow, and that at potential vorticity ratios exceeding 4:1 the flow is unstable to short wave disturbances.

In chapter 4 we return to the Lighthill theory of gravity wave generation, to assess its predictive power in cases where the Froude number is not small. Webster (1970) has investigated the validity of the  $F^{-7}$  power scaling law experimentally for a non-rotating jet in shallow water, and found that it applied for Froude number up to approximately  $F = 1$ . In this thesis I present a numerical investigation of barotropically unstable jets which generate gravity waves as a result of coupling between vortex motions and gravity waves as the instability saturates and the potential vorticity rolls up.4:1

It is found that, when background rotation is included, the vortical dynamics will tend to become less unsteady as the Froude number is increased. This effect, combined with the fact

that gravity waves can not propagate with frequencies below the inertial frequency, acts to reduce the amplitude of gravity wave radiation at larger Froude numbers, unless the potential vorticity in the strip is zero or of opposite sign to the background potential vorticity.

In the final chapter, I summarise the results obtained in the thesis, discuss possible connections between this work and observed phenomena in atmospheres and oceans, and make some suggestions for further research.

## Chapter 2

# Asymptotic analysis at low Froude number

## 2.1 Introduction

It is now more than forty years since Lighthill (1952) proposed his successful theory for predicting the intensity acoustic emissions from turbulent jets. The starting point for any theory of aerodynamic sound generation must be the compressible fluid equations:

$$\frac{\partial}{\partial t}\rho u_i + \frac{\partial}{\partial x_j}\rho u_i u_j + \frac{\partial p}{\partial x_i} = 0 \quad (2.1)$$

$$\frac{\partial \rho}{\partial t} + \frac{\partial}{\partial x_i}\rho u_i = 0 \quad (2.2)$$

$$\left(\frac{p}{p_0}\right) = \left(\frac{\rho}{\rho_0}\right)^\gamma, \quad (2.3)$$

where  $\gamma$  is the adiabatic gas exponent. For a diatomic gas, one takes  $\gamma = 1.4$ , but for our purposes it is important to note that if the fluid is assumed to be two-dimensional, the choice  $\gamma = 2$  yields the (non-rotating) shallow water equations, with density  $\rho$  in place of the shallow water height. Gravity waves in the shallow water system are the counterpart of acoustic waves in the compressible gas equations, and it follows that any analysis of sound wave generation by vortical motions in two-dimensional compressible fluids should be equally valid in analysing gravity wave generation by vortical motions in the shallow water equations.

The crucial step of Lighthill's (*op. cit.*) so-called "acoustic analogy" theory is to combine (2.1) – (2.3) to yield

$$\left(\frac{\partial^2}{\partial t^2} - c_0^2 \nabla^2\right) \rho' = \frac{\partial^2}{\partial x_i \partial x_j} T_{ij}, \quad (2.4)$$

where  $c_0^2 = \gamma p_0 / \rho_0$ ,  $\rho = \rho_0 + \rho'$ ,  $\rho_0$  is constant, and

$$T_{ij} = \rho u_i u_j + (p - c_0^2 \rho) \delta_{ij}. \quad (2.5)$$

The left hand side of (2.4) is then simply the acoustic wave operator acting on the density field, and the right hand side is to be regarded as the effective acoustic source.

So far we have proceeded by formal manipulation of (2.1 - 2.3). The predictive power of (2.4), however, comes only as a result of making certain assumptions about the nature of the source tensor  $T_{ij}$ .

Lighthill (*op. cit.*) proceeded by assuming that the eddy Mach number is small, so that each eddy is acoustically compact. Scaling arguments for small Mach numbers imply that  $T_{ij} \approx \rho_0 u_i u_j$ . In deriving scaling laws for the wave field due to a low Mach number eddy, it is

convenient to follow Crighton (1975) and work in the frequency domain  $(\mathbf{x}, \omega)$ , rather than the time domain  $(\mathbf{x}, t)$ .

The solution to (2.4) may then be written down as

$$\rho'(\mathbf{x}, \omega) = -\frac{1}{4\pi c_0^2} \int \frac{\partial^2}{\partial x'_i \partial x'_j} T_{ij}(\mathbf{x}', \omega) \frac{\exp(i\omega|\mathbf{x} - \mathbf{x}'|/c_0)}{|\mathbf{x} - \mathbf{x}'|} d^3 \mathbf{x}' \quad (2.6)$$

in three space dimensions, and

$$\rho'(\mathbf{x}, \omega) = \frac{1}{16\pi i c_0^2} \int \frac{\partial^2}{\partial x'_i \partial x'_j} T_{ij}(\mathbf{x}', \omega) H_0(\omega|\mathbf{x} - \mathbf{x}'|/c_0) d^2 \mathbf{x}' \quad (2.7)$$

in two space dimensions, where  $H_0$  is the Hankel function of the first kind of order zero. If the source  $T_{ij}$  is assumed acoustically compact, we may expand the integrals (2.6) and (2.7) to obtain far field expressions for the radiated waves as

$$\rho' \sim \frac{1}{4\pi c_0^2} \frac{\omega^2}{c_0^2} \frac{x_i x_j}{|\mathbf{x}|^2} \frac{1}{|\mathbf{x}|} \exp(i\omega|\mathbf{x}|/c_0) \int T_{ij}(\mathbf{x}', \omega) d^3 \mathbf{x}' \quad (2.8)$$

in three space dimensions, and

$$\rho' \sim \frac{i}{16\pi c_0^2} \frac{\omega^2}{c_0^2} \frac{x_i x_j}{|\mathbf{x}|^2} \frac{1}{(\omega|\mathbf{x}|/c_0)^{1/2}} \int T_{ij}(\mathbf{x}', \omega) d^2 \mathbf{x}' \quad (2.9)$$

in two. The asymptotic expressions (2.8) and (2.9) enable us to obtain the dependence of the radiated far wave field upon the parameters of the source flow. In three dimensions, we have

$$\rho' \sim \frac{1}{c_0^2} \frac{\omega^2}{c_0^2} \frac{1}{|\mathbf{x}|} \rho_0 u^2 l^3 = \rho_0 \frac{l}{|\mathbf{x}|} \left(\frac{u}{c_0}\right)^2 \left(\frac{\omega l}{c_0}\right)^2 \quad (2.10)$$

and in two dimensions

$$\rho' \sim \frac{1}{c_0^2} \frac{\omega^{3/2}}{c_0^{3/2}} \frac{1}{|\mathbf{x}|^{1/2}} \rho_0 u^2 l^2 = \rho_0 \left(\frac{l}{|\mathbf{x}|}\right)^{1/2} \left(\frac{u}{c_0}\right)^2 \left(\frac{\omega l}{c_0}\right)^{3/2}. \quad (2.11)$$

Typically, one assumes that the frequency  $\omega$  is set by the velocity and length scales of the eddies, so that  $\omega \sim u/l$ . These expressions then lead directly to the most startling results of the theory – that at low Mach number the acoustic intensity  $I \equiv (c_0^3/\rho_0)\rho'^2$  of the radiated waves at fixed  $l/|\mathbf{x}|$  obeys the scaling laws

$$I \sim \begin{cases} M^8 & 3 \text{ dimensions} \\ M^7 & 2 \text{ dimensions} \end{cases}, \quad (2.12)$$

where  $M$  is Mach number of the turbulence in the eddy, holding  $c_0$  and  $\rho_0$  constant. The high exponent in the power scaling law derives from three facts: power is a quadratic quantity in

wave amplitude; the power radiated will depend on the intensity of the turbulence generating it; and the effective source term for the acoustic radiation corresponds to a quadrupole source distribution in the compact limit, cancelling out the potentially stronger effects of monopoles or dipoles. The implication is that acoustic disturbances generated by vortical motions will be exceptionally weak, at least in the limit of low Mach number, and can be expected to have a negligible impact on the flows which generate them.

One shortcoming of the Lighthill theory is that there is no way to quantify the effect of acoustic wave radiation on the vortical flows which generate the acoustic waves. A significant advance in the general theory of aerodynamic sound generation was made when several workers (Obermeier, 1967; Lauvstad, 1968; Crow, 1970) independently developed analyses of the phenomenon using the method of matched asymptotic expansions, taking the Mach number  $M$  as the small asymptotic parameter. Two asymptotic regions are established: a source region of length scale  $l$ , in which the flow is nearly incompressible, and a wave region of length scale  $lM^{-1}$ , in which acoustic waves are linear at the leading two orders in Mach number at which they appear.

One generally assumes that the vorticity in the eddy is zero outside a region of finite extent on the  $l$  length scale. In the vortical flow region, the flow is incompressible at leading order in Mach number. Therefore, if the vorticity field is specified, the velocity and pressure fields at leading order in Mach number can be obtained directly from it. If the vorticity is zero except in some bounded domain, the velocity fields will decay as  $r^{-3}$  in three dimensions, or  $r^{-1}$  in two dimensions. Higher order Mach number corrections to the velocity and pressure in the vortical region are obtained by perturbation expansion. The expansion is singular, with acoustic waves on a length scale of order  $lM^{-1}$ , which is long compared with the scale of the vortical region. At high order in Mach number, details of the matching conditions are required to uniquely determine the velocity and height fields in the vortical regions.

The principal acoustic waves obtained by the matched asymptotic analysis correspond exactly to those predicted by the original Lighthill theory as described above, provided  $T_{ij}$  is formed from the incompressible velocity field associated with the vorticity distribution for the eddy. The analysis of Crow is distinguished among these studies in that he carries out the Mach number expansion in the source region to a sufficiently high order in  $M$  to establish that corrections due to the compressibility of the vortical region do not introduce monopoles or

dipoles, which could in principle give rise to waves of the same amplitude as the leading order quadrupole.

In addition to a general analysis of the radiated sound field, the method of matched asymptotic expansions has also been used to obtain expressions for the sound radiated from flows whose leading order incompressible solution may be expressed analytically. Two-dimensional flows analysed in this way include point vortex flows (Klyatskin 1966; Stuber 1970; Rahman 1971; Crighton 1972a; Gryanik 1983), vortex sheets (Crighton 1972b; Crighton & Leppington, 1974) and a limited class of flows with distributed vorticity (Zeitlin 1988, 1991).

Application of the theory to simple three-dimensional flows is less common since, unlike a large class of two-dimensional point vortex solutions, there are comparatively few three dimensional flows with confined vorticity whose solution can be expressed in closed analytical form. The only reported calculations of sound generation by three dimensional ideal flows in free space are for interacting vortex rings (Klyatskin 1966; Kambe & Minota 1981), and for the Hasimoto soliton (Kimura 1989). Kambe and Minota have subsequently obtained good agreement between experimental measurements of the acoustic sound field generated by low Mach number colliding vortex rings in the laboratory and the corresponding theoretical predictions (Kambe & Minota 1983; Minota & Kambe 1986; Kambe, 1986).

Despite considerable interest in the sound field generated by two and three dimensional vortical motions, comparatively little attention has been paid to the effect of sound radiation upon the flow which generates it. Exceptions are the papers of Klyatskin (1966) and Gryanik (1983) for simple point vortex flows, and Zeitlin (1988, 1991) for two dimensional flows with distributed vorticity.

In the point vortex paper of Gryanik (1983), the flows consist of rotating configurations of point vortices. The point vortices are of equal strength, and placed at the vertices of a regular polygon. The acoustic wave field is calculated using the leading order of matched asymptotic expansions, and the radiated power computed from it. The interaction energy of the point vortex configurations depends on a single parameter: the distance from the centre of the polygon to the vortices, which is assumed to adjust slowly to account for the energy lost due to the acoustic wave radiation. However, a difficulty with point vortex calculations for essentially compressible fluid dynamics problems is that the point vortex model collapses at order  $M$  in the expansion as an evacuated region forms at a finite  $O(M)$  distance from the

vortex core (see Barsony-Nagy *et al.*, 1987; Moore & Pullin, 1987). The resulting complexity of the asymptotic expansions makes it practically impossible to continue the analysis to sufficiently high order in  $M$  to account for the effect of acoustic radiation within a matched asymptotic framework, and we feel it is therefore desirable to investigate the effect of radiation on some distributed vortex flows, such as those analysed by Zeitlin (1988, 1991).

However, one can raise concerns about the analysis of Zeitlin (*op. cit.*). In his study, he took the initial vorticity distribution to be a member of the class of steadily rotating two dimensional vortical flows with vorticity of finite extent investigated by Abrashkin & Yakubovich (1984). The flows belong to distinct one-parameter families, each family being characterised by its circulation and degree of rotational symmetry. Again, using the leading order of matched asymptotics, Zeitlin obtains the wave field, and hence rate of energy radiation. He then assumes that the flows evolve to take account of this energy loss by adjusting the available free parameter, conserving circulation but reducing the energy of the vortical flow.

The important point is that, although distributed vorticity makes it quite possible to construct a singular perturbation expansion in  $M$  which remains regular over the vortical scale, and requires rescaling only to account for acoustic wave radiation, there seems to be no reason to assume, as Zeitlin does, that the effect of the acoustic radiation is to cause the vortex to evolve slowly between different states of the one parameter family. Williams (1992) has undertaken a weakly nonlinear analysis of the case with  $180^\circ$  rotational symmetry, in which the steadily rotating states are ellipses with small aspect ratio. His analysis showed that the vortex could split at a time of  $O(F^{-4})$ , which seems inconsistent with the supposition of Zeitlin that the ellipses would simply elongate, conserving their area, but remaining elliptical.

It is therefore of interest to perform a full analysis of this flow using matched asymptotic expansions, expanding the vortical and acoustic scale flows in the small parameter  $M$  until the matching condition between them requires a term to be introduced to the vortical scale flow which accounts for the loss of energy to the acoustic waves at some (high) order in  $M$ . The behaviour would then be described entirely in terms of advection of potential vorticity in the vortical region. The flow evolution should be consistent with energy arguments in cases where the latter apply, but would also be able to show when energy arguments would not apply.

Norton (personal communication) has shown how to recast the  $f$ -plane shallow water equa-

tions

$$\frac{D\mathbf{u}}{Dt} + f\mathbf{k} \times \mathbf{u} + g\nabla h = 0 \quad (2.13)$$

$$\frac{Dh}{Dt} + h\nabla \cdot \mathbf{u} = 0 \quad (2.14)$$

into a similar form to (2.4), viz:

$$\left( \frac{\partial^2}{\partial t^2} + f^2 - c_0^2 \nabla^2 \right) \frac{\partial h}{\partial t} = \frac{\partial^2}{\partial x_i \partial x_j} T_{ij}, \quad (2.15)$$

where now

$$T_{ij} = \frac{\partial}{\partial t}(hu_i u_j) + f\varepsilon_{ik} h u_j u_k + \frac{1}{2}g \frac{\partial}{\partial t}(h - h_0)^2 \delta_{ij}. \quad (2.16)$$

Now, (2.15) will have propagating wave solutions if and only if their frequency exceeds the magnitude of the inertial frequency  $|f|$ . If  $T_{ij}$  is formed as the result of some fully nonlinear evolution, it would seem unlikely that all frequencies in all of its components will fall below the inertial frequency  $f$ , however small the Rossby number of the flow may be in some averaged sense. Therefore, it seems highly likely that gravity wave radiation is the inevitable consequence of fully nonlinear flow evolution.

Since balanced models do not admit freely propagating gravity waves, one might suppose that the present analysis shows that it is unlikely that one could construct a balanced model of the vortical flow at all orders in the Froude number expansion. This conclusion, however, should not be drawn too quickly, and we are certainly in no position to draw it as a result of the analysis presented so far.

To summarize, the essential feature of the matched asymptotic approach when used in aeroacoustics is that the Mach number is low, so that the source scale flow is nearly incompressible, and can be described by its vorticity alone. The sound field is obtained by an asymptotic matching process, which does not affect the source flow at leading order.

In the shallow water equations, if a low Froude number approximation is made, and  $T_{ij}$ , given by (2.16), is constructed using the incompressible velocity field, a similar matched asymptotic analysis may be used to predict the leading order gravity wave radiation due to a localized vortical flow knowing only the evolution of the potential vorticity field. With the gravity wave field now obtained, we might tentatively suggest that the vortical flow could be corrected at subsequent orders in Froude number to take account of the both the effects of divergence in

the vortical region and of gravity wave radiation. If so, then the entire perturbation expansion in Froude number for all fields could be constructed knowing only the potential vorticity. This would therefore constitute a balanced model which actually takes into account all the gravity wave radiation that is necessarily generated by the Lighthill mechanism, and would remain valid as the vortical flow is adjusted to take account of the gravity wave radiation. This would seem contrary to the intuitive notion that balanced models should not be able to take propagating gravity waves into account.

It is clear that the only way to address the possibility of a balanced model incorporating gravity wave radiation is to perform a matched asymptotic analysis of the entire problem. That analysis forms the basis for the rest of this chapter, which is organised as follows:

In §2.2 I present a matched asymptotic analysis of a compact vortical source in the  $f$ -plane shallow water equations at low Froude number. I assume throughout that the potential vorticity is confined to a finite compact region for all time. The applicability of the method of matched asymptotic expansions to gravity wave generation in the two-dimensional shallow water equations in a rotating frame is established. The analysis is carried sufficiently far to obtain the principal effect of the wave radiation on the source region.

In §2.3 the effect of the radiation on the source region is discussed within the context of balance and potential vorticity inversion.

In §2.4 the effect of gravity wave radiation on an ellipse of uniform potential vorticity is examined. The degree to which the solution agrees with, and differs from, the analysis of Zeitlin (1988, 1991) is clarified.

In §2.5, I offer some concluding remarks about the nature of the effect of gravity wave radiation on vortical sources, with particular reference to the “generalized adjustment” ideas of Vallis (1992) and Shepherd (personal communication), which were discussed briefly in chapter 1.

## 2.2 Gravity wave generation as a singular perturbation problem

To establish the nature of gravity wave generation by vortical motions at low Froude number, we are considering single layer shallow water dynamics on an  $f$ -plane. In the absence of motion,

we assume the layer has uniform depth  $H_0$ , and hence uniform potential vorticity  $Q_0 = f/H_0$ .

Suppose now that the potential vorticity  $Q$  differs from  $Q_0$  only in some vortical region of finite extent, which is of dimension  $L$ . We must now turn to deriving a scaling of the shallow water equations valid in the limit of order-one Rossby number and small Froude number. From the definition of potential vorticity, it follows that the relative vorticity  $\zeta$  scales as  $\zeta \sim Q'H_0$ , where  $Q' \sim Q - Q_0$ , and hence that the typical velocities  $U$  in the region of non-uniform potential vorticity scale according to  $U \sim Q'H_0L$ . The Rossby number  $Ro$  and Froude number  $F$  are defined by  $F \sim U/(gH_0)^{1/2}$ ,  $Ro = U/fL \sim Q'/Q$ . We shall assume for the remainder of this chapter that  $Q'/Q_0 = O(1)$ , so that  $Ro = O(1)$ , and we shall also assume that  $F \ll 1$ .

Now we let the total layer depth be  $H$ . By considering the balance of terms in the momentum equation, it follows from the assumption of order-one Rossby number that the advective and Coriolis terms are of the same order. Consistency requires that all terms in the momentum equation are of the same order. This implies that  $H - H_0 = O(F^2)$ , and hence that the continuity equation reduces to the incompressibility constraint at leading order.

With velocity  $\mathbf{u}$  scaled on  $U$ , length scaled on  $L$ , time  $t$  scaled on  $U/L$ , and writing  $H - H_0 = F^2H_0h$ , the shallow water equations take the nondimensional form:

$$\frac{D\mathbf{u}}{Dt} + f\mathbf{k} \times \mathbf{u} + \nabla h = 0 \quad (2.17)$$

$$F^2 \left( \frac{Dh}{Dt} + h\nabla \cdot \mathbf{u} \right) + \nabla \cdot \mathbf{u} = 0. \quad (2.18)$$

The nondimensionalised potential vorticity takes the form

$$Q = \frac{f + \zeta}{1 + F^2h}. \quad (2.19)$$

The leading order dynamics are thus simply two-dimensional incompressible vortex dynamics. The presence of background rotation plays no part in the leading order evolution of the potential vorticity field, although the associated height field  $h$  will be modified due to background rotation.

With the nondimensional form of the equations now established for the vortical region which “drives” the flow, we may proceed to develop the singular perturbation expansion for the entire

flow which will enable us to determine the radiated wave field and the nature of its effect on the vortical flow.

### 2.2.1 Perturbation expansion for the vortical flow

We begin by developing the perturbation expansion for the vortical flow region. We write  $\mathbf{u} = \nabla\phi + \mathbf{k} \times \nabla\psi$ , and expand  $\phi$ ,  $\psi$  and  $h$  in perturbation expansions as

$$\psi = \psi_0 + F^2\psi_2 + \dots; \quad \phi = F^2\phi_2 + \dots; \quad h = h_0 + F^2h_2 + \dots. \quad (2.20)$$

The expansion for  $\phi$  starts at  $O(F^2)$  because from (2.18) we see that at leading order the flow is non-divergent.

We consider a flow in which initially the potential vorticity  $Q$  is specified as a function of position.

As the flow evolves, the potential vorticity is advected by all orders of the velocity field  $\mathbf{u}$ :

$$\frac{\partial Q}{\partial t} + (\mathbf{u}_0 + F^2\mathbf{u}_2 + \dots) \cdot \nabla Q = 0. \quad (2.21)$$

As it stands, this equation cannot be correct, since there are advective terms at all orders in  $F$ , but the time derivative term  $\partial Q/\partial t$  occurs only at the leading order in  $F$ .

For times of order unity, the difficulty may be easily resolved by expanding  $Q$  as an asymptotic series in  $F$ :

$$Q = Q_0 + F^2Q_2 + \dots. \quad (2.22)$$

However, over longer times, it is possible that this formulation might give rise to secular growth in  $Q_2$  – for example, if there is a component of  $\mathbf{u}_2$  which acts to slow down the rotation of vortices, or to move two vortices apart. To resolve these difficulties, we must introduce a long time scale  $T = F^2t$ , and the potential vorticity evolution equation at  $O(F^2)$  becomes

$$\frac{\partial Q_2}{\partial t} + \frac{\partial Q_0}{\partial T} + \mathbf{u}_0 \cdot \nabla Q_2 + \mathbf{u}_2 \cdot \nabla Q_0 = 0. \quad (2.23)$$

In general, there is no straightforward way to distinguish between the advective terms in (2.23) which give rise to slow secular behaviour in the order-unity potential vorticity field from those which give rise to  $O(F^2)$  fluctuations of the potential vorticity on the fast ( $O(1)$ ) timescale. Fortunately, this distinction is not important in analysing gravity wave generation and its effect

on the vortical flow, although it is important when specific flows are to be described, as in §2.4 below.

We shall now assume that  $Q = f$  everywhere except in some finite domain, which we refer to as the vortex. Then, since  $\nabla \cdot \mathbf{u}_0 = 0$ , we may write  $\mathbf{u}_0 = \mathbf{k} \times \nabla \psi_0$ , and obtain

$$\nabla^2 \psi_0 = Q_0 - f. \quad (2.24)$$

$Q_0 - f$  represents the leading order relative vorticity  $\mathbf{k} \cdot (\nabla \times \mathbf{u})$ , which for convenience we shall refer to as  $\zeta_0$ , so that  $\zeta_0$  is zero outside some finite region on the vortical length scale. In general, the Laplacian can only be inverted up to non-singular harmonic terms. By Liouville's theorem, any nonsingular harmonic terms must be unbounded at infinity. Assuming, that  $\psi_0$  does not contain any non-singular growing terms, we can obtain  $\psi_0$  from (2.24) in terms of a Green function integral

$$\psi_0 = \frac{1}{2\pi} \int \zeta_0(\mathbf{x}') \ln |\mathbf{x} - \mathbf{x}'| d^2 \mathbf{x}'. \quad (2.25)$$

For the present analysis, we are primarily concerned with obtaining expressions for the vortical flow fields  $\psi_0, h_0, \psi_2, \phi_2, \dots$  in sufficient generality that we may evaluate them in the limit as  $|\mathbf{x}| \rightarrow \infty$ , in preparation for matching onto the wave region. First, we expand  $\ln |\mathbf{x} - \mathbf{x}'|$  for  $|\mathbf{x}| > |\mathbf{x}'|$ , using the Taylor expansion for the logarithm:

$$\ln |\mathbf{x} - \mathbf{x}'| = \ln |\mathbf{x}| + x'_i \frac{\partial}{\partial x_i} \ln |\mathbf{x}| + \frac{1}{2} x'_i x'_j \frac{\partial^2}{\partial x_i \partial x_j} \ln |\mathbf{x}| + \dots, \quad (2.26)$$

and substitute this for  $\ln |\mathbf{x} - \mathbf{x}'|$  in (2.25). Since  $Q - f$  is of compact support, all the resulting moment integrals converge, and it is simple to show that the remainder is of smaller order than the last moment integral taken. Taking terms to  $O(r^{-2})$ , we have

$$\psi_0 = \frac{1}{2\pi} \ln |\mathbf{x}| \int \zeta_0(\mathbf{x}') d^2 \mathbf{x}' \quad (2.27)$$

$$+ \frac{1}{2\pi} \frac{x_i}{|\mathbf{x}|^2} \int x'_i \zeta_0(\mathbf{x}') d^2 \mathbf{x}' \quad (2.28)$$

$$+ \frac{1}{2\pi} \left( \frac{\delta_{ij}}{|\mathbf{x}|^2} - \frac{2x_i x_j}{|\mathbf{x}|^4} \right) \int \frac{1}{2} x'_i x'_j \zeta_0(\mathbf{x}') d^2 \mathbf{x}' \quad (2.29)$$

$$+ O(r^{-3}).$$

Now, we may note that the integral in (2.27) is an  $O(1)$  approximation to the circulation  $\int \zeta d^2 \mathbf{x}'$ , and that in (2.28) is an  $O(1)$  approximation to the Kelvin impulse  $\int \zeta \mathbf{x}' d^2 \mathbf{x}'$ . These

are both constant on the  $O(1)$  timescale  $t$ , and so the fluctuating part of the leading order streamfunction  $\psi_0$  is  $O(r^{-2})$  as  $r \rightarrow \infty$ . Since  $\int(x^2 + y^2)\zeta$  is also independent of time on the  $O(1)$  timescale, the time-dependent part of (2.29) may be represented as

$$\frac{A(t)}{r^2} \cos 2\theta + \frac{B(t)}{r^2} \sin 2\theta. \quad (2.30)$$

This represents a quadrupolar far field for  $\psi_0$ , and will clearly match to a radiating wave field of quadrupole form.

It is straightforward to see from dimensional grounds, and it will be verified in §2.2.2 below, that if the vortical source has a length scale of order unity, then the gravity waves generated will have a long wavelength of order  $F^{-1}$ . It follows that the leading order temporally fluctuating quadrupole in  $\psi_0$ , given by (2.30), will be of order  $F^2$  in the wave region, where the radial variable is  $R \equiv Fr$ .

On the other hand, it is clear that  $O(F^2)$  fields will arise in the vortical region as a direct result of the local effects of divergence. If any of these fields should have a temporally fluctuating monopolar far field, they would give rise to monopolar gravity wave radiation at  $O(F^2)$ , which would be formally of the same order as the quadrupolar radiation obtained from the incompressible source scale dynamics. We shall therefore proceed to obtain the far field expressions for  $\psi_2$  and  $\phi_2$ , to determine whether the leading order quadrupole is the only  $O(F^2)$  wave field.

To obtain expressions for  $\psi_2$  and  $\phi_2$ , we must first obtain an expression for  $h_0$ . If we attempt to use the divergence of the momentum equation (2.17):

$$\nabla \cdot (\mathbf{u}_0 \cdot \nabla \mathbf{u}_0) + f \nabla \cdot (\mathbf{k} \times \mathbf{u}_0) + \nabla^2 h_0 = 0 \quad (2.31)$$

directly to obtain  $h_0$ , we obtain the integral expression

$$h_0 = f\psi_0 - \frac{1}{2\pi} \int \frac{\partial^2}{\partial x'_i \partial x'_j} (u_{0i}(\mathbf{x}') u_{0j}(\mathbf{x}')) \ln |\mathbf{x} - \mathbf{x}'| d^2 \mathbf{x}'. \quad (2.32)$$

Although  $\partial^2(u_{0i}u_{0j})/\partial x_i \partial x_j = O(r^{-4})$  as  $r \rightarrow \infty$ , and therefore the integral in (2.32) converges, it is not straightforward to extract the asymptotic form of  $h_0$  for large  $|\mathbf{x}|$  from (2.32). To see this, substitute the expansion for  $\ln |\mathbf{x} - \mathbf{x}'|$  into (2.32). The  $\ln r$  and  $r^{-1}$  terms vanish after integration by parts, and we are left with a divergent integral:

$$h_0 \sim f\psi_0 - \frac{1}{2\pi} \left( \frac{\partial^2}{\partial x_i \partial x_j} \ln |\mathbf{x}| \right) \int (u_{0i}(\mathbf{x}') u_{0j}(\mathbf{x}')) d^2 \mathbf{x}'. \quad (2.33)$$

The integrand is now of order  $r^{-2}$  for large  $r$ , and therefore the moment integrals for the far field of  $h_0$  fail to converge at the first order at which they are non-zero. We are therefore unable to predict the far-field behaviour of  $h_0$  directly from (2.31), and some other method must be found to obtain the far-field expression for  $h_0$ .

The resolution to the difficulty is to introduce the Bernoulli variable  $B = h + \frac{1}{2}\mathbf{u}^2$  in (2.17), which was used extensively by Howe (1975) for his study of the aerodynamic sound generation problem, to obtain Crocco's equation:

$$\frac{\partial \mathbf{u}}{\partial t} + (f + \zeta)(\mathbf{k} \times \mathbf{u}) + \nabla B = 0. \quad (2.34)$$

As with  $\psi$ ,  $\phi$  and  $h$ , we expand  $B$  in an asymptotic series in  $F$ :

$$B = B_0 + F^2 B_2 + \dots. \quad (2.35)$$

From (2.34) one then obtains at order unity

$$\nabla^2 B_0 = -\nabla \cdot (\zeta_0 \mathbf{k} \times \mathbf{u}) + f \nabla^2 \psi_0. \quad (2.36)$$

Inverting the Laplacian, we obtain<sup>1</sup>

$$B_0 = f\psi_0 + \frac{1}{2\pi} \int \nabla \cdot (\zeta_0 \nabla \psi_0) \ln |\mathbf{x} - \mathbf{x}'| d^2 \mathbf{x}'. \quad (2.37)$$

The important point is that  $\zeta_0$  is zero outside some finite domain. Therefore we may obtain the far field expansion for  $B_0$  by expanding the logarithm in the form (2.26) and substituting it into the integral in (2.37). Moreover, since the leading order term in the far field expansion of (2.37) has the coefficient

$$\int \zeta_0 \nabla \psi_0 d^2 \mathbf{x}' = 0, \quad (2.38)$$

---

<sup>1</sup>In (2.37) and, except where otherwise stated, in all subsequent integrals in §2.2.1, all terms in integrands are functions of  $\mathbf{x}'$ , and all gradients, represented by  $\nabla$ , when acting on integrands, are gradients with respect to  $\mathbf{x}'$ .

it follows from conservation of Kelvin's impulse on timescale  $t$  (see, e.g. Batchelor, 1967) that the far field expansion of  $B_0$  to  $O(r^{-2})$  takes the form

$$B_0 \sim f\psi_0 - \frac{1}{2\pi} \left( \frac{\delta_{ij}}{|\mathbf{x}|^2} - \frac{2x_i x_j}{|\mathbf{x}|^4} \right) \int \zeta_0(\mathbf{x}') x'_i \frac{\partial \psi_0}{\partial x'_j} d^2 \mathbf{x}' + O(r^{-3}) \quad (2.39)$$

in the limit of large  $r$ . Consequently, the leading order Bernoulli function  $B_0$  has a quadrupolar far field. To obtain the far field for  $h_0$ , we then use  $h_0 = B_0 - \frac{1}{2}\mathbf{u}_0^2$ . From the far field expression for  $\psi_0$  (2.27-2.29), we can see that  $u_0 = O(r^{-1})$  in the far field, and the only  $r^{-1}$ -like term in  $\mathbf{u}_0$  is the circulation, which is independent of time. Therefore, at  $O(r^{-2})$ ,  $B_0$  and  $h_0$  differ in the far field by a time-independent term only, and the principal time fluctuating part of  $h_0$  is therefore also quadrupolar in the far field.

This resolves our first difficulty, which arose due to the nonconvergence of the integral in (2.33). We must now proceed to resolve whether there are competing monopoles introduced by compressibility at  $O(F^2)$ . If the time fluctuating parts of the far fields of  $\psi_2$  and  $\phi_2$  at  $O(1)$  have only  $e^{2i\theta}$  dependence, then they will correspond to higher order matching for the quadrupole in the wave region. If, on the other hand, they contain components which are independent of  $\theta$ , these would correspond to an  $O(F^2)$  monopole. The principal wave field could not then be deduced directly from the incompressible velocity field, and we could not truly refer to the radiation as ‘‘quadrupole’’.

To resolve this, we carry out the perturbation expansion to the next order in  $F$  in the source region. Writing  $\mathbf{u}_2 = \nabla\phi_2 + \mathbf{k} \times \nabla\psi_2$ , we have

$$\nabla^2 \phi_2 = -\frac{\partial h_0}{\partial t} - \nabla \cdot (\mathbf{u}_0 h_0) \quad (2.40)$$

$$\nabla^2 \psi_2 = (f + \zeta_0)h_0 + Q_2. \quad (2.41)$$

From (2.37), and using the identity

$$\mathbf{u}_0^2 \equiv |\nabla\psi|^2 = \frac{1}{2}\nabla^2\psi_0^2 - \psi_0\nabla^2\psi_0, \quad (2.42)$$

we may write  $h_0$  as

$$h_0 = \left( f + \frac{1}{2}\zeta_0 \right) \psi_0 - \frac{1}{4}\nabla^2\psi_0^2 + \frac{1}{2\pi} \int \nabla \cdot (\zeta_0 \nabla \psi_0) \ln |\mathbf{x} - \mathbf{x}'| d^2 \mathbf{x}'. \quad (2.43)$$

In addition, it is helpful to note the identity:

$$\nabla \cdot (\psi_0 \mathbf{u}_0) = 0, \quad (2.44)$$

and hence to use the expression

$$\nabla \cdot (h_0 \mathbf{u}_0) = \nabla \cdot ((h - f\psi_0) \mathbf{u}_0) \quad (2.45)$$

in (2.40). The point here is that  $h_0 = O(\ln r)$  as  $r \rightarrow \infty$ , whereas, from (2.39), it is straightforward to show that  $h_0 - f\psi_0 = O(r^{-2})$ . This turns out to be essential in determining the far field expression for  $\phi_2$ .

With  $h_0$  now in a suitable form for integration, the solution to (2.40) may be written as

$$\phi_2 = - \frac{f}{8\pi} \frac{\partial}{\partial t} \int \zeta_0 |\mathbf{x} - \mathbf{x}'|^2 (\ln |\mathbf{x} - \mathbf{x}'| - 1) d^2 \mathbf{x}' \quad (2.46)$$

$$- \frac{1}{4\pi} \frac{\partial}{\partial t} \int \psi_0 \zeta_0 \ln |\mathbf{x} - \mathbf{x}'| d^2 \mathbf{x}' \quad (2.47)$$

$$+ \frac{1}{2} \psi_0 \frac{\partial \psi_0}{\partial t} \quad (2.48)$$

$$- \frac{1}{8\pi} \frac{\partial}{\partial t} \int \nabla \cdot (\zeta_0 \nabla \psi_0) |\mathbf{x} - \mathbf{x}'|^2 (\ln |\mathbf{x} - \mathbf{x}'| - 1) d^2 \mathbf{x}' \quad (2.49)$$

$$- \frac{1}{2\pi} \int \nabla \cdot ((h_0 - f\psi_0) \mathbf{u}_0) \ln |\mathbf{x} - \mathbf{x}'| d^2 \mathbf{x}'. \quad (2.50)$$

The first four terms (2.46 - 2.49) all come from inversion of the Laplacian on  $-\partial h_0/\partial t$ , using (2.43) to first obtain an expression for  $-\partial h_0/\partial t$ . The last term (2.50) comes from inversion of the Laplacian on  $-\nabla \cdot (h_0 \mathbf{u}_0)$ . However,  $h_0 \mathbf{u}_0 = O((\ln r)/r)$ , and it is not immediately clear that the Laplacian can be inverted via an integral expression such as (2.50). Using expression (2.45) makes it clear that the integrand in (2.50) is of order  $O(r^{-4})$  as  $r \rightarrow \infty$ , and hence the integral converges.

The solution to (2.41) for  $\psi_2$  can also be written down as an integral expression:

$$\psi_2 = - \frac{1}{4} f \psi_0^2 \quad (2.51)$$

$$+ \frac{1}{2\pi} \int Q_2 + \zeta_0 \left( h_0 + \frac{1}{2} f \psi_0 \right) \ln |\mathbf{x} - \mathbf{x}'| d^2 \mathbf{x}' \quad (2.52)$$

$$+ \frac{1}{8\pi} f^2 \int \zeta_0 |\mathbf{x} - \mathbf{x}'|^2 (\ln |\mathbf{x} - \mathbf{x}'| - 1) d^2 \mathbf{x}' \quad (2.53)$$

$$+ \frac{1}{8\pi} f \int \nabla \cdot (\zeta_0 \nabla \psi_0) |\mathbf{x} - \mathbf{x}'|^2 (\ln |\mathbf{x} - \mathbf{x}'| - 1) d^2 \mathbf{x}'. \quad (2.54)$$

We must now obtain the far field expansions of these expressions for  $\phi_2$  and  $\psi_2$ .

Consider first the far field form of  $\phi_2$  (2.46-2.50). We shall consider the far field form of each of expressions (2.46-2.50) in turn.

Starting with (2.46), we have

$$\frac{\partial}{\partial t} \int \zeta_0 |\mathbf{x} - \mathbf{x}'|^2 (\ln |\mathbf{x} - \mathbf{x}'| - 1) d^2 \mathbf{x}' = |\mathbf{x}|^2 (\ln |\mathbf{x}| - 1) \frac{d}{dt} \int \zeta_0 d^2 \mathbf{x}' \quad (2.55)$$

$$+ \frac{\partial}{\partial x_i} (|\mathbf{x}|^2 (\ln |\mathbf{x}| - 1)) \frac{d}{dt} \int x'_i \zeta_0 d^2 \mathbf{x}' \quad (2.56)$$

$$+ \frac{1}{2} \frac{\partial^2}{\partial x_i \partial x_j} (|\mathbf{x}|^2 (\ln |\mathbf{x}| - 1)) \frac{d}{dt} \int x'_i x'_j \zeta_0 d^2 \mathbf{x}' \quad (2.57)$$

$$+ O(r^{-1} \ln r). \quad (2.58)$$

Now, since

$$\frac{d}{dt} \int \zeta_0 d^2 \mathbf{x}' = 0 \quad (2.59)$$

by conservation of circulation, and

$$\frac{d}{dt} \int x'_i \zeta_0 d^2 \mathbf{x}' = 0 \quad (2.60)$$

by conservation of Kelvin's impulse, it follows that

$$\frac{\partial}{\partial t} \int \zeta_0 |\mathbf{x} - \mathbf{x}'|^2 (\ln |\mathbf{x} - \mathbf{x}'| - 1) d^2 \mathbf{x}' = \frac{1}{2} \frac{\partial^2}{\partial x_i \partial x_j} (|\mathbf{x}|^2 (\ln |\mathbf{x}| - 1)) \frac{\partial}{\partial t} \int x'_i x'_j \zeta_0 d^2 \mathbf{x}' \quad (2.61)$$

$$+ O(r^{-1} \ln r). \quad (2.62)$$

We can now show that (2.46) does not contribute a monopolar source term. We start by noting that

$$\frac{d}{dt} \int (x'^2 + y'^2) \zeta_0 d^2 \mathbf{x}' = 0. \quad (2.63)$$

It then follows that the tensor integral in (2.61) is traceless. The  $O(1)$  far field component of (2.61) therefore corresponds to the higher order in Froude number matching conditions for the quadrupolar wave field, but contributes no further monopolar wave field of its own.

Continuing to analyse (2.47), it follows from conservation of energy in the source region on the timescale of the vortex dynamics that

$$\frac{d}{dt} \int \zeta_0 \psi_0 d^2 \mathbf{x}' = 0. \quad (2.64)$$

Expanding the logarithm and substituting, it follows that the far field of (2.47) is  $O(r^{-1})$ .

Since  $\psi_0 \sim \ln r$ , and  $\partial\psi_0/\partial t \sim r^{-2}$ , it follows that (2.48) is  $O(r^{-2} \ln r)$  in the far field, so we need not consider it further.

For (2.49), it follows again from conservation of Kelvin's impulse that

$$\begin{aligned} \frac{\partial}{\partial t} \int \nabla \cdot (\zeta_0 \nabla \psi_0) |\mathbf{x} - \mathbf{x}'|^2 (\ln |\mathbf{x} - \mathbf{x}'| - 1) d^2 \mathbf{x}' = \\ \frac{1}{2} \frac{\partial^2}{\partial x_i \partial x_j} (|\mathbf{x}|^2 (\ln |\mathbf{x}| - 1)) \frac{\partial}{\partial t} \int x'_i \zeta_0 \frac{\partial \psi_0}{\partial x'_j} d^2 \mathbf{x}' \\ + O(r^{-1} \ln r) \end{aligned} \quad (2.65)$$

Like (2.46), this also has a fluctuating far field at  $O(1)$ , but also like (2.46), we can show that the trace of the tensor integral is zero, and therefore this too corresponds only to higher order matching for the quadrupolar waves, and does not introduce a monopole either.

To see this, note that the trace of (2.65) is proportional to  $\int (xv_0 - yu_0)$ . One can see that this is zero from conservation of  $\int (x^2 + y^2) \zeta_0$ , and therefore we can conclude that (2.49) has only  $e^{2i\theta}$  behaviour at  $O(1)$  in the far field. Consequently, (2.49) does not contribute a monopole in the far field.

Finally we consider (2.50). If we proceed by expanding the logarithm and integrating by parts, as before, the first term we obtain is

$$\int \nabla \cdot ((h_0 - f\psi_0) \mathbf{u}_0) \ln |\mathbf{x} - \mathbf{x}'| d^2 \mathbf{x}' = \frac{\mathbf{x}}{|\mathbf{x}|^2} \cdot \int (h_0 - f\psi_0) \mathbf{u}_0 d^2 \mathbf{x}'. \quad (2.66)$$

However, we should note that, unlike the other integrals for which far field expressions have been obtained, the integrand here is not of compact support, and is of order  $O(r^{-3})$  as  $r \rightarrow \infty$ . At the next order in the expansion of the logarithm, a factor  $x'$  is introduced into the integrand, making the integral non-convergent. It follows that the order of the remainder in this case cannot be determined from subsequent terms in the asymptotic expansion of the logarithm, and extensive analysis is required to show that the order of the remainder is  $(r^{-2} \ln r)$ , thus confirming that (2.50) is of order  $O(r^{-1})$  for large  $r$ , and therefore does not contribute a monopole to the wave field. The analysis to show that the order of the remainder in (2.66) is  $r^{-2} \ln r$  is presented in Appendix A.

We turn now to examining the far field of  $\psi_2$ .

Two of the four integrals in the representation of  $\psi_2$  have counterparts in the representation of  $\phi_2$ . They are (2.53), which is the counterpart of (2.46), and (2.54), which is the counterpart of (2.49). The only difference between (2.46) and (2.53) is a factor of  $f^{-1}\partial/\partial t$ . This is also the difference between (2.49) and (2.54). It follows from the analyses presented for (2.46) and (2.49) that neither (2.53) nor (2.54) can have time dependent monopoles in their far fields, although both terms do contain components of the time dependent quadrupole.

To show that (2.51) does not have a time dependent monopolar far field, we recall that although  $\psi_0 = O(\ln r)$  for large  $r$ ,  $\psi_{0t} = O(r^{-2})$ . Therefore, the time dependent part far field of (2.51) is of order  $O(r^{-2} \ln r)$ , and hence does not constitute a time dependent monopole.

To show that (2.52) does not have a time dependent monopolar far field, we first recall that  $\int \zeta_0 \psi_0$  is independent of time, and therefore we need only consider the term

$$\frac{1}{2\pi} \ln r \int Q_2 + \zeta_0 h_0. \quad (2.67)$$

However, it is simply the  $O(F^2)$  contribution to the circulation. Since conservation of circulation is true of a general shallow water system, and does not rely on any small Froude number limit, it should be independent of time at all orders. To show that (2.67) is independent of time, we note that

$$\frac{\partial \zeta_0}{\partial t} = -\nabla \cdot (\mathbf{u}_0 \zeta_0); \quad \frac{\partial h_0}{\partial t} = -\nabla \cdot (\mathbf{u}_0 h_0 + \mathbf{u}_2). \quad (2.68)$$

Hence

$$\frac{\partial}{\partial t} (\zeta_0 h_0) = -\nabla \cdot (\zeta_0 h_0 \mathbf{u}_0) - \zeta_0 \nabla \cdot \mathbf{u}_2. \quad (2.69)$$

Moreover, if we also recall that

$$\frac{\partial Q_2}{\partial t} + \frac{\partial \zeta_0}{\partial T} = -\mathbf{u}_0 \cdot \nabla Q_2 - \mathbf{u}_2 \cdot \nabla Q_0, \quad (2.70)$$

we obtain

$$\frac{d}{dt} (Q_2 + \zeta_0 h_0) = -\nabla \cdot (\mathbf{u}_0 Q_2 + h_0 \zeta_0 \mathbf{u}_0 + \zeta_0 \mathbf{u}_2) - \frac{\partial \zeta_0}{\partial T}. \quad (2.71)$$

It follows that

$$\frac{d}{dt} \int Q_2 + \zeta_0 h_0 = -\frac{d}{dT} \int \zeta_0 - \int (\mathbf{u}_0 Q_2 + \zeta_0 \mathbf{u}_2 + \zeta_0 h_0 \mathbf{u}_0) \cdot d\mathbf{s}. \quad (2.72)$$

Now since  $\zeta_0$  vanishes outside some finite region, the boundary integral on the right hand side of (2.72) vanishes. Then, since  $\int \zeta_0$  is independent of  $t$ , it follows that (2.52) does not have a time dependent far field at  $O(1)$  in  $r$  for large  $r$ .

To obtain an integral representation for  $h_2$ , we expand (2.34) at order  $F^2$  to obtain

$$\nabla^2 \left( B_2 + \frac{\partial \phi_2}{\partial t} - f\psi_2 - \frac{1}{2}f^2\psi_0^2 \right) = \nabla \cdot (h_0\zeta_0\nabla\psi_0 + (h_0 - f\psi_0)\nabla\psi_0 - \zeta_0(\mathbf{k} \times \mathbf{u}_2)). \quad (2.73)$$

Now  $\phi_2$  and  $\psi_2$  have already been shown to contribute only quadrupoles. It is straightforward to show that the right hand side contributes a dipole only (in an analysis similar to that given for (2.50) in appendix A). Therefore  $B_2$ , and hence  $h_2$ , are also quadrupole at leading order in the far field. This is reassuring, since gravity waves involve perturbations in both velocity and height fields, and it should not have been possible to have a monopole in  $h_2$  without a corresponding monopole in at least one of  $\psi_2$  or  $\phi_2$ .

### 2.2.2 Dynamics of the wave zone resulting from the vortical flow

Considering the orders of the unsteady terms in the limit  $r \rightarrow \infty$  in the vortical flow, we have terms of orders  $1 \times r^{-2}$  and  $F^2 \times 1$ , reminding us that the expansion becomes disordered when  $r \sim F^{-1}$ . To obtain the dynamics of the wave zone, we must rescale the equations using the long length scale  $F^{-1}$  corresponding to the wavelength of gravity waves. We therefore introduce the wave region spatial variable  $\mathbf{X}$ , defined such that  $\mathbf{X} = F\mathbf{x}$ . Rescaling the equations, we obtain

$$\begin{aligned} \frac{\partial}{\partial t}(\nabla\phi + \mathbf{k} \times \nabla\psi) + (f + \zeta)\mathbf{k} \times (\nabla\phi + \mathbf{k} \times \nabla\psi) + \nabla h \\ + \frac{1}{2}F^2\nabla(\nabla\phi + \mathbf{k} \times \nabla\psi)^2 = 0 \end{aligned} \quad (2.74)$$

$$\frac{\partial h}{\partial t} + \nabla^2\phi + F^2\nabla \cdot ((\nabla\phi + \mathbf{k} \times \nabla\psi)h) = 0, \quad (2.75)$$

where now  $\nabla$  represents  $\partial/\partial\mathbf{X}$ . These equations admit propagating gravity waves as solutions. In the wave region it is the nonlinear terms, rather than the divergence terms, which are of small order in the limit of small Froude number.

We now proceed to the details of matching the asymptotic expansions in the source region and the wave zone together. We start by expanding  $\psi$ ,  $\phi$  and  $h$  in asymptotic series in  $F$ :

$$\psi = \psi_0 + F\psi_1 + F^2\psi_2 + \dots \quad (2.76)$$

$$\phi = \phi_0 + F\phi_1 + F^2\phi_2 + \dots \quad (2.77)$$

$$h = h_0 + Fh_1 + F^2h_2 + \dots \quad (2.78)$$

Firstly, since, for the vortical region,  $\psi_0$  and  $h_0$  are independent of  $t$  at orders 1 and  $r^{-1}$  in their far field limits, it is sufficient in the expansion in the wave zone to take  $\psi_0, \psi_1, h_0$  and  $h_1$  to be independent of  $t$ , and to take  $\phi_0 = \phi_1 = 0$ . Thus, in the wave zone,

$$\{h_0, h_1\} = f\{\psi_0, \psi_1\} \quad (2.79)$$

$$(\nabla^2 - f^2)\{\psi_0, \psi_1\} = 0, \quad (2.80)$$

and it follows from applying decaying boundary conditions at infinity that

$$\psi_0 = C_0 K_0(|f|R) \quad (2.81)$$

$$\psi_1 = C_1 K_1(|f|R). \quad (2.82)$$

The values of the constants  $C_0$  and  $C_1$  are determined by matching conditions onto the source scale flow in the limit  $R \rightarrow 0$ .

The expansion of  $K_0(|f|R)$  for small  $R$  implies that constant corrections to  $h$  will be required at  $O(1)$  and  $O(\ln F)$ , which will in turn affect the velocity field at  $O(F^2)$  and  $O(F^2 \ln F)$ . Since these are time-independent terms, we shall not discuss them further here. We shall return to them in §2.4, where the complete solution to  $O(F^2)$  is obtained for the model problem of the Kirchoff ellipse (Lamb, 1932).

At the next two orders ( $O(F^2)$  and  $O(F^3)$ ) in the wave zone, it is convenient to separate the fields into two parts: one part which is independent of  $t$ , and one part which is oscillatory in  $t$ . Taking, for example,  $\psi_2$ , we use  $\hat{\psi}_2$  to represent the part which is independent of  $t$ , and  $\tilde{\psi}_2$  to represent the oscillatory part. For the  $t$ -independent parts, we obtain from (2.74) at  $O(F^2)$ :

$$(\nabla^2 - f^2)\hat{\psi}_2 = -\frac{1}{2}f|\nabla\psi_0|^2 + \frac{1}{2}f^3\psi_0^2. \quad (2.83)$$

A similar equation can be obtained for  $\hat{\psi}_3$ . Again, the boundary conditions on these equations are decaying at infinity, and matching conditions onto the source flow as  $|\mathbf{X}| \rightarrow 0$ .

For the oscillatory parts, we then have

$$\left(\frac{\partial^2}{\partial t^2} + f^2 - \nabla^2\right) \{\tilde{\phi}_2, \tilde{\psi}_2, \tilde{h}_2, \tilde{\phi}_3, \tilde{\psi}_3, \tilde{h}_3\} = 0, \quad (2.84)$$

with

$$\frac{\partial}{\partial t} \{\tilde{\psi}_2, \tilde{\psi}_3\} + f \{\tilde{\phi}_2, \tilde{\phi}_3\} = 0. \quad (2.85)$$

Here, the boundary conditions which we shall impose are a radiation condition at infinity, and matching onto the source flow as  $|\mathbf{X}| \rightarrow 0$ . When matching  $\tilde{\phi}_2$  and  $\tilde{\phi}_3$  onto the vortical region, we do not match  $\phi$  and  $\psi$  individually, because the decomposition of the velocity field into streamfunction  $\psi$  and velocity potential  $\phi$  is non-unique. In the vortical region, the leading order far field quadrupole comes about directly as a result of incompressible flow, and in the previous section we chose to represent that flow using only a streamfunction. Therefore, its far field does not satisfy the condition (2.85). However, since the vorticity is confined to a finite area of the vortical region, the flow is both incompressible and irrotational in the limit  $r \rightarrow \infty$ , and hence we are free to represent it far from the vortex using either a streamfunction or a velocity potential, or any combination of the two, including a combination which satisfies the constraint (2.85).

It is convenient to work in frequency space for the details of wave matching, in which the general solutions of (2.84) are the Hankel functions

$$H_m^{(\cdot)} \left( \sqrt{\omega^2 - f^2} R \right) e^{im\theta}, \quad (2.86)$$

where  $m$  is the order, determined by the required  $\theta$  dependence of the match on to the source flow;  $(\cdot) = 1, 2$  is the type, determined by the radiation condition; and  $R = |\mathbf{X}|$  as before. The order  $m = 0$  corresponds to a monopole wave,  $m = 1$  a dipole,  $m = 2$  a quadrupole, and so on. Normally the Hankel functions  $H_m^{(1,2)}$  are defined to be  $J_m \pm iY_m$ , where  $J$  and  $Y$  are Bessel and associated Bessel functions respectively (Abramowitz & Stegun, 1965). For convenience in the present analysis, we shall multiply  $H$  by  $\pm i$ , so that in our case  $H_m^{(1,2)} = -Y_m \pm iJ_m$ . Throughout, we shall represent the Fourier transform of a function  $f(t)$  by  $\tilde{f}(\omega)$ , where

$$\tilde{f}(\omega) = \int_{-\infty}^{\infty} f(t) e^{i\omega t} dt. \quad (2.87)$$

Now, the time-dependent far field form of  $\psi_0$  in the vortical region, given in (2.30), may be taken as

$$\psi_0 \sim \frac{4\alpha(t)}{\pi r^2} e^{2i\theta}. \quad (2.88)$$

Therefore, the outer limit of the inner expansion for  $\psi$  takes the form  $r^{-2}e^{2i\theta}$ . To satisfy the matching conditions for the wave fields at  $O(F^2)$ , we will require them to have  $2\theta$  angular dependence. Hence we choose mode  $m = 2$  and write the general solution for the  $O(F^2)$  wave fields in frequency space:

$$\tilde{\phi}_2 = A(\omega)(\omega^2 - f^2)H_2^{(1)}\left(\sqrt{\omega^2 - f^2}R\right)e^{2i\theta} \quad (2.89)$$

$$\tilde{\psi}_2 = B(\omega)(\omega^2 - f^2)H_2^{(1)}\left(\sqrt{\omega^2 - f^2}R\right)e^{2i\theta} \quad (2.90)$$

$$\tilde{h}_2 = C(\omega)(\omega^2 - f^2)H_2^{(1)}\left(\sqrt{\omega^2 - f^2}R\right)e^{2i\theta}. \quad (2.91)$$

One matches the velocity  $\nabla\phi + \mathbf{k} \times \nabla\psi$  and the height field  $h$  to get

$$A = \frac{f\tilde{\alpha}}{\omega + f}; \quad B = \frac{i\omega\tilde{\alpha}}{\omega + f}; \quad C = (\omega - f)\tilde{\alpha}, \quad (2.92)$$

where  $\tilde{\alpha}(\omega)$  is the Fourier transform of  $\alpha(t)$ , defined by (2.87).

Since we have shown that there are no  $O(F^2)$  monopoles in the source region, this is the complete representation of the leading order (i.e.  $O(F^2)$ ) wave field. Thus we have confirmed that the principal radiation is quadrupole. In general, the  $O(F^3)$  wave field will be composed of a dipole and an octupole.

### 2.2.3 The effect of wave radiation on the vortical flow

We have now determined the principal wave radiation in terms of integrals over the vortex. These integrals can be regarded as known functions of time. At any time, they can be determined by knowing only the potential vorticity distribution at that time.

We turn now to considering the “back-reaction” problem. That is, we calculate the effect of the radiation on the flow which is generating it. This consists in matching the wave solution back onto the source flow. To do this, we must consider the expansion of the Hankel function in the limit  $R \rightarrow 0$ :

$$\pi(\omega^2 - f^2)H_2^{(1)}(\sqrt{\omega^2 - f^2}R) = \frac{4}{R^2} \quad (2.93)$$

$$+ (\omega^2 - f^2) \quad (2.94)$$

$$- \frac{1}{4}(\omega^2 - f^2)^2 R^2 \ln \left( \frac{1}{2} \sqrt{\omega^2 - f^2} R \right) \quad (2.95)$$

$$+ \frac{1}{8}(\omega^2 - f^2)^2 (\psi(1) + \psi(3)) R^2 \quad (2.96)$$

$$\pm i\pi \frac{1}{8}(\omega^2 - f^2)^2 R^2 \quad (2.97)$$

$$+ O(R^4 \ln R),$$

where  $\psi(\cdot)$  is the logarithmic derivative of the  $\Gamma$  function (Abramowitz & Stegun, 1965, p.258).

Expanding this in the source scale variables we get

$$F^2 \pi(\omega^2 - f^2) H_2^{(\cdot)}(\sqrt{\omega^2 - f^2} R) = \frac{4}{r^2} \quad (2.98)$$

$$+ F^2(\omega^2 - f^2) \quad (2.99)$$

$$- F^4 \ln F \frac{1}{4}(\omega^2 - f^2)^2 r^2 \quad (2.100)$$

$$+ F^4 \frac{1}{4}(\omega^2 - f^2)^2 r^2 \left( \ln 2 - \ln(\sqrt{(\omega^2 - f^2)} r) \right) \quad (2.101)$$

$$+ F^4 \frac{1}{8}(\omega^2 - f^2)^2 \left( \frac{3}{2} - 2\gamma \right) r^2 \quad (2.102)$$

$$\pm i\pi \frac{F^4}{8}(\omega^2 - f^2)^2 r^2 \quad (2.103)$$

$$+ O(F^4 \ln F),$$

where  $\gamma \approx 0.5772$  is Euler's constant.

At this point, any attempt to separate the matching procedure into terms which are “due to the radiation” and “other terms” might seem somewhat arbitrary. For a start, there is the term (2.100) of order  $F^4 \ln F$ , which could certainly not have been predicted from considering the expansion for the source flow alone. However, it has none of the features that we would expect of a term due to the radiation. In particular, it is independent of the sign of  $\pm$  in (2.103) taken to satisfy the radiation condition! The only term which actually depends on application of the radiation condition is (2.103). However, one can see that, when we take the convolution with  $\tilde{\alpha}(\omega)$  to invert the Fourier transform, we recover an integral which depends on both past and future values of  $\alpha(t)$ , which appears to violate the radiation condition. Thus it seems misleading to regard term (2.103) alone as representing the effect of radiation on the source. Instead, we

amalgamate the  $\ln(\omega^2 - f^2)$  term in (2.101) with (2.103) and the  $\gamma$  term from (2.102) to give

$$- F^4(\omega^2 - f^2)^2 r^2 \left( \frac{1}{8} (\ln(\omega^2 - f^2)r + 2\gamma) \mp \frac{i\pi}{8} \right) \tilde{\sigma}(\omega), \quad (2.104)$$

where  $\tilde{\sigma}$  is the Fourier transform of a source function. For the present analysis,  $\tilde{\sigma}$  is  $A(\omega)$ ,  $B(\omega)$  or  $C(\omega)$ , where  $A$ ,  $B$  and  $C$  are given by (2.92), depending on whether we are considering the matching conditions for  $\phi$ ,  $\psi$  or  $h$ , respectively. When (2.104) is converted back into the time domain, we recover an integral in the matching condition which depends only on the past history of the dynamics:

$$r^2 \int_0^\infty \ln \tau [\cos(f\tau)g(t - \tau)]_\tau d\tau, \quad (2.105)$$

where  $g(t)$  is the inverse Fourier transform of  $\tilde{g}(\omega) \equiv (\omega^2 - f^2)^2 \tilde{\sigma}(\omega)/16$  (the details are given in appendix B). A term (2.105)  $\times e^{2i\theta}$  is thus required in  $\phi$ ,  $\psi$  and  $h$ , in the vortical region, at order  $O(F^4)$ . The exact form of  $g$  depends, of course, on whether we are performing the match for  $\phi$ ,  $\psi$  or  $h$ . The important point is that, since  $\tilde{\sigma}$  is related to  $\tilde{\alpha}$  through (2.92), with  $\sigma = A, B$ , or  $C$ ,  $g(t)$  may be expressed as a sum of instantaneous time derivatives of  $\alpha(t)$  defined by (2.88), and is therefore a known function of the dynamics of the vortex region. The choice of  $\mp$  in (2.104), required to obtain an integral (2.105) over the past history only, and not involving the future evolution, can be shown to be equivalent to requiring an outgoing wave form for  $H_2^{(\cdot)}$  as  $R \rightarrow \infty$ .

We further remark that  $O(F^3)$  dipoles in the wave zone also give rise to non-local time integrals at  $O(F^4)$  in the source region. In this case the flow induced in the source region is a uniform velocity which has no effect on the energy of the source at leading order, although it must be retained if the  $O(F^6)$  and  $O(F^6 \ln F)$  flows in the source are to be computed.

### 2.3 Implications for balance and potential vorticity inversion

The foregoing study was motivated by a desire to understand the fundamental limitations of the concept of balanced dynamics. We shall now discuss this concept in the context of the isolated low Froude number vortex which we have studied here.

At  $O(1)$ , the dynamics are just two-dimensional incompressible vortex dynamics. This clearly does not depend on any knowledge of the past history of the flow in the vortex region, or of the gravity wave field, and so the dynamics are balanced in the sense that the instantaneous

potential vorticity field is sufficient to determine the velocity and height fields, and hence to integrate the equations of motion by advecting the potential vorticity field.

At  $O(F^2 \ln F)$ , there is a non-uniform correction to the vorticity of the vortical region as a result of the matching conditions. Although it arises as a result of the matching conditions between the vortical region and the wave region, it is independent of time. It can therefore be obtained from instantaneous fields, and should be regarded as a balanced correction to the vortical dynamics.

At  $O(F^2)$ , the corrections to the dynamics are expressible entirely in terms of inversions of the Laplacian on the  $O(1)$  fields and further time-independent terms introduced by the asymptotic matching conditions. At this order, still no knowledge of the gravity wave field or of the past history of the vortex dynamics is required. This means that we can think of corrections at this order as balanced corrections to the dynamics, which represent the effects of local divergence, but not of gravity wave generation.

However, at  $O(F^4)$ , terms arise which come about as a result of matching to the wave zone, which are non-local in time, and which depend on the gravity wave radiation condition. We should note, however, that the integral (2.105) is not strictly an integral over the past history of an actual flow. The source term  $g(t - \tau)$  in the integral is to be regarded as a term  $g(t - \tau, T_2, T_4, \dots)$  in which only the shortest time variable  $t$  is allowed to vary, and all other time variables are kept fixed. Formally we regard the integral as bounded because, implicit in our scaling analysis, we have assumed that terms associated with two-dimensional vortex dynamics remain bounded as the integration proceeds for arbitrarily long times. In reality this may be true only for a very small number of vorticity distributions, such as the solutions presented by Abrashkin and Yakubovich (1984).

Interestingly, then, this integral can be computed, in principle, by knowing only the instantaneous potential vorticity, and then integrating the two-dimensional incompressible vortex dynamics equations backwards in time. One might be tempted to think that we could therefore regard this correction as known in terms of the potential vorticity evolution, and therefore part of the balanced dynamics. However, it is then not clear how far back into the past they should be integrated. If we assume that the disturbance is turned on at some time  $t_0$  then, for consistency, we would have to integrate back to time  $t_0$ . We would then expect (2.105) to be sensitive to the value of  $t_0$  chosen. In the standard situation we are given *no* information about

the past history of the flow: we are given a potential vorticity distribution and nothing else. The choice of  $t_0$  then becomes entirely arbitrary, and we cannot satisfactorily say that we have evaluated (2.105).

If we were to try to integrate (2.105) back to  $\tau = -\infty$ , then there is no reason to expect the integral to converge, even if it remains bounded. One might be slightly worried by this, since it is the result of inverting an apparently well-behaved Fourier transform. Formally one should say that the integral (2.105) is defined by its Cauchy Principal Value, so that  $\int_0^\infty \ln \tau \cos \Omega \tau d\tau$  is given by the corresponding Fourier Transform (2.104), with  $\omega \equiv \Omega$  and  $\tilde{\sigma} \equiv 1$ .

Another interesting feature is the logarithmic kernel, which means that contributions to (2.105) are significant for times arbitrarily far into the past. This may seem surprising because one would expect activity in the source region not to continue to affect the source region at the same strength long after the waves have propagated away. If  $g$  is truly of compact support, then we can integrate (2.105) once by parts to obtain

$$\int_{t-a}^{t-b} \tau^{-1} \cos(f\tau) g(t-\tau) d\tau, \quad (2.106)$$

where  $a$  and  $b$  are the limits of the range over which  $g$  is non-zero. It follows that if  $g$  is bounded then the importance of its contribution to the back reaction decays as  $t^{-1}$  for large  $t$ . However, we cannot dispense with past history in this manner unless we know that  $g$  is zero for all times before some initial time  $t_0$ . This is because although the individual impact of finite time sources decays as  $t^{-1}$ , there are in principle an infinite number of such sources.

Finally, we should note that the “radiation term” (2.104) is non-vanishing even when all the frequencies in  $\tilde{\sigma}(\omega)$  lie below the inertial frequency  $f$  in magnitude. This corresponds to the case where all the gravity waves are evanescent. Therefore, they do not transport energy to infinity, and we would not wish to refer to this term as the effect of radiation in this context. However, we can see that in the case where  $|\omega| < |f|$ , we can obtain an expression for (2.104) which requires only instantaneous time derivatives of  $\alpha(t)$  at the current time to be known. If  $|\omega| < f$  we may write

$$-F^4 \pi (\omega^2 - f^2)^2 r^2 \left( \frac{1}{8\pi} \left( \ln(f^2 - \omega^2) r + i \arg(\omega^2 - f^2) + 2\gamma \right) \mp i \frac{1}{8} \right) \tilde{\sigma}(\omega). \quad (2.107)$$

Then, selecting the sign  $\mp$  appropriately, according to whether we take  $\arg(-1)$  as  $\pm\pi$ , we

are left with the so-called radiation term expressed as

$$\frac{1}{8}F^4(f^2 - \omega^2)^2 r^2 \left( \ln(f^2 - \omega^2)r + 2\gamma \right) \tilde{\sigma}(\omega). \quad (2.108)$$

The selection of the  $\mp$  here is equivalent to an evanescence boundary condition in the wave far field.

The logarithmic term  $\ln(f^2 - \omega^2)$  can now be expanded as

$$\ln(f^2 - \omega^2) = \ln f^2 + \ln(1 - \omega^2/f^2) = 2 \ln f - \omega^2/f^2 + \omega^4/2f^4 - \omega^6/3f^6 + \dots, \quad (2.109)$$

i.e.  $2 \ln f$  plus a convergent Taylor series in which only integer powers of  $\omega$  appear. The recovery of only integral powers of  $\omega$  implies that we need only find the inverse Fourier transform of  $\tilde{\sigma}(\omega)$  multiplied by integral powers of  $\omega$ , and hence only instantaneous time derivatives of  $\alpha(t)$  are required: no integral over the past history of evolution, such as (2.105), need be evaluated.

Technically, any finite truncation of this expansion defines a balanced model for the single compact vortex. One could perhaps argue that, in a source whose frequencies lie largely, but not entirely, below the inertial frequency, taking a few terms in the expansion of  $\ln(f^2 - \omega^2)$  might lead to a general improvement to the  $O(F^4)$  dynamics, even though the series would ultimately diverge. This sort of behaviour is qualitatively familiar from the studies of Norton (1988) and McIntyre & Norton (1993), where a hierarchy of balanced models produces successively better approximations to shallow water dynamics at the first few orders, but ultimately fails to converge.

The notions discussed above have some bearing on the concept of “superbalance”, as proposed by J. J. Tribbia (personal communication). In a “superbalance”, one is supposed to diagnose all the past history of gravity wave radiation consistent with the given potential vorticity distribution. “Superbalance” might therefore be regarded as a gravity wave minimization, and as such deserves some consideration.

Tribbia has proposed the following scheme:

- Choose height and velocity fields consistent with the current PV distribution
- Integrate backwards in time (in principle to  $t = -\infty$ )
- Compute a time-integrated measure of total gravity wave activity

- Iterate the height and velocity fields at  $t = 0$  (subject to the prescribed PV field) to minimise the integrated gravity wave activity

In a sense, we might regard the flow given by the low Froude number matched asymptotic analysis as precisely the flow which minimises the total gravity wave activity, since we include only that gravity wave field which is essential for an asymptotic match onto the vortex dynamics. If so, then the foregoing analysis gives some idea of the characteristics which supposed superinversion operators are likely to possess. In particular, it suggests (a) that they are unlikely to converge unless some “initial instant” is assumed for the model, before which there is assumed to be no gravity wave activity, and (b) that the superinversion operator will in general be sensitive (at  $O(F^4)$ ) to the choice of initial instant.

## 2.4 The effect of gravity wave radiation upon a rotating elliptical patch of uniform potential vorticity – an explicit example of generalized adjustment

In a pioneering paper, Broadbent & Moore (1979) investigated the stability of a Rankine vortex to two-dimensional perturbations. A Rankine vortex is an axisymmetric vortical column, with uniform vorticity within the column and zero vorticity without. In the low Mach number limit, therefore, the Rankine vortex corresponds to a vortex of uniform potential vorticity. They showed numerically that disturbances with axial mode numbers of two, three, four and six were unstable over a wide range of Mach numbers, and obtained an expression for the growth rate of the mode two instability at low Mach number by a matched asymptotic analysis.

Subsequently, Kop’ev & Leont’ev (1983) argued that the expression for the growth rate at low Mach number which was obtained by Broadbent & Moore (1979) could also be derived from energetic arguments, which made it possible to obtain growth rates for higher axial modes without significantly greater effort. Their analysis depends on assuming that the boundary perturbations are of small amplitude, of the form  $e^{im\theta}$ .

Recently, Zeitlin (1988, 1991) has suggested that the energetic arguments of Kop’ev & Leont’ev (1983) could be applied to flows with nonlinear departures from axisymmetry. He used these arguments to predict the way in which a class of exact solutions to the two-dimensional Euler equations found by Abrashkin & Yakubovich (1984) would respond to acoustic wave

radiation.

The Abrashkin & Yakubovich flows are categorized according to their degree of rotational symmetry, and the simplest class, with two-fold rotational symmetry, corresponds to the rotating ellipse of uniform vorticity found by Lamb (1932).

The analysis of Zeitlin (1988, 1991) assumed that the Abrashkin & Yakubovich flows adjusted to take account of gravity wave radiation simply by evolving to another such flow with the same degree of rotational symmetry and the same circulation but with less energy. For a rotating ellipse, this corresponds to increasing the aspect ratio of the ellipse while keeping its area constant. Most significantly, it implicitly assumes that, to a first approximation at least, the ellipse remains elliptical as it adjusts to the effect of gravity wave radiation.

Zeitlin's analysis might be regarded as unsatisfactory, however, since nothing is done to check that ellipses will simply elongate without significant change of form. The purpose of this section is to investigate the evolution of the rotating ellipse by a matched asymptotic analysis, thus enabling us to obtain the significant characteristics of the flow at every order in Froude number up to the order at which the vortical flow loses energy in response to gravity wave radiation. The present analysis is therefore able to investigate the validity of Zeitlin's assumption that the ellipse remains elliptical.

### 2.4.1 Evolution of the vortex boundary

A compact description of the rotating elliptical vortex requires construction of an "elliptical" coordinate system in order to describe the flow outside the vortex by means of elementary functions.

It is convenient to work in the complex plane, in which  $z = x + iy$ , where  $x$  and  $y$  are cartesian coordinates in physical space. One can then define elliptical coordinates  $\xi$  and  $\eta$ , via a new complex variable  $w = \xi + i\eta$ , such that  $z = c \cosh w$ . In  $w$ -space, the azimuthal coordinate  $\eta$  runs from 0 to  $2\pi$ , and the ellipse in  $z$ -space lies within the region  $0 < \xi < 1$  in  $w$ -space. For an ellipse with semi-major axis  $a$  and semi-minor axis  $b$ , Lamb (1932) showed that  $c$  is given by

$$c = (a^2 + b^2)^{1/2}. \quad (2.110)$$

An alternative description, which appears to be more readily generalizable in the present

context, is to work in  $\ln w$ -space, to which we assign the complex variable  $\zeta$ . In the following analysis, we use a conformal mapping from  $z$ -space to  $\zeta$ -space such that the ellipse in  $z$ -space is mapped onto the unit disc  $|\zeta| < 1$  in  $\zeta$ -space.

Recently, Legras & Zeitlin (1992) have used this formalism to develop the elliptical moment model of Legras & Dritschel (1991), Dritschel & Legras (1991). They begin by postulating a conformal mapping  $f(\zeta)$  from the exterior of the unit disk in the  $\zeta$ -plane to the exterior of a simply connected area in the  $z$ -plane, given by

$$f(\zeta) = \Gamma\zeta + \frac{\nu}{\zeta} + \sum_{i=3}^{\infty} \frac{\mu_i}{\zeta^i}. \quad (2.111)$$

Without loss of generality,  $\Gamma$  is taken to be real throughout. They were interested in the interaction between a number of different ellipses in two dimensional incompressible flow, in which the shape of each ellipse was represented in the form (2.111). The essence of their approach was that the evolution of the ellipses could be described by obtaining evolution equations for  $\nu$  and the  $\mu_i$  for each ellipse. They developed their so-called elliptical moment model by assuming that the  $\mu_i$  were small, and so neglecting nonlinear products of the  $\mu_i$  in the derivation of the evolution equations.

To obtain the evolution equations for the coefficients of the conformal map, it is convenient to consider the Lagrangian time derivative of  $z$ .

We start from the statement

$$\dot{z} \equiv \frac{Dz}{Dt} = u + iv \quad (2.112)$$

and convert this via (2.111) into its equivalent statement in the  $\zeta$ -plane

$$\frac{Df}{Dt} \equiv \frac{\partial f}{\partial t} + \frac{\partial f}{\partial \zeta} \dot{\zeta} = u + iv. \quad (2.113)$$

Rearranging (2.113), we obtain

$$\frac{\dot{\zeta}}{\zeta} + \frac{1}{\zeta} \frac{\partial f}{\partial \zeta} \frac{\partial f}{\partial t} = \frac{u + iv}{\zeta \frac{\partial f}{\partial \zeta}}. \quad (2.114)$$

Now, since the elliptical vortex boundary is a material line in  $z$ -space, so it must also be a material line in  $\zeta$ -space. Recalling that in  $\zeta$ -space the vortex boundary is the unit circle, particle velocities on  $|\zeta| = 1$  must be tangent to the unit circle, and therefore on  $|\zeta| = 1$ , we

will have

$$\operatorname{Re} \left[ \frac{\dot{\zeta}}{\zeta} \right] = 0, \quad (2.115)$$

and hence

$$\operatorname{Re} \left[ \frac{1}{\zeta f'} \frac{\partial f}{\partial t} \right] = \operatorname{Re} \left[ \frac{u + iv}{\zeta f'} \right]. \quad (2.116)$$

Legras & Zeitlin (1992) now invoke a classical theorem of complex analysis, which states that a complex function which is analytic in  $|z| < 1$  is known, up to a purely imaginary constant, if its real part is known in the unit circle  $|z| = 1$ . Hence, the right hand side of (2.116) can be used to define a function  $h(\zeta)$ , which is analytic in  $1/\zeta$ , and for which

$$\operatorname{Re} h(\zeta)|_{|\zeta|=1} = \operatorname{Re} \left[ \frac{u + iv}{\zeta f'} \right]_{|\zeta|=1}. \quad (2.117)$$

The evolution of the conformal mapping function  $f(\zeta)$  can then be obtained from

$$\frac{\partial f}{\partial t} = \zeta \frac{\partial f}{\partial \zeta} h(\zeta). \quad (2.118)$$

The temporal evolution of the vortex is now described entirely by the temporal evolution of the conformal map  $f(\zeta)$ , using (2.118). If  $h(\zeta)$  is expressed in the form of a Laurent series in  $\zeta^{-1}$ , setting the (arbitrary) imaginary part of the constant term in the expansion to zero is equivalent to imposing that  $\Gamma$  remains real throughout the evolution of the vortex.

### 2.4.2 The solution at leading order in $F$

We shall begin by obtaining Kirchoff's famous solution for the rotation rate of the elliptical vortex (see Lamb 1932) using the method outlined in the previous section. Although there are many ways to derive the solution, the presentation given here is intended to describe how the method presented above will work when we proceed to obtain evolution equations for the coefficients of the conformal map at higher orders in  $F$ . Without loss of generality, we shall assume that the potential vorticity within the ellipse exceeds its value outside the ellipse by unity.

To obtain the leading order streamfunction  $\psi_0$ , we must solve

$$\nabla^2 \psi_0 = \begin{cases} 1 & \text{inside ellipse} \\ 0 & \text{outside ellipse} \end{cases}. \quad (2.119)$$

Using the complex variables  $z$  inside the ellipse and  $\zeta$  outside it, (2.119) becomes

$$4 \frac{d^2 \psi_0^{(i)}}{dz d\bar{z}} = 1, \quad |\zeta| < 1 \quad (2.120)$$

$$4 \frac{d^2 \psi_0^{(e)}}{d\zeta d\bar{\zeta}} = 0, \quad |\zeta| > 1, \quad (2.121)$$

where  $\psi_0^{(i)}$  and  $\psi_0^{(e)}$  are the expressions for the leading order streamfunction for the interior and exterior of the ellipse respectively. Integrating these equations, and imposing continuity of  $\psi$  and its normal derivative on the boundary of the ellipse, we obtain

$$\psi_0^{(i)} = \frac{1}{4} z \bar{z} - \frac{1}{8\Gamma} (\bar{\nu} z^2 + \nu \bar{z}^2) - \frac{1}{4} (\Gamma^2 - |\nu|^2) \quad (2.122)$$

$$\psi_0^{(e)} = \frac{1}{4} (\Gamma^2 - |\nu|^2) \ln \zeta \bar{\zeta} + \frac{1}{8\Gamma} (\Gamma^2 - |\nu|^2) (\nu \zeta^{-2} + \bar{\nu} \bar{\zeta}^{-2}) \quad (2.123)$$

as the leading order solution for  $\psi$ .

It is straightforward to show that the velocity, on the boundary of the ellipse, is then

$$\frac{1}{2\Gamma} i(\Gamma^2 - |\nu|^2) \zeta. \quad (2.124)$$

To obtain the evolution equations for  $\Gamma$  and  $\nu$ , we note that

$$\operatorname{Re} \left[ \frac{u + iv}{\zeta f'} \right] = \operatorname{Re} \left[ \frac{i}{2\Gamma} \frac{\Gamma^2 - |\nu|^2}{\Gamma - \nu/\zeta^2} \right] = \operatorname{Re} \left[ \frac{i}{2\Gamma^2} \frac{\nu(\Gamma^2 - |\nu|^2)}{\Gamma\zeta^2 - \nu} \right], \quad (2.125)$$

and hence, by (2.118),

$$\frac{\partial f}{\partial t} = \frac{1}{2} i\nu \left( 1 - \frac{|\nu|^2}{\Gamma^2} \right) \zeta^{-1}, \quad (2.126)$$

which implies

$$\frac{d\Gamma}{dt} = 0; \quad \frac{d\nu}{dt} = \frac{1}{2} i\nu \left( 1 - \frac{|\nu|^2}{\Gamma^2} \right), \quad (2.127)$$

with solution

$$\Gamma = \text{constant}; \quad |\nu| = \text{constant}; \quad \nu = |\nu| e^{i\Omega t}; \quad \Omega = \frac{1}{2} \left( 1 - \frac{|\nu|^2}{\Gamma^2} \right). \quad (2.128)$$

There are no higher order matching terms which would require the introduction of any of the  $\mu_i$  terms in (2.111), thus confirming that at leading order the ellipse remains elliptical.

The rotation rate of the vortex is therefore  $(1 - |\nu|^2/\Gamma^2)/4$ , the factor of four rather than two coming from the fact that the conformal mapping description of the vortex boundary is unable to distinguish between  $0^\circ$  and  $180^\circ$ .

### 2.4.3 The solution to $O(F^2)$

To proceed to higher order in  $F$ , we must first compute the leading order height field  $h_0$ . It is convenient to work with the Bernoulli function  $B$ , for which

$$\nabla^2 B_0 = \begin{cases} 1 + f & \text{inside ellipse} \\ 0 & \text{outside ellipse} \end{cases} . \quad (2.129)$$

In the interior of the ellipse,  $h_0$  can be readily obtained from  $B_0$  via the relation  $h_0 = B_0 - \frac{1}{2}\mathbf{u}_0^2$ . Outside the ellipse, a possible difficulty arises, since the calculation of  $\mathbf{u}_0$  from  $\psi_0$  will introduce a Jacobian factor:

$$h_0^{(e)} = B_0^{(e)} - 2 \left( \frac{d\psi_0^{(e)}}{d\zeta} \frac{d\psi_0^{(e)}}{d\bar{\zeta}} \right) \times \left( \frac{df}{d\zeta} \frac{d\bar{f}}{d\bar{\zeta}} \right)^{-1} . \quad (2.130)$$

At first, the appearance of the Jacobian factor in (2.130) would seem to imply that, outside the ellipse, the expression for  $h_0$  will contain all even inverse powers of  $\zeta$ . and the simplicity of the analytical expression of the rotating elliptical vortex solution would be lost. Fortunately, however, (2.130) can be simplified. After imposing continuity of  $h_0$  and its normal derivative across the elliptical boundary, we obtain

$$\begin{aligned} h_0^{(i)} &= \frac{1}{16} (1 + 2f - |\nu|^2) \left( 2z\bar{z} - \frac{\bar{\nu}}{\Gamma} z^2 - \frac{\nu}{\Gamma} \bar{z}^2 \right) \\ &- \frac{1}{4} \left( \Gamma^2(1 + f) - |\nu|^2(2 + f) \right) + \text{constant} \end{aligned} \quad (2.131)$$

$$\begin{aligned} h_0^{(e)} &= \frac{1}{4} f \left( \Gamma^2 - |\nu|^2 \right) \ln \zeta\bar{\zeta} + \frac{1}{16\Gamma^3} \left( \Gamma^4(1 + 2f) - 2|\nu|^2\Gamma^2(1 + f) + |\nu|^4 \right) \left( \nu\zeta^{-2} + \bar{\nu}\bar{\zeta}^{-2} \right) \\ &- \frac{1}{8\Gamma^2} \left( \Gamma^2 - |\nu|^2 \right)^2 (\zeta\bar{\zeta})^{-1} + \text{constant}. \end{aligned} \quad (2.132)$$

The Jacobian factor has been cancelled exactly from the denominator by the derivatives of  $\psi$ . It follows that, as in the case of  $\psi_0$ , only quadratic terms in  $z$  or  $\zeta^{-1}$  and their conjugates need be retained in the solution.

The arbitrary constant in (2.131) and (2.132) must be determined through the matching conditions to the outer flow.

We first note that in the limit  $r \rightarrow \infty$ , (2.123) implies

$$\psi_0^{(e)} \sim \frac{1}{2} (\Gamma^2 - |\nu|^2) \ln r. \quad (2.133)$$

From (2.81), this implies an outer scale flow streamfunction

$$\psi_0 = -\frac{1}{2} (\Gamma^2 - |\nu|^2) K_0(|f|Fr), \quad (2.134)$$

and a height field

$$h_0 = -f \frac{1}{2} (\Gamma^2 - |\nu|^2) K_0(|f|Fr). \quad (2.135)$$

This in turn induces a uniform correction to  $h$  in the vortical flow:

$$h_{0l} = f \frac{1}{2} (1 - |\nu|^2) (\ln(|f|F\Gamma) + \gamma), \quad (2.136)$$

which implies an  $O(F^2)$  streamfunction in the vortical region:

$$\nabla^2 \psi_{2l} = \begin{cases} (1+f)h_{0l} & \text{inside ellipse} \\ fh_{0l} & \text{outside ellipse} \end{cases}, \quad (2.137)$$

which has components at  $O(F^2)$  and  $O(F^2 \ln F)$ .

Converting into complex coordinates and solving this equation, we obtain the streamfunction inside the elliptical vortex:

$$\psi_{2l}^{(i)} = h_{0l} \left( \frac{1}{4} z \bar{z} (1+f) - \frac{1}{8\Gamma} (\bar{\nu} z^2 + \nu \bar{z}^2) - \frac{1}{4} (\Gamma^2 - |\nu|^2) \right), \quad (2.138)$$

and the streamfunction outside the ellipse:

$$\begin{aligned} \psi_{2l}^{(e)} &= \frac{1}{8} h_{0l} \left( 2f\Gamma^2 \zeta \bar{\zeta} + 2f\Gamma (\bar{\nu} \zeta \bar{\zeta}^{-1} + \nu \bar{\zeta} \zeta^{-1}) \right. \\ &\quad \left. + (\Gamma^2 - |\nu|^2) \left( 2 \ln \zeta \bar{\zeta} + \frac{\nu}{\Gamma} \zeta^{-2} + \frac{\bar{\nu}}{\Gamma} \bar{\zeta}^{-2} \right) + 2f|\nu|^2 \zeta^{-1} \bar{\zeta}^{-1} \right). \end{aligned} \quad (2.139)$$

Repeating the procedure to obtain the leading order solution described in §4.2, we obtain an evolution equation for  $\nu$  at  $O(F^2 \ln F)$ :

$$\frac{d\nu}{dT_l} = \frac{1}{2} i h_{0l} \nu (2f + 1 - (|\nu|/\Gamma)^2). \quad (2.140)$$

There is no correction to the higher  $\mu_i$  coefficients at  $(F^2 \ln F)$ .

Equation (2.140) implies a correction to the rotation rate  $\omega$  at  $O(F^2 \ln F)$ , such that

$$\omega = \frac{1}{4} \left( \Gamma^2 - |\nu|^2 + F^2 \ln F \frac{1}{2} f (\Gamma^2 - |\nu|^2) (2f + 1 - (|\nu|/\Gamma)^2) + O(F^2) \right). \quad (2.141)$$

Recalling that  $\ln F < 0$ , this corresponds to a reduction in the rotation rate if and only if  $f(2f + 1 - (|\nu|/\Gamma)^2) > 0$ . The implication is that, as  $|f|$  becomes large, the vortex always slows down compared with its incompressible rotation rate. Its rotation rate increases only if  $-(1 - (|\nu|/\Gamma)^2)/2 < f < 0$ .

We are now in a position to write down the equations for the second order velocity potential and streamfunction  $\phi_2$  and  $\psi_2$  respectively.

$$4 \frac{d^2 \phi_2^{(i)}}{dz d\bar{z}} = -\frac{1}{32\Gamma^5} i(\Gamma^2 - |\nu|^2)(\Gamma^2(1 + 2f) - |\nu|^2)(\bar{\nu}z^2 - \nu\bar{z}^2) \quad (2.142)$$

$$\begin{aligned} 4 \frac{d^2 \phi_2^{(e)}}{d\zeta d\bar{\zeta}} = & -\frac{1}{32\Gamma^4} i(\Gamma^2 - |\nu|^2)^2(\Gamma^2(1 + 2f) - |\nu|^2)(\nu^2\zeta^{-4} - \bar{\nu}^2\bar{\zeta}^{-4}) \\ & -\frac{1}{32\Gamma^3} i(\Gamma^2 - |\nu|^2)^2(\Gamma^2(1 - 2f) - |\nu|^2)(\nu\zeta^{-2} - \bar{\nu}\bar{\zeta}^{-2}) \\ & -\frac{1}{16\Gamma^5} (\Gamma^2 - |\nu|^2)^2(\Gamma^4 - |\nu|^4 - f\Gamma^2|\nu|^2)(\nu\zeta^{-4}\bar{\zeta}^{-2} - \bar{\nu}\bar{\zeta}^{-4}\zeta^{-2}) \\ & +\frac{1}{8\Gamma^3} i(\Gamma^2 - |\nu|^2)^3(\nu\zeta^{-3}\bar{\zeta}^{-1} - \bar{\nu}\bar{\zeta}^{-3}\zeta^{-1}) \end{aligned} \quad (2.143)$$

$$4 \frac{d^2 \psi_2^{(i)}}{dz d\bar{z}} = (1 + f) \left[ \frac{1}{16} (1 + 2f - |\nu|^2) \left( 2z\bar{z} - \frac{\bar{\nu}}{\Gamma} z^2 - \frac{\nu}{\Gamma} \bar{z}^2 \right) - \frac{1}{4} (\Gamma^2(1 + f) - |\nu|^2(2 + f)) \right] \quad (2.144)$$

$$\begin{aligned} 4 \frac{d^2 \psi_2^{(e)}}{d\zeta d\bar{\zeta}} = & f(\Gamma - \nu\zeta^{-2})(\Gamma - \bar{\nu}\bar{\zeta}^{-2}) \left[ \frac{1}{4} f (\Gamma^2 - |\nu|^2) \ln \zeta\bar{\zeta} \right. \\ & \left. + \frac{1}{16\Gamma^3} (\Gamma^4(1 + 2f) - 2|\nu|^2\Gamma^2(1 + f) + |\nu|^4) (\nu\zeta^{-2} + \bar{\nu}\bar{\zeta}^{-2}) \right. \\ & \left. \frac{1}{8\Gamma^2} (\Gamma^2 - |\nu|^2)^2 (\zeta\bar{\zeta})^{-1} \right] \end{aligned} \quad (2.145)$$

The result is that  $\phi_2$  and  $\psi_2$  will require only constant, logarithmic, quadratic and quartic terms in their expressions, and the full solution of the problem to  $O(F^2)$  can be written down in a finite expression involving only products of algebraic and logarithmic functions. The evolution of the boundary of the ellipse will require  $\mu_3$  to be non-zero at order  $O(F^2)$ , but all the other  $\mu_i$  may be set to zero without approximation.

A considerable amount of manipulation is required to obtain expressions for  $\phi_2$  and  $\psi_2$ , and a program was written to undertake the integration and matching using the REDUCE symbolic manipulation language.

After obtaining the  $O(F^2)$  velocity fields and substituting into (2.111 - 2.118), one obtains:

$$\begin{aligned} \frac{d\mu_3}{dt} &= -\frac{i}{2}\bar{\mu}_3\frac{\nu^4}{\Gamma^4} - 2i\mu_3\frac{|\nu|^2}{\Gamma^2} + \frac{3i}{2}\mu_3 \\ &+ \frac{i\Gamma\nu^2}{96}\left(1 - (|\nu|/\Gamma)^2\right) \left[ f^2\left(6 - 2(|\nu|/\Gamma)^2\right) \right. \\ &\quad \left. + f\left(1 - (|\nu|/\Gamma)^2\right)\left(7 + 3(|\nu|/\Gamma)^2\right) \right. \\ &\quad \left. + 2\left(1 - (|\nu|/\Gamma)^2\right)^2\left(1 + (|\nu|/\Gamma)^2\right) \right] \end{aligned} \quad (2.146)$$

$$\begin{aligned} \frac{d\mu_1}{dt} + \frac{d\nu}{dT} &= \frac{i\nu|\nu|^2}{2\Gamma^3}(\mu_{-1} + \mu_{-1}^-) \\ &+ \frac{i}{2}(\mu_1 - 2(|\nu|/\Gamma)^2\mu_1 - (\nu/\Gamma)^2\bar{\mu}_1) \\ &+ \frac{i}{4}(1 - (|\nu|/\Gamma)^2)(4(\nu/\Gamma)^3\bar{\mu}_3 + 2(\bar{\nu}/\Gamma)\mu_3 + (\bar{\nu}|\nu|^2/\Gamma^3)\mu_3) \\ &+ \frac{i\nu}{96}(1 - (|\nu|/\Gamma)^2) \left( f^2(4 + 18(|\nu|/\Gamma)^2 - 2(|\nu|/\Gamma)^4) \right. \\ &\quad \left. - f(1 - (|\nu|/\Gamma)^2)(29 - 2(|\nu|/\Gamma)^2 - 3(|\nu|/\Gamma)^4) \right. \\ &\quad \left. - (1 - (|\nu|/\Gamma)^2)^2(11 + (|\nu|/\Gamma)^2 - 2(|\nu|/\Gamma)^4) \right) \\ &+ \frac{i}{4}f\nu(\Gamma^2 - |\nu|^2)(2f + 1 - (|\nu|/\Gamma)^2)(\ln(|f|\Gamma) + \gamma) \end{aligned} \quad (2.147)$$

$$\frac{d\mu_{-1}}{dt} = \frac{1}{4}((\nu^2|\nu|^2/\Gamma^4)\bar{\mu}_3 + (\bar{\nu}/\Gamma)^2\mu_3 - (\nu/\Gamma)^2\bar{\mu}_3 - (\bar{\nu}^2|\nu|^2/\Gamma^4)\mu_3). \quad (2.148)$$

The solution for  $\nu$  is known on the shortest timescale  $t$ , and this system of equations describes oscillations of  $\mu_3, \mu_1$  and  $\mu_{-1}$ , where  $\mu_1$  and  $\mu_{-1}$  are used to represent  $O(F^2)$  corrections of  $\nu$  and  $\Gamma$  respectively. The oscillations are forced in the  $\mu_3$  equation, with a forcing frequency of  $2\Omega$  – i.e. four times the rotational frequency of the vortex. Forcing in the  $\mu_1$  equation is secular, and is absorbed into the  $d\nu/dT$  component, leading to an  $O(F^2)$  modification to the rotation rate of the vortex.

It is convenient to investigate solutions for  $\mu_3$  with the frequency of the forcing. These solutions will give weakly perturbed elliptical vortex shapes which rotate without change of form. Vortical patches which rotate without change of form have been termed V-states by Deem & Zabusky (1978), the simplest example of a V-state being the rotating ellipse of uniform

vorticity in the two-dimensional incompressible Euler equations.

Once the V-states of our system are found, the forcing is effectively removed from the system of equations describing the  $O(F^2)$  perturbations to the elliptical vortex shape. They are then the same equations which describe free perturbations to an elliptical vortex boundary in incompressible flow. The perturbations will therefore be oscillatory provided the vortex is stable to incompressible mode-4 perturbations, and exponential otherwise.

The stability of an incompressible elliptical vortex was investigated by Love (1893). He found that the ellipse was always stable if it had an aspect ratio  $\lambda = (\Gamma + |\nu|)/(\Gamma - |\nu|)$  of less than 3. At an aspect ratio  $\lambda = 3$ , the ellipse became unstable to mode 3 perturbations (i.e.  $\mu_2 \neq 0$ ). In the present study, we impose  $180^\circ$  rotational symmetry, and therefore we do not encounter mode 3 perturbations. As the aspect ratio is increased further, so successively more modes become unstable. The first one of interest to us here is mode 4, which becomes unstable when the aspect ratio  $\lambda = (\sqrt{2} + 2\sqrt{\sqrt{2} - 1})(1 + 1/\sqrt{2}) \approx 4.61$ . In the variables  $\Gamma$  and  $|\nu|$  to be used here, this corresponds to  $|\nu|/\Gamma = \sqrt{\sqrt{2} - 1}$ .

#### 2.4.4 V-states for weakly divergent flow

In finding the V-state with  $180^\circ$  rotational symmetry for incompressible flow, the conformal map (2.111) from the unit disc in  $\zeta$ -space to the shape of the rotating vortex patch in  $z$ -space was postulated. The evolution equations for the coefficients showed that  $\mu_i = 0$  for all  $i$  was a consistent solution. A single evolution equation remained for  $\nu$ , and it followed that  $|\nu|$  was a constant, corresponding to vortex patch rotating at a constant rate.

With the effects of divergence introduced, we have seen that  $\mu_3$  may not be assumed to be zero for all time, although all the other  $\mu_i$  for  $i > 3$  may be taken to be zero.

We start by searching for a solution for  $\mu_3$  of the form

$$\mu_3(t) = Me^{2i\Omega t}, \quad (2.149)$$

where  $M$  is a constant (which will depend on  $|\nu|$ ), and  $\Omega = (\Gamma^2 - |\nu|^2)/2$ . This solution should be regarded as the particular integral of (2.148). Substituting (2.149) into (2.148) and factorizing,

we obtain

$$M = -\frac{\Gamma|\nu|^2(1 - (|\nu|/\Gamma)^2)}{48(1 - 2(|\nu|/\Gamma)^2 - (|\nu|/\Gamma)^4)} (f^2(6 - 2(|\nu|/\Gamma)^2) + f(1 - (|\nu|/\Gamma)^2)(7 + 3(|\nu|/\Gamma)^2) + 2(1 - (|\nu|/\Gamma)^2)^2(1 + (|\nu|/\Gamma)^2)). \quad (2.150)$$

Thus, provided that the denominator  $1 - 2(|\nu|/\Gamma)^2 - (|\nu|/\Gamma)^4 \neq 0$ , there is a unique solution for  $M$  in terms of  $|\mu|$ . This is equivalent to the condition  $(|\nu|/\Gamma)^2 \neq \sqrt{2} - 1$ . One can readily verify that  $\mu_1$  and  $\mu_{-1}$  may be set to zero with this solution. The rotation rate of the vortex is changed by  $O(F^2)$ .

It is also straightforward to show that the solution describes a vortex which is rotating without change of form. The conformal mapping function  $f(\zeta)$  is now

$$f(\zeta) = \Gamma\zeta + |\nu|e^{i\Omega t}\zeta^{-1} + F^2Me^{2i\Omega t}\zeta^{-3}. \quad (2.151)$$

Moving into a frame of reference rotating with the vortex, we define the complex coordinate in the rotating frame  $Z$  by  $\zeta = Ze^{i\Omega t/2}$ . Then

$$f(\zeta) = e^{i\Omega t/2} (\Gamma Z + |\nu|Z^{-1} + F^2MZ^{-3}). \quad (2.152)$$

In the rotating  $Z$ -frame, therefore, the conformal mapping is rotating at a constant rotation rate  $\Omega/2$ . Apart from this uniform background rotation, the coefficients of the mapping are constants, and hence the vortex rotates without change of shape.

From (2.150), we can see that  $M$  can be positive or negative, depending upon  $|\nu|/\Gamma$  and  $f$ . In figures 2.1–2.4 rotating V-state shapes are shown for various  $|\nu|$  and various  $M$ , both positive and negative.

The ellipses are normalised to have a semi-major axis of unit length. A clear distinction is to be drawn between positive  $M$  and negative  $M$ . When  $M$  is positive, the ellipses seem to become more distorted towards square shapes, and for larger values of  $M$  appear to develop cusps. When  $M$  is negative, however, the ends of the ellipses tend to round out, and the V-states become more peanut-shaped. Now, it also follows from (2.150) that for moderate to large  $|f|$ , we will have  $M < 0$ , and therefore the  $M < 0$  solutions should be qualitatively similar to the V-states of the single layer quasi-geostrophic equations. A study of these V-states was carried

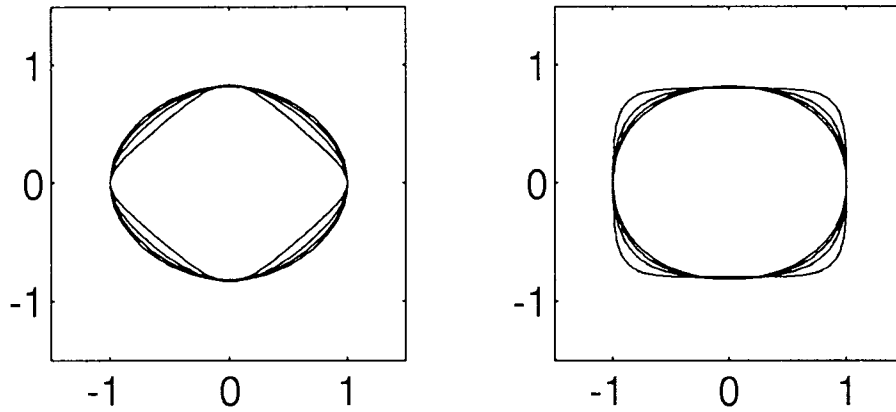


Figure 2.1: Shapes of rotating weakly compressible steadily rotating V-states for positive  $\mu_3$  (left) and negative  $\mu_3$  (right), with small aspect ratio ( $|\nu|/\Gamma = 0.1$ )

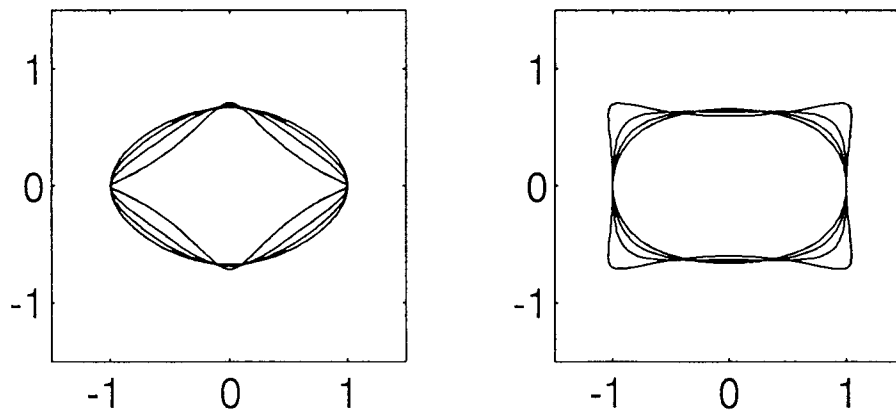


Figure 2.2: As figure 2.1, but with  $|\nu|/\Gamma = 0.2$

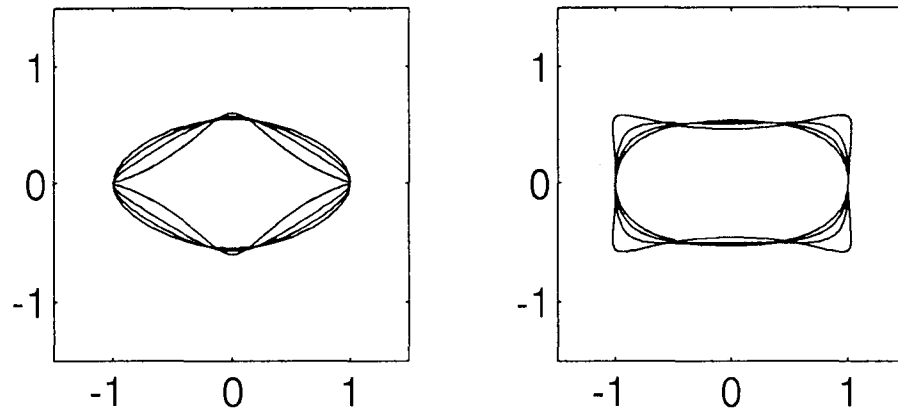


Figure 2.3: As figure 2.1, but with  $|\nu|/\Gamma = 0.3$

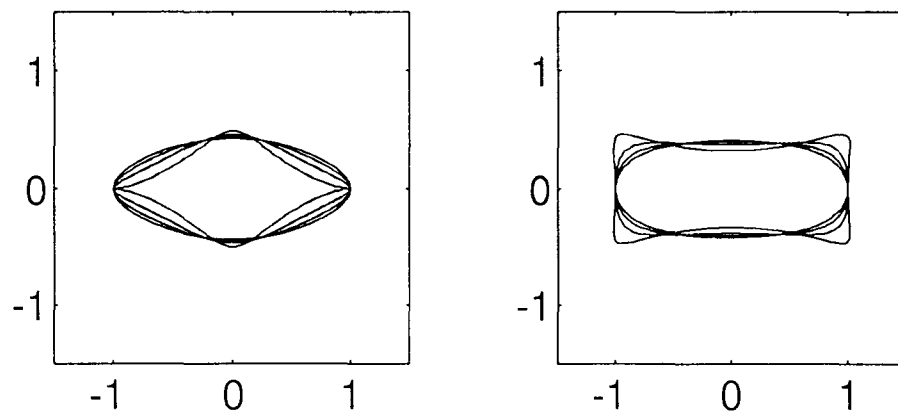


Figure 2.4: As figure 2.1, but with  $|\nu|/\Gamma = 0.4$

out by Polvani *et al.* (1989), who found that the V-states of the single layer quasigeostrophic equations were more peanut-shaped than their elliptical counterparts for the incompressible Euler equations. It seems, therefore, that the asymptotic expansion presented here is capable of capturing the qualitative of V-states of the quasigeostrophic system.

In addition to the  $O(F^2)$  change of shape of the V-states, the rotation rate is adjusted by an amount of  $O(F^2)$ , due to local divergence effects. However, except when the background rotation is absent, the dominant correction to the rotation rate comes about from matching conditions with the wave scale flow. The correction introduced from the matching conditions when background rotation is present is  $O(F^2 \ln F)$  (equation 2.141).

#### 2.4.5 The effect of gravity wave radiation

We turn now to the effect of gravity wave radiation on the rotating nearly-elliptical vortex. As we have seen, the effect of wave radiation does not enter the problem at  $O(F^2)$ , but does enter the problem at  $O(F^4)$ , in the form of a matching condition in the far field, imposing a uniform straining flow.

If one attempts to perform a complete asymptotic analysis of the fields to  $O(F^4)$ , it is not possible to express them in closed analytical form, unlike the  $O(1)$ ,  $O(F^2)$  and  $O(F^2 \ln F)$  fields. The problem arises because, although the Bernoulli function to second order in  $F^2$  outside the ellipse can be expressed in a finite sum of powers of  $\zeta$  and  $\bar{\zeta}$ , multiplied, by logarithms of  $\zeta$  and  $\bar{\zeta}$ , obtaining the height field from the Bernoulli function involves dividing by the Jacobian of the transformation. At  $O(F^2)$ , unlike the leading order analysis, it does not seem possible to factor out the Jacobian from the corresponding numerator. Thus although the second order height field may be expressed in closed (albeit cumbersome) form, integration with respect to  $\zeta$  and  $\bar{\zeta}$  will not lead to a closed form expression for the velocity potential at  $O(F^4)$ .

It follows that at  $O(F^4)$ , the representation of any V-state by a conformal mapping of form (2.111) will require  $\mu_i \neq 0$  for all odd  $i$ . However, it is clear that even if it were possible to obtain equations for the evolution of the  $\mu_i$ , the contributions from the fields obtained in the way described above would give rise only to adjustments to the rotation rate of the structure at  $O(F^4)$ , and some further  $O(F^4)$  corrections to the amplitudes of  $\nu$  and the  $\mu_i$ .

On the other hand, matching of the leading order solution to the gravity wave region will

give rise to a radiating wave field, one result of which is to introduce in the wave field a Hankel function of the appropriate type, corresponding to a radiating boundary condition. Matching conditions then imply that a large scale straining flow of form  $r^2 \sin 2\theta$  will be introduced at  $O(F^4)$  in the region of the vortex, in a sense which will cause the ellipse to elongate and lose energy, consistent with the associated radiating wave field. Since we know that ellipses remain elliptical under the influence of a large scale straining flow (Kida, 1981), it follows that we may simply regard  $\nu$  as a slowly varying parameter.

To see this in detail, we must first obtain the wave-like part of the far field. First, therefore, we must obtain the time fluctuating part of the far field of  $\psi_0^{(i)}$  in the limit  $r \rightarrow \infty$ . In doing so, however, we must recall that the  $\zeta$ -coordinate is itself evolving in time, and hence the  $\ln \zeta \bar{\zeta}$  term will contribute to the quadrupolar far field in (2.123).

From (2.123), the time-fluctuating part of  $\psi_0^{(e)}$  is

$$-\frac{\Gamma}{8r^2} |\nu| (\Gamma^2 - |\nu|^2) \left( e^{-i(2m\theta - \Omega t)} + e^{i(2m\theta - \Omega t)} \right). \quad (2.153)$$

Matching onto the wave field, this implies a leading order ( $O(F^2)$ ) wave field, which consists of wavelike perturbations for streamfunction  $\psi$  and velocity potential  $\phi$ , related via (2.85). In this case, we therefore have

$$-i\Omega\psi + f\phi = 0 \quad (2.154)$$

$$\phi + i\psi \sim \frac{i\Gamma}{8r^2} |\nu| (\Gamma^2 - |\nu|^2) \left( e^{-i(2m\theta - \Omega t)} + e^{i(2m\theta - \Omega t)} \right) \quad \text{as } r \rightarrow 0, \quad (2.155)$$

which implies  $O(F^2)$  wave fields:

$$\psi_2 = \frac{i\pi\Gamma}{16} \frac{f}{\Omega + f} |\nu| (\Gamma^2 - |\nu|^2) (\Omega^2 - f^2) \text{H}_2^{(1)}((\Omega^2 - f^2)^{1/2} R) e^{i(2m\theta - \Omega t)} \quad (2.156)$$

$$\phi_2 = -\frac{\pi\Gamma}{16} \frac{\Omega}{\Omega + f} |\nu| (\Gamma^2 - |\nu|^2) (\Omega^2 - f^2) \text{H}_2^{(1)}((\Omega^2 - f^2)^{1/2} R) e^{i(2m\theta - \Omega t)}. \quad (2.157)$$

The imaginary part of this corresponds to a streamfunction at  $O(F^4)$  in the vortical region:

$$\psi_4 = -\frac{\pi\Gamma}{128} \frac{\Omega - f}{\Omega + f} (\Gamma^2 - |\nu|^2) (\Omega^2 - f^2)^2 (\bar{\nu}z^2 - \nu\bar{z}^2). \quad (2.158)$$

Adding this streamfunction to the velocity field at  $O(F^4)$  and using (2.116), we obtain

$$\frac{d\Gamma^2}{dt} = F^4 \frac{\pi}{32} \Gamma^2 |\nu|^2 (\Gamma^2 - |\nu|^2) (\Omega^2 - f^2) (\Omega - f)^2 \quad (2.159)$$

$$\frac{d|\nu|^2}{dt} = F^4 \frac{\pi}{32} \Gamma^2 |\nu|^2 (\Gamma^2 - |\nu|^2) (\Omega^2 - f^2) (\Omega - f)^2. \quad (2.160)$$

Conservation of the circulation,  $(\Gamma^2 - |\nu|^2)/4$ , was not used explicitly in deriving these equations, and serves as an independent check on the analysis.

If we introduce the constant  $C$ , defined such that  $C^2 = \Gamma^2 - |\nu|^2$ , we can obtain an evolution equation for  $\Gamma^2$ :

$$\frac{d\Gamma^2}{dt} = F^4 \frac{\pi}{32\Gamma^6} C^2 (\Gamma^2 - C^2) \left( \frac{1}{4} C^4 - \Gamma^4 f^2 \right) \left( \frac{1}{2} C^2 - f\Gamma^2 \right)^2. \quad (2.161)$$

Let us consider first the non-rotating case, which was considered by Zeitlin (1991). In this case, (2.161) reduces to:

$$\frac{d\Gamma^2}{dt} = \frac{\pi F^4}{512\Gamma^6} C^{10} (\Gamma^2 - C^2). \quad (2.162)$$

In this case, we may obtain the solution:

$$\Gamma^6/3 + C^2\Gamma^4/2 + C^4\Gamma^2 + C^6 \ln(\Gamma^2 - C^2) = \frac{\pi F^4 C^{10} t}{512} + \text{constant}. \quad (2.163)$$

Since  $\Gamma^2 > C^2$ , we know that  $\Gamma$  is a monotonically increasing function of time, and hence as  $t \rightarrow \infty$  we will have

$$\Gamma \sim \left( \frac{3\pi}{512} \right)^{1/6} C^{5/3} (F^4 t)^{1/6} + O(1). \quad (2.164)$$

Since  $\Gamma$  increases without bound in this case, it follows from conservation of  $\Gamma^2 - |\nu|^2$  that, for large  $t$ ,  $|\nu| \sim \Gamma - O(\Gamma^{-1})$ . The ellipse has thus become infinitely long and this, with semi-major axis  $\Gamma + |\nu| \rightarrow \infty$ , and semi-minor axis  $\Gamma - |\nu| \rightarrow 0$  as  $t \rightarrow \infty$ . The result is that the vortex evolves through a succession of V-states, with rapid oscillations about them on the  $O(1)$  timescale.

However, we already know that if  $(|\nu|/\Gamma)^2 = \sqrt{2} - 1$ , the perturbation expansion breaks down because the ellipse departs from elliptical form as  $\mu_3$  in the conformal mapping (2.111) becomes unbounded. In the case  $f = 0$ , we also know that  $\mu_3 < 0$ , and hence we can make some qualitative statement about the nature of distortion of the ellipse.

In figure 2.5, the evolution of an ellipse with  $f = 0$  is shown approaching the critical aspect ratio  $(|\nu|/\Gamma)^2 = \sqrt{2} - 1$ . The perturbation expansion suggests that, as the critical aspect ratio is reached, the ellipse becomes progressively more “peanut”-shaped. Eventually, the expansion procedure breaks down, and the mapping  $f(\zeta)$  ceases to be single-valued. By this time, the lobes of the “peanut” have grown significantly, and there is a tendency to pinch in the middle, creating two separate vortices.

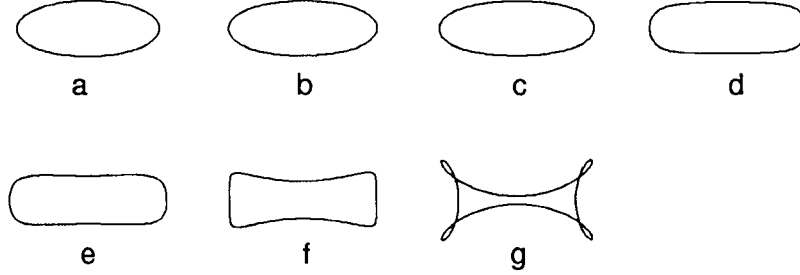


Figure 2.5: V-states of the rotating ellipse in the non-rotating frame ( $f = 0$ ). Fig (a) represents the aspect ratio at which mode 3 instability would first occur, if  $180^\circ$  symmetry were relaxed. Figures (a) to (g) show the V-states as the ellipse extends due to wave radiation. The splitting ratio is  $(|\nu|/\Gamma)^2 = 0.4142$ .

Some support for this scenario is provided by the analytical work of Williams (1992), and the numerical work of Chan *et al.* (1993). Williams performs a weakly nonlinear version of the present analysis, equivalent to assuming that  $|\nu|/\Gamma = O(F^2)$ . He shows that the weakly nonlinear development of the elliptical perturbation also leads to a “pinch” at a time of order  $\ln F/F^4$ . The numerical work of Chan *et al.* confirms this, but their Froude number is of order one. It seems that this analysis is in agreement with the existing literature, though not with Zeitlin’s (1991) remarks, where he supposed that a secondary barotropic instability mechanism would have to be invoked to explain the subsequent breakup of the ellipse into two vortices. That is not the conclusion of the present study, nor is it the conclusion of Williams. The present study provides an interesting counterpart to the study of Williams in that it shows that  $O(F^2)$  terms are sufficient to explain the principal dynamics, and one does not need to take into account terms at high order in  $F$  to obtain the nonlinear breakdown of the ellipse, even though they are required for the weakly nonlinear analysis.

Now, we notice that, as the aspect ratio of the ellipse increases, the frequency of the radiated waves  $\Omega = (1 - (|\nu|^2/\Gamma^2))/2 = C^2/(2\Gamma^2)$  decreases. Provided  $\Omega > |f|$ , waves will radiate and the ellipse will continue to elongate. However, if  $\Omega < |f|$ , then waves will not radiate,  $\Gamma^2$  and  $|\nu|^2$  will be constant, and the ellipse will not elongate with time. The values of the constants  $|f|$  and  $C$  will determine whether the ellipse reaches the splitting aspect ratio, at which it breaks in two. At the splitting aspect ratio, the frequency of radiated waves is  $\Omega_c = 1 - 1/\sqrt{2}$ . Therefore,

if  $|f| > 1 - 1/\sqrt{2}$ , the ellipse will gradually approach the aspect ratio, at which it no longer excites radiating gravity waves. If, on the other hand,  $|f| < 1 - 1/\sqrt{2}$ , we expect the ellipse to split in two as it approaches the critical aspect ratio. It will then be necessary to determine the sign of  $\mu_3$  to describe the nature of the breakup of the ellipse.

To determine the sign of  $\mu_3$  at the splitting aspect ratio, we set  $(|\nu|/\Gamma)^2 = \sqrt{2} - 1$  in (2.150) and determine the roots of  $M = 0$  as a function of  $f$ . This leads to the equation

$$(4 - \sqrt{2})f^2 + (\sqrt{2} - 1)f + 6\sqrt{2} - 8 = 0, \quad (2.165)$$

which has solutions

$$f_1 = -(1 - 1/\sqrt{2}) \approx -0.29; \quad f_2 = -2(3\sqrt{2} - 2)/7 \approx -0.64. \quad (2.166)$$

If  $f$  lies between  $f_1$  and  $f_2$ , then  $M > 0$ , otherwise  $M < 0$ .

The magnitude of  $f_1$ , the smaller of the two roots of (2.166), is the same as the magnitude of the critical background rotation rate, above which the inhibiting effect of background rotation on the radiation will prevent ellipses from reaching their splitting aspect ratio. It follows that if  $|f| < 1 - 1/\sqrt{2}$ , we will always have  $M < 0$  at the critical aspect ratio  $(|\nu|/\Gamma)^2 = \sqrt{2} - 1$ . Therefore, the nature of the breakup of an elliptical vortex by elongation due to gravity wave radiation can be described entirely by considering a succession of V-states in which  $\mu_3 \rightarrow -\infty$  while  $(|\nu|/\Gamma)^2 = \sqrt{2} - 1$  — the same as for the case without background rotation.

Finally, in cases where the background rotation is sufficiently strong to inhibit the breakup of the vortex, it is interesting to note the differences in the approach to the equilibrium aspect ratio of the ellipse between positive and negative  $f$ .

Returning to (2.161), we can write

$$\begin{aligned} \int \left( \frac{\alpha}{\Gamma^2 - C^2} + \frac{\beta}{f\Gamma^2 + C^2/2} + \frac{\gamma}{f\Gamma^2 - C^2/2} + \frac{\delta}{(f\Gamma^2 - C^2/2)^2} + \frac{\epsilon}{(f\Gamma^2 - C^2/2)^3} \right) d\Gamma^2 \\ = \int \frac{F^4 \pi C^2}{32} dt \end{aligned} \quad (2.167)$$

for constants  $\alpha, \beta, \gamma, \delta, \epsilon$ . For  $f > 0$ , at large times we will have

$$\int \frac{\epsilon d\Gamma^2}{(f\Gamma^2 - C^2/2)^3} \sim \int \frac{F^4 \pi C^2}{32} dt, \quad (2.168)$$

where  $\epsilon = -C^2/(64f^2(1 - 2f))$ . Hence, for large times, we will have

$$\Gamma^2 \sim \frac{C^2}{2f} - \frac{1}{2\sqrt{\pi}f(1 - 2f)^{1/2}} (F^4 t)^{-1/2}. \quad (2.169)$$

The cyclonic ellipse approaches its final aspect ratio algebraically in time for large times.

On the other hand, if  $f < 0$  then, for large  $t$ , we have

$$\int \frac{\beta d\Gamma^2}{f\Gamma^2 + C^2/2} \sim \int \frac{F^4 \pi C^2}{32} dt, \quad (2.170)$$

where  $\beta = 1/(64f^2C^2(1 + 2f))$ . From this it follows that

$$\Gamma^2 - \frac{C^2}{2|f|} \propto \exp(-2\pi C^4 |f|^3 (1 - 2|f|) F^4 t), \quad (2.171)$$

so that, when  $-1/2 < f < 0$ , the final approach of the anticyclonic ellipse to its steady aspect ratio is exponential in time, and hence rather more rapid than the corresponding cyclonic case.

The particular case  $f = 1 - 1/\sqrt{2}$  requires special attention. In this case, the radiating ellipse equilibrates at the critical aspect ratio. However,  $\mu_3$  is unbounded at the critical aspect ratio (unlike the corresponding anticyclonic case  $f = -(1 - 1/\sqrt{2})$ , in which case it remains bounded as it approaches its critical aspect ratio). Since only other radiation terms can affect the growth of  $\Gamma$ , it is probably necessary to consider higher order radiation fields to resolve this singularity, perhaps with  $f$  differing from  $1 - 1/\sqrt{2}$  by  $O(F^2)$ . However, it seems that the principal features of the response of the ellipse to gravity wave radiation have been captured by the present analysis, and no further analysis has been attempted to clarify this remaining limiting case.

## 2.5 Discussion

The material presented in this chapter has focussed on the asymptotic limit of small Froude number. This is the limit in which the Lighthill analysis of aerodynamic sound generation is formally valid.

We have seen that it is possible to perform a matched asymptotic analysis and recover a quadrupolar far field, in a manner similar to Crow (1970) for the three-dimensional case. That result alone is non-trivial: if the incompressible velocity field is used in computing the Lighthill source term for a single two-dimensional eddy, the resulting integrals for the quadrupole moments are divergent.

The matched asymptotic analysis enabled us to analyse the general form of the back-reaction — i.e. the effect of the radiating gravity waves on the vortical flow. We showed that it was not

in general possible to determine the back reaction, which occurs at  $O(F^4)$  in the source flow, in terms of the instantaneous potential vorticity field, even if one is permitted to integrate the equations of motion backwards in time. This is because history integrals are in general sensitive to the initial instant which is selected in the integration over the past times. However, if no radiating gravity waves were present, it was possible to obtain an expression for the  $O(F^4)$  flow evaluating only instantaneous time derivatives of the potential vorticity field, and without reference to any initial instant. It follows that, at low Froude number, it is not in general possible to construct a balanced model which incorporates gravity wave emission without specifying a time in the past before which there are supposed to be no gravity waves.

An example of a flow subject to gravity wave radiation is the rotating ellipse of uniform potential vorticity. This flow was analysed to elucidate some more features of the effect of gravity wave radiation in a low Froude number limit. It was found that the ellipse tended to elongate in response to gravity wave radiation until it reached a certain aspect ratio, at which point it appeared to split into two vortices, and beyond which point the asymptotic analysis is not valid. The effect of the elongation is to reduce the radiation frequency of the quadrupolar gravity waves. Therefore, if the background rotation is sufficiently rapid, the ellipse might not reach its splitting aspect ratio, whereas for weaker background rotation the splitting aspect ratio is always attained on times such that  $t = O(F^{-4})$ .

If the splitting aspect ratio is not achieved, a remarkable degree of asymmetry in  $f$  is observed in the way in which the final aspect ratio of the ellipse is approached – exponentially in  $F^4 t$  for anticyclones, but algebraically in  $F^4 t$  for cyclones.

From time to time it is suggested that the nonlinear shallow water equations might exhibit a phenomenon of generalized adjustment, in which the vortical flow is continually adjusting itself to emit as few gravity waves as possible. Although the general analysis suggests that this is never truly possible for flows with a full spectrum of frequencies, the generalized adjustment hypothesis is supported by the model problem of the rotating ellipse. The ellipse elongates, and if the background rotation is sufficiently strong, will ultimately stop emitting gravity waves. If the background rotation is not sufficiently strong, it will split into two vortices, which will presumably move apart until they no longer radiate gravity waves. At that point, if they are sufficiently far apart, elliptical perturbation might once again grow on the boundaries of each separately, and the process will repeat itself. By this mechanism, the overall intensity of

radiation will decrease as more and more smaller vortices are responsible for the radiation. To see this, first note that the scaling law (2.9) can be modified to take account of the effect of the Coriolis force:

$$h' \sim \begin{cases} h_0 \left(\frac{l}{|\mathbf{x}'|}\right)^{1/2} \left(\frac{u}{c_0}\right)^2 \left(\frac{(\omega^2 - f^2)^{1/2} l}{c_0}\right)^{3/2} & \omega^2 > f^2 \\ 0 & \omega^2 < f^2 \end{cases}. \quad (2.172)$$

Now,  $\omega$  is set by the vorticity, and  $u \sim \omega l$ . Hence, keeping  $l/|\mathbf{x}'|$  fixed, we have

$$h' \sim l^{7/2}. \quad (2.173)$$

Each time the vortex splits, two vortices are formed, each with  $l \rightarrow l/\sqrt{2}$ . Ultimately, we suppose that there are  $n$  vortices, each of dimension  $l/\sqrt{n}$ . Then

$$h' \sim n \times \left(\frac{l}{n^{1/2}}\right)^{7/2} \sim n^{-3/4}. \quad (2.174)$$

Alternatively, keeping  $|\mathbf{x}'|$  fixed,  $h' \sim n^{-1}$ . Consequently, as  $n \rightarrow \infty$ , the overall radiated gravity wave amplitude decreases, supporting the concept of generalized adjustment, in which the flow evolves so as to decrease the amplitude of the gravity waves it radiates.

There is, however, one key point about the generalized adjustment hypothesis. In the usual Rossby adjustment problem, the adjustment happens on the timescale of the inertial period, which is assumed short compared with the timescale of motions. Rossby adjustment is a fast process, as far as the balanced dynamics are concerned. For the type of adjustment due to gravity wave radiation experienced by the rotating ellipse, the opposite is true: the adjustment occurs on a very long timescale compared with the balanced dynamics.

## 2.6 Appendix A

The aim of this appendix is to show that the far field of (2.50) takes the form of the expected dipole when the logarithmic kernel is expanded for  $|\mathbf{x}'| \ll |\mathbf{x}|$ , and the error is an order of magnitude smaller, except for a logarithmic factor. We note that Crow (1970) remarks that his integrals will fail to converge after a certain number of moment expansions, but he does not rigorously address their asymptotic form. Ting & Miksis (1990) have presented a more careful analysis of the corresponding asymptotic forms in the three-dimensional problem, and

the analysis presented here is in the spirit of their paper, although the details are somewhat different.

In this appendix, we are considering the far field form of

$$\int_{\mathbb{R}^2} \nabla \cdot ((h_0 - f\psi_0)\mathbf{u}_0) \ln |\mathbf{x} - \mathbf{x}'| d^2\mathbf{x}'. \quad (2.175)$$

We note that, integrating (2.175) once by parts, this is equivalent to

$$\int_{\mathbb{R}^2} (h_0 - f\psi_0)\mathbf{u}_0 \cdot \frac{\mathbf{x} - \mathbf{x}'}{|\mathbf{x} - \mathbf{x}'|^2} d^2\mathbf{x}'. \quad (2.176)$$

We start by considering the form of the far field for  $\psi_0(\mathbf{x})$ . In (2.25), we suppose that  $\zeta_0$  is a  $C^\infty$  function of two variables. We assume further that  $\zeta_0$  is of compact support, so  $\exists \rho > 0$  such that  $\zeta_0(\mathbf{x}) = 0 \forall |\mathbf{x}| > \rho$ . Therefore  $|\zeta_0|$  is bounded with  $|\zeta_0| < Q \forall \mathbf{x}$ . It follows that,  $\forall |\mathbf{x}| > 2\rho$ ,

$$\left| \frac{\partial \psi}{\partial x_i} \right| = \frac{1}{2\pi} \left| \int_{\mathbb{R}^2} \zeta_0(\mathbf{x}') \frac{x_i - x'_i}{|\mathbf{x} - \mathbf{x}'|^2} d^2\mathbf{x}' \right| \quad (2.177)$$

$$\leq \frac{Q}{2\pi} \int_{|\mathbf{x}'| < \rho} \frac{1}{|\mathbf{x}| - \rho} d^2\mathbf{x}' \quad (2.178)$$

$$\leq \frac{Q\rho^2}{|\mathbf{x}|}, \quad (2.179)$$

where we obtain (2.178) from (2.177) by using Schwartz' formula in the form  $|\mathbf{x} - \mathbf{x}'| > |\mathbf{x}| - |\mathbf{x}'|$ .

Similarly

$$\left| \frac{\partial^2 \psi_0}{\partial x_i \partial x_j} \right| = \frac{1}{2\pi} \left| \int_{\mathbb{R}^2} \zeta_0(\mathbf{x}') \left( \frac{\delta_{ij}}{|\mathbf{x} - \mathbf{x}'|^2} - \frac{2(x_i - x'_i)(x_j - x'_j)}{|\mathbf{x} - \mathbf{x}'|^4} \right) d^2\mathbf{x}' \right| \quad (2.180)$$

$$\leq \frac{Q}{2\pi} \int_{|\mathbf{x}'| < \rho} \left( \frac{1}{(|\mathbf{x}| - \rho)^2} + \frac{2}{(|\mathbf{x}| - \rho)^2} \right) d^2\mathbf{x}' \quad (2.181)$$

$$\leq \frac{6Q\rho^2}{|\mathbf{x}|^2}. \quad (2.182)$$

Now let  $\chi = B_0 - f\psi_0$ . Since  $\zeta_0$  is a  $C^\infty$  function of compact support, so is  $\zeta_0 \nabla \psi_0$ , which is bounded with bound  $U$  (say). Then

$$|\chi(\mathbf{x})| = \frac{1}{2\pi} \left| \int_{\mathbb{R}^2} \zeta_0 \frac{\partial \psi_0}{\partial x'_j} \left( \frac{x_j - x'_j}{|\mathbf{x} - \mathbf{x}'|^2} - \frac{x_j}{|\mathbf{x}|^2} \right) d^2\mathbf{x}' \right| \quad (2.183)$$

$$= \frac{1}{2\pi} \left| \int_{\mathbb{R}^2} \zeta_0 \frac{\partial \psi_0}{\partial x_j} \left( \frac{2x_j \mathbf{x} \cdot \mathbf{x}' - x'_j |\mathbf{x}|^2 - x_j |\mathbf{x}'|^2}{|\mathbf{x}|^2 |\mathbf{x} - \mathbf{x}'|^2} \right) d^2 \mathbf{x}' \right| \quad (2.184)$$

$$\leq \frac{\mathcal{U}}{2\pi} \int_{|\mathbf{x}'| < \rho} \frac{3\rho |\mathbf{x}|^2 + \rho^2 |\mathbf{x}|}{|\mathbf{x}|^2 (|\mathbf{x}| - \rho)^2} d^2 \mathbf{x}' \quad (2.185)$$

$$\leq \frac{7\mathcal{U}\rho^3}{|\mathbf{x}|^2}, \quad (2.186)$$

where here we obtain (2.185) from (2.184) by expanding the numerator as a sum of the moduli of its components, and expand the denominator in the same way as in the step from (2.177) to (2.178). Similarly,

$$\left| \frac{\partial \chi}{\partial x_i} \right| = \frac{1}{2\pi} \left| \int_{\mathbb{R}^2} \zeta_0 \frac{\partial \psi_0}{\partial x'_j} \left( \frac{\delta_{ij}}{|\mathbf{x} - \mathbf{x}'|^2} - \frac{2(x_i - x'_i)(x_j - x'_j)}{|\mathbf{x} - \mathbf{x}'|^4} - \frac{\delta_{ij}}{|\mathbf{x}|^2} + \frac{2x_i x_j}{|\mathbf{x}|^4} \right) d^2 \mathbf{x}' \right| \quad (2.187)$$

$$\leq \frac{\mathcal{U}}{2\pi} \int_{|\mathbf{x}'| < \rho} \left( \frac{2|\mathbf{x}|\rho + \rho^2}{|\mathbf{x}|^2 (|\mathbf{x}| - \rho)^2} + \frac{12|\mathbf{x}|^2 \rho + 6|\mathbf{x}|^4 \rho^2 + 2|\mathbf{x}|^2 \rho^4}{|\mathbf{x}|^4 (|\mathbf{x}| - \rho)^4} \right) d^2 \mathbf{x}' \quad (2.188)$$

$$\leq \frac{126\mathcal{U}\rho^3}{|\mathbf{x}|^3}. \quad (2.189)$$

Now let  $\mathbf{g} = (h_0 - f\psi_0)\mathbf{u}$ . From (2.179, 2.182, 2.186, 2.189) we have:

**Lemma 1**  $\exists A, B > 0$  such that  $|g_i| < A|\mathbf{x}|^{-3}$  and  $|\partial g_i / \partial x_j| < B|\mathbf{x}|^{-4} \quad \forall |\mathbf{x}| > 2\rho$  and for  $i = 1, 2; j = 1, 2$ .

To proceed with our analysis of (2.176), we split the domain of integration  $\mathbb{R}^2$  into three parts:

$$\text{I } |\mathbf{x}'| < |\mathbf{x}| - 1$$

$$\text{II } |\mathbf{x}| - 1 < |\mathbf{x}'| < |\mathbf{x}| + 1$$

$$\text{III } |\mathbf{x}'| > |\mathbf{x}| + 1$$

### 2.6.1 Region I

In region (I), we consider

$$\int_{|\mathbf{x}'| < |\mathbf{x}| - 1} \mathbf{g}(\mathbf{x}') \cdot \left( \frac{\mathbf{x} - \mathbf{x}'}{|\mathbf{x} - \mathbf{x}'|^2} - \frac{\mathbf{x}}{|\mathbf{x}|^2} \right) d^2 \mathbf{x}' \quad (2.190)$$

in (2.176). We split region (I) into three subregions:

Ia  $|\mathbf{x}'| < 2\rho$

Ib  $2\rho < |\mathbf{x}'| < |\mathbf{x}|/2$

Ic  $|\mathbf{x}|/2 < |\mathbf{x}'| < |\mathbf{x}| - 1$

In region (Ia) we have

$$\left| \int_{I_a} g_j(\mathbf{x}') \frac{2x_j \mathbf{x} \cdot \mathbf{x}' - x'_j |\mathbf{x}|^2 - x_j |\mathbf{x}'|^2}{|\mathbf{x}|^2 |\mathbf{x} - \mathbf{x}'|^2} \right| \quad (2.191)$$

$$\leq \mathcal{G} \int_{|\mathbf{x}'| < 2\rho} \frac{6\sigma |\mathbf{x}|^2 + 4\sigma^2 |\mathbf{x}|}{|\mathbf{x}|^2 (|\mathbf{x}| - \sigma)^2} d^2 \mathbf{x}' \quad (2.192)$$

$$\leq 8\pi \mathcal{G} \rho^3 \frac{3|\mathbf{x}| + 2\rho}{|\mathbf{x}| (|\mathbf{x}| - 2\rho)^2} \quad (2.193)$$

$$\sim O\left(\frac{1}{|\mathbf{x}|^2}\right), \quad (2.194)$$

where, in (2.192),  $\sigma = |\mathbf{x}'|$ .

In region (Ib) we have

$$\left| \int_{I_b} g_j(\mathbf{x}') \frac{2x_j \mathbf{x} \cdot \mathbf{x}' - x'_j |\mathbf{x}|^2 - x_j |\mathbf{x}'|^2}{|\mathbf{x}|^2 |\mathbf{x} - \mathbf{x}'|^2} \right| \quad (2.195)$$

$$\leq 4\pi \int_{2\rho}^{\frac{1}{2}|\mathbf{x}|} \frac{A}{\sigma^3} \frac{3\sigma |\mathbf{x}|^2 + \sigma^2 |\mathbf{x}|}{|\mathbf{x}|^2 (|\mathbf{x}| - \sigma)^2} \sigma d\sigma \quad (2.196)$$

$$= \frac{4\pi A}{|\mathbf{x}|^2} \left[ 8 - \frac{4|\mathbf{x}|}{|\mathbf{x}| - 2\rho} + 3 \ln(|\mathbf{x}| - 2\rho) - 3 \ln 2\rho \right] \quad (2.197)$$

$$\sim O\left(\frac{\ln |\mathbf{x}|}{|\mathbf{x}|^2}\right). \quad (2.198)$$

In region (Ic) we have

$$\left| \int_{I_c} g_j(\mathbf{x}') \frac{2x_j \mathbf{x} \cdot \mathbf{x}' - x'_j |\mathbf{x}|^2 - x_j |\mathbf{x}'|^2}{|\mathbf{x}|^2 |\mathbf{x} - \mathbf{x}'|^2} \right| \quad (2.199)$$

$$\leq \int_{\frac{1}{2}|\mathbf{x}|}^{|\mathbf{x}|-1} \frac{3}{|\mathbf{x}| - \sigma} \frac{A}{\sigma^3} \sigma d\sigma \quad (2.200)$$

$$= \frac{3A}{|\mathbf{x}|^2} \left[ \ln(|\mathbf{x}| - 1) + 2 - \frac{|\mathbf{x}|}{|\mathbf{x}| - 1} \right] \quad (2.201)$$

$$\sim O\left(\frac{\ln |\mathbf{x}|}{|\mathbf{x}|^2}\right). \quad (2.202)$$

### 2.6.2 Region II

In region II we must consider the subregions

$$\text{IIa } |\mathbf{x} - \mathbf{x}'| < 1$$

$$\text{IIb } |\mathbf{x} - \mathbf{x}'| > 1$$

First we note that, from lemma 1 and Taylor's theorem with differential form of the remainder, we have that,  $\forall |\mathbf{x}|, |\mathbf{x}'| > 2\rho$ ,  $\exists C$  independent of  $|\mathbf{x}|$  such that

$$|\mathbf{g}(\mathbf{x}) - \mathbf{g}(\mathbf{x}')| < \frac{C}{|\mathbf{x}|^4} |\mathbf{x} - \mathbf{x}'|. \quad (2.203)$$

Thus, we write (IIa) as

$$\int_{|\mathbf{x}-\mathbf{x}'|<1} \frac{(\mathbf{g}(\mathbf{x}') - \mathbf{g}(\mathbf{x})) \cdot (\mathbf{x} - \mathbf{x}')}{|\mathbf{x} - \mathbf{x}'|^2} d^2 \mathbf{x}' + \mathbf{g}(\mathbf{x}) \cdot \int_{|\mathbf{x}-\mathbf{x}'|<1} \frac{\mathbf{x} - \mathbf{x}'}{|\mathbf{x} - \mathbf{x}'|^2} d^2 \mathbf{x}'. \quad (2.204)$$

Now,

$$\left| \int_{|\mathbf{x}-\mathbf{x}'|<1} \frac{(\mathbf{g}(\mathbf{x}') - \mathbf{g}(\mathbf{x})) \cdot (\mathbf{x} - \mathbf{x}')}{|\mathbf{x} - \mathbf{x}'|^2} d^2 \mathbf{x}' \right| < \frac{C}{|\mathbf{x}|^4} \int_0^{2\pi} \int_0^1 r dr d\theta = \pi C / |\mathbf{x}|^4, \quad (2.205)$$

whereas

$$\mathbf{g}(\mathbf{x}) \cdot \int_{|\mathbf{x}-\mathbf{x}'|<1} \frac{\mathbf{x} - \mathbf{x}'}{|\mathbf{x} - \mathbf{x}'|^2} d^2 \mathbf{x}' = |\mathbf{g}(\mathbf{x})| \int_0^{2\pi} \int_0^1 \frac{1}{r} r dr d\theta = 0. \quad (2.206)$$

In (IIb) we have

$$\left| \int_{\text{IIb}} \frac{\mathbf{g}(\mathbf{x}') \cdot (\mathbf{x} - \mathbf{x}')}{|\mathbf{x} - \mathbf{x}'|^2} d^2 \mathbf{x}' \right| < 8\pi A / |\mathbf{x}|^2, \quad (2.207)$$

since  $|\mathbf{x} - \mathbf{x}'|^{-1} < 1$  in IIb.

### 2.6.3 Region III

In III, we consider

$$\left| \int_{|\mathbf{x}'|>|\mathbf{x}|+1} \mathbf{g}(\mathbf{x}') \cdot \frac{\mathbf{x} - \mathbf{x}'}{|\mathbf{x} - \mathbf{x}'|^2} d^2 \mathbf{x}' \right| \quad (2.208)$$

$$< 2A \int_{|\mathbf{x}'|>|\mathbf{x}|+1} |\mathbf{x}'|^{-3} \left( \frac{1}{|\mathbf{x}'| - |\mathbf{x}|} \right) d^2 \mathbf{x}' \quad (2.209)$$

$$= 4\pi A \int_{|\mathbf{x}+1|}^{\infty} \frac{1}{r^2} \frac{1}{r-|\mathbf{x}|} dr \quad (2.210)$$

$$= 4\pi A \left( \frac{1}{|\mathbf{x}|^2} \ln(|\mathbf{x}|+1) - \frac{1}{|\mathbf{x}|(|\mathbf{x}|+1)} \right) \quad (2.211)$$

$$\sim O\left(\frac{\ln|\mathbf{x}|}{|\mathbf{x}|^2}\right). \quad (2.212)$$

Collecting (2.194, 2.198, 2.202, 2.205, 2.206, 2.207, 2.212) together we arrive at

$$\int_{\mathbb{R}^2} \nabla \cdot ((h_0 - f\psi_0)\mathbf{u}_0) \ln|\mathbf{x} - \mathbf{x}'| d^2\mathbf{x}' \quad (2.213)$$

$$\sim \frac{\mathbf{x}}{|\mathbf{x}|^2} \cdot \int_{\mathbb{R}^2} (h_0 - f\psi_0)\mathbf{u}_0(\mathbf{x}') d^2\mathbf{x}' + O\left(\frac{\ln|\mathbf{x}|}{|\mathbf{x}|^2}\right) \quad \square \quad (2.214)$$

## 2.7 Appendix B

We define the Fourier Transform  $\tilde{f}(\omega)$  of the function  $f(t)$  by

$$\tilde{f}(\omega) = \int_{-\infty}^{\infty} f(t) e^{i\omega t} dt, \quad (2.215)$$

as in equation (2.87). From Lighthill (1958), the Fourier Transform of  $\ln|x|H(x)$  is

$$\ln|\tilde{t}|H(t) = -\frac{1}{i\omega} \left( \frac{i\pi}{2} \operatorname{sgn}\omega + \ln|\omega| \right) + \frac{\gamma}{i\omega}. \quad (2.216)$$

Using shifting formulae, it follows that the Fourier Transform of  $e^{ift} \ln|t|H(t)$  is

$$e^{ift} \ln|\tilde{t}|H(t) = -\frac{1}{i(\omega-f)} \left( \frac{i\pi}{2} \operatorname{sgn}(\omega-f) + \ln|\omega-f| \right) + \frac{\gamma}{i(\omega-f)}, \quad (2.217)$$

and hence the Fourier transform of the integral

$$\int_0^{\infty} \ln \tau e^{if\tau} (g'(t-\tau) - ifg(t-\tau)) \quad (2.218)$$

is

$$-\tilde{g}(\omega) \left( \frac{i\pi}{2} \operatorname{sgn}(\omega-f) + \ln|\omega-f| + \gamma \right). \quad (2.219)$$

and hence the Fourier transform of

$$2 \int_0^{\infty} \ln \tau \frac{d}{d\tau} [\cos f\tau g(t-\tau)] \quad (2.220)$$

is

$$-\tilde{g}(\omega) \left[ \frac{i\pi}{2} (\operatorname{sgn}(\omega-f) + \operatorname{sgn}(\omega+f)) + \ln|\omega^2 - f^2| + 2\gamma \right]. \quad (2.221)$$

Now,

$$\ln |\omega^2 - f^2| + \operatorname{sgn}(\omega - f) + \operatorname{sgn}(\omega + f) = \ln(\omega^2 - f^2) \mp i\pi, \quad (2.222)$$

where the sign of  $\mp$  in (2.222) is set by the choice of analytic branch of the logarithm function. Therefore, with the appropriate choice of the branch of the logarithm,

$$-(\omega^2 - f^2)^2 \tilde{\sigma}(\omega) \left( \frac{1}{8} \left( \ln(\omega^2 - f^2) + 2\gamma \right) \mp \frac{i\pi}{8} \right) \quad (2.223)$$

has an inverse Fourier transform

$$\int_0^\infty \ln \tau \frac{d}{d\tau} (\cos f\tau g(t - \tau)), \quad (2.224)$$

where

$$\tilde{g}(\omega) = \frac{1}{16} (\omega^2 - f^2)^2 \tilde{\sigma}(\omega), \quad (2.225)$$

and where (2.224) is an integral over the entire past history of the dynamics. If the other analytic branch of the logarithm is taken in (2.222), the result is that the integral (2.224) becomes an integral over the entire future evolution of the dynamics. The radiation condition is equivalent to imposing the choice of branch of logarithm which gives rise to (2.224).

## Chapter 3

# Instability of vortices and jets

### 3.1 Introduction

In chapter 2, some general properties of gravity wave generation by vortical motions were derived in the asymptotic limit of low Froude number  $F$ . It was shown that, in the vortical region, the first corrections to the incompressible vortical dynamics which are required to take account of non-zero divergence occur at  $O(F^2)$  and  $O(F^2 \ln F)$ . On the basis of this elementary scale analysis, one might therefore expect gravity wave activity to be observed in the vortical flow at  $O(F^2)$ . However, the  $O(F^2)$  and  $O(F^2 \ln F)$  corrections can be determined entirely in terms of the instantaneous vortical flow, and thus represent balanced corrections to the leading order dynamics. The effect of gravity wave radiation is felt in the vortical region at  $O(F^4)$ , two orders higher in the expansion parameter than might have been expected from elementary scale analysis. The particular flow of the Kirchoff ellipse of uniform potential vorticity was analysed. The ellipse experienced elongation as a result of gravity wave radiation. The elongation either ceased at the aspect ratio at which the radiation from the ellipse was reduced to the inertial frequency, or continued until the ellipse reached a “splitting” aspect ratio of 4.6:1, at which the ellipse split in two. The elongation of the ellipse represents the effect of gravity wave radiation in the vortical flow which generates it, and the elongation rate of the ellipse was therefore  $O(F^4)$ . If we suppose now that the eccentricity of the ellipse is small, we may regard this elongation as the growth of a mode of instability on an axisymmetric vortex, with an eigenfunction of the form  $f(r)e^{i(2\theta-\omega t)}$ , where  $\theta$  is the azimuthal angle, and  $\omega$  is the eigenfrequency. Here,  $\omega$  is real at  $O(1)$  and  $O(F^2)$ , but contains an imaginary part at  $O(F^4)$ . The eigenmode consists of a vortical or Rossby wave on the boundary of the vortex, coupled to a gravity wave far from the vortex. The growth rate of the instability is a measure of the degree of interaction between vortical motions and gravity waves in the system.

The concept of instabilities due to coupling between different waves has been the subject of a paper by Sakai (1989). In the most general form of the theory, he advocates decomposing the system of eigenvector equations to be studied into distinct wave vectors, which are neutral non-interacting modes of some reference system, but which interact in the system of interest due to the presence of a mean flow, second layer or other destabilizing phenomenon. Once the decomposition into a system of wave functions is accomplished, the resulting matrix eigenvalue analysis for the system of interest is lengthy but routine. The structure of the unstable eigenmodes in terms of the modes of the reference system elucidates which wave – wave inter-

actions are responsible for the instability. However, if the eigenmodes can be analysed in some asymptotic limit, as here in the case of low Froude number or high mode number, it is possible to elucidate the nature of the wave mode interactions which are responsible for the instability without recourse to lengthy matrix eigenvalue analysis. This asymptotic approach has been used by Knessel & Keller (1992) in their analysis of a short wavelength instability found by Griffiths *et al.* (1982) which is due to gravity wave – gravity wave interaction.

Within this wave mode instability framework, conventional barotropic instability and baroclinic instability are to be regarded as due to Rossby wave – Rossby wave interactions. They both arise due to opposite signs of the potential vorticity gradient in the flow, either at different horizontal locations (in the case of barotropic instability) or on different vertical levels (in the case of baroclinic instability).

Gravity wave – gravity wave instabilities are also fairly common, and have been found in single layer shear flows with uniform potential vorticity (Satomura 1981; Kubokawa 1986; Hayashi & Young 1987). Kelvin – Helmholtz instability is also a manifestation of gravity wave – gravity wave instability. The instability exists due to gravity waves which develop on either side of a density jump in stratified shear flow, just as Rossby waves develop on either side of a strip of potential vorticity in barotropic instability.

Rossby wave – gravity wave instability, however, is a comparatively unfamiliar phenomenon. Sakai (1989) has clearly demonstrated a Rossby wave – gravity wave instability in a two-layer parallel shear flow at moderate Rossby number. He has also suggested the several previously discovered instabilities are candidates for a description in terms of Rossby wave – gravity wave interaction. In many of the studies he discusses, an interface between two fluids of different density intersects a free surface, and the “gravity wave” part of the Rossby wave – gravity wave instability is supposed to be the wave at the free surface intersection.

Within the context of barotropic shallow water vortex dynamics, which is the topic of this thesis, the model problem consists of a semi-infinite layer of light fluid, of finite depth, on top of an infinite layer of heavy fluid of infinite depth (see figure 3.1). Paldor (1983) has shown that, if the potential vorticity in the upper layer is uniform everywhere where it has non-zero depth, the eigenmodes of the system are always neutral. Killworth & Stern (1982) have shown that an instability will always be present when the potential vorticity in the upper layer increases away from the interface. I believe that this wave is more properly a generalization of a Rossby

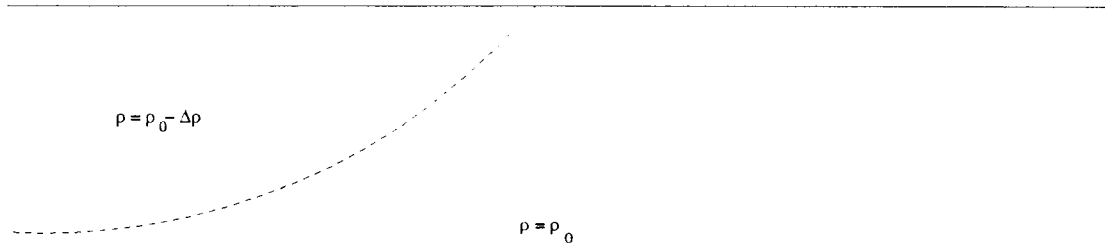


Figure 3.1: Schematic diagram depicting a semi-infinite single layer of fluid.

wave in the upper layer, with finite potential vorticity on one side of the interface, and infinite potential vorticity (zero depth) on the other side. Consider first the case where the potential vorticity is finite on both sides of the interface. In such circumstances, a wave on the boundary between the two regions would clearly be regarded as a Rossby wave. Then, since at all finite values of potential vorticity we would regard the wave on the interface between the two regions of different potential vorticity as a Rossby wave, it seems perverse to suggest, as Sakai (1989) does, that we should regard it as a gravity wave in the singular case of infinite potential vorticity on one side of the interface. The condition for instability found by Killworth & Stern (1982), that the potential vorticity increase away from the interface, is simply a condition which ensures that the interface is a minimum of potential vorticity, and that there is therefore a change in the potential vorticity gradient in the upper layer at the interface.

The shallow water vortex instability, discussed partially in chapter 2 in terms of the elongation of the elliptical vortex, is a clear case of Rossby wave – gravity wave instability in a single layer model. It was discovered first in the non-rotating two dimensional ideal gas equations by Broadbent & Moore (1979). They consider a vortex of radius  $a$ , with uniform vorticity  $2\Omega$  for  $r < a$ , and zero vorticity for  $r > a$ . Such a vortex is commonly referred to as a “Rankine vortex”. They define a Mach number  $M$  based on the vortex boundary velocity, so that  $M = \Omega a / c_0(a)$ , where  $c_0$  is the sound speed  $c_0^2(r) = \gamma p_0(r) / \rho_0(r)$ . They consider eigenfunctions of the form  $f(r)\epsilon^{i(m\theta - \omega t)}$ , where  $m$  represents the azimuthal mode number of the disturbance. They show numerically that, as  $M$  is increased away from zero, the growth rates of instabilities are non-zero for mode numbers  $m = 2, 3, 4, 6, 8$ . For each  $m$ , they investigate only one eigenmode, which reduces to the neutral mode found by Kelvin (1880) in the limit  $M \rightarrow 0$ , with eigenfrequency  $\omega = \Omega - 1$ . At small  $M$  the growth rates scale as  $M^{2m}$  (Kop’ev & Leont’ev, 1983), meaning that large mode numbers are less unstable than small ones for small  $M$ . Indeed, it can be clearly seen from figure 3 of Broadbent & Moore (1979) that, for moderate Mach number  $M$ , growth

rates of the instability remain smaller for larger mode numbers than smaller ones.

For  $M < 2.236$ , modes  $m = 2, 3, 4, 6, 8$  are found to be unstable for all  $M$ . The maximum growth rates obtained by Broadbent & Moore for a given  $M$  were always found at mode  $m = 2$ . The overall maximum growth rate occurred at  $M \approx 1.5$ , with  $\text{Im}(\omega) \approx 0.012$ . The growth rates remain small over the whole range of values of  $M < 2.236$ , suggesting that the strength of Rossby wave – gravity wave coupling might be small even at quite large Froude numbers. When  $M = 2.236$  Broadbent & Moore are obliged to terminate their numerical eigenvalue calculations, since then the density vanishes at the centre of the vortex.

Sozou (1987) showed that the mode investigated by Broadbent & Moore (1979) is not the only unstable mode in the compressible Rankine vortex, and that there are an infinite number of modes for which  $\omega = \Omega - O(M^2)$ . These modes are singular in the limit  $M = 0$ , but non-singular for all non-zero  $M$ . They typically have growth rates at least an order of magnitude smaller than the corresponding Broadbent – Moore mode (Sozou 1987, table 1).

A general stability theorem for axisymmetric shallow water vortices was given by Ripa (1987). It was derived by variational methods, and therefore provides a sufficient condition for stability. The condition is that the axisymmetric flow with azimuthal velocity  $V(r)$  and height field  $H(r)$  is stable if

$$(V - \lambda r)^2 < H(r) \quad (3.1)$$

$$(V - \lambda r) \frac{dQ}{dr} \geq 0 \quad (3.2)$$

$$\text{for some } \lambda, \quad (3.3)$$

where  $Q = (f + dV/dr + V/r)/H(r)$  is the potential vorticity in the basic state. In the case of an isolated vortex in unbounded shallow water, (3.1) can only be satisfied if  $\lambda = 0$ . Then, if the vortex is cyclonic, with the potential vorticity inside the vortex exceeding the value outside, we would expect the azimuthal velocity  $V(r)$  at the boundary of the vortex to be anticlockwise, i.e. positive. Consequently,  $VdQ/dr$  will be zero everywhere except at the boundary of the vortex, where it will be negative. Similarly, if the vortex is anticyclonic, with  $dQ/dr > 0$ , we expect  $V(r) < 0$  at the vortex boundary. In either case,  $V(r)dQ/dr < 0$  at the vortex boundary, and (3.2) is not satisfied. Therefore it is not possible to obtain any stability results for an axisymmetric vortex with a monotonic potential vorticity profile by variational methods, no matter how small the Froude and Rossby numbers might be.

A general stability theorem for parallel flow stability in shallow water was given by Ripa (1983). In this case, the sufficient condition for stability of the flow with jet velocity  $U(y)$  and layer depth  $H(y)$  is

$$(\lambda - U(y)) \frac{dQ}{dy} \geq 0 \quad (3.4)$$

$$(\lambda - U(y))^2 < H(y) \quad (3.5)$$

$$\text{for some } \lambda. \quad (3.6)$$

Now, if the potential vorticity gradient is concentrated in a single jump, at  $y = 0$ , say, then  $U(y)dQ/dy < 0$  at  $y = 0$ , and we may take  $\lambda = U(0)$  to satisfy (3.4). The remaining condition (3.5) then states that the flow must be everywhere subsonic with respect to the velocity of the potential vorticity jump  $(U(0) - U(y))^2 < H(y)$ . Unlike the case of axisymmetric flow, it is now possible to show that the flow is stable provided the ratio of potential vorticities across the jump is less than 4.

One of the aims of this thesis is to investigate the strength of Rossby wave – gravity interactions in the shallow water system. The growth rates of Rossby wave – gravity wave instabilities in axisymmetric and parallel flows are therefore of fundamental interest, and the remainder of the chapter is organised as follows:

In §3.2, the instability of an axisymmetric vortex with a single discontinuity in potential vorticity is analysed. The results at finite Froude number will differ from those of Broadbent & Moore (1979) at finite Mach number, in that in this study the potential vorticity, rather than vorticity, is taken to be constant within the vortex. This prevents the evacuation of the basic state found by Broadbent & Moore. As the background rotation rate  $f$  is increased, the low mode number disturbances cease to be unstable. A WKBJ analysis is therefore performed, and it is found that large mode number disturbances to an axisymmetric vortex are always unstable, no matter how small the Froude and Rossby numbers might be.

In §3.3 we investigate the effect of smoothing the potential vorticity profile within the context of the WKBJ analysis. It is found that the instability persists, provided the potential vorticity gradient is confined to within a region of size  $o(m^{-1})$ , so that Rossby wave critical layers at  $\omega = mV/r$  induce phase shifts which are no more than exponentially weak in  $m$ . The Sozou modes are shown to exist due to the non-uniform potential vorticity within the Rankine vortex at non-zero Mach number, which therefore supports a spectrum of Rossby waves within

the vortex in addition to the single Rossby wave on the vortex boundary.

In §3.4, we discuss the results of the analysis in §3.2 in relation to the question of existence or non-existence of a slow manifold for the shallow water equations. Since the WKBJ analysis has shown that a Rossby wave – gravity wave instability exists at arbitrarily small Rossby number, the result is that a true slow manifold, in the sense of no identifiable gravity wave – like structure at small non-zero Rossby number, cannot exist, because the large mode number eigenmodes will always possess a gravity wave - like tail. Mathematically, one can show that a slow manifold, if it exists at all, cannot then be unique, precisely because of the presence of the instability at arbitrarily small Rossby number.

In §3.5 the instability of a parallel flow with a single discontinuity of potential vorticity is investigated. The potential vorticity in the region  $y < 0$  is taken to be unity, while the potential vorticity in the region  $y > 0$  takes a value  $q > 1$ . It is found via a WKBJ analysis that the stability bound found by Ripa (1983) is an exact stability boundary, with unstable modes for all  $q > 4$ . The limit  $q \rightarrow \infty$  is singular, and if  $q$  is rescaled such that  $q = O(k^{4/3})$ , the growth rate of the instability tends to zero, as  $q/k^{4/3} \rightarrow \infty$ , consistent with the analysis of Paldor (1983), and supporting the contention that the interfacial wave should be viewed as a Rossby wave, rather than a gravity wave.

In §3.6, some final conclusions to this chapter are offered.

## 3.2 Instability of a circular vortex with discontinuous potential vorticity

### 3.2.1 The basic state

In this section, we shall restrict our attention to basic states with a single radial discontinuity of potential vorticity. Following the same scaling of the shallow water equations as in chapter 2, but not now assuming  $F \ll 1$ , the basic state equations are

$$\frac{d\bar{h}}{dr} = f\bar{v} + \frac{\bar{v}^2}{r} \quad (3.7)$$

$$\frac{d\bar{v}}{dr} + \frac{\bar{v}}{r} = Q(1 + F^2\bar{h}) - f. \quad (3.8)$$

These must be solved subject to regularity conditions at  $r = 0$ , and decay conditions as  $r \rightarrow \infty$ . The nonlinearity in (3.7) means that we must use numerical means to solve (3.7,3.8), except in

the limit  $F \ll 1$ , where they can be solved by matched asymptotic expansion.

The free parameters in the problem are  $f$  and  $F$ . The nondimensionalizations of chapter 2 allow us to take the vortex to be of unit radius, the potential vorticity jump across the boundary of the vortex to be of unit strength, and the layer to be of unit mean depth. Then  $Q = f$  for  $r > 1$ , and  $Q = f + 1$  for  $r < 1$ .

### 3.2.2 The disturbance equations

Disturbance equations are derived for a single azimuthal wavenumber  $m$  and frequency  $\omega$ , so that the disturbance variables are expressible in the form  $g(r)e^{im\theta - i\omega t}$ . They are

$$i\sigma v_r - (f + 2\bar{v}/r)v_\theta + \frac{dh}{dr} = 0 \quad (3.9)$$

$$i\sigma v_\theta + Q(1 + F^2\bar{h})v_r + \frac{1}{r}imh = 0 \quad (3.10)$$

$$F^2 \left( i\sigma h + (f\bar{v} + \bar{v}^2/r)v_r \right) + (1 + F^2\bar{h}) \left( \frac{dv_r}{dr} + \frac{v_r}{r} + \frac{1}{r}imv_\theta \right) = 0, \quad (3.11)$$

where  $\sigma = -\omega + m\bar{v}/r$ .

This set of equations must be solved subject to regularity conditions at  $r = 0$ , and a radiation/evanescence condition as  $r \rightarrow \infty$ .

The equations (3.9 - 3.11) contain only two radial derivatives, and therefore represent a second order differential equation for the eigenfunctions. If one chooses  $v_r$  and  $h$  as variables,  $v_\theta$  must be obtained from (3.10). The possibility of a critical layer at  $\sigma = 0$  makes it impossible to ensure that this will be a successful method. Instead, we choose to eliminate  $h$ . After some algebra, one obtains a pair of first order ordinary differential equations for the eigenmodes:

$$\frac{dv_r}{dr} = A(r)v_r + B(r)v_\theta \quad (3.12)$$

$$\frac{dv_\theta}{dr} = C(r)v_r + D(r)v_\theta, \quad (3.13)$$

where

$$A(r) = \frac{F^2\sigma Q r}{m} - \frac{1}{r} \frac{d}{dr} \ln H \quad (3.14)$$

$$B(r) = \frac{iF^2\sigma^2 r}{H m} - \frac{im}{r} \quad (3.15)$$

$$C(r) = \frac{iF^2 H Q^2 r}{m} + \frac{im}{r} + \frac{iH}{\sigma} \frac{dQ}{dr} \quad (3.16)$$

$$D(r) = -\frac{F^2 Q \sigma r}{m} - \frac{1}{r}, \quad (3.17)$$

and  $H = 1 + F^2\bar{h}$ .

The advantage of this formulation over the standard formulation (3.9 - 3.11) is that the critical layer singularity  $\sigma = 0$  occurs only where there are radial gradients of the basic state potential vorticity  $Q(r)$ . If the potential vorticity gradients are confined to a single discontinuity in potential vorticity at the vortex boundary, the eigenfunction equations are non-singular, and at the vortex boundary we impose continuity of  $h$  and  $v_r$ . Dividing (3.10) by  $v_r$ , we thereby obtain a continuity equation

$$\left[ \sigma \frac{v_\theta}{v_r} \right] = \left[ iQ(1 + F^2\bar{h}) \right], \quad (3.18)$$

where  $[\alpha]$  represents the jump in a quantity  $\alpha$  across the vortex boundary.

### 3.2.3 The limit $F \ll 1$

Before proceeding to numerical calculation of the eigenvalues of the system (3.12 - 3.17), we consider the limit  $F \ll 1$ .

In chapter 2 we showed that matching conditions between the vortical region and the gravity wave region led to a wave field in which the principal wave component was a quadrupole. This was forced by unsteady terms of the form  $r^{-2}e^{2i\theta}$  present in the streamfunction in the limit of  $r \rightarrow \infty$ . In the case of a mode 2 perturbation to an axisymmetric vortex, these terms appear due to the unsteadiness in velocity and height fields induced by the perturbation of the vortex boundary. The effect of the radiation appears at  $O(F^4)$ , the effect of which is to destabilize the vortex.

From the viewpoint of an instability, we therefore have growth of a mode 2 perturbation to an axisymmetric vortex, with a growth rate of order  $F^4$ . Higher order perturbations to the vortex do not produce quadrupole far fields, since they have  $m$ -fold rotational symmetry, and their streamfunction far fields take the form  $r^{-m}e^{im\theta}$ . Rescaling the radial coordinate to  $R = Fr$ , appropriate for the wave region, we have wave fields in streamfunction, velocity potential and height of form  $H_m(\sqrt{\omega^2 - f^2}R)e^{i(m\theta - \omega t)}$  at order  $F^m$ , and therefore the first out of phase contribution in the matching conditions for the inner problem occurs at order  $O(F^{2m})$ . Hence in general at low Froude number the vortex has mode  $m$  instabilities with growth rates  $O(F^{2m})$ .

However, we must also consider the real part of the frequency, which must lie above the

inertial frequency  $|f|$  if waves are to propagate and the out of phase terms are to appear in the matching conditions. The analysis for the circular vortex at  $F = 0$  was first performed by Kelvin (1880), who found that

$$\omega = \frac{1}{2}(m - 1). \quad (3.19)$$

It follows that we shall require  $m > 1 + 2|f|$  for instability at low  $F$ . The fastest growing  $m = 2$  modes are inhibited by the presence of background rotation, and for small to moderate Rossby numbers the first unstable mode could occur at quite a large value of  $m$ , and hence quite a small growth rate of order  $F^{2m}$ .

### The basic state

We begin our analysis by establishing the form of the basic state from considering the basic state equations (3.7-3.8) in the limit  $F \ll 1$ . From the analysis of chapter 2, we require two asymptotic regions –  $r = O(1)$  and  $r = O(F^{-1})$ .

We begin with the region  $r = O(1)$ . We expand

$$\bar{v} = \bar{v}_0 + F^2 \bar{v}_2 + \dots \quad (3.20)$$

$$\bar{h} = \bar{h}_0 + F^2 \bar{h}_2 + \dots \quad (3.21)$$

Here we allow for the possibility that the matching conditions might introduce  $\ln F$  terms into the expansions (3.20,3.21). Substituting (3.20,3.21) into (3.8) gives, at leading order

$$\frac{d\bar{v}_0}{dr} + \frac{\bar{v}_0}{r} = \begin{cases} 1 & \text{for } r < 1 \\ 0 & \text{for } r > 1 \end{cases}. \quad (3.22)$$

Imposing regularity at  $r = 0$ , and  $r^{-1}$  decay at  $r \rightarrow \infty$ , we have

$$\bar{v}_0 = \begin{cases} \frac{1}{2}r & \text{for } r < 1 \\ \frac{1}{2}r^{-1} & \text{for } r > 1 \end{cases}. \quad (3.23)$$

The equation for  $\bar{h}_0$  is

$$\frac{d\bar{h}_0}{dr} = f\bar{v}_0 + \frac{\bar{v}_0^2}{r}. \quad (3.24)$$

Substituting (3.23) into (3.24) we find

$$\bar{h}_0 = \begin{cases} \frac{1}{8}(2f + 1)r^2 + C_1 & \text{for } r < 1 \\ \frac{1}{2}f \ln r - \frac{1}{8}r^{-2} + C_2 & \text{for } r > 1 \end{cases}, \quad (3.25)$$

where  $C_1$  and  $C_2$  are constants, to be determined by continuity of  $\bar{h}_0$  at  $r = 1$ , and matching to the outer solution.

Proceeding now to the outer region, we define a long range variable  $R = Fr$ . Since  $\bar{v}_0 \sim r^{-1}$  as  $r \rightarrow \infty$ , we rescale  $\bar{v}_0$  by  $F$ , so

$$\bar{h}_0 = H(R) + O(F^2) \quad (3.26)$$

$$\bar{v}_0 = FV(R) + O(F^3). \quad (3.27)$$

Then substituting (3.26, 3.27) into (3.7,3.8) we obtain

$$\frac{dV}{dR} + \frac{V}{R} = fH \quad (3.28)$$

$$\frac{dH}{dR} = fV. \quad (3.29)$$

Combining (3.28) & (3.29) into a single equation for  $V(R)$ , we have

$$\frac{d^2V}{dR^2} + \frac{1}{R} \frac{dV}{dR} - \left( f^2 + \frac{1}{R^2} \right) V = 0. \quad (3.30)$$

Imposing decaying boundary conditions as  $R \rightarrow \infty$ , (3.30) has solution

$$V(R) = AK_1(|f|R), \quad (3.31)$$

where  $K_1$  is the modified Bessel function of order one, and  $A$  is a constant. Matching to the velocity field in the vortical region (3.23) gives

$$A = \frac{1}{2}|f|. \quad (3.32)$$

It follows that

$$H(R) = -\frac{1}{2}fK_0(|f|R). \quad (3.33)$$

For small  $R$ , we have

$$H(r) = \frac{1}{2}f \left( \ln \left( \frac{1}{2}|f|R \right) + \gamma \right) + O(R^2 \ln R). \quad (3.34)$$

and matching to (3.25) gives

$$C_2 = \frac{1}{2}f \left( \ln \left( \frac{1}{2}|f|F \right) + \gamma \right). \quad (3.35)$$

Note the appearance of the  $\ln F$  term. This means that  $\bar{h}_0$  starts at  $O(\ln F)$ . Then finally

$$C_1 = \frac{1}{2}f \left( \ln \left( \frac{1}{2}|f|F \right) + \gamma \right) - \frac{1}{4}(f+1). \quad (3.36)$$

The analysis presented is valid in the limit  $f \rightarrow 0$ , in which limit

$$V(R) = \frac{1}{2R}; \quad H(R) = O(F^2); \quad C_1 = -\frac{1}{4}; \quad C_2 = 0. \quad (3.37)$$

Having obtained the leading order solutions for  $\bar{v}_0$  and  $\bar{h}_0$  in both asymptotic regions, we could now go on to develop perturbation expansions to obtain equations for  $\bar{v}_2, \bar{h}_2 \dots$ . However, as we shall see, such corrections are not required to compute the growth rate of the instability, and serve only to correct the real part of the eigenfrequency. Indeed, the expression for  $\bar{h}_0$  is not really essential to the  $F \ll 1$  analysis, although it is required to initialize the numerical eigenvalue calculations in the  $F \ll 1$  limit.

### The disturbance equations

As for the analysis of the basic state, we expand  $v_r$  and  $v_\theta$  in asymptotic series with  $F^2$  as the expansion parameter. The asymptotic expansions are matched between two regions, with range variables  $r$  and  $R \equiv Fr$  as before (see also chapter 2). Additionally, the eigenvalue  $\omega$  must be expanded in powers of  $F^2$ , with logarithmic terms as necessary.

Substituting (3.14 - 3.17) into (3.12,3.13) in the limit  $F \ll 1$  gives equations for  $v_r$  and  $v_\theta$

$$\frac{dv_r}{dr} = -\frac{1}{r}v_r - \frac{im}{r}v_\theta \quad (3.38)$$

$$\frac{dv_\theta}{dr} = \frac{im}{r}v_r - \frac{1}{r}v_\theta. \quad (3.39)$$

The solutions are

$$v_r = r^{m-1}; \quad v_\theta = ir^{m-1} \quad (3.40)$$

or

$$v_r = r^{-m-1}; \quad v_\theta = -ir^{-m-1}. \quad (3.41)$$

Regularity as  $r \rightarrow 0$  implies we take an eigenfunction of form (3.40) in  $r < 1$ . Decay as  $r \rightarrow \infty$  implies we take an eigenfunction of form (3.41) in  $r > 1$ . Then, substituting into the continuity equation (3.18) gives  $\omega = m\bar{v}(1) - 1/2$ , which gives Kelvin's result (3.19) on substitution of the basic state (3.23), for which  $\bar{v}(1) = 1/2$ , valid in the limit  $F = 0$ .

Rather than proceeding to consider higher orders in  $F$  in the inner expansion, we will

consider the leading order outer expansion. There the disturbance equations are

$$\frac{dv_r}{dR} = -\left(\frac{\omega f R}{m} + \frac{1}{R}\right)v_r + \left(\frac{i\omega^2 R}{m} - \frac{im}{R}\right)v_\theta \quad (3.42)$$

$$\frac{dv_\theta}{dR} = \left(\frac{if^2 R}{m} + \frac{im}{R}\right)v_r + \left(\frac{f\omega R}{m} - \frac{1}{R}\right)v_\theta. \quad (3.43)$$

They have solution

$$v_r = A \left[ i\omega\lambda H_{m-1}(\lambda R) - i\frac{m}{R}(\omega + f)H_m(\lambda R) \right] \quad (3.44)$$

$$v_\theta = A \left[ f\lambda H_{m-1}(\lambda R) - \frac{m}{R}(\omega + f)H_m(\lambda R) \right], \quad (3.45)$$

where  $\lambda^2 = (\omega^2 - f^2)$ ,  $H_m$  is a Hankel function of degree  $m$ , of the first or second kind, and  $A$  is an arbitrary constant. The kind of the Hankel function is chosen to give radiation conditions at infinity. With  $e^{-i\omega t}$  time dependence, one chooses Hankel functions of the first kind for radiation conditions.

Now the outer limit of the inner expansions for  $v_r$  and  $v_\theta$  have  $r^{-m-1}$  behaviour. Therefore in the outer region we start our expansions for  $v_r$  and  $v_\theta$  at  $O(F^{m+1})$ . This is consistent with waves in  $\psi$ ,  $\phi$  and  $h$  at  $O(F^m)$ . If a formal expansion is carried out for the inner region, we see from (3.14 - 3.17) that it proceeds by first obtaining the fields at a given order, and then obtaining  $\omega$  at that order from the matching conditions. To obtain  $v_r$  and  $v_\theta$  to order  $F^{2n}$  for some integer  $n$ , one need only know  $\omega$  to order  $F^{2(n-1)}$ . The continuity condition (3.18) then gives  $\omega$  at order  $F^{2n}$ .

Since the eigenvalue equations are linear in  $v_r$  and  $v_\theta$ , the amplitude of the leading order solution given by (3.40) for  $r < 1$  and (3.41) for  $r > 1$  is not specified uniquely, and at higher orders in the perturbation expansion it is possible to add to the solution at that order a component of the leading order eigenfunction. To specify the eigenfunction uniquely, we impose the condition that the coefficients of  $r^{m-1}$  in the expansions of  $v_r$  and  $v_\theta$  in the limit  $r \rightarrow 0$  are zero at all orders in  $F$  except the leading order. This then fixes the amplitude and phase of the eigenfunction at all orders in  $F$ . Then, without reference to the outer expansion, one can see that the velocity components  $v_r$  and  $v_\theta$  remain  $\pi/2$  out of phase with each other at all subsequent orders in  $F$  in the inner expansion, and therefore  $\omega$  remains real until the matching conditions with the wave region must be taken into account.

Matching (3.41) onto (3.44,3.45) to determine the amplitude of the gravity waves in the outer expansion gives

$$A = -\frac{\pi \lambda^m}{2^m m! (\omega + f)}. \quad (3.46)$$

Then matching the out-of-phase  $J_m$  terms in the Hankel functions (3.44, 3.45) back onto the inner solution at order  $O(F^{2m})$  gives a contribution to the inner solution of the form

$$v_r = -iBr^{m-1}; \quad v_\theta = Br^{m-1}, \quad (3.47)$$

where  $B$  is determined from  $A$  and the properties of the Hankel function in the limit  $R \rightarrow 0$ . It is given by

$$B = \frac{\pi m}{(m!)^2} \left( \frac{\omega^2 - f^2}{4} \right)^m \left( \frac{\omega - f}{\omega + f} \right). \quad (3.48)$$

As we discussed above, to make the expansion procedure well defined, the expansions for  $v_r$  and  $v_\theta$  in  $r < 1$  are to be  $o(r^{m-1})$  for  $r \ll 1$ , and hence we must add to (3.47) functions of form (3.41) to ensure continuity of  $v_r$  at  $r = 1$ . All other contributions to  $v_r$  and  $v_\theta$  at all orders up to and including  $F^{2m}$  contribute only to the real part of  $\omega$ , and not to the growth of the instability.

To calculate the growth rate of the instability, it is therefore sufficient to consider the velocity fields

$$v_r = \begin{cases} r^{m-1} & \text{for } r < 1 \\ r^{-m-1} - iBF^{2m}(r^{m-1} - r^{-m-1}) & \text{for } r > 1 \end{cases} \quad (3.49)$$

$$v_\theta = \begin{cases} ir^{m-1} & \text{for } r < 1 \\ -ir^{-m-1} + BF^{2m}(r^{m-1} + r^{-m-1}) & \text{for } r > 1 \end{cases}. \quad (3.50)$$

Returning to the jump condition (3.18), we obtain

$$\text{Im}(\omega) = \frac{\pi m F^{2m}}{2(m!)^2} \left( \frac{\omega^2 - f^2}{4} \right)^m \left( \frac{\omega - f}{\omega + f} \right) + O(F^{2m+2}). \quad (3.51)$$

### 3.2.4 Numerical eigenvalue calculations

#### Numerical technique

We start by considering techniques for solving numerically the basic equations (3.7, 3.8) for the basic state variables  $\bar{v}$  and  $\bar{h}$ . The numerical difficulties arise in that both  $r = 0$  and  $r = \infty$  are singular points of the system, and we can only apply boundary conditions there by making use of some expansion of the solutions for small  $r$  and large  $r$  respectively. Given initial guesses for  $\bar{h}(0)$  and  $\bar{h}(\infty)$ , the basic state equations can then be integrated to  $r = 1$ , and iteration on  $\bar{h}(0)$  and  $\bar{h}(\infty)$  used to make  $\bar{h}$  and  $\bar{v}$  continuous across the vortex boundary  $r = 1$ .

We consider first the singular point  $r = \infty$ . In this limit, we will impose conditions that  $\bar{v}$  and  $\bar{h}$  tend to zero as  $r \rightarrow \infty$ . By manipulation of the equations (3.7, 3.8), one obtains

$$\frac{d^2\bar{h}}{dr^2} + \frac{1}{r} \frac{d\bar{h}}{dr} - F^2 f^2 \bar{h} = \frac{2\bar{v}}{r} \frac{d\bar{v}}{dr} \quad (3.52)$$

$$\frac{d^2\bar{v}}{dr^2} + \frac{1}{r} \frac{d\bar{v}}{dr} - \left( F^2 f^2 + \frac{1}{r^2} \right) \bar{v} = F^2 f \frac{\bar{v}^2}{r}. \quad (3.53)$$

Imposing evanescence conditions as  $r \rightarrow \infty$ , we note that the nonlinear right hand sides of (3.52) and (3.53) will be of small order compared with  $\bar{v}$  and  $\bar{h}$  in the limit  $r \rightarrow \infty$ . A convenient form of solution for  $r \rightarrow \infty$  is therefore

$$h = K_0(\alpha r) H(r) \quad (3.54)$$

$$v = K_1(\alpha r) V(r), \quad (3.55)$$

where  $H(r)$  and  $V(r)$  tend to some finite non-zero limits  $H_\infty$  and  $V_\infty$  respectively as  $r \rightarrow \infty$ , and  $\alpha^{-1} = (F|f|)^{-1}$  is the Rossby deformation radius for this problem. Differential equations for  $H$  and  $V$  are

$$\frac{dV}{dr} = \frac{K_0(\alpha r)}{K_1(\alpha r)} (\alpha V + F^2 f H) \quad (3.56)$$

$$\frac{dH}{dr} = \frac{K_1(\alpha r)}{K_0(\alpha r)} \left( fV + \alpha H + \frac{K_1(\alpha r)}{r} V^2 \right), \quad (3.57)$$

from which it follows that

$$V_\infty = -\frac{\alpha}{f} H_\infty. \quad (3.58)$$

Then, given an initial estimate for  $H_\infty$ , and taking some  $R \gg \alpha^{-1}$ , we take  $H = H_\infty$  at  $r = R$ , and (3.58) as the relationship between  $H$  and  $V$  at  $r = R$ . We can then integrate (3.56, 3.57) backwards to the boundary of the vortex.

The sole exception is in the case  $f = 0$ , where the form of the solution for  $\bar{v}$  is known outside the vortex boundary:

$$\bar{v} = \frac{A}{r}; \quad \bar{h} = -\frac{A^2}{2r^2}, \quad (3.59)$$

where  $A$  is an arbitrary constant, and hence  $\bar{v}$  and  $\bar{h}$  are known in terms of the constant  $A$  rather than the constant  $H_\infty$ .

In the vicinity of  $r = 0$ ,  $\bar{h} \sim O(1)$  and  $\bar{v} \sim O(r)$  as  $r \rightarrow 0$ . In this case, simple power series expansions in  $r$  of the form

$$\bar{h}(r) = h_0 + h_2 r^2 + h_4 r^4 + h_6 r^6 + \dots \quad (3.60)$$

$$\bar{v}(r) = v_1 r + v_3 r^3 + v_5 r^5 + v_7 r^7 + \dots \quad (3.61)$$

are sufficient to give  $\bar{h}(r)$  and  $\bar{v}(r)$  at some small, non-zero  $r$ , given a guess  $h_0$  for  $h(0)$ . We can then integrate (3.7, 3.8) forwards in  $r$  to the boundary of the vortex.

At the boundary of the vortex, we impose continuity of  $\bar{h}$  and  $\bar{v}$ . A Newton method was used to iterate on  $h_0$  and  $H_\infty$  (and  $h_0$  and  $A$  in the case of  $f = 0$ ) until the discontinuities in  $\bar{h}$  and  $\bar{v}$  across the boundary fell below some prescribed tolerance. To employ a Newton method, the differential equations (3.7, 3.8, 3.56, 3.57) and the starting series (3.58, 3.60, 3.61) were differentiated with respect to the parameters  $h_0$  and  $H_\infty$ , so that the variation of  $\bar{v}$  and  $\bar{h}$  with respect to  $h_0$  and  $H_\infty$  on either side of the vortex boundary could be obtained (in the case  $f = 0$ , it is trivial to obtain expressions for the derivatives of the boundary velocity and height with respect to  $A$ ). For  $F \ll 1$ , good initial guesses for  $h_0$  and  $H_\infty$  or  $A$  were obtained from a matched asymptotic analysis, with  $\bar{h}$  given by  $C_1$  due to (3.25) and (3.36), and  $H_\infty = -f/2$  due to (3.33), or  $A = 1/2$ .

We now turn to the disturbance equations.

The analysis of the eigenvalue equations is simplified by realising that the amplitude of the eigenfunctions is irrelevant, and that only the ratio of  $v_r/v_\theta$  on either side of the vortex boundary is required to compute the eigenvalue  $\omega$ .

As for the basic state, both  $r = 0$  and  $r = \infty$  are singular points of the equations, and

some use must be made of the asymptotic form of the solution in these limits to apply the appropriate boundary conditions, which are boundedness at  $r = 0$  and evanescence as  $r \rightarrow \infty$ .

We start by considering the limit  $r \rightarrow 0$ . Here, we may take  $v_r = r^{m-1} + k_1 r^{m+1} + \dots$ . Regularity at  $r = 0$  then implies that  $v_\theta = i r^{m-1} + k_2 r^{m+1} + \dots$ . The constants  $k_1$  and  $k_2$  can then be obtained from the eigenvalue equations, and

$$v_r/v_\theta = -i + K_2 r^2 + O(r^4). \quad (3.62)$$

The constant  $K_2$  depends on the eigenvalue  $\omega$ . Hence, given an initial guess for  $\omega$ , the ratio of  $v_r$  to  $v_\theta$  is known in the limit  $r \rightarrow 0$  from the series (3.62). The ratio is used to initialize the  $r$ -integration of the eigenvalue equations with a starting value of  $r = 0.01$ . In all eigenvalue calculation, the starting series (3.62) was terminated at  $O(r^2)$ . Hence, the ratio  $v_r/v_\theta$  is known just inside the vortex boundary.

At infinity, since the background flow is exponentially small there, we have

$$h \sim H_m^{(1)}(\lambda r) \quad (3.63)$$

with exponentially small corrections, where

$$\lambda^2 = (\omega^2 - f^2)F^2, \quad (3.64)$$

and the type of the Hankel function is chosen to satisfy the radiation condition. Rearranging (3.9, 3.10, 3.11) we have a relationship between  $v_r$  and  $v_\theta$  through

$$(f^2 - \omega^2)v_r + i\omega \frac{dh}{dr} + \frac{1}{r} imfh = 0 \quad (3.65)$$

$$(f^2 - \omega^2)v_\theta - f \frac{dh}{dr} - \frac{1}{r} m\omega h = 0. \quad (3.66)$$

In the case where  $\omega^2 \sim f^2$  we can still find a non-singular expression for the ratio  $v_r/v_\theta$  by expanding the Hankel function representation of  $h$ . Again, the amplitude of  $h$  is not important – it is sufficient to know the ratio of the velocities  $v_r/v_\theta$ .

Note that there is no need to integrate the disturbance equations in from the radiation far field of the Hankel function. This is fortunate, since, if  $\omega^2 \sim f^2$ , this would require a very large range of integration indeed. The equations (3.65, 3.66) assume negligible basic state velocity and height fields, but not a far field form of the wave field. Therefore, it is sufficient to integrate in from a radius where the basic state is sufficiently small. Since the basic state decay

is independent of the eigenvalue, the required position of the integration for the eigenfunction equations in the region  $r > 1$ , is fixed for given  $F$  and  $|f|$ , and decreases as  $F$  and  $|f|$  increase.

Given an initial guess for  $\omega$ , we must iterate on  $\omega$  to satisfy the continuity equation (3.18). Here it is not so convenient to use a Newton method, due to the non-analytic behaviour of the solution at  $\omega = \pm f$ . However, iteration from two initial guesses using linear interpolation to predict the location of the root was found to perform reasonably well, typically converging in 5 or 6 iterations.

At low Froude number, we supply an initial guess for  $\omega$  by considering the Kelvin modes on a circular incompressible vortex, with frequency given by (3.19). This can be used as a first guess  $\omega_0$  for the eigenfrequency, and a second guess can be supplied which is not too far away ( $\omega_0 - 0.05$  say).

At low Froude number, growth rates are typically very low, and this places a strain on the numerical accuracy required. In all cases presented here, NAG routines were used for integrating the ODEs for both the basic state problem and the eigenvalue problem. In the exterior of the vortex, the differential equations are stiff, and a backward differencing method was used. A forward differencing method was used for the interior of the vortex. Tolerances of  $10^{-15}$  were specified in all numerical integrations. In the disturbance problem, the computational values of the eigenfunctions were kept of order unity throughout the ranges of integration by applying the scaling function  $(1 + (Fr)^{2m})^{-1} r^{-1/2} e^{-\lambda r}$  to the variables in the exterior of the vortex (where  $\lambda_r$  is the real part of  $\lambda$ , and  $\lambda$  is given by (3.64)), and the function  $r^{m-1}$  to the interior variables. The very low tolerance specification, together with the rescaling to make the computational variables of order unity throughout the domains of integration, means that we can have some confidence in the imaginary parts of the eigenvalues down to around  $10^{-14}$ .

### Results of the eigenvalue calculations

The growth rate of the instability of the axisymmetric vortex depends on three parameters: the Froude number  $F$ ; the Rossby number  $f^{-1}$ ; and the azimuthal mode number of the instability  $m$ .

We begin by investigating the growth rates of the instability in the case of infinite Rossby number ( $f = 0$ ). This limit is most similar to the study of Broadbent & Moore (1979), except

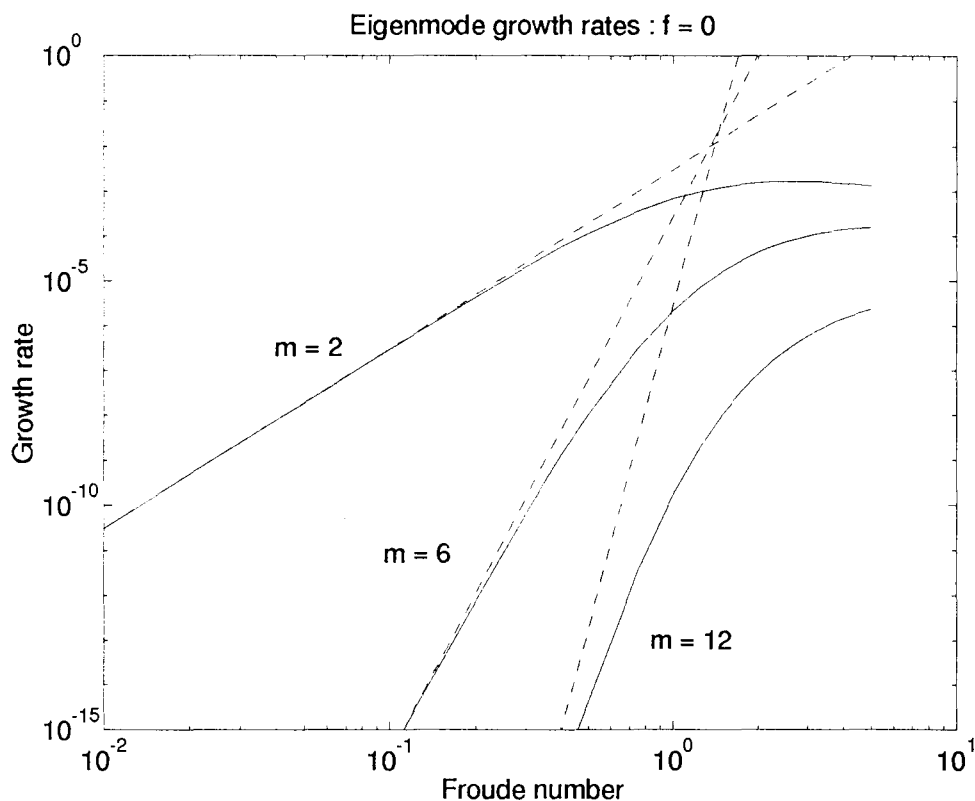


Figure 3.2: Axisymmetric vortex with  $f = 0$ . Growth rates of unstable modes (solid lines), and their low Froude number limits (dashed lines).

here we take the vortex to have uniform potential vorticity, rather than uniform vorticity as they did.

Figure 3.2 shows the growth rates of the instability for Froude numbers from 0 to 5 and for mode numbers  $m = 2, 6, 12$ . Solid lines are growth rates obtained from the numerical eigenvalue calculation, and dotted lines are the growth rates given by the low Froude number analysis (equation 3.51). The graph is plotted on a log-log scale, so that at low Froude number the slope of the lines is  $2m$ . Mode 2 is found to be the most unstable, and grows more slowly with Froude number than the higher mode numbers. The numerical eigenvalue calculations are apparently reproducing the eigenvalues obtained from low Froude number limit with growth rates down to  $10^{-14}$ , and we can be confident that numerical algorithm used to integrate (3.12) & (3.13) is performing adequately.

The real part of the eigenfrequency divided by  $m$  is shown in figure 3.3. It is always bounded between 0 and  $m \times V(1)$ , apparently approaching  $m \times V(1)$  at large  $m$ .

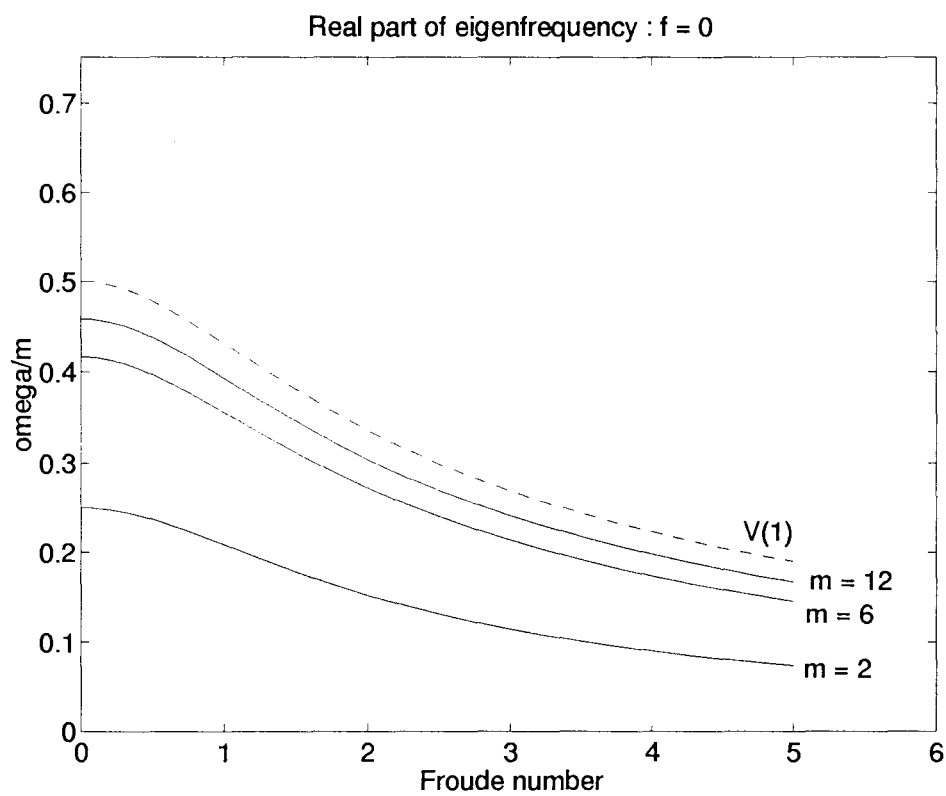


Figure 3.3: Axisymmetric vortex with  $f = 0$ . Real parts of eigenfrequencies /  $m$  (solid lines), with  $V(1)$  (dashed line) for comparison.

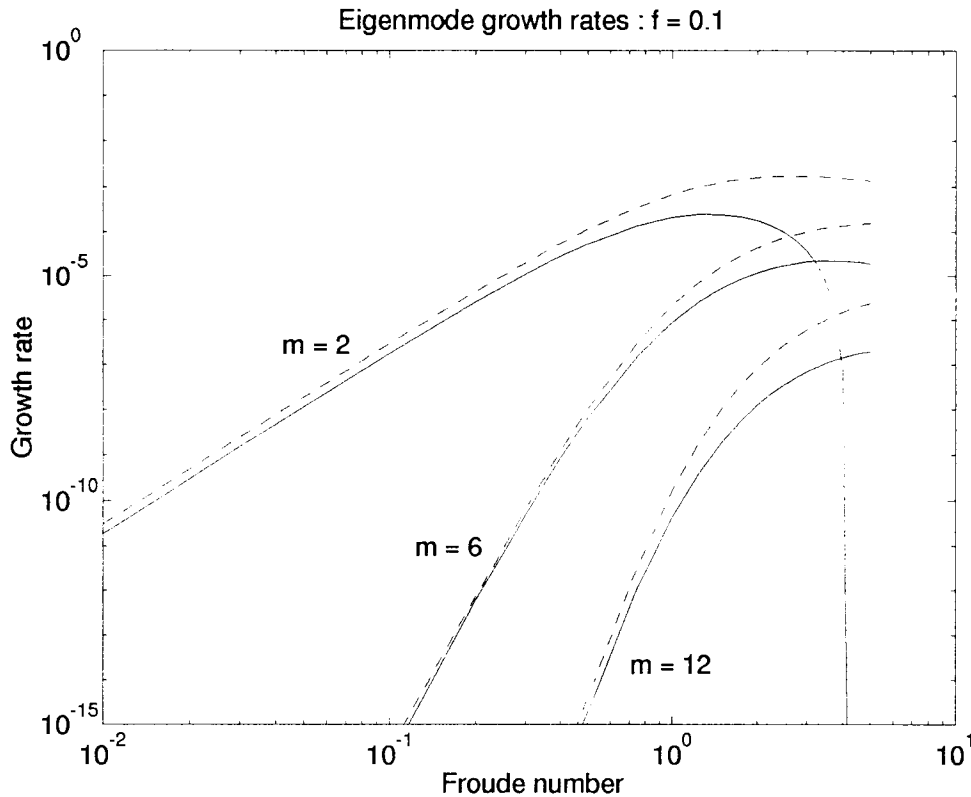


Figure 3.4: Axisymmetric vortex with  $f = 0.1$ . Growth rates of unstable modes (solid lines), together with growth rates of modes with  $f = 0$  (dashed lines) for comparison.

We now turn to investigating the instability at non-zero  $f$ . In particular, it is important to note that for  $f$  between 0 and  $-1$ , the vortices are anticyclones with potential vorticity of opposite sign to the background potential vorticity. For  $f > 0$  the vortices are always cyclones, and for  $f < -1$ , they are anticyclones with potential vorticity of the same sign as the background. If  $f \neq 0$ , we expect the effect of background rotation to inhibit the instability if the real part of the eigenfrequency is below  $|f|$ . We start by investigating the effect on the instability of weak background rotation, in the first case taking  $|f| = 0.1$ .

In figure 3.4, growth rates are shown for  $f = 0.1$ , and in figure 3.5 they are shown for  $f = -0.1$ . For reference, the dashed lines in figures 3.4 & 3.5 show the corresponding growth rates of the instability for  $f = 0$ . In the case  $f = 0.1$ , the vortices should be regarded as very intense cyclones, with potential vorticity equal to 11 times the background value, whereas in the case  $f = -0.1$  they are very intense anticyclones, with potential vorticity equal to  $-9$  times the background value. The corresponding real parts of the eigenfrequencies divided by  $m$  are

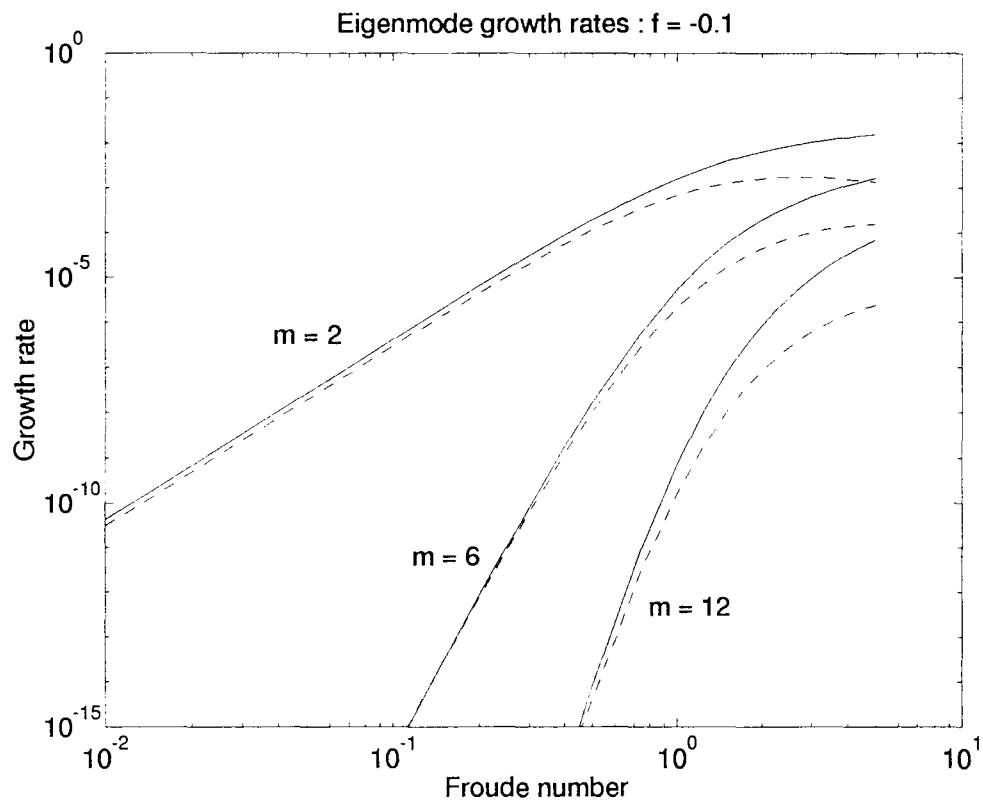


Figure 3.5: Axisymmetric vortex with  $f = -0.1$ . Growth rates of unstable modes (solid lines), together with growth rates of modes with  $f = 0$  (dashed lines) for comparison.

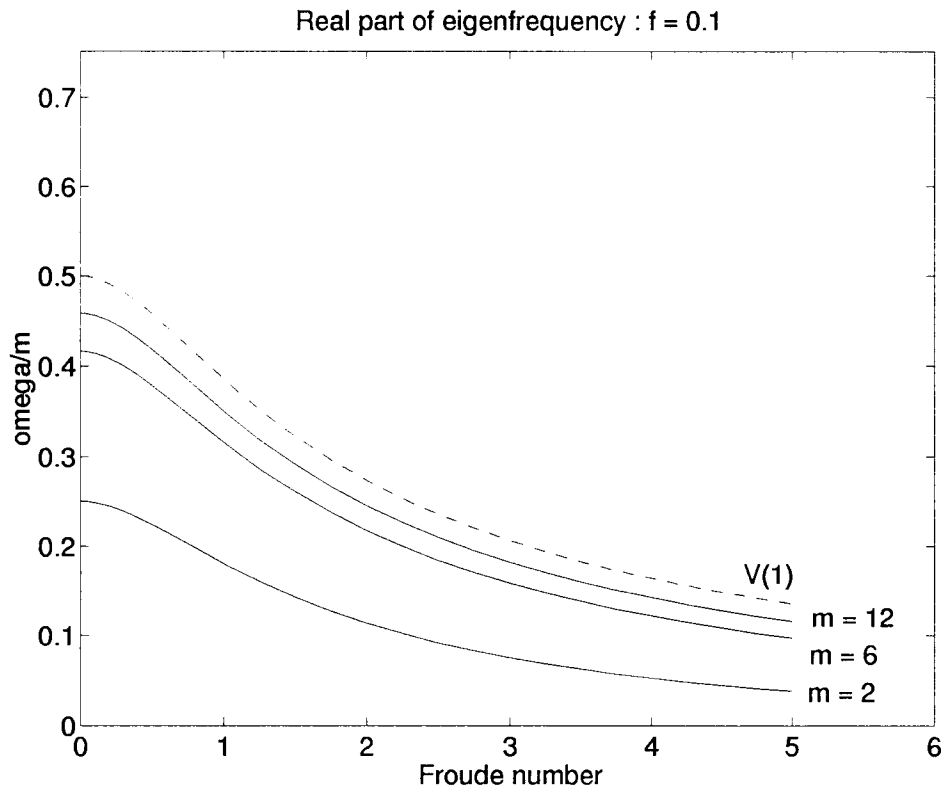


Figure 3.6: Axisymmetric vortex with  $f = 0.1$ . Real parts of eigenfrequencies  $/ m$  (solid lines), with  $V(1)$  (dashed line) for comparison.

shown in figures 3.6 & 3.7.

Notice that  $V(1)$  is quite different for  $f > 0$  and  $f < 0$  as  $F$  is varied, but that the real part of the eigenfrequency is still bounded between 0 and  $m \times V(1)$ , approaching  $m \times V(1)$  at large  $m$ .

Figures 3.4 & 3.5 show that a small amount of background rotation has a significant effect on the growth rate of the instability in both the cyclonic and anticyclonic cases, although in opposite senses. In figure 3.4 we see that the background rotation inhibits the instability of the cyclone. One would expect it to do so, but to completely cut off the instability the real part of the eigenfrequency must be reduced from 0.5 at  $F = 0$  to 0.1 at  $F \approx 4$ . It is perhaps surprising that the velocity at the boundary of the vortex, and hence the real part of the eigenfrequency, decreases so markedly with increasing Froude number. By contrast, in the anticyclonic case  $f = -0.1$ , the growth rates of the instability are markedly increased over their corresponding  $f = 0$  values, and the real part of the eigenfrequency does not decrease nearly so rapidly with

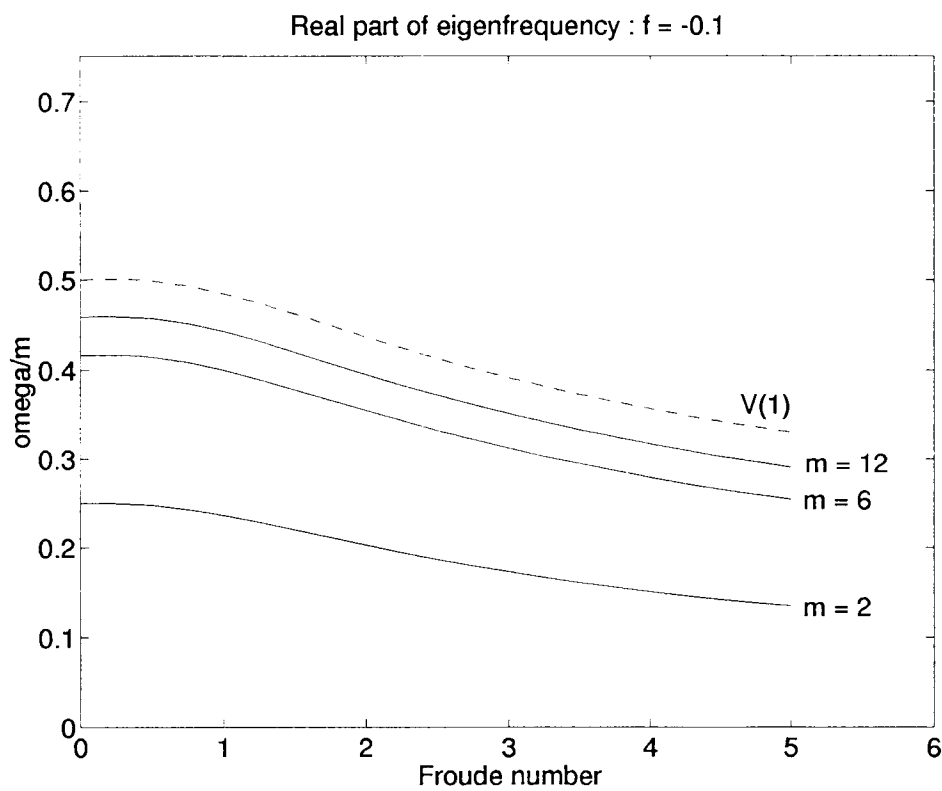


Figure 3.7: Axisymmetric vortex with  $f = -0.1$ . Real parts of eigenfrequencies /  $m$  (solid lines), with  $V(1)$  (dashed line) for comparison.

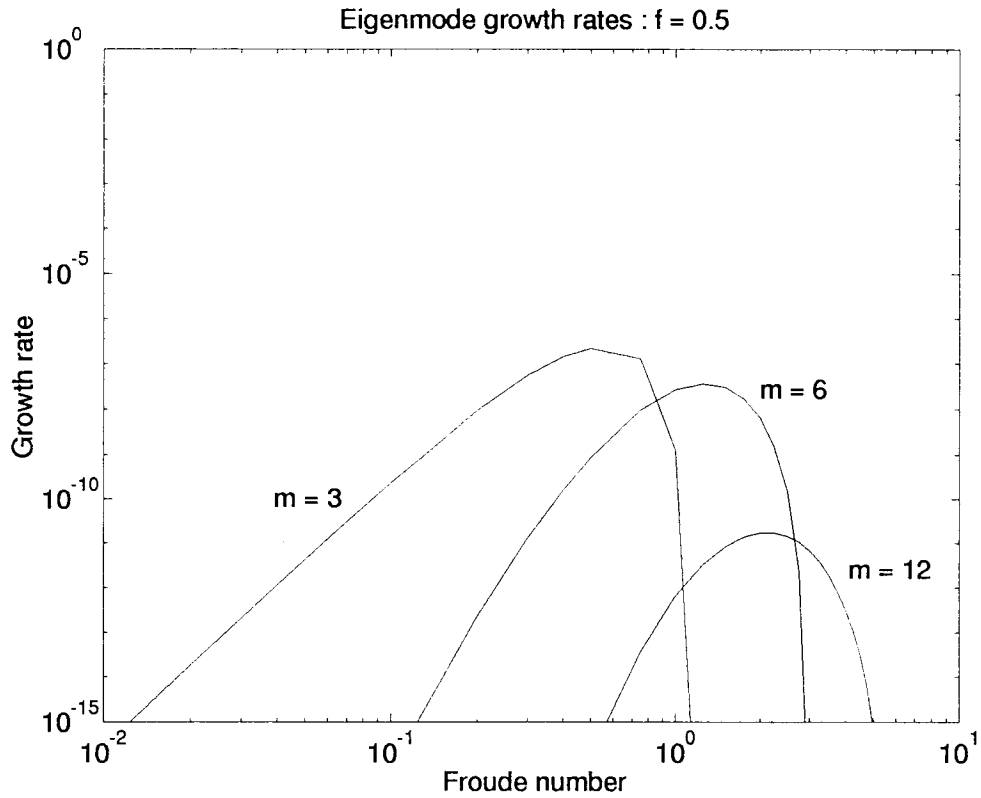


Figure 3.8: Axisymmetric vortex with  $f = 0.5$ . Growth rates of unstable modes.

increasing Froude number.

When  $|f| = 0.5$ , we reach the situation where the mode  $m = 2$  instability is not unstable at leading order in Froude number, since then we have  $\omega = |f|$  at leading order in  $F$ . In figure 3.8 growth rates are shown for  $f = 0.5$ . Mode 2 is stable over all Froude number shown on the graph, and growth rates for modes 3, 6 and 12 are shown. As  $F$  is increased, so more and more modes become stabilized, as the vortex boundary velocity decreases and the real part of the eigenfrequency falls below  $f$ . This is shown in figure 3.9. The instability of the vortex at  $f = 0.5$  is summarized in figure 3.10. In figure 3.10a we see that the maximum growth rate, over all Froude numbers, occurs at a Froude number of about 0.9. As  $F$  is increased further, the mode number of the fastest growing mode increases, apparently almost linearly with  $F$  (see figure 3.10b), and the growth rate of the fastest growing mode decreases, being barely greater than  $10^{-15}$  at  $F = 5.0$ .

In the anticyclonic case  $f = -0.5$ , shown in figure 3.11, the mode 2 instability persists for

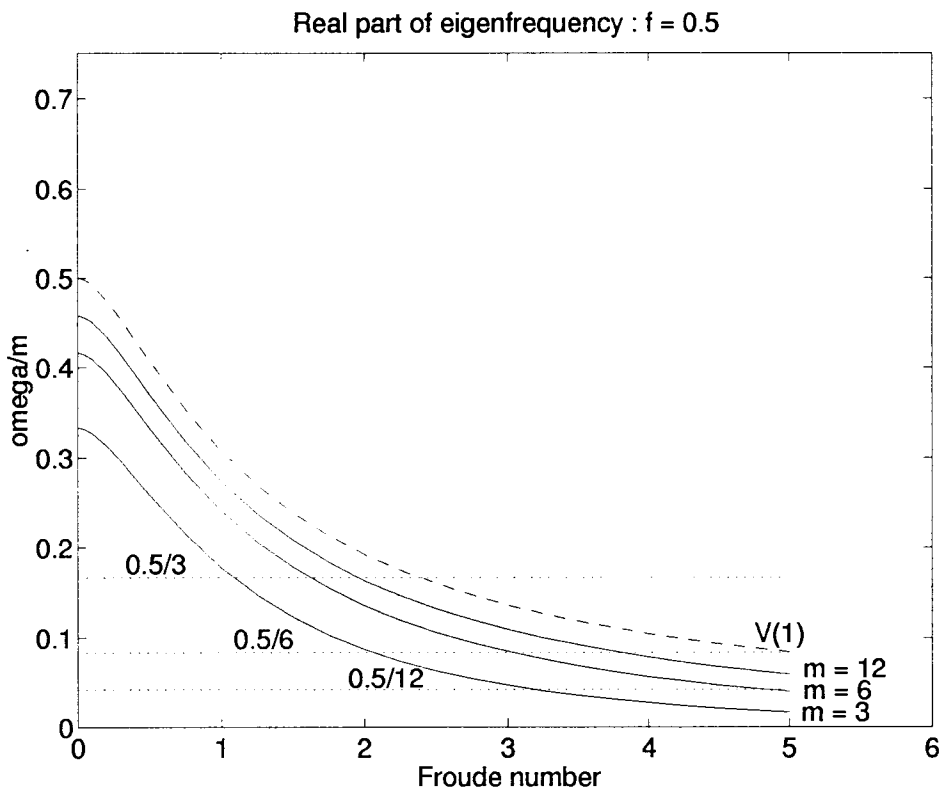


Figure 3.9: Axisymmetric vortex with  $f = 0.5$ . Real parts of eigenfrequencies  $\omega/m$  (solid lines), with  $V(1)$  (dashed line) for comparison. Dotted lines are the critical values of  $\omega/m$ , below which the instability is inhibited for each given  $m$ . Modes  $m = 3$  and  $m = 6$  are inhibited at some  $F < 5$ . Mode 12 is not inhibited for  $F < 5$ , but the growth rate of mode 12 is less than  $10^{-15}$  at  $F = 5$  (see figure 3.8).

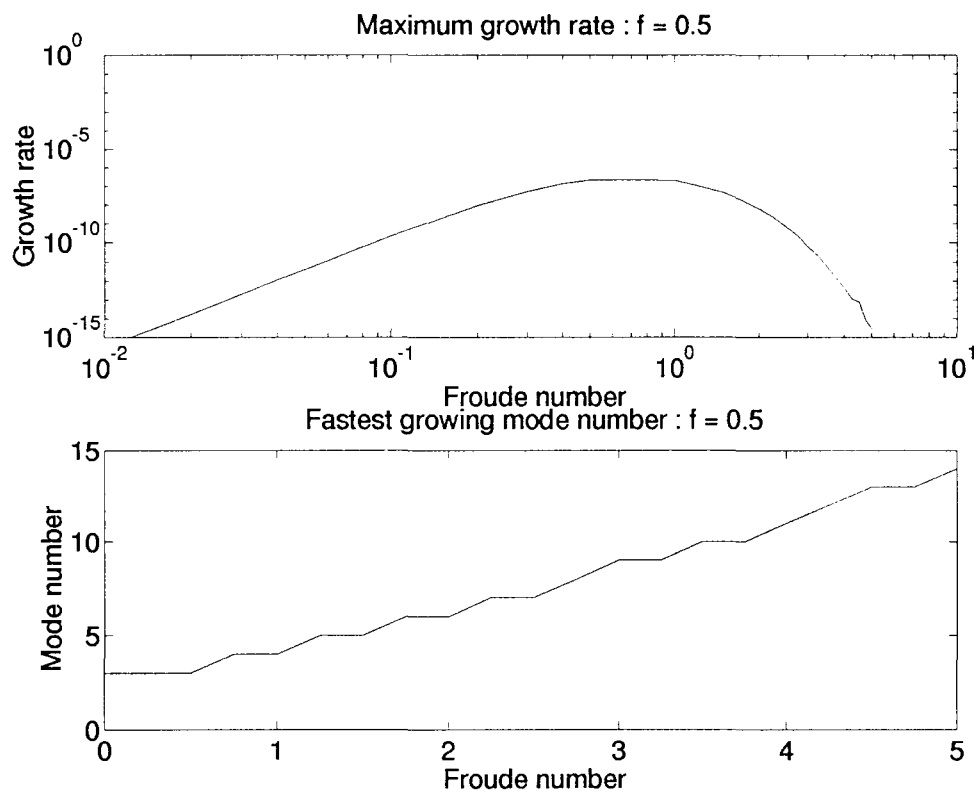


Figure 3.10: Axisymmetric vortex with  $f = 0.5$ . (a): Growth rate of fastest growing mode, and (b): Mode number of fastest growing mode

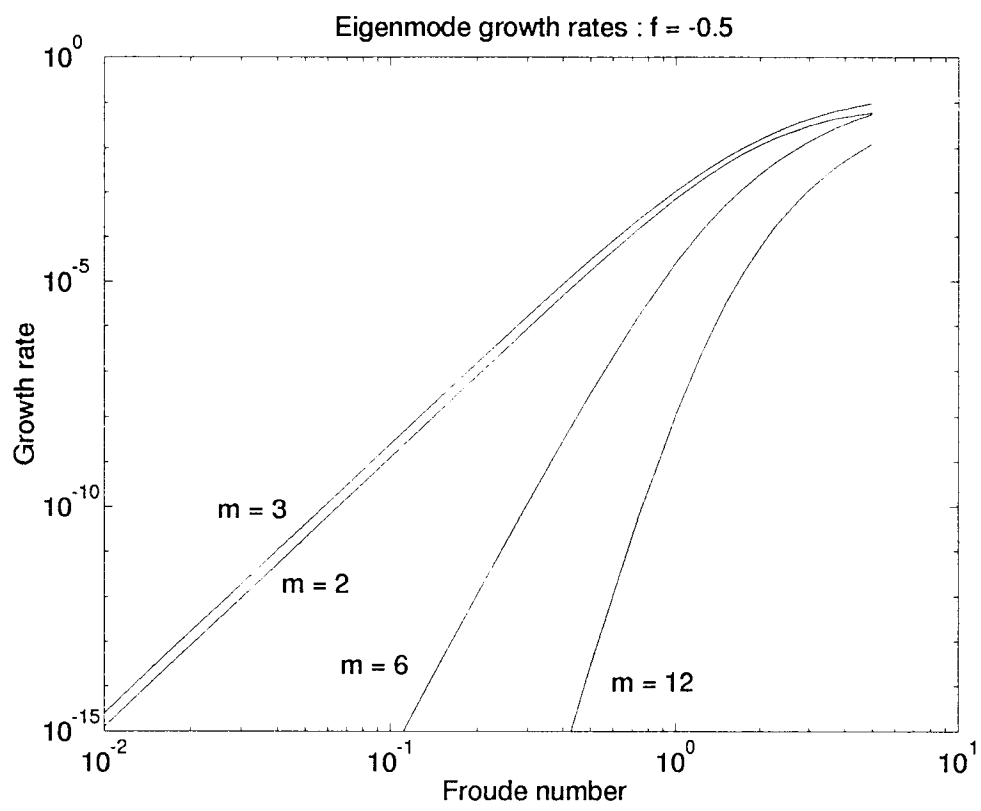


Figure 3.11: Axisymmetric vortex with  $f = -0.5$ . Growth rates of unstable modes.

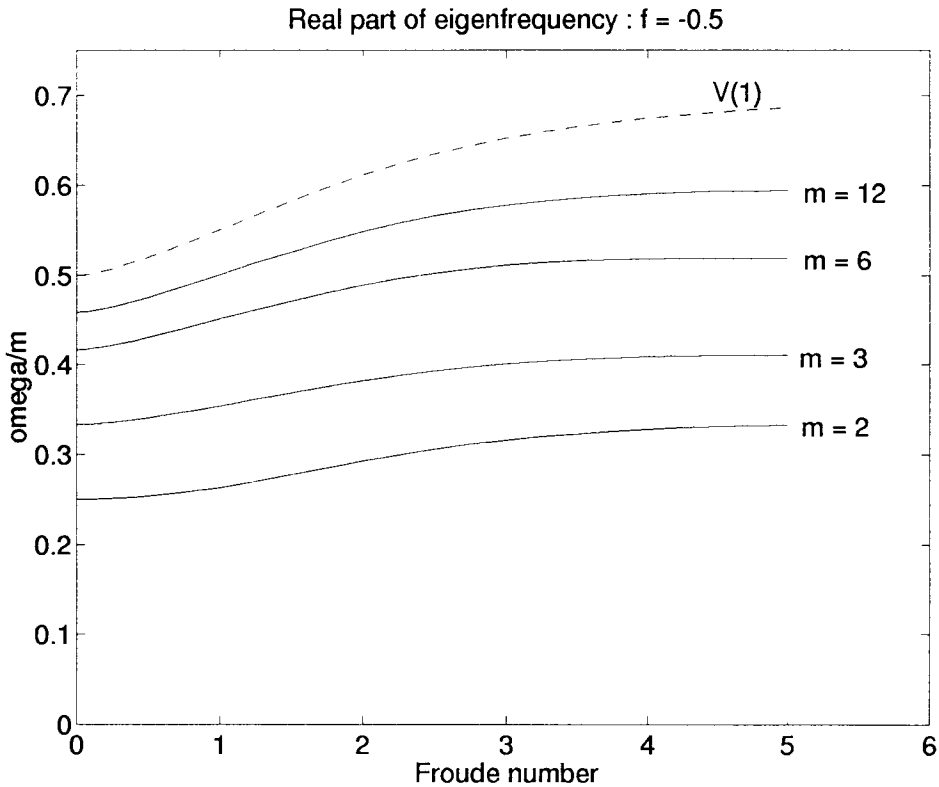


Figure 3.12: Axisymmetric vortex with  $f = -0.5$ . Real parts of eigenfrequencies /  $m$  (solid lines), with  $V(1)$  (dashed line) for comparison.

all non-zero  $F$ , but its behaviour at small  $F$  is changed, increasing with the 6th power of the Froude number, rather than the 4th. In this case, the real part of the eigenfrequency tends to increase as  $F$  is increased, consistent with an increase of  $V(1)$  (figure 3.12).

When  $|f| = 1.0$ , mode 3 ceases to be unstable at small Froude number. Moreover, for  $|f| > 1.0$  the anticyclones have potential vorticity  $(f + 1)$  of the same sign as the background potential vorticity  $f$ , and the case  $f = -1$  corresponds to a vortex of zero potential vorticity. Figure 3.13 shows the growth rates of the instability for  $f = 1$ . The maximum growth rate never exceeds  $10^{-10}$ , and the growth rate of mode  $m = 12$  never exceeds  $10^{-15}$ . The real part of the eigenfrequency behaves much as before, with  $V(1)$  now decreasing very rapidly as  $F$  is increased (figure 3.14).

In figure 3.15, the growth rates of the instability are shown for  $f = -1.0$ . In contrast to the case  $f = 1.0$ , the instabilities persist over a wide range of  $F$ . The vortex boundary velocity is always 0.5, and the real parts of the eigenfrequencies do not decrease markedly as

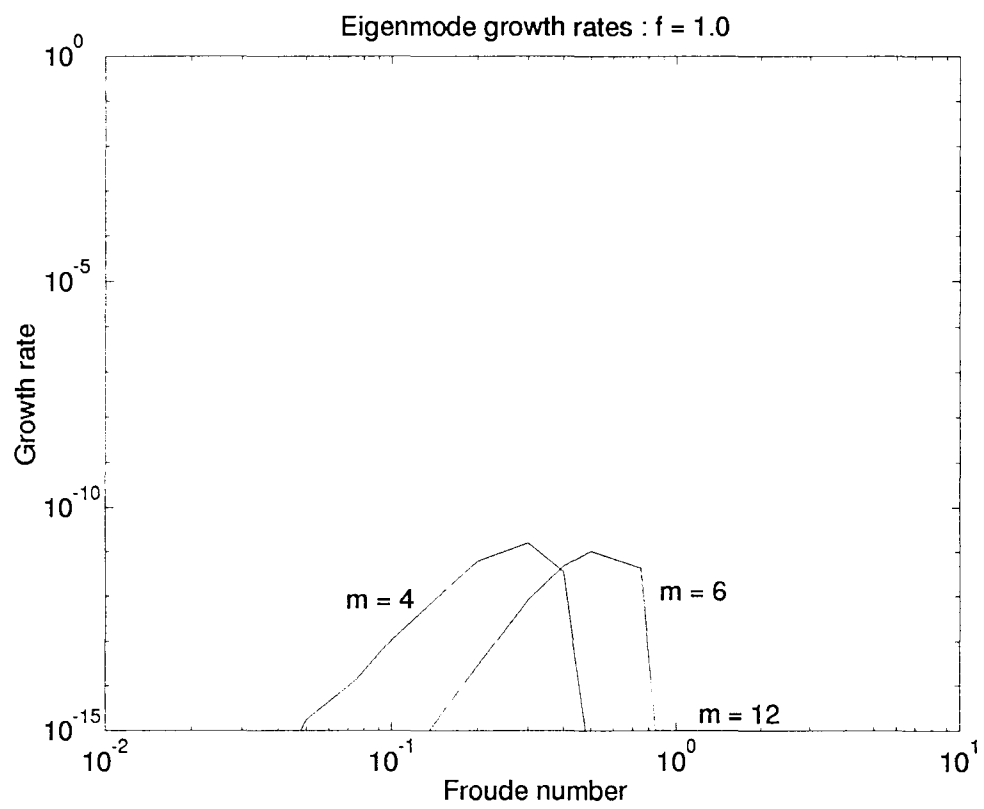


Figure 3.13: Axisymmetric vortex with  $f = 1.0$ . Growth rates of unstable modes.

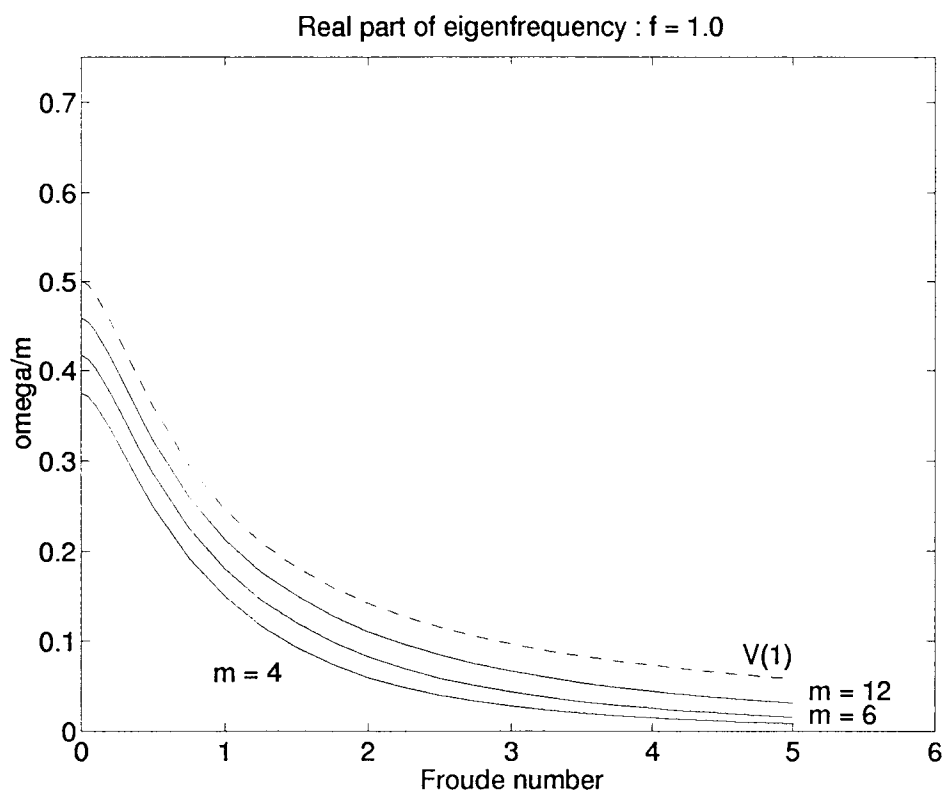


Figure 3.14: Axisymmetric vortex with  $f = 1.0$ . Real parts of eigenfrequencies /  $m$  (solid lines), with  $V(1)$  (dashed line) for comparison.

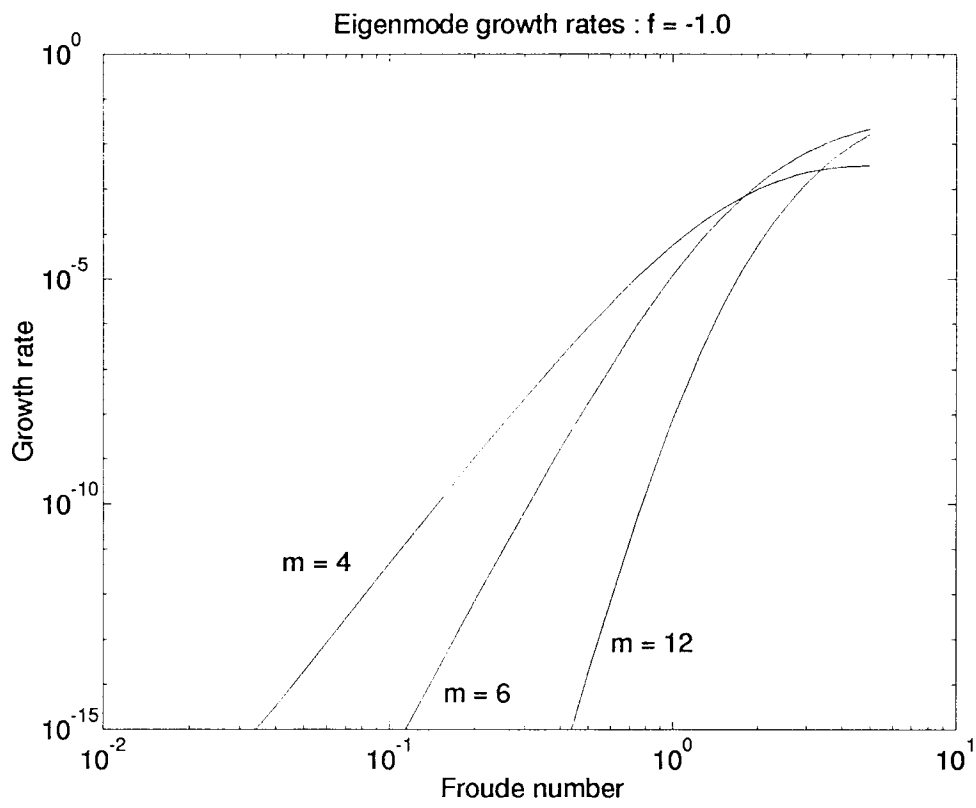


Figure 3.15: Axisymmetric vortex with  $f = -1.0$ . Growth rates of unstable modes.

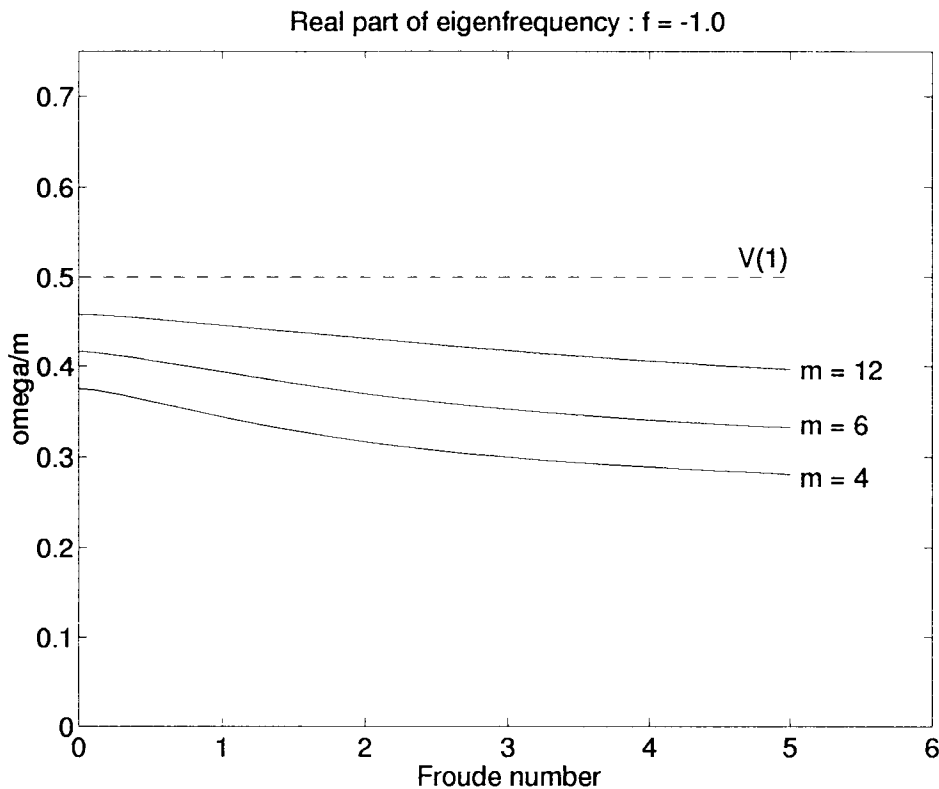


Figure 3.16: Axisymmetric vortex with  $f = -1.0$ . Real parts of eigenfrequencies /  $m$  (solid lines), with  $V(1)$  (dashed line) for comparison.

$F$  is increased (see figure 3.16). Mode 3, which is marginally stable at  $F = 0$ , for  $f = \pm 1.0$ , is never unstable for  $|f| = 1.0$ , either for positive or negative  $f$ . This is quite different from the case  $f = -0.5$ , where the marginally stable mode,  $m = 2$ , became unstable in the anticyclonic case, but remained stable in the cyclonic case.

For  $f \sim 1$  it appears that the cyclones have instabilities with only very weak growth rates, if at all, and it seems likely that increasing  $f$  still further will continue to reduce the growth rates, at the same time requiring larger and larger  $m$  for the instability to exist at all. However, for  $f \sim -1$ , the anticyclones still have comparatively large growth rates, and in figures 3.17 & 3.18 we see the effect of increasing  $|f|$  above 1 in the anticyclonic case.

In figure 3.17 the growth rates of mode 4 instabilities are shown for  $f = -1.1, -1.2, -1.3$ . We can see that as  $|f|$  is increased beyond 1.0, the effect of background rotation very rapidly reduces instability at mode number 4, the maximum growth rate at  $f = -1.3$  being four order of magnitude smaller than the maximum growth rate at  $f = -1.1$ . Figure 3.18 shows growth

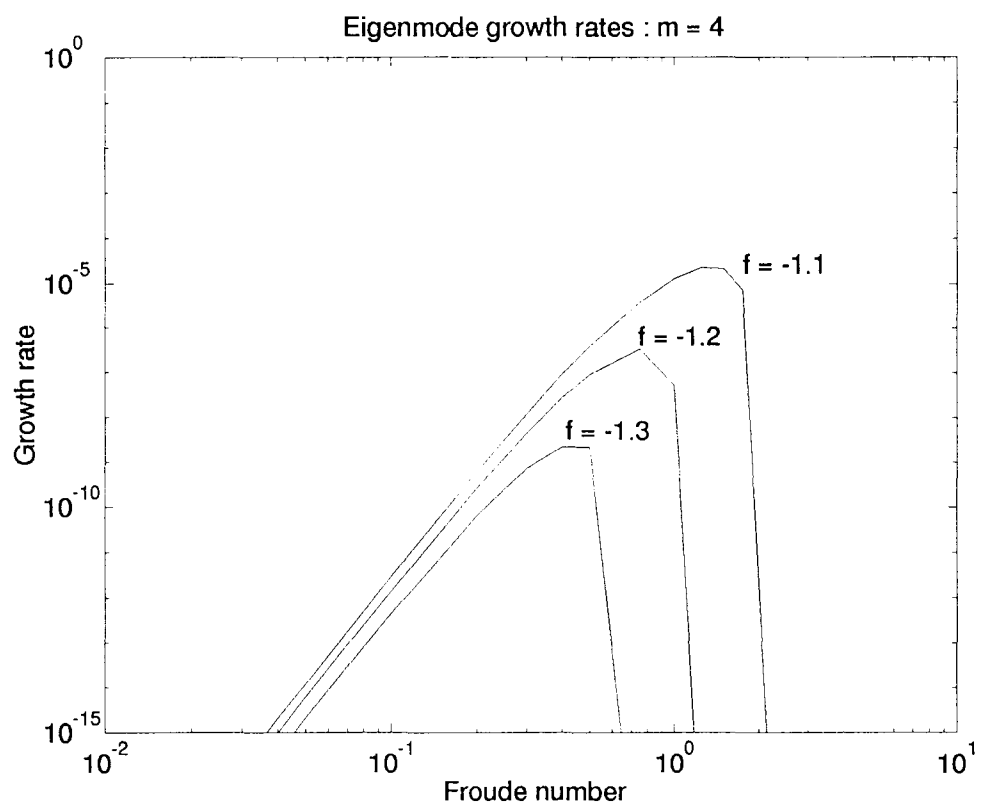


Figure 3.17: Growth rates of mode number 4 disturbances to vortices with  $f = -1.1, -1.2, -1.3$ .

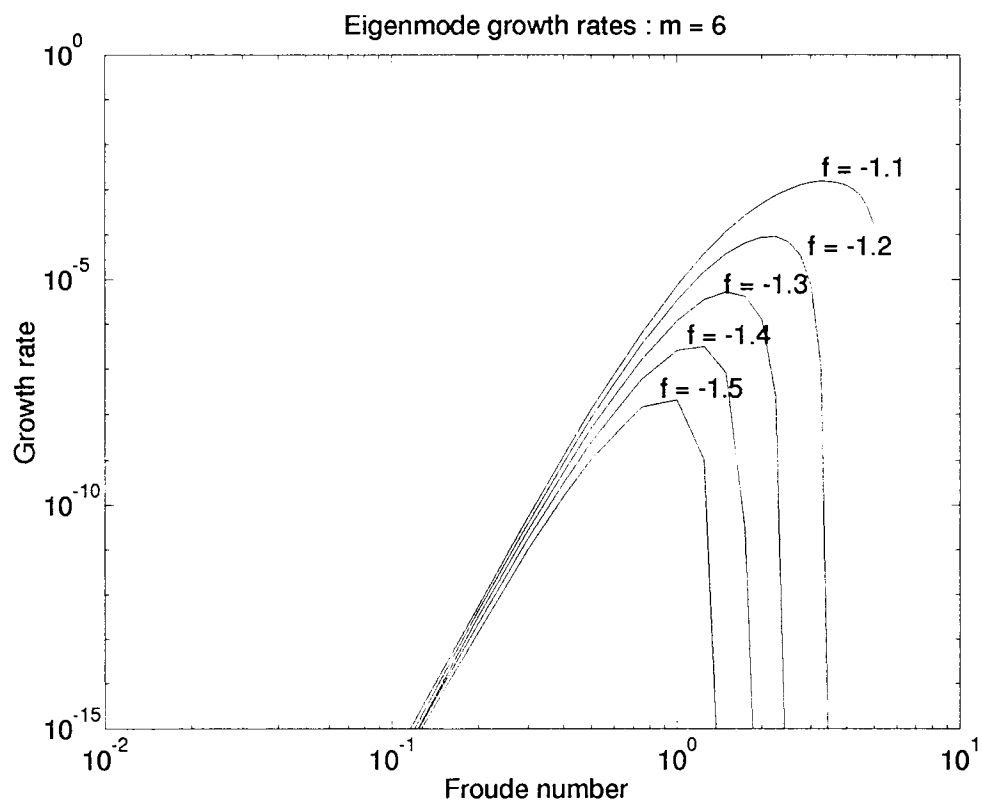


Figure 3.18: Growth rates of mode number 6 disturbances to vortices with  $f = -1.1, -1.2, -1.3, -1.4, -1.5$ .

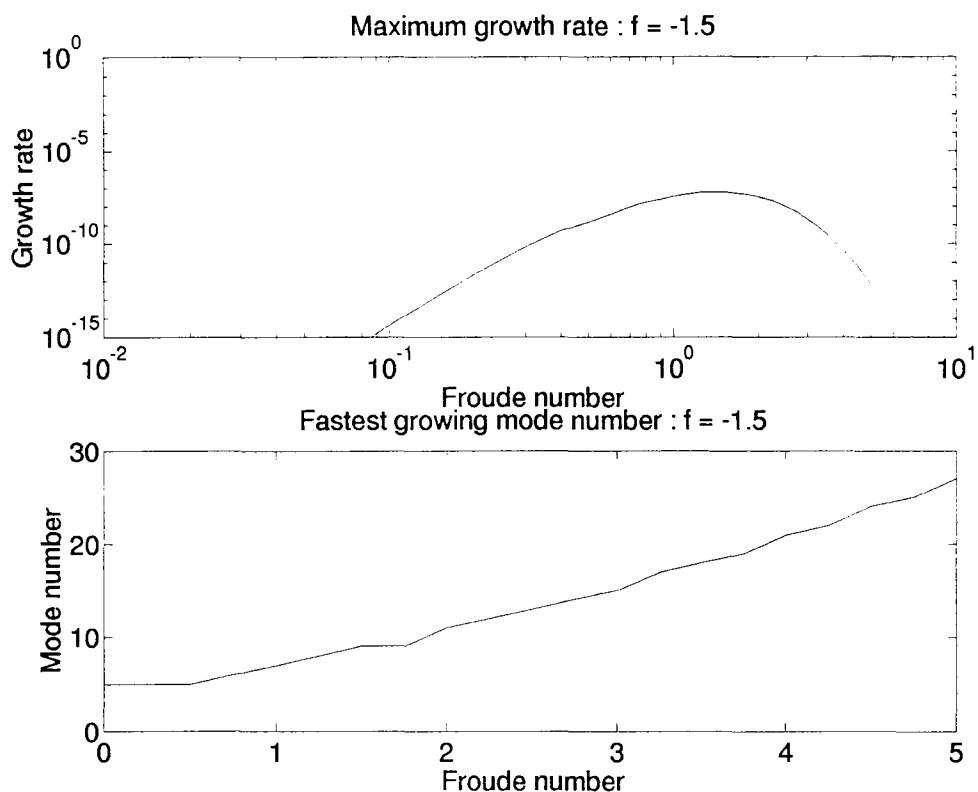


Figure 3.19: Axisymmetric vortex with  $f = -1.5$ . (a): Growth rate of fastest growing mode, and (b): Mode number of fastest growing mode.

rates of mode 6 instabilities for  $f = -1.1, -1.2, -1.3, -1.4, -1.5$ . For this higher mode number the instabilities persist for larger  $|f|$  than in the case  $m = 4$ , but are still significantly inhibited as  $|f|$  is increased. It seems that the instabilities of the anticyclones with  $f < -1$  are very similar to instabilities of the cyclones  $f > 1$ , with the instability at moderate to large Froude numbers persisting only at very high mode numbers.

The instability of the vortex at  $f = -1.5$  is summarized in figure 3.19, which is to be compared with figure 3.10 for the vortex with  $f = 0.5$ . The overall maximum growth rate now occurs at a Froude number of about 1.1, with the fastest growth rate reducing to about  $10^{-12}$  at  $F = 5.0$ . The mode number of the fastest growing mode increases almost linearly with  $m$ , reaching  $m = 27$  at  $F = 5.0$ . The picture is broadly similar to the case  $f = 0.5$ , shown in figure 3.10, although the mode numbers in this case are larger, and the growth rates slightly greater at larger values of  $F$ . It is in contrast to what is found for  $0 > f \geq -1$ , where the growth rates apparently increased without bound as  $F$  was increased.

We turn now to an explanation of the difference in behaviour of the instability between cyclonic and anticyclonic vortices. At low Froude number, a difference between positive and negative  $f$  exists in the expression (3.51) for the growth rate of the instability in the  $F \ll 1$  limit. The difference is a factor of  $(\omega - f)/(\omega + f)$ , which is smaller if  $\omega$  and  $f$  have the same sign than it is if they are of opposite sign. Since  $\omega$  is always positive, this factor means that anticyclones are always more unstable to Rossby wave – gravity wave instability than cyclones. The difference lies in the nature of the coupling between the vortical region and the wave region. This difference is small, however, and amounts only to a constant factor. It cannot explain why low wave number disturbances to cyclonic vortices are stabilized as the Froude number is increased, whereas low wave number disturbances to anticyclonic vortices are destabilized.

The key to understanding the difference lies in the nature of the basic states. For small  $F$ , the azimuthal velocity at the vortex boundary is always 0.5. Since the wave on the boundary of the vortex is a Rossby wave, we expect it to propagate in a pseudo-westward direction – i.e. with a real frequency between 0 and  $m \times V(1)$  in the case of a vortex of unit radius. Therefore the azimuthal velocity at the boundary of the vortex sets a bound for the real part of the eigenfrequency.

Of course, one reason why eigenmodes with comparatively high frequencies will be more unstable is that they are less influenced by the inertial cut-off  $\omega = |f|$ . While this is one explanation, it is not the only one, and is probably not the most significant. Regardless of the inertial cut-off frequency, we would still expect higher frequency eigenmodes to be more unstable than lower frequency modes, because at higher frequencies the interaction between vortical and gravitational motions becomes stronger.

To see this, first recall that we expect the growth rate of the instability to depend on the strength of coupling between the Rossby wave, on the vortex boundary, and the gravity waves, found distant from the vortex boundary. The character of the eigenmodes changes from being Rossby wave - like to gravity wave - like at the “sonic radius”, at which the intrinsic angular phase speed of disturbances,  $\omega r/m - V(r)$ , is equal to the gravity wave phase speed  $F^{-1} H^{1/2}(r)$ . At a given  $F$ , it follows that, the larger the value of  $\omega$ , the smaller  $r$  will have to be to achieve a given angular phase speed, and hence the closer the sonic radius will be to the boundary of the vortex. We should expect this to lead to an enhanced coupling between the Rossby

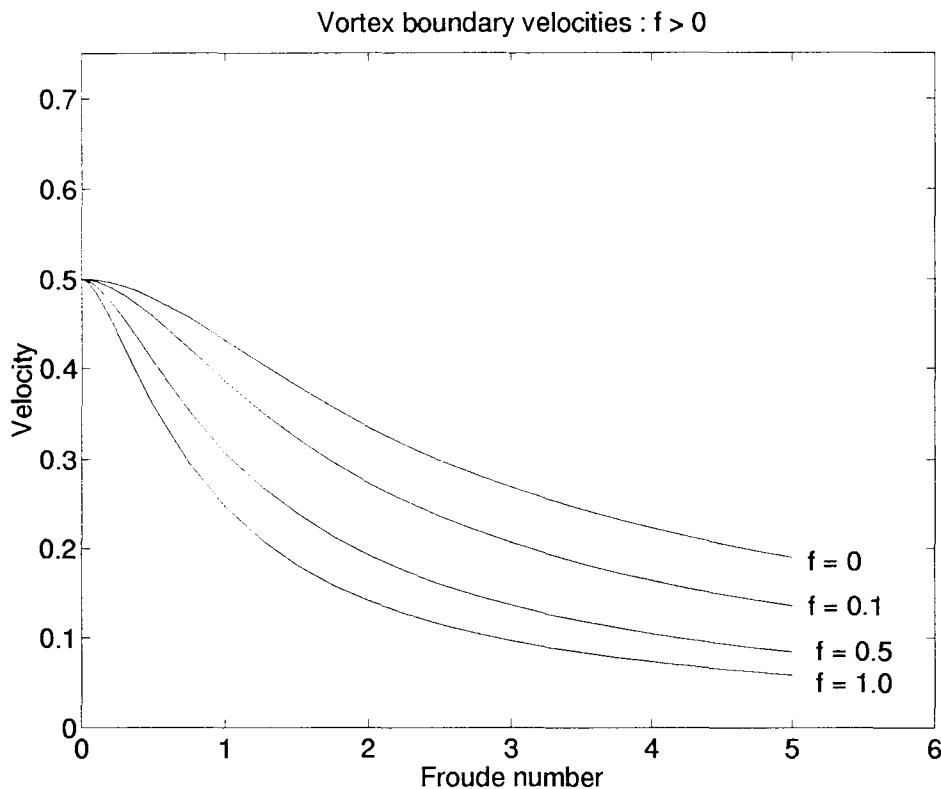


Figure 3.20: Azimuthal velocity at boundary of vortices,  $f > 0$ .

wave on the vortex boundary and the gravity wave beyond the sonic radius in cases where  $\omega$  is comparatively large.

We shall return to this point in the next section, with reference to the WKBJ analysis. The analysis enables us to distinguish between the effect of the inertial cut-off, which primarily affects the growth rates of low mode number disturbances, and the effect of variation in the location of the sonic radius, which affects the growth rates at all mode numbers. For the present, however, we shall simply examine the large degree of variation in the vortex boundary velocities which is experienced as  $F$  and  $f$  are varied, and defer a quantitative discussion to the end of the next section.

In figure 3.20, the azimuthal vortex boundary velocity is shown as a function of Froude number for cyclones with various values of  $f$ . In all cases the vortex boundary velocity decreases very rapidly as the Froude number is increased, from a velocity of 0.5 at  $F = 0$  to less than 0.2 at  $F = 5$ . Therefore, we expect the real part of the eigenfrequency to decrease as  $F$  is

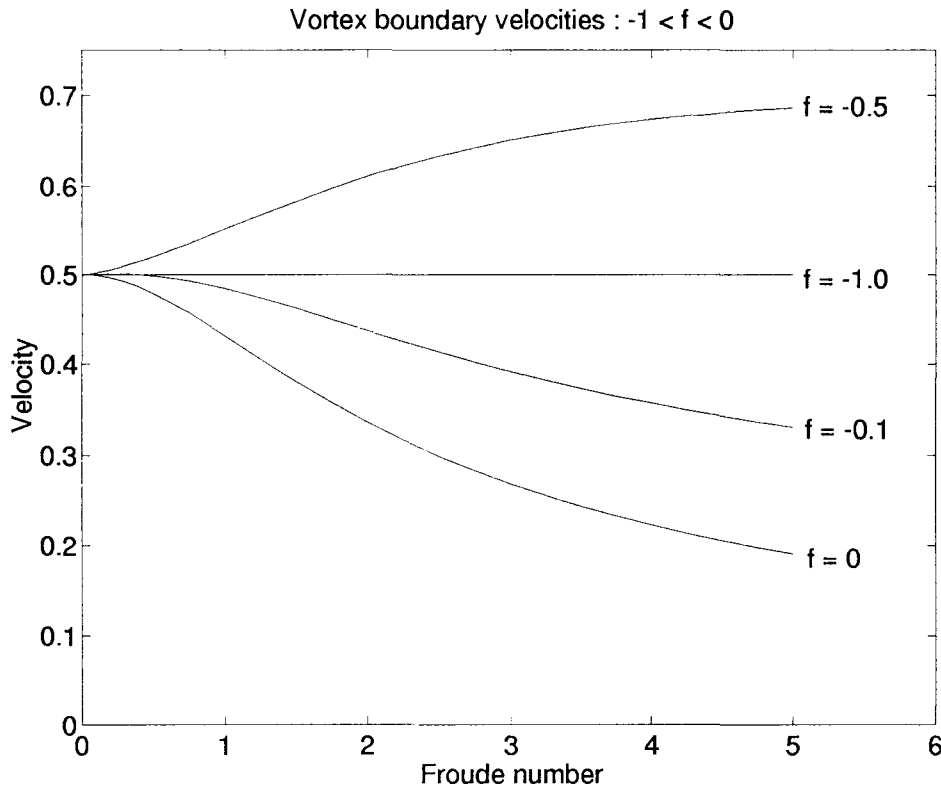


Figure 3.21: Azimuthal velocity at boundary of vortices,  $-1 < f < 0$ .

increased.

Vortex boundary velocities for anticyclones with  $|f| < 1$  are shown in figure 3.21. For small  $|f|$ , the vortex boundary velocity decreases, just as in the cyclonic case, but much less rapidly. For example, with  $f = -1/10$ , the velocity decreases from 0.5 to 0.33 as  $F$  increases from 0 to 5, whereas with  $f = 1/10$  it decreases from 0.5 to 0.14. The most striking difference comes for larger  $f$ , where the vortex boundary velocity increases as  $F$  is increased. The most extreme example is the case  $f = -1/2$ , where the velocity increases from 0.5 at  $F = 0$  to 0.68 at  $F = 5$ . When  $f = -1$ , the vortex boundary velocity is exactly 0.5 for all  $F$ .

For  $f < -1$ , the vortex boundary velocities always decrease as  $F$  is increased. This is shown in figure 3.22. The growth rates of these instabilities tend to behave more like those of cyclones than the anticyclones with  $-1 < f < 0$ .

The results of the eigenvalue calculations may be summarized as follows. In the absence of background rotation, the eigenmode with  $m = 2$  is always unstable in the range  $0 < F < 5$ ,

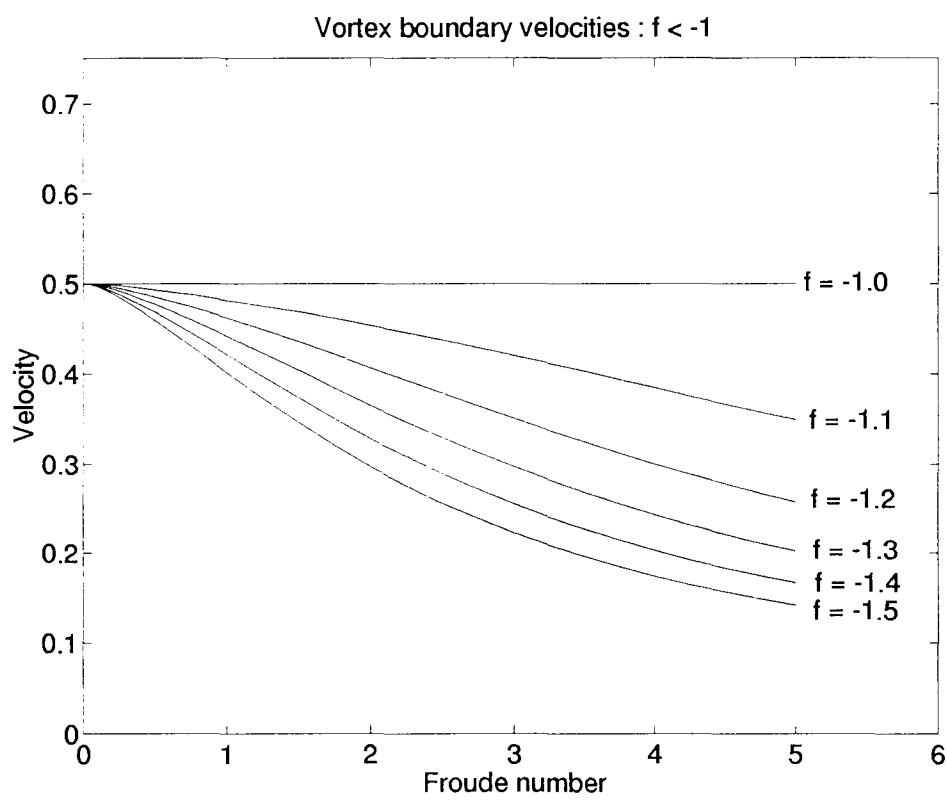


Figure 3.22: Azimuthal velocity at boundary of vortices,  $f < -1$ .

and is probably unstable for all  $F$ . With background rotation present, low mode number eigenmodes may be unstable at small Froude numbers, but become stabilized as the Froude number is increased. This is because the real part of the eigenfrequency decreases as the Froude number is increased, and eventually falls below  $|f|$ , at which point the instability mechanism no longer exists.

The maximum growth rates (taken over all  $m$ ) are shown as a function of  $F$  and  $f$  in figures 3.23a & 3.24a. The growth rate and fastest growing mode number surfaces are shown from two different orientations for ease of visualization. With the exception of the vortices for which  $-1 < f < 0$ , the growth rate of the instability generally peaks at a finite value of the Froude number, and with a fairly low growth rate. However, when  $-1 < f < 0$ , it seems that the growth rate of the instability may increase without bound as  $F$  is increased. The corresponding fastest growing mode number is shown in figures 3.23b & 3.24b. For  $-1 < f < 0$ , the fastest growing mode number is typically small (either 2 or 3), whereas for values of  $f$  outside this range, the fastest growing mode number can be quite large. In the most extreme case shown, when  $F = 5$  and  $f = -1.5$ , the fastest growing mode number is 27.

Thus, the cyclones all tend to exhibit the same dependence on  $F$  and  $f$ . As  $f$  and  $F$  are increased, successively higher mode numbers must be taken to retain the instability, whereas the anticyclones fall into two categories. When  $-1 < f < 0$ , the vortex has potential vorticity of opposite sign to the background. In these cases, there is no marked tendency to stabilize as  $F$  is increased. In the particular case  $f = -1/2$  the instability becomes markedly stronger as  $F$  increases, with maximum growth rate for  $m = 3$ . When  $f < -1$ , however, the dependence of the instability on  $|f|$  and  $F$  is similar to the cyclonic cases, and again large mode numbers are required to retain the instability. Strong instability by the Rossby wave – gravity wave instability mechanism seems possible only when  $-1 < f < 0$  and the mode number  $m$  is not too large. These are the cases where the sonic radius is closest to the boundary of the vortex.

From a practical point of view, we have almost certainly identified those cases in which this instability is sufficiently vigorous that it might be observed in nature. However, we are interested not only in cases of practical significance, but also in whether coupling between vortical motions and gravity waves exists at all Rossby numbers, or whether there is a value of  $|f|$  above which the instability ceases to exist, at least for some range of  $F$ , and in which cases the vortical motions could then be separated from the gravity waves in the problem.

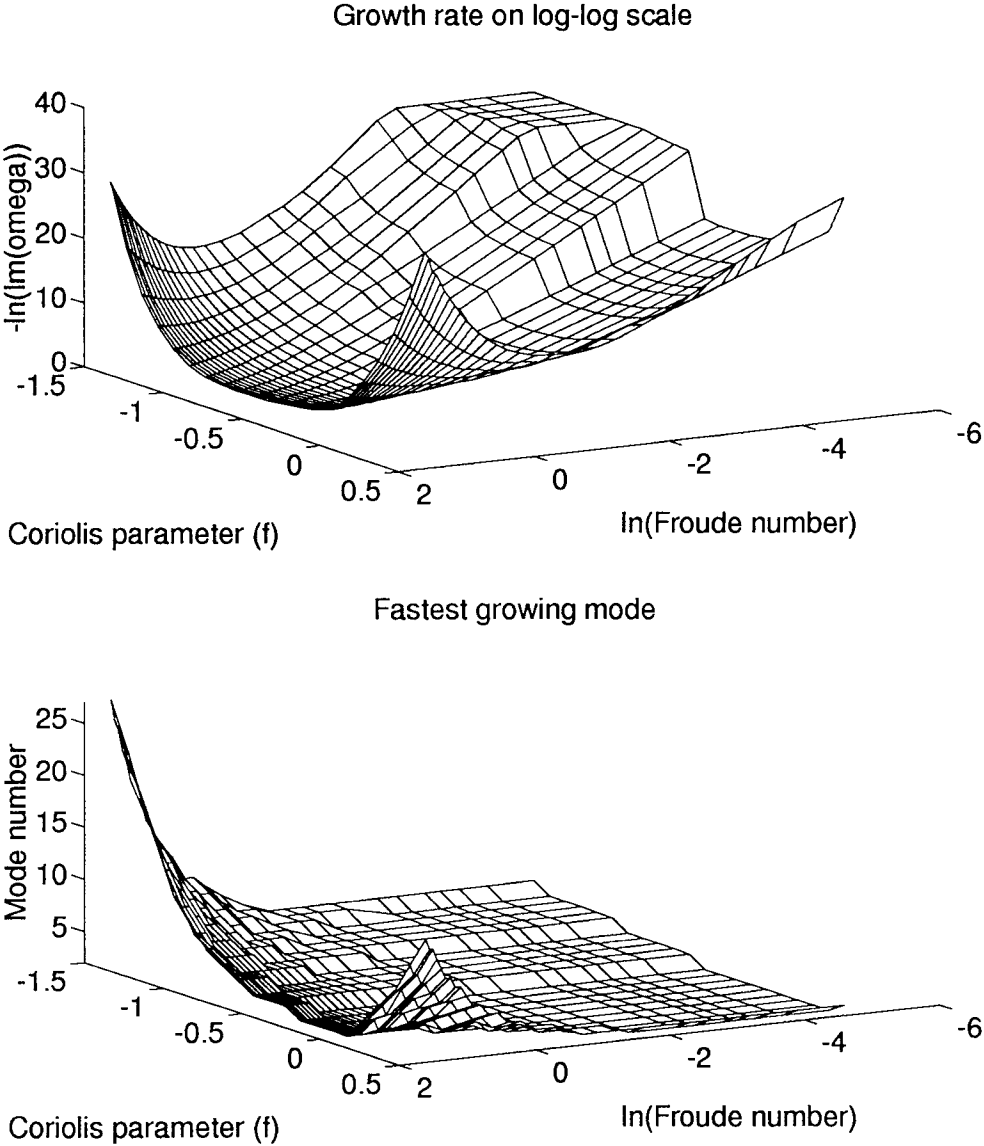


Figure 3.23: Summary of axisymmetric vortex instability calculations, viewed from orientation giving most complete view of growth rate surface.

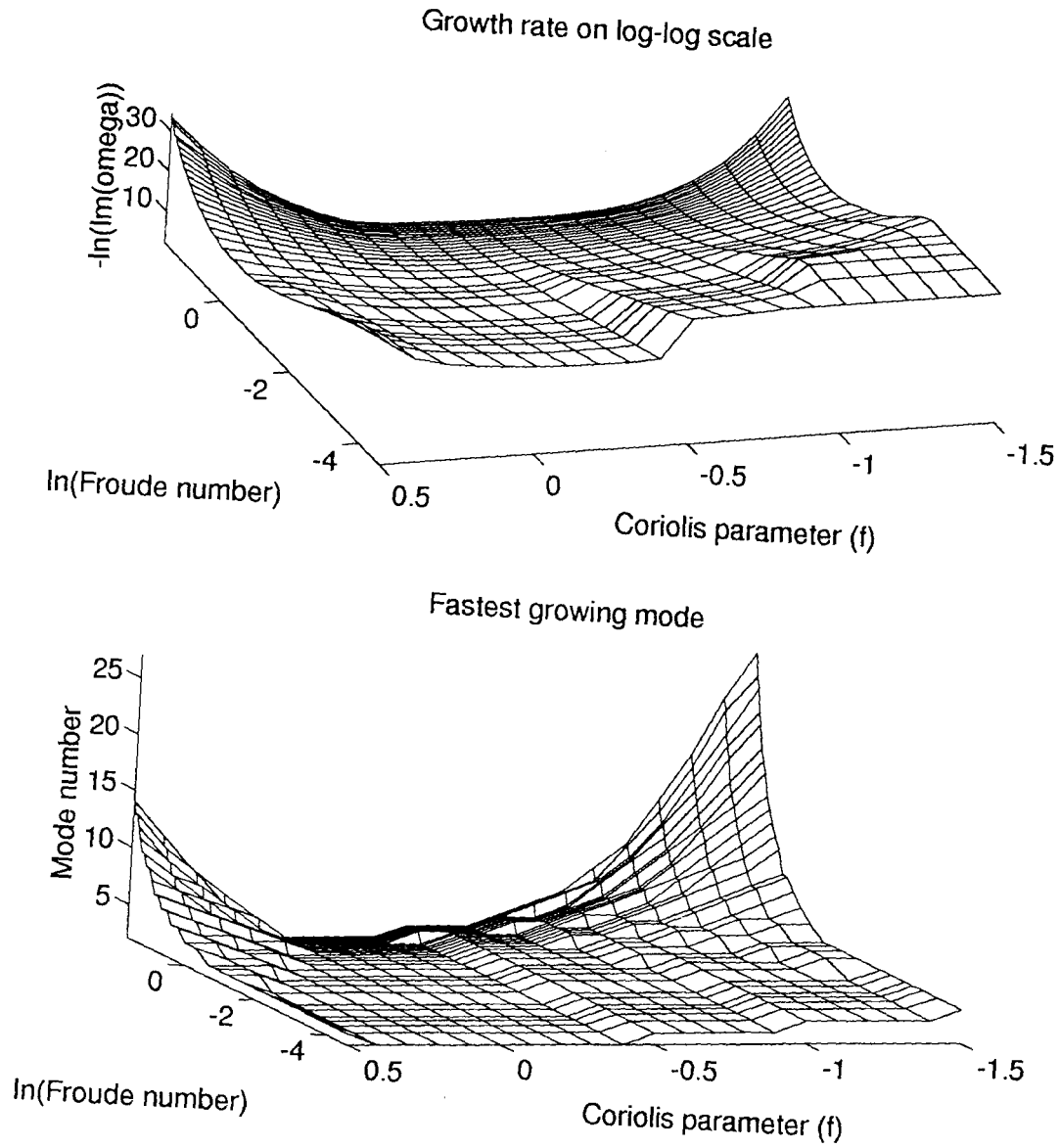


Figure 3.24: As figure 3.23, but viewed from orientation giving most complete view of fastest growing mode number surface. Note that (a) is viewed from a greater elevation than (b).

The next section therefore examines this instability for arbitrary  $f$  and  $F$  in the limit  $m \gg 1$ . The WKBJ analysis has the added advantage that it assumes *a priori* that  $\omega \gg f$ . Therefore any distinction between cyclones and anticyclones which can be accounted for by the WKBJ analysis must be due to the general nature of the basic state, and the strength of Rossby wave – gravity wave interactions on it, and any distinction not accounted for must be due to the specific effects of the inertial cut-off frequency.

### 3.2.5 The limit of large mode number

We start by writing (3.12,3.13) as a single second order ordinary differential equation for  $v_\theta$ :

$$\frac{d^2 v_\theta}{dr^2} + F(r) \frac{dv_\theta}{dr} + G(r) v_\theta = 0, \quad (3.67)$$

where

$$F = -\frac{C'}{C} - A - D; \quad G = \frac{C'D}{C} + AD - BC - D', \quad (3.68)$$

where here  $A, B, C$  and  $D$  are given by (3.14-3.17). Equation (3.67) must be solved subject to certain boundary conditions. These are regularity at  $r = 0$ , and an evanescence/radiation condition as  $r \rightarrow \infty$ . The latter of these conditions requires some care. Any unstable mode must be exponentially weak at infinity, and therefore an evanescence condition should suffice. However, we shall for convenience state the radiation condition, bearing in mind that when the eigenfrequency becomes slightly complex, perhaps at some high order in the expansion parameter  $m$ , the solution of (3.67) acquires some weak exponential decay.

Following standard WKBJ analysis, we write

$$v_\theta = A(r) e^{im\psi(r)}, \quad (3.69)$$

where now  $A(r)$  is an amplitude function and  $\psi(r)$  is a phase function, made rapidly varying through the factor of  $m$  in the exponent. Substituting (3.69) into (3.67) gives

$$A'' + 2im\psi'A' + im\psi''A - m^2\psi'^2A + F(r)(A' + im\psi'A) + G(r)A = 0. \quad (3.70)$$

In general  $\psi$  and  $A$  must be expanded in inverse powers of the WKBJ expansion parameter  $m$ . The decomposition of  $v_\theta$  into  $A(r)$  and  $\psi(r)$  is not unique. A small ( $O(m^{-1})$ , say), correction to  $v_\theta$  through  $\psi$  could just as easily be made by an  $O(m^{-1})$  correction to  $A$ . However, the decomposition can be made unique, and a great deal more convenient to work with, if we insist

that  $A(r)$  and  $\psi(r)$  naturally take the roles of amplitude and phase in that, if  $\{A(r), \psi(r)\}$  is a solution of (3.70), then so is  $\{A(r), -\psi(r)\}$ .

Equation (3.70) can then be separated into two equations:

$$A'' - m^2 \psi'^2 A + F(r)A' + G(r)A = 0 \quad (3.71)$$

$$2\psi'A' + \psi''A + \psi'AF(r) = 0, \quad (3.72)$$

which latter equation can be integrated at once to

$$2 \ln |A| + \ln |\psi'| + \int F = 0. \quad (3.73)$$

We now start our asymptotic analysis of (3.71). Since we know from (3.19) that  $\omega$  is of order  $m$ , at least in the limit  $F \ll 1$ , it is convenient to work with an intrinsic angular frequency  $c$  defined by  $c \equiv \omega/m$ . Bearing Kelvin's expression  $\omega = (m-1)/2$  in mind, and in the spirit of asymptotic expansions, we must expand  $c$  in the form

$$c = c_0 + m^{-1}c_1 + \dots \quad (3.74)$$

In fact, it will turn out that  $c$  has not only an algebraic expansion in  $m^{-1}$ , but also requires terms exponentially small in  $m$  to describe the instability.

From (3.14-3.17) we know that, expanding in  $m$ ,  $F(r)$  is  $O(1)$ , while  $G(r)$  takes the form

$$G(r) = m^2 \left[ \frac{(-c + \bar{v}/r)^2 F^2}{1 + F^2 \bar{h}} - \frac{1}{r^2} \right] + O(1), \quad (3.75)$$

which can, by virtue of the expansion (3.74) have terms of order  $O(m^2)$  and  $O(m)$ . From (3.71), at  $O(m^2)$ , the equation for  $\psi_0$  is

$$\psi_0'^2 = \frac{(-c_0 + \bar{v}/r)^2 F^2}{1 + F^2 \bar{h}} - \frac{1}{r^2}. \quad (3.76)$$

The expression for  $A_0$  can be obtained from (3.73). Notice that, since  $F(r)$  is regular for all  $r \neq 0$ , there is a singularity in the expression for  $A_0$  at a radius  $r = r_c$  where  $\psi_0'(r_c) = 0$ . We can see at once that, for  $c_0 \neq 0$ , there is at least one such radius, since  $\psi_0'^2 \sim -r^{-2} < 0$  as  $r \rightarrow 0$ , but  $\psi_0'^2 \sim c_0^2 F^2 > 0$  as  $r \rightarrow \infty$ .

Now,  $v_\theta = A(r)e^{im(\psi_0 + m^{-1}\psi_1 + \dots)}$ , and since we will require an expression for both the amplitude and phase of  $v_\theta$ , we must obtain expressions for both  $\psi_0$  and  $\psi_1$ . The equation for

$\psi_1$  is obtained from (3.71) at  $O(m)$ , and is

$$\psi'_0 \psi'_1 + \frac{F^2 c_1 (-c_0 + \bar{v}/r)}{1 + F^2 h} = 0. \quad (3.77)$$

Now, the nature of the solutions for  $v_\theta$  differs significantly on either side of  $r = r_c$ . On one side, and in particular in the limit  $r \rightarrow \infty$ , the solutions are oscillatory (for real  $c_0$ ), whereas on the other side, and in particular in the limit  $r \rightarrow 0$ , they are growing and decaying exponentials. We refer to the radius  $r = r_c$  as the “turning radius”, and in the following analysis we shall assume that there is precisely one turning radius for the vortex. There is always precisely one turning radius for  $F \ll 1$ , whatever the magnitude of the Coriolis parameter  $f$ , and hence the assumption includes the basic state in the “quasigeostrophic” limit, in which one might expect interactions between vortices and gravity waves to be weakest. All vortices investigated numerically in the previous section were found to have precisely one turning radius.

The expansion (3.69) for  $v_\theta$  is not valid in the neighbourhood of  $r = r_c$ , since  $\psi'_0$  is zero there, and so by (3.73)  $A$  would be unbounded. We must therefore rescale the equations in the neighbourhood of  $r = r_c$  and derive equations for the perturbation expansion in this inner asymptotic region. In the vicinity of  $r = r_c$ , we have

$$G(r) = m^2 a_1 (r - r_c) + \dots, \quad (3.78)$$

where  $a_1$  is a positive constant. Rescaling the radial coordinate as  $x = m^{2/3}(r - r_c)$  the leading order equation for  $v_\theta$  from (3.67) becomes

$$\frac{d^2 v_\theta}{dx^2} + a_1 x v_\theta = 0. \quad (3.79)$$

Equation (3.79) has solutions  $v_\theta = A_i(-a_1^{1/3}x), B_i(-a_1^{1/3}x)$ , where  $A_i(z)$  and  $B_i(z)$  are Airy functions (Abramowitz & Stegun, 1965).

Four asymptotic regions have now been established, and the method of matched asymptotic expansions will now be used to relate the solutions in the different regions. The asymptotic regions are

- 1 :  $r > r_c$
- 2 :  $r - r_c = O(m^{-2/3})$
- 3 :  $1 < r < r_c$

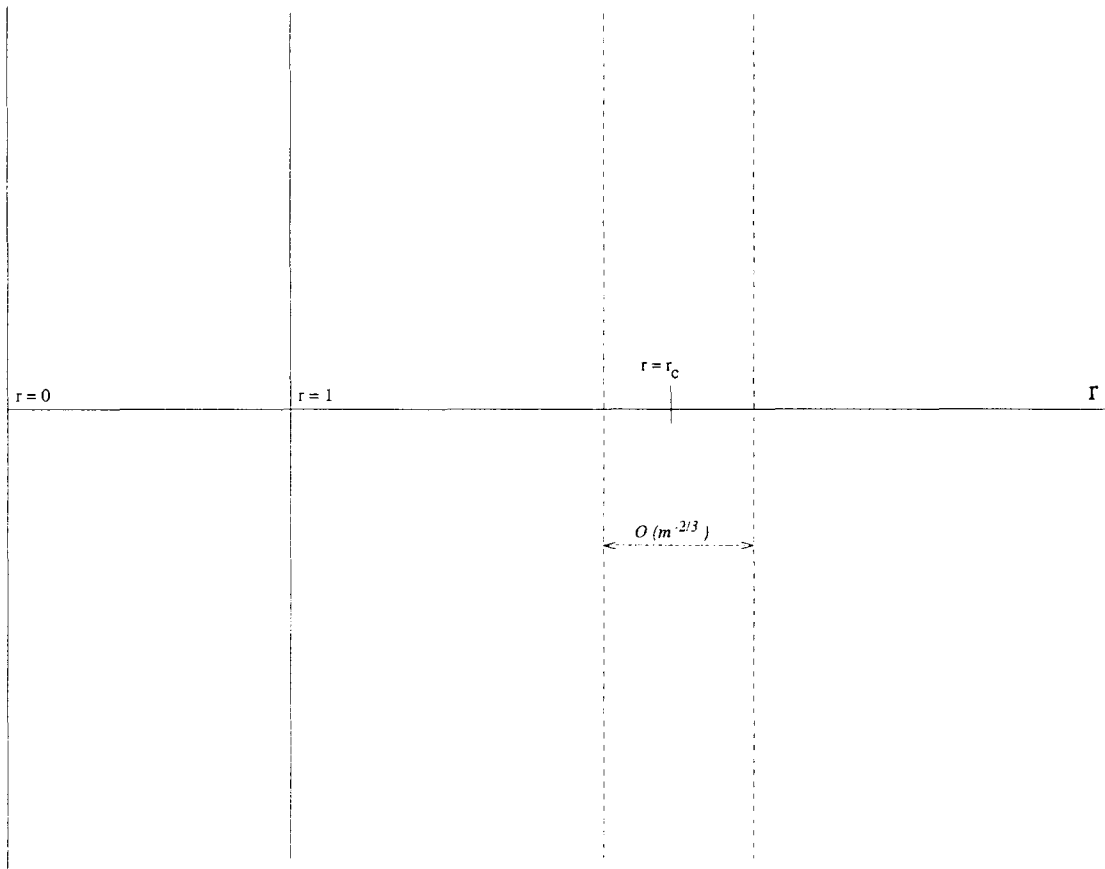


Figure 3.25: Asymptotic regions of shallow water vortex instability analysis.

4 :  $0 < r < 1$

The situation is depicted in figure 3.25.

**Region 1:**  $r > r_c$

As  $r \rightarrow \infty$ , we can place conditions on the branch of square root to take in the solution of (3.76) by imposing a radiation boundary condition, so that  $\psi'_0 > 0$  as  $r \rightarrow \infty$ . This immediately implies, through the matching condition in the limit  $x \rightarrow \infty$ , the ratio of  $A_i$  to  $B_i$  to take in the solution of (3.79). The expansions of  $A_i(z)$  and  $B_i(z)$  in the limit  $z \rightarrow \infty$  then gives, through the matching conditions, the ratio of the growing to decaying exponential solutions to (3.67) for  $1 < r < r_c$ .

**Region 2:**  $r - r_c = O(m^{-2/3})$

For  $z \rightarrow -\infty$ , the Airy functions take the asymptotic forms

$$A_i(-z) \sim \pi^{-1/2} z^{-1/4} \sin(2/3 z^{3/2} + \pi/4) \quad (3.80)$$

$$B_i(-z) \sim \pi^{-1/2} z^{-1/4} \cos(2/3 z^{3/2} + \pi/4). \quad (3.81)$$

Therefore, if we write  $v_\theta = \alpha A_i(-a_1^{1/3} x) + \beta B_i(-a_1^{1/3} x)$ , matching to a radiating field as  $x \rightarrow \infty$  implies  $\alpha/\beta = i$ .

In the limit  $x \rightarrow -\infty$  we have

$$A_i(z) \sim \frac{1}{2} \pi^{-1/2} z^{-1/4} e^{-2/3 z^{3/2}} \quad (3.82)$$

$$B_i(z) \sim \pi^{-1/2} z^{-1/4} e^{2/3 z^{3/2}}. \quad (3.83)$$

**Region 3:**  $1 < r < r_c$

Now if we let

$$\Psi_0(r) = - \int_r^{r_c} \left( \frac{1}{r^2} - \frac{(-c_0 + \bar{v}/r)^2 F^2}{1 + F^2 \bar{h}} \right)^{1/2} dr \quad (3.84)$$

and

$$\Psi_1(r) = \int_r^{r_c} \frac{c_1(-c_0 + \bar{v}/r)}{\Psi_0'(1 + F^2 \bar{h})} dr \quad (3.85)$$

then, for  $1 < r < r_c$ , we have

$$v_\theta = A(r) \left( a e^{m\Psi_0 + \Psi_1} + b e^{-m\Psi_0 - \Psi_1} \right), \quad (3.86)$$

where the ratio of  $b$  to  $a$  is to be determined by the matching conditions to the Airy function region. Now the  $B_i(-a_1^{1/3} x)$  term is, by (3.83), exponentially growing away from  $r = r_c$  - i.e. it is exponentially decaying with radius in  $1 < r < r_c$ . It therefore matches to the term  $b e^{-m\Psi_0 - \Psi_1}$  in the solution in the region  $1 < r < r_c$ . Correspondingly, the  $A_i(-a_1^{1/3} x)$  term matches to the solution which is exponentially growing with radius - that is, the term  $a e^{m\Psi_0 + \Psi_1}$ . Hence by considering (3.82-3.83) in the limit  $z \rightarrow \infty$ , the ratio of exponentially growing to exponentially decaying terms in the region  $1 < r < r_c$  satisfies the relation  $a/b = i/2$ . Up to an arbitrary amplitude, therefore, this completes the solution in the range  $r > 1$ .

**Region 4:**  $0 < r < 1$ 

In the range  $r < 1$ , the crucial boundary condition is regularity at  $r = 0$ . This implies only solutions of the form

$$v_\theta = de^{m\Psi_0 + \Psi_1} \quad (3.87)$$

are possible, where  $\Psi_0$  is given by (3.84), and  $\Psi_1$  by (3.85).

**Jump conditions at  $r = 1$** 

The final task, which determines the eigenvalue  $c$  at successive orders, is to apply continuity of  $v_r$  and  $h$  at  $r = 1$ , which is expressed in the continuity condition (3.18).

To find  $v_r$ , we may use to sufficient accuracy

$$\frac{dv_\theta}{dr} \sim \frac{im}{r} v_r. \quad (3.88)$$

For  $r < 1$ , this leads to

$$\left. \frac{v_\theta}{v_r} \right|_{r=1-} = i + O(m^{-1}). \quad (3.89)$$

On the other hand, for  $r > 1$ , we obtain

$$\left. \frac{v_\theta}{v_r} \right|_{r=1+} = i \frac{e^{-m\Psi(1)} + i/2e^{m\Psi(1)}}{-e^{-m\Psi(1)} + i/2e^{m\Psi(1)}}, \quad (3.90)$$

where here

$$\Psi(1) = \Psi_0(1) + m^{-1}\Psi_1(1). \quad (3.91)$$

Recalling that  $\Psi < 0$ , this takes the asymptotic form for large  $m$ :

$$\frac{v_\theta}{v_r} \sim \frac{i}{r\Psi'_0} \left( 1 + ie^{2m\Psi(1)} \right). \quad (3.92)$$

There are algebraic corrections to these terms, but because of our judicious decomposition of  $A$  and  $\psi$ , the expression (3.92) expresses the principal exponential terms. In particular, then, it has the correct expression for the leading order (exponentially small) imaginary part of  $v_\theta/v_r$ .

Returning to the continuity condition (3.18), at order  $O(m)$ , we simply have

$$c_0 = \bar{v}(1). \quad (3.93)$$

At the next order, we obtain

$$c_1 = -\frac{1}{2}H_1 \left(1 - \frac{1}{2}ie^{2m\Psi(1)}\right), \quad (3.94)$$

where  $H_1 = 1 + F^2\bar{h}(1)$ .

There are two things to note about (3.94). Firstly, the correction to the real phase speed of the disturbance is negative, and is in accordance with Kelvin's expression (3.19) in the limit  $F \ll 1$ . This is consistent with the claim that the disturbance on the boundary of the vortex has locally the character of a Rossby wave, with a pseudo-westward phase speed. The second thing is that the imaginary correction to  $c$  is always positive, corresponding to a temporally growing disturbance of form  $e^{-imct}$  at any value of  $F$  or  $f$ . Since the asymptotic limit in this case is of a particular type of disturbance, rather than a particular type of basic state, as it was in the  $F \ll 1$  analysis of chapter 2, we conclude that all basic states which satisfy the assumption of a single turning point are unstable, at least to large mode number disturbances.

### The low Froude number limit

We can obtain an independent check on the expression (3.94) in the limit of low Froude number by expanding it for  $F \ll 1$  and comparing the result with the expression (3.51) expanded in the limit of large  $m$ .

We start by expanding the expression (3.84) for  $\Psi_0(1)$  in the limit  $F \ll 1$ . Firstly, we recall that  $\bar{v}$  is of order  $O(F)$  everywhere except where  $r$  is of order  $O(1)$ . Therefore, to leading order in  $F$ , and recalling that  $c_0 = 1/2$  at leading order in  $F$ , we have that  $r_c = 2F^{-1}$  at leading order in  $F$ .

Now the integrand in (3.84) takes the asymptotic forms

$$\left(\frac{1}{r^2} - \frac{(-c_0 + \bar{v}/r)^2 F^2}{1 + F^2\bar{h}}\right)^{1/2} \sim \begin{cases} \frac{1}{r} + O(F) & \text{for } r = O(1) \\ F \left(\frac{1}{F^2 r^2} - \frac{1}{4}\right)^{1/2} + O(F^2) & \text{for } r = O(F^{-1}) \end{cases} \quad (3.95)$$

The technique is to split up the range of integration into two sub domains:  $[1, F^{-1/2}]$  and  $[F^{-1/2}, 2F^{-1}]$ . In the latter of these two domains we use a rescaled variable  $R \equiv Fr$ . The leading order expansion of  $\Psi_0(1)$  is then

$$\Psi_0(1) \sim \int_2^{F^{1/2}} \left(\frac{1}{R^2} - \frac{1}{4}\right)^{1/2} dR + \int_{F^{-1/2}}^1 \frac{1}{r} dr. \quad (3.96)$$

Integrating, substituting, and expanding for small  $F$ , we obtain

$$\Psi_0(1) \sim 1 + \ln F - \ln 4 + O(F). \quad (3.97)$$

The asymptotic evaluation of (3.85) for  $\Psi_1(1)$  is simpler, because the integrand has a regular expansion in  $F$ . The leading contribution comes from the range  $r = O(F^{-1})$ , and  $\Psi_1(1)$  takes the form

$$\Psi_1(1) \sim \frac{1}{4} \int_2^0 \left( \frac{1}{R^2} - \frac{1}{4} \right)^{-1/2} = -1. \quad (3.98)$$

It follows from (3.94) that the growth rate of the instability is

$$\frac{1}{4} e^{2m\Psi(1)} = \frac{1}{4} \left( \frac{F}{4} \right)^{2m} e^{2(m-1)}. \quad (3.99)$$

To compare the expression (3.99) with the predictions of the analysis for  $F \ll 1$ , we expand  $\text{Im}(\omega)$  for large  $m$ , where  $\text{Im}(\omega)$  is given by (3.51). For large  $m$  we have

$$\text{Im}(\omega) \sim \frac{\pi F^{2m}}{2m((m-1)!)^2} \frac{1}{4^{2m}} (m-1)^{2m}. \quad (3.100)$$

Using Stirling's formula for  $(m-1)!$ :

$$(m-1)! = (2\pi)^{1/2} (m-1)^{m-1/2} e^{-(m-1)}, \quad (3.101)$$

we have

$$\text{Im}(\omega) \sim \frac{1}{4} \frac{e^{2(m-1)}}{4^{2m}} F^{2m}, \quad (3.102)$$

and hence the low Froude number and large mode number analyses agree in the limit in which they are both valid.

### Comparison with numerical eigenvalue calculations

In addition to the analysis in the low Froude number limit, we can also test the validity of the general expression (3.94) given for the growth rate of the instability in the WKBJ limit against the numerical eigenvalue calculations.

Growth rates of the instability against mode number are shown in figures 3.26 & 3.27.

The basic states chosen all have Froude number  $F = 2.5$  in figure 3.26, and  $F = 5$  in figure 3.27, with varying values of  $f$  indicated on the graphs. Overall there seems to be good

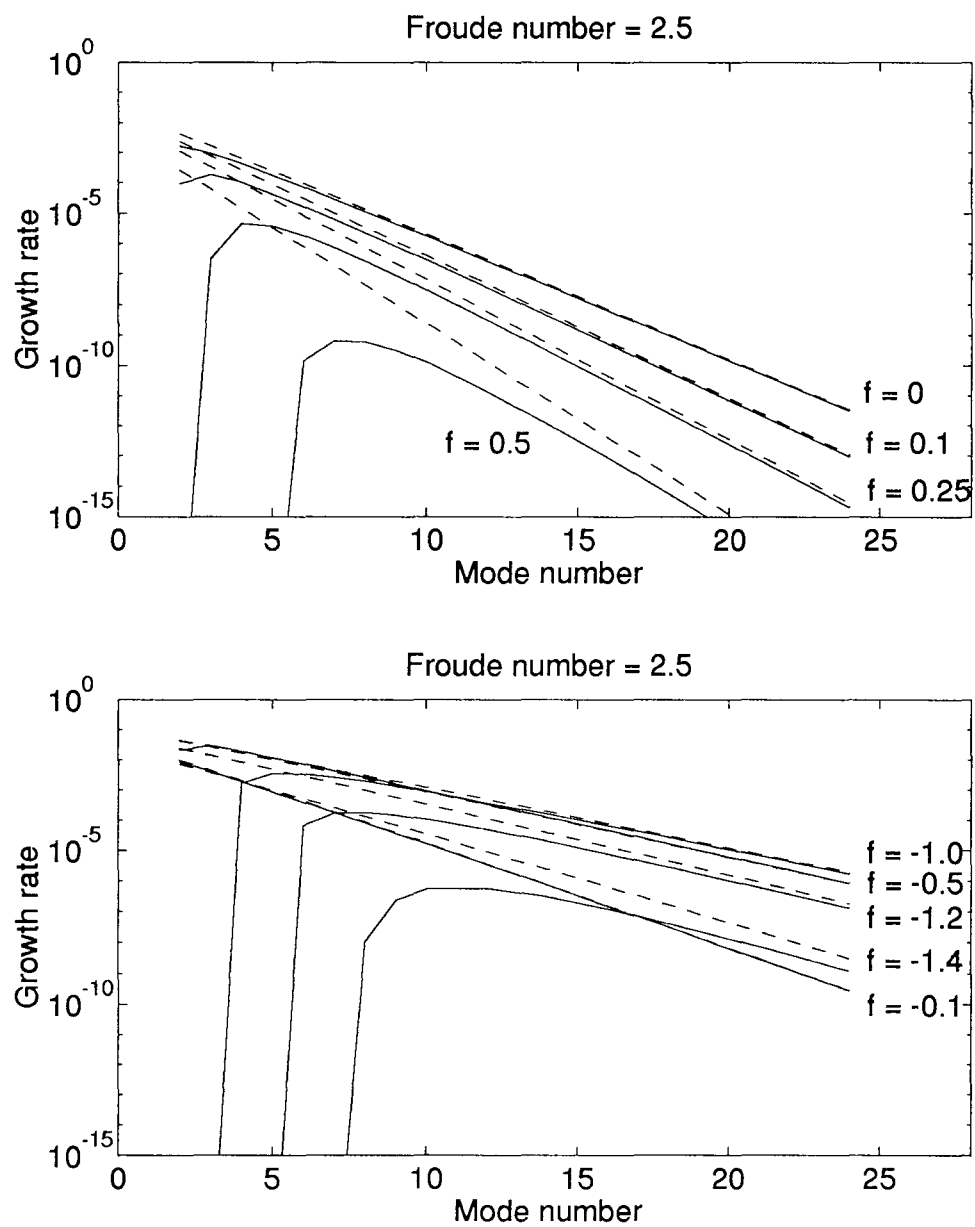


Figure 3.26: Comparison of eigenmode growth rates (solid lines) with WKBJ predictions (dashed lines),  $F = 2.5$ , for  $m = 0$  to 25, at various values of  $f$ .

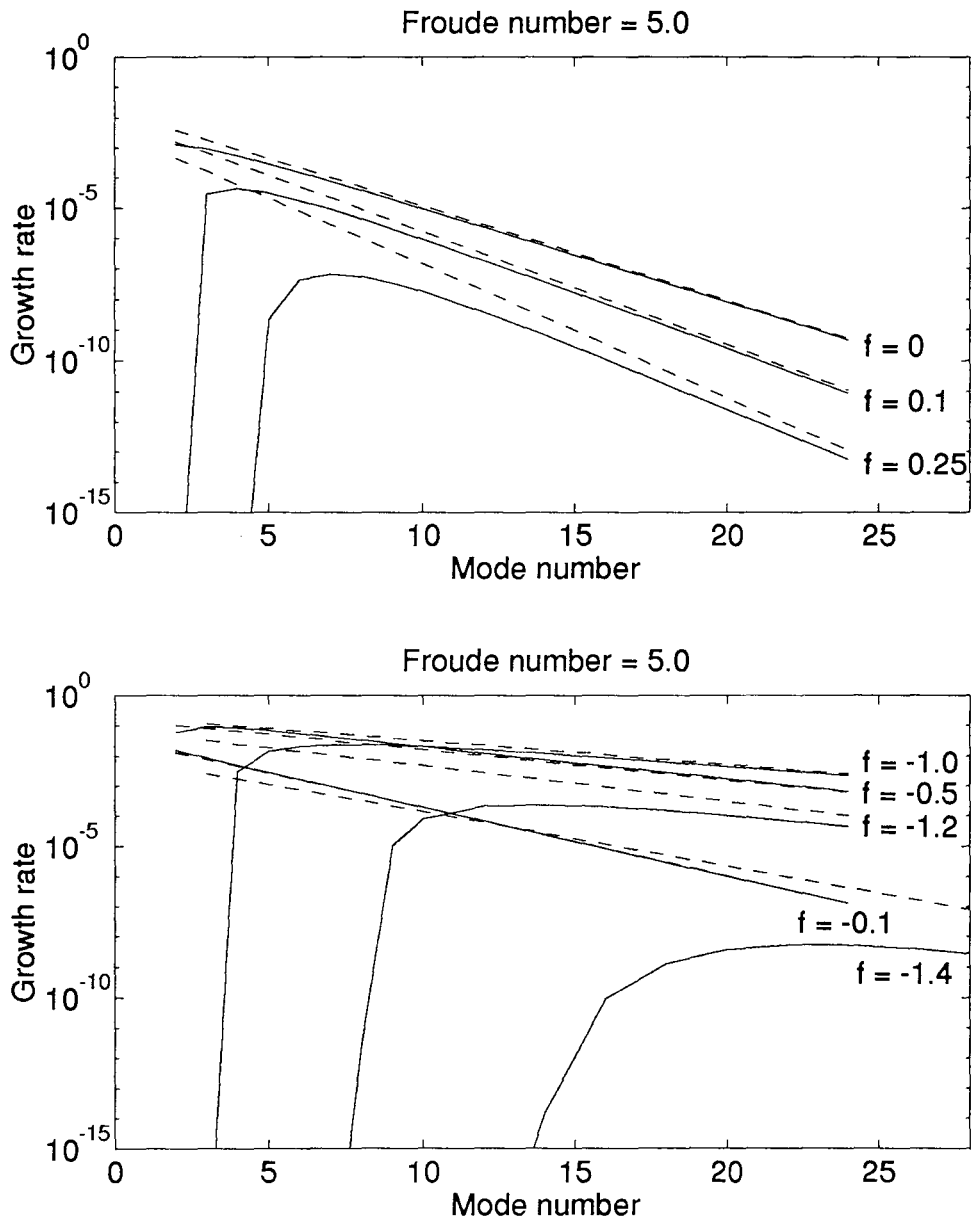


Figure 3.27: Comparison of eigenmode growth rates (solid lines) with WKBJ predictions (dashed lines),  $F = 5.0$ , for  $m = 0$  to 25.

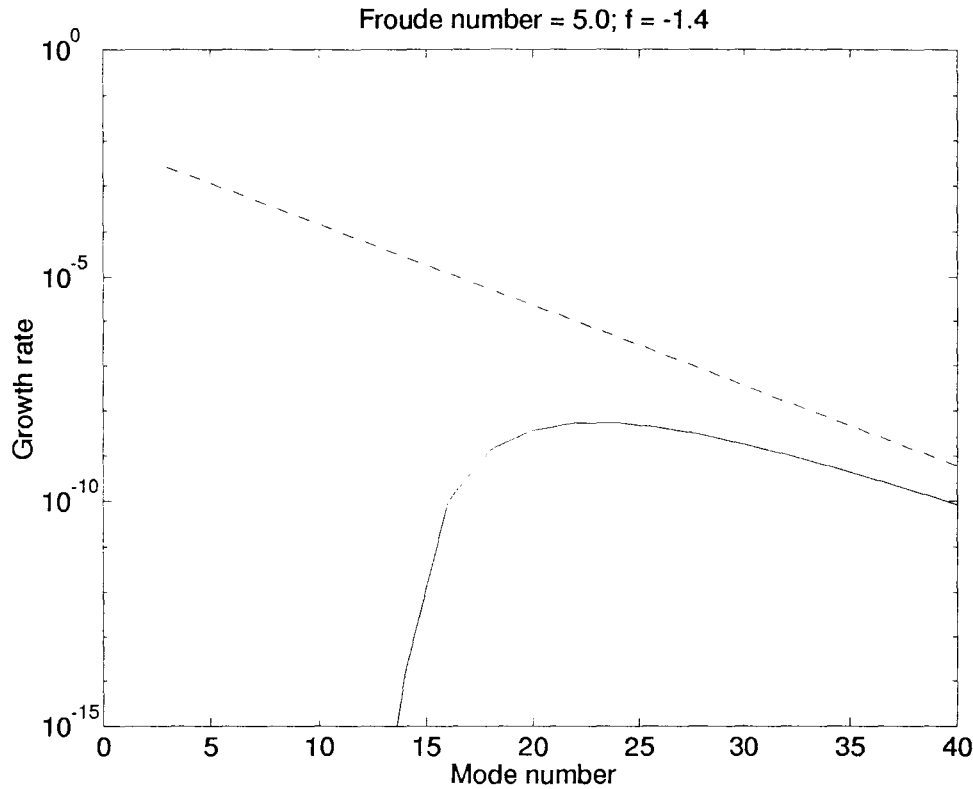


Figure 3.28: Comparison of eigenmode growth rate (solid line) with WKB prediction (dashed line) for  $F = 5.0$  and  $f = -1.4$ , extended to  $m = 40$ .

agreement between the WKB analysis (dashed lines) and the numerical eigenvalue code (solid lines), even for quite moderate values of  $m$ . The case  $F = 5$ ,  $f = -1.4$  is extended to  $m = 40$  in figure 3.28 to demonstrate agreement in this case.

A significant distinction is to be drawn between  $f > 0$  and  $f < 0$ . For given  $F$ , the magnitudes of  $\Psi_0(1)$  and  $\Psi_1(1)$  are always greater when  $f > 0$  than when  $f < 0$ . It follows immediately that the instability will be weaker for  $f > 0$  in the limit of large  $m$ . This is significant, in that it is dependent entirely upon the nature of the basic state, and independent of the effects of inertial cut-off, which are assumed not to apply, since the WKB analysis assumes that  $f$  is of order unity, whereas  $\omega$  is of order  $m \gg 1$ . Where the numerical eigenvalues are in good qualitative agreement with the WKB prediction, any differences between them for different values of  $f$  must be directly attributable to the nature of the basic state alone, and independent of the effects of the inertial cut-off.

For small  $m$  and small  $|f|$ , the eigenmodes are unstable, and their growth rates are broadly

in line with the values predicted by the WKBJ analysis. However, as  $|f|$  is increased, the eigenmodes become stable at small  $m$ . Since this effect is not predicted by the WKBJ analysis, it must be due to the fact that the eigenfrequencies are comparable with the magnitudes of the inertial frequency, and hence the inertial cut-off is significant.

As a heuristic way of thinking about the behaviour of the growth rates, I propose that in the region where they are seen to be increasing with increasing  $m$ , it is because the real part of the eigenvalue is increasing. The growth rate is therefore dominated by effects of the inertial cut-off. Examination of figures 3.26 & 3.27 shows that, once the instability has set in, this range of  $m$  tends to be quite small. However, in the range where the growth rate of the instability decreases with  $m$ , I propose that the WKBJ analysis is broadly valid in this limit, and the dependence of the growth rate of the instability on  $f$  is determined largely by the nature of induced basic state, and not directly by the effect of the inertial cut-off. Even in the range where the inertial cut-off is dominating the lower eigenmodes, the nature of the basic state is clearly important, in that it sets the real part of the eigenfrequency, and hence determines whether the eigenmodes are unstable or not.

In conclusion, the axisymmetric vortex is always unstable, but as  $F$  and  $|f|$  are increased, larger and larger values of  $m$  must be taken to obtain the instability. Almost all the asymmetry between cyclones and anticyclones can be explained in terms of the basic state. At large  $m$ , the nature of the basic state determines the strength of Rossby wave – gravity wave interactions, and at small  $m$  it determines whether and by how much the real part of the eigenfrequency will exceed  $|f|$ , and hence how significantly the instability is affected by the inertial cut-off.

### 3.2.6 The Sozou modes

The analysis of the previous sections is distinguished by the fact that only one eigenmode has been found, whereas Sozou (1987) found an infinite set of modes in the Rankine vortex at non-zero Mach number.

The purpose of this section is to explain the difference between Sozou's results, both analytical and numerical, and the present analysis. It turns out that the difference lies in the fact that the Rankine vortex has uniform vorticity and non-uniform potential vorticity for all  $M \neq 0$ , whereas in the analysis of the previous section, we have assumed the potential vorticity to be piecewise constant.

We start by obtaining the potential vorticity of the Rankine vortex. The Rankine vortex has uniform vorticity, which we shall set to unity. Then

$$\bar{v}(r) = \begin{cases} \frac{1}{2}r & r < 1 \\ \frac{1}{2r} & r > 1 \end{cases}. \quad (3.103)$$

Using  $d\bar{h}/dr = \bar{v}^2/r$ , and applying continuity of  $\bar{h}$  at  $r = 1$ , we have

$$\bar{h}(r) = \begin{cases} -\frac{1}{4} + \frac{1}{8}r^2 & r < 1 \\ -\frac{1}{8}r^{-2} & r > 1 \end{cases}. \quad (3.104)$$

Hence the potential vorticity and its gradient in the radial direction are given respectively by

$$Q = \frac{1}{1 - \frac{1}{8}F^2(2 - r^2)}; \quad \frac{dQ}{dr} = -\frac{F^2r}{\left[2 - \frac{1}{4}F^2(2 - r^2)\right]^2}. \quad (3.105)$$

From this we see that  $dQ/dr < 0$  for all  $r < 1$ , and the potential vorticity is zero for  $r > 1$ . Hence the potential vorticity gradient is monotonic, and the vortex is not unstable to a barotropic Rossby wave – Rossby wave type of instability. However, the non-zero potential vorticity gradient means that, in addition to the Rossby wave on the boundary of the vortex, it is capable of supporting an infinite set of Rossby wave modes within the vortex.

We now consider the limit  $m \gg 1$ . Returning to the eigenvalue equations (3.12 - 3.17), if additional modes are to be introduced in this large  $m$  limit as a result of the non-zero gradient of potential vorticity, it can only be because  $(H/\sigma)dQ/dr \sim O(m)$  over a range of order unity within the vortex. Only then is the balance of terms in the equation for  $\psi_0$  changed at leading order in  $m$ .

In fact, the uniform vorticity of the Rankine vortex is significant, as well as its non-uniform potential vorticity. Within the vortex,  $\sigma = -\omega + m$ , i.e.  $\sigma$  is constant within the vortex, and there are no critical layers there (unless  $\sigma = 0$  throughout the vortex). In this case we may take  $\sigma = m + m^{-1}c_2$ , where  $c_2$  is constant, so that  $\sigma$  is of order  $m^{-1}$  throughout the vortex. It turns out that the equation for  $v_\theta$  is singular in the general cases to be described below, and it is more convenient to work with an equation for  $v_r$ . Writing  $v_r(r) = A(r)e^{im\psi(r)}$ , the equation for  $\psi_0$  then becomes

$$\psi_0'^2 = -\left(\frac{1}{r^2} + \frac{F^2}{4c_2H(r)}\right), \quad (3.106)$$

where  $H(r) = 1 + F^2\bar{h}(r)$ . In this case, it is convenient to note that  $c_1 = 0$ , and hence  $\psi_1 = 0$ .

Now, we consider the continuity condition (3.18). At order unity, it is

$$-\frac{c_2}{m} \left[ \frac{v_\theta}{v_r} \right] = [iH(1)Q], \quad (3.107)$$

and therefore we require  $v_\theta/v_r$  to be of order  $m$  at  $r = 1^-$ . Since  $v_\theta \sim (ir/m)dv_r/dr$ , this can only be achieved if  $v_r = O(m^{-1})$  at  $r = 1$ .

We must now consider two possible cases:  $c_2 > 0$  and  $c_2 < 0$ . If  $c_2 > 0$ , we can write down the solution for  $v_\theta$  over the range  $0 < r < 1$  as

$$v_r = A(r) \exp \left[ m \int_0^r \left( \frac{1}{r^2} + \frac{F^2}{4c_2 H(r)} \right)^{1/2} dr \right]. \quad (3.108)$$

In this case,  $v_r$  is always of order 1, and hence it will not be possible to satisfy the continuity conditions at  $r = 1$ .

Therefore, we seek solutions with  $c_2 < 0$ . For convenience, we introduce a new constant  $\kappa$ , and let  $c_2 = -4F^2\kappa^{-2}$ . Then

$$\psi_0'^2 = \left( \frac{\kappa^2}{H(r)} - \frac{1}{r^2} \right). \quad (3.109)$$

There is now a turning point at  $r_c$ , given by  $H(r_c)/r_c^2 = \kappa^2$  and, provided  $\kappa$  is sufficiently large, this turning point will occur at some  $r_c < 1$ . It is simple to show from the form  $H(r)$  that the turning point is unique for a given  $\kappa$ . The solution in  $0 < r < 1$  is now divided into three asymptotic regions

$r < r_c$  Exponentially growing solution

$r - r_c = O(m^{-2/3})$  Airy functions

$r_c < r < 1$  Oscillatory functions

For  $0 < r < r_c$ , we will have

$$v_r = A(r) \exp \left[ m \left( \frac{1}{r^2} - \frac{\kappa^2}{H(r)} \right)^{1/2} dr \right]. \quad (3.110)$$

In the region  $r - r_c = O(m^{-2/3})$ , the solution will be represented in terms of Airy functions. What is important for the eigenvalue equation is the solution in  $r > r_c$ . Now, if the solution

in  $r < r_c$  consists of only an exponential term which is growing in  $r$ , then the solution in the neighbourhood of  $r = r_c$  will be represented by  $A_i(z)$ , where  $z$  is proportional to  $r^{2/3}$ . Then in  $r > r_c$ , matching to the Airy function gives a solution for  $v_r$ :

$$v_r = A(r) \cos \left[ m \int_{r_c}^r \left( \frac{\kappa^2}{H(r)} - \frac{1}{r^2} \right)^{1/2} dr - \frac{\pi}{4} \right]. \quad (3.111)$$

If we now wish to have  $v_r = 0$  at leading order in  $m$  then,

$$m \int_{r_c}^r \left( \frac{\kappa^2}{H(r)} - \frac{1}{r^2} \right)^{1/2} dr = \left( n - \frac{1}{4} \right) \pi; \quad n = 1, 2, 3, \dots \quad (3.112)$$

This equation is the leading order eigenvalue equation for  $\kappa$  at arbitrary Froude number  $F$ . To make further progress, and to compare this result with that obtained by Sozou (1987), we shall make the assumption  $F \ll 1$ , but  $\kappa = O(1)$ . The only approximation to make is that  $H(r) = 1$  in (3.112). Then we obtain a dispersion relation for  $\kappa$

$$\sqrt{\kappa^2 - 1} - \arccos \kappa^{-1} = m^{-1} \left( n - \frac{1}{4} \right) \pi. \quad (3.113)$$

Sozou works with a frequency divided by the vorticity in the vortex  $f = m - 2m\omega^2/s^2$ , where  $\omega$  is the vorticity in the vortex. After rescaling Sozou's (1987) equations, one can show that his variable  $s$  should correspond to our variable  $m\kappa$ . Sozou claims that roots of his dispersion relation satisfy  $J_m(s) = 0$ . It is more convenient to work with  $\kappa$  than  $s$ , so we solve  $J_m(m\kappa) = 0$  for large  $m$  and  $\kappa$  of order unity.

From Abramowitz & Stegun (1965),

$$J_m(m \sec \beta) \sim \sqrt{2/(\pi m \tan \beta)} \cos(m \tan \beta - m\beta - \pi/4). \quad (3.114)$$

Identifying  $\sec \beta \equiv \kappa$  gives  $\tan \beta \equiv \sqrt{\kappa^2 - 1}$ , and hence Sozou's condition is

$$m\sqrt{\kappa^2 - 1} - m \arccos \kappa^{-1} - \pi/4 = (n - 1/2)\pi, \quad (3.115)$$

which is the same as equation (3.113).

The important point is that the additional roots found by Sozou are only possible at large  $m$  because of the uniform vorticity and non-uniform potential vorticity in the Rankine vortex

at non-zero Mach number. The large mode number analysis reveals that there is a turning point within the vortex in these cases, implying that the eigenmodes have a wave-like structure for  $r_c < r < 1$ . The turning point is possible only because  $\sigma = O(m^{-1})$  and  $dQ/dr \neq 0$  throughout the vortex region, neither of which can be true for a vortex with uniform potential vorticity, except in the singular limit  $F = 0$ . The conclusion is that they are associated with Rossby waves propagating on the potential vorticity gradient within the Rankine vortex. The fact that  $c_2 < 0$  once again reminds us that they have a retrograde or pseudo-westward phase progression, consistent with their being Rossby-wave like.

An expression for the growth rate of the instability can also be obtained, by considering the leading order real terms in (3.18). Outside the vortex, the equations for the disturbances are the same as before, except that now  $c_1$  in (3.74) is zero, and hence  $\Psi_1 = 0$ . Outside the vortex, therefore, the first real terms in  $v_\theta/v_r$  are  $e^{2m\Psi_0(1)}$ , where  $\Psi_0$  is given by (3.84).

Now, at  $r = 1^+$ ,  $v_\theta/v_r = -i$ , whereas at  $r = 1^-$ ,  $v_\theta/v_r = -imH_1/c_2 = imH_1\kappa^2/(4F^2)$ . Therefore, the real part of (3.18) is

$$-c_i m^2 H_0 / c_2 + \frac{c_2}{m} e^{2m\Psi_0(1)} = 0, \quad (3.116)$$

and hence we may write down an expression for the principal imaginary part of  $\omega$

$$\omega_i = c_2^2 / (m^2 H_0) e^{2m\Psi_0(1)}. \quad (3.117)$$

### 3.3 Instability of a circular vortex with smooth potential vorticity

We turn now to showing that, under certain assumptions, the vortex instability found in the previous section can be generalized to vortices with a smooth (analytic) potential vorticity profile, provided the potential vorticity gradient is sufficiently steep. I show how to scale the potential vorticity gradient so that the instability threshold is found at a finite value of the gradient.

#### 3.3.1 Disturbance equations

To begin, we consider how the behaviour of differential equations (3.9-3.11) are modified when there is a non-zero potential vorticity gradient in the basic state.

The equations for the eigenfunctions were stated in the previous section as

$$\frac{dv_r}{dr} = A(r)v_r + B(r)v_\theta \quad (3.118)$$

$$\frac{dv_\theta}{dr} = C(r)v_r + D(r)v_\theta, \quad (3.119)$$

where

$$A(r) = \frac{F^2\sigma Qr}{m} - \frac{d}{dr} \ln H \frac{1}{r} \quad (3.120)$$

$$B(r) = \frac{iF^2\sigma^2r}{Hm} - \frac{im}{r} \quad (3.121)$$

$$C(r) = \frac{iF^2HQ^2r}{m} + \frac{im}{r} + \frac{iH}{\sigma} \frac{dQ}{dr} \quad (3.122)$$

$$D(r) = -\frac{F^2Q\sigma r}{m} - \frac{1}{r}, \quad (3.123)$$

and  $H = 1 + F^2\bar{h}$ . We now consider the order of terms in the case where  $dQ/dr \neq 0$ .

In general,  $\sigma$  is of order  $O(m)$ , and the principal behaviour of the eigenmodes will not be affected by the term  $(H/\sigma)dQ/dr$  in  $C(r)$ , not present in the case of piecewise uniform potential vorticity. However, we know from the eigenmodes found above that  $\sigma > 0$  at the vortex boundary, but tends to a negative constant value as  $r \rightarrow \infty$ . Therefore, there must exist at least one zero of  $\sigma$  in  $r > 1$  and, if  $\bar{v}$  approaches  $r = 1$  faster than linearly in  $r$ , there will exist another zero of  $\sigma$  in  $r < 1$ . In particular, if  $f$  is large, then the basic state flow could be taken to be approximated by the quasigeostrophic equations, in which case the velocity field takes the form  $I_0(F|f|r)$  for  $r < 1$ , and  $K_0(F|f|r)$  for  $r > 1$ .

To derive a distinguished asymptotic scaling for the problem, we consider a limit in which the potential vorticity gradient at the boundary of the vortex, although finite, is very sharp. In this limit, we expect to recover the results of the previous section, in which the eigenmode was exponentially growing in  $r$  for  $r < 1$ , and exponentially decaying in  $r$  for  $r > 1$ . To achieve this transition in the form of the eigenmode there must be an asymptotic region in the neighbourhood of  $r = 1$  in which the potential vorticity gradient enters the eigenfunction equations at the leading order in  $m$ . Across this region the nature of the solution will change from exponentially growing to exponentially decaying. There is only one way in which this can be achieved, and that is by bringing  $(H/\sigma)dQ/dr$  into leading order balance in (3.119).

Now, to change the balance in (3.119), we shall require  $(H/\sigma)dQ/dr$  to be of order  $m$ , in order to balance  $m/r$ . Furthermore, in the limit of a very sharp potential vorticity jump

(abbreviated to PV jump), we know that  $\sigma = H(1)/2$  at the boundary of the vortex. Over a range of order  $\delta$ ,  $\sigma$  is of order  $1 + m\delta$ , and if  $Q$  varies by order unity across this region, its gradient is of order  $1/\delta$ .

It remains to show that the required scaling is  $\delta \sim m^{-1}$ . If we take  $\delta \ll m^{-1}$ , then  $(H/\sigma)dQ/dr \sim 1/\delta$ , which is required to balance  $m/r$ . This contradicts the assumption  $\delta \ll m^{-1}$ , and hence we require  $\delta \geq O(m^{-1})$ . On the other hand, if  $\delta \gg m^{-1}$ , then  $(H/\sigma)dQ/dr \sim 1/(m\delta^2)$ . Requiring this to balance  $m/r$  leads to another contradiction, and hence we arrive at the scaling  $\delta = O(m^{-1})$ .

The situation now being considered is a potential vorticity jump of order one over a distance of order  $m^{-1}$ , with a gradient of order  $m$ . This is internally consistent – if  $Q'$  is of order  $m$  over a range of order  $m^{-1}$  then this will lead to a net PV jump of order one over this range. The amplitude of the eigenfunction  $e^{\pm im\Psi}$  varies by order unity over this range, and hence  $\delta \sim m^{-1}$  represents the distinguished scaling for the problem, in which the potential vorticity changes by order unity over the length scale of amplitude variations of order unity in the eigenfunctions.

Now recall that the vortex is of unit radius, so the region of sharp PV gradients is centred on  $r = 1$ . Introducing a new range variable  $z = m(r - 1)$ , and assuming  $\sigma \sim O(1)$ , we obtain an equation for  $v_r$  at leading order in  $m$ :

$$\frac{d^2 v_r}{dz^2} - \left(1 + \frac{H}{\sigma} \frac{dQ}{dz}\right) v_r = 0. \quad (3.124)$$

To make further progress, we may assume initially that the PV jump occupies a small region in  $z$  (of order  $\epsilon$ ). In fact, it turns out that this is sufficient to understand the problem in full. We shall assume as before that  $Q(r = 1^-) = Q(r = 1^+) + 1$ . To fix ideas, we shall assume that the PV across the vortex boundary takes a hyperbolic tangent profile. Then

$$\frac{dQ}{dz} = -\frac{1}{2\epsilon} \operatorname{sech}^2(z/\epsilon), \quad (3.125)$$

so that

$$Q = -\frac{1}{2} \tanh(z/\epsilon) + b, \quad (3.126)$$

where  $b$  is an arbitrary constant, required for matching to the outer flow. The equations for the velocity and height fields of the basic state in the asymptotic region  $z = O(1)$  are

$$\frac{m}{F^2} \frac{dH}{dz} = f\bar{v} + \frac{\bar{v}^2}{r} \quad (3.127)$$

$$m \frac{d\bar{v}}{dz} = QH - f - \bar{v}(1 + z/m)^{-1}. \quad (3.128)$$

From (3.128) it follows that  $\bar{v}(z) = V_0(\text{constant}) + O(m^{-1})$ , and from (3.127) it follows that  $H(z) = H_0(\text{constant}) + O(m^{-1})$ . If we expand  $\bar{v} = V_0 + m^{-1}V_1 + \dots$ , then from (3.128) we obtain an equation for  $V_1$ :

$$\frac{dV_1}{dz} = QH_0 - f - V_0, \quad (3.129)$$

with solution

$$V_1 = -\frac{1}{2}\epsilon H_0 \ln \cosh(z/\epsilon) + (bH_0 - f - V_0)z. \quad (3.130)$$

Without loss of generality, we may take the associated constant of integration to be zero in this case by absorbing it into  $V_0$ . The variable  $\sigma = m(-c + V/r)$  now takes the form

$$\sigma = -c_1 - \frac{1}{2}\epsilon H_0 \ln \cosh(z/\epsilon) + (bH_0 - f - 2V_0)z + O(m^{-1}). \quad (3.131)$$

The requirement  $\sigma = O(1)$  is met by setting  $c_0 = V_0$ . This is consistent with equation (3.94) the limit of a single discontinuity in potential vorticity.

We now have sufficient details of the basic state in the region  $z = O(1)$  to enable us to analyse the nature of the unstable eigenmode.

We start with the inner region,  $z = O(\epsilon)$ , across which the PV varies by an amount of order  $O(1)$ . Introducing a further variable  $\zeta = z/\epsilon$ , and expanding  $v_r = v_r^{(0)} + \epsilon v_r^{(1)} + \dots$  gives

$$v_r^{(0)} = \text{constant} = 1 \quad \text{say}. \quad (3.132)$$

Then

$$\frac{d^2 v_r^{(1)}}{d\zeta^2} = \frac{H_0}{2c_1} \text{sech}^2 \zeta. \quad (3.133)$$

Integrating for  $v_r^{(1)}$  gives

$$v_r^{(1)} = \frac{H_0}{2c_1} \ln \cosh \zeta + k_1 \zeta + k_2, \quad (3.134)$$

where  $k_1$ ,  $k_2$  and  $c_1$  are found by matching to  $v_r$  in the region  $z = O(1)$ .

Now, for  $z = O(1)$ ,  $\sigma$  takes the form

$$\sigma \sim -c_1 - \frac{H_0}{2}(|z| - \alpha z), \quad (3.135)$$

where  $\alpha = 2(bH_0 - f - 2V_0)/H_0$ . If  $|\alpha| < 1$ , then there are two roots of the equation  $\sigma = 0$ . As discussed above, this will be the generic case for low Rossby number flow, in which  $\sigma$  has a

zero on either side of the PV jump. Since the WKBJ ( $m \gg 1$ ) analysis was motivated by the difficulty of finding unstable modes numerically in the low Rossby number limit, I shall assume  $|\alpha| < 1$  for the remainder of the analysis of this section. The equation governing  $v_r$  is then

$$\frac{d^2 v_r}{dz^2} - \left(1 - \frac{1}{2\epsilon\sigma} \operatorname{sech}^2(z/\epsilon)\right) v_r = 0. \quad (3.136)$$

It follows that, to leading order of approximation,

$$\frac{d^2 v_r}{dz^2} - v_r = -\frac{4}{\epsilon} (-2c_1/H_0 - |z| + \alpha z)^{-1} e^{-z^2/\epsilon^2} v_r. \quad (3.137)$$

We retain the exponentially small term on the right hand side of (3.137) due to its possible singularities at  $\sigma = 0$ . We denote these positions by  $z = z_-$  and  $z = z_+$ .

Analysis of these points shows that they are regular singular points, with indicial exponents 0 and 1. Moreover, writing the solution with the logarithmic term in the form

$$v_r = 1 + \delta(z - z_0) \log(z - z_0) + \dots, \quad (3.138)$$

(where here  $z_0$  stands for  $z_-$  or  $z_+$ ) we can easily see that  $\delta$  will be exponentially small in  $\epsilon$ . It follows that the critical layers  $\sigma = 0$  are insignificant to the eigenfunctions at all algebraic orders in  $\epsilon$ , and the eigenfunctions and their derivatives will be continuous across  $\sigma = 0$  at all algebraic orders in  $\epsilon$ . Hence the leading order solutions are  $v_r = e^{\pm z}$ .

Now, we know from the analysis for the case of a sharp PV interface that we will require  $v_r$  to be exponentially decaying at leading order away from  $r = 1$ , and hence we take  $v_r = e^{-|z|}$  as the leading order solutions in the regions  $|z| = O(1)$ . It follows from matching to the inner region  $z = O(\epsilon)$  that  $v_r^{(1)} \sim -|\zeta|$  as  $|\zeta| \rightarrow \infty$ , and this matching to (3.134) fixes  $k_1 = k_2 = 0$ , and

$$c_1 = -\frac{1}{2} H_0. \quad (3.139)$$

This is consistent with the expression for  $c_1$  given by (3.94) in the analysis for the discontinuous potential vorticity. Hence,

$$\sigma = \frac{H_0}{2} (1 - |z| + \alpha z), \quad (3.140)$$

and the zeros of  $\sigma$  occur at two locations  $z_+$  and  $z_-$ , given by

$$z_+ = \frac{1}{1 - \alpha} > 0; \quad z_- = -\frac{1}{1 + \alpha} < 0. \quad (3.141)$$

We now turn to analysing the effect of the exponentially small  $\delta$  in the neighbourhood of the critical layers. We start by analysing  $v_r$  in the neighbourhood of  $z = z_-$ . Writing  $y = z - z_-$ , and substituting (3.139) into (3.137), we have

$$\sigma = \frac{H_0}{2|z_-|} y \quad (3.142)$$

$$\frac{d^2 v_r}{dy^2} - \left( 1 - \frac{4|z_-| e^{-z_-^2/\epsilon^2}}{\epsilon y} \right) v_r = 0. \quad (3.143)$$

Substitution of (3.138) with  $z_0 \equiv z_-$  into (3.143) gives

$$\delta = -4|z_-| \epsilon^{-1} e^{-z_-^2/\epsilon^2}. \quad (3.144)$$

Now, if we are constructing an unstable mode, it follows that  $\text{Im}\sigma < 0$ , and that therefore there is not really a singularity at  $\sigma = 0$  at all. If  $\sigma$  has a small negative imaginary part as we pass through  $y = 0$ , it follows from (3.142) that  $y$  must also have a small negative imaginary part ( $-i\mu$ , say). Since  $\ln(z - z_-)$  has branch points at the zeros of  $\sigma$ , the effect of this small negative imaginary part of  $\sigma$  is to displace the branch point of the logarithm from  $y = 0$  to  $y = i\mu$  for some small positive  $\mu$ . As  $y$  is increased through zero along the real axis, the argument of  $y$  must therefore increase by  $\pi$  to be consistent with the branch cut of the logarithm. The situation is depicted in figure 3.29. Since  $\ln y = \ln|y| + i\text{Arg}y$ , and since  $v_r$  takes the value  $e^{-|z_-|}$  to leading order at  $y = 0$ , it follows that the leading order contribution to the phase shift of the solution as we pass through  $y = 0$  is given by  $i\pi\delta e^{-|z_-|} y + \dots$ . The solution satisfies (3.137), and therefore for  $y > 0$ , the leading order contribution to the imaginary part of the solution introduced by the branch cut is

$$v_r^i = -4\pi i |z_-| e^{-|z_-|} \epsilon^{-1} e^{-|z_-|^2/\epsilon^2} \sinh y. \quad (3.145)$$

In addition to an imaginary part of the solution due to the presence of critical layers in the flow, an imaginary contribution to  $v_r$  can also be introduced by having a small imaginary part of  $c$ , which we shall denote as  $ic_i$ . Near  $z = 0$ , in the region where  $\zeta = O(1)$ ,  $v_r^{(i)}$  is expanded in powers of  $\epsilon$ :

$$v_r^i = v_0^i + \epsilon v_1^i + \dots \quad (3.146)$$

Then  $v_0^i$  is constant, and  $v_1^i$  satisfies

$$\frac{d^2 v_1^i}{d\zeta^2} = \frac{H_0 v_0^i}{2c_1} \text{sech}^2 \zeta - \frac{i H_0 c_i}{2c_1^2} \text{sech}^2 \zeta. \quad (3.147)$$

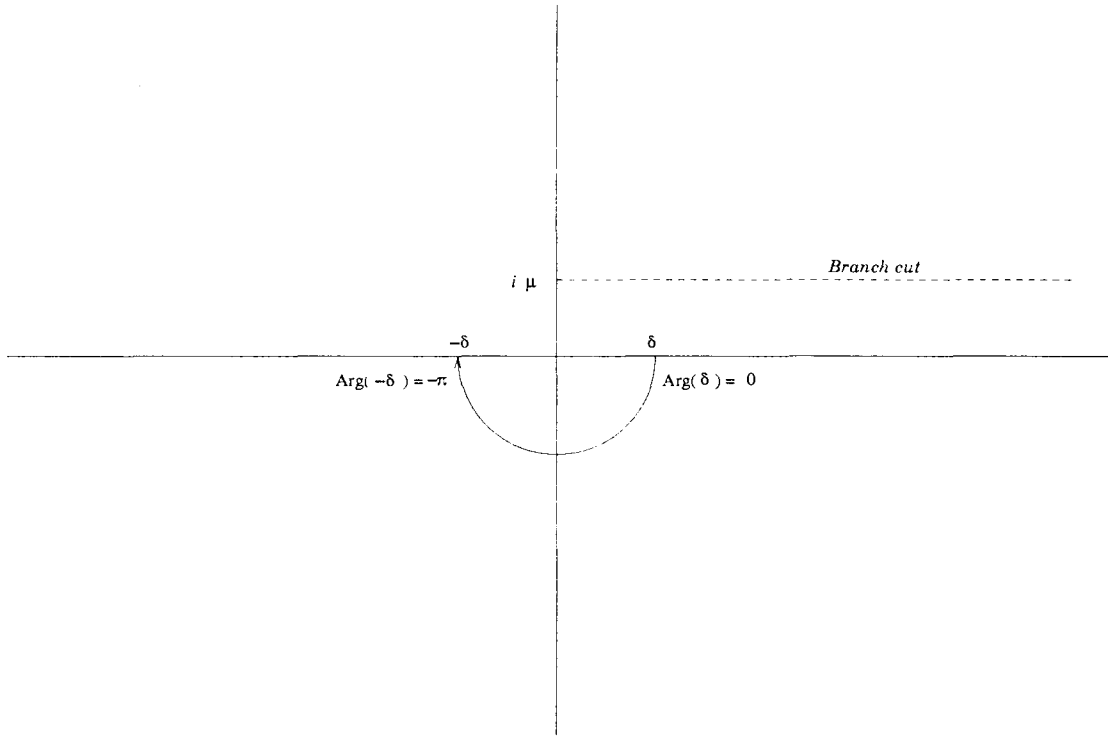


Figure 3.29: Schematic showing how argument changes in the neighbourhood of a branch point displaced slightly from the real axis.

This equation has solution

$$v_1^i = - \left( v_0^i + \frac{2ic_i}{H_0} \right) \ln \cosh \zeta + k_1 \zeta + k_2. \tag{3.148}$$

As  $\zeta \rightarrow -\infty$ ,

$$v_r^i \sim -4\pi i |z_-| e^{-|z_-|} \epsilon^{-1} e^{-|z_-|^2/\epsilon^2} (\sinh |z_-| + \epsilon \zeta \cosh |z_-| + O(\epsilon^2)). \tag{3.149}$$

Hence

$$v_0^i = -4\pi i |z_-| e^{-|z_-|} \sinh |z_-| \epsilon^{-1} e^{-|z_-|^2/\epsilon^2} \tag{3.150}$$

$$v_0^i + \frac{2ic_i}{H_0} + k_1 = -4\pi i |z_-| e^{-|z_-|} \cosh |z_-| \epsilon^{-1} e^{-|z_-|^2/\epsilon^2}. \tag{3.151}$$

Then, as  $\zeta \rightarrow \infty$ , we will have

$$v_r^i \sim v_0^i + \epsilon \left( -v_0^i - \frac{2ic_i}{H_0} + k_1 \right) \zeta. \quad (3.152)$$

The solution in the region  $z > 0$  is now written as

$$v_r^i = A\epsilon^z + B\epsilon^{-z}. \quad (3.153)$$

Matching implies

$$A + B = v_0^i; \quad A - B = -v_0^i - \frac{2ic_i}{H_0} + k_1. \quad (3.154)$$

It is the exponentially growing part of this solution which will match to the exponentially growing (and imaginary) part of the solution in  $r > 1$ , introduced in the region  $1 < r < r_c$  by the matching procedure across the sonic radius  $r = r_c$ . Of particular interest is therefore the value of  $A$ , which is given by

$$A = \frac{k_1}{2} - \frac{ic_i}{H_0} = -\frac{2ic_i}{H_0} - 2\pi i |z_-| \epsilon^{-2|z_-|}. \quad (3.155)$$

Finally, we must attend to the matching conditions across the second critical layer at  $z = z_+$ . In the same manner as the critical layer at  $z = z_-$ , this introduces a further small imaginary part to  $v_r$  as the leading order solution crosses the critical layer. The existing imaginary part is not changed at leading order. At this second critical layer we use the variable  $y = z - z_+$ . Then

$$\sigma = -\frac{H_0}{2|z_+|} y \quad (3.156)$$

$$\frac{d^2 v_r}{dy^2} - \left( 1 + \frac{4|z_+| e^{-|z_+|^2/\epsilon^2}}{\epsilon y} \right) v_r = 0. \quad (3.157)$$

Now recall that the singularity is to be removed by introducing a small negative imaginary part to  $\sigma$ . In the case  $z \sim z_+$ , we see from (3.156) that  $y$  therefore has a small positive imaginary part as we pass through  $y = 0$  along the real line. This is the opposite sign to the case  $z = z_-$ , in which  $y$  was required to have a small negative imaginary part. In the present case the branch

point of the logarithm is therefore displaced to  $y = -i\mu$ , and the argument of  $y$  decreases by  $\pi$  as  $y$  is increased through  $y = 0$ . Hence to the imaginary part of the solution we add

$$-4\pi i |z_+| e^{-|z_+|} \epsilon^{-1} e^{-|z_+|^2/\epsilon^2} \sinh y. \quad (3.158)$$

The exponentially growing part of this solution is

$$-2\pi i |z_+| e^{-2|z_+|} \epsilon^{-1} e^{-|z_+|^2/\epsilon^2} e^z. \quad (3.159)$$

Hence the sum of the exponentially growing imaginary terms in the region  $z > z_+$  will be

$$\left[ -2\pi i \epsilon^{-1} \left( |z_+| \epsilon^{-2|z_+|} e^{-z_+^2/\epsilon^2} + |z_-| e^{-2|z_-|} e^{-z_-^2/\epsilon^2} \right) - \frac{2ic_i}{H_0} \right] e^z. \quad (3.160)$$

Exponentially growing real terms can be removed by a small change to the real part of  $c$ .

We now turn to matching this to the region  $1 < r < r_c$ . In this region, the expansion of the leading order term for  $r \rightarrow 1^+$  gives an exponential function which is decaying with increasing  $r$ . However, as discussed in the analysis for the vortex with discontinuous PV, the radiation condition introduces an exponentially growing term, which is exponentially small (in  $m$ ), and out of phase with the leading order exponentially decaying term. The ratio of growing to decaying terms in  $v_r$  as  $r \rightarrow 1^+$  is  $-(i/2)e^{2m|\Psi(1)|}$ , where  $\Psi(1)$  is given by (3.84, 3.85, 3.91). Since we took  $v_r$  to be one at leading order in this region, matching conditions in the limit  $z \rightarrow \infty$  for the imaginary component of  $v_r$  from (3.160) imply

$$\frac{2\pi}{\epsilon} \left( |z_+| e^{-2|z_+|} \epsilon^{-z_+^2/\epsilon^2} + |z_-| e^{-2|z_-|} e^{-z_-^2/\epsilon^2} \right) + \frac{2ic_i}{H_0} = \frac{1}{2} e^{2m\Psi(1)}. \quad (3.161)$$

Now let  $Z = \max(|z_+|, |z_-|)$ . Then if

$$\epsilon = Z/(2|\Psi(1)|)^{1/2} m^{-1/2}, \quad (3.162)$$

with small corrections, then (3.161) is solved with  $c_i = 0$ , and the necessary imaginary part of  $v_r$  in the limit  $z \rightarrow \infty$  exists without introducing an imaginary part to  $c$ . If  $\epsilon$  is smaller than, but of the same order as, the value given by (3.162), then  $c_i$  will be of order  $e^{2m|\Psi(1)|}$ .

If  $\epsilon \ll m^{-1/2}$ , then the principal phase shift across the PV gradient is due to the imaginary part of  $c$ , and

$$c_i = \frac{1}{4} e^{2m\Psi(1)}. \quad (3.163)$$

Again, this is consistent with equation (3.94), derived in the limit of discontinuous potential vorticity.

Finally, if  $\epsilon > Z/(2|\Psi(1)|)^{1/2}m^{-1/2}$ , the equation (3.161) can only be satisfied with  $c_i < 0$ . This is a contradiction, since the analytic continuation used at the critical layers assumed  $c_i > 0$ . Consequently the eigenmode structure of the problem is lost if  $\epsilon > Z/(2|\Psi(1)|)^{1/2}m^{-1/2}$ .

It is interesting to see how some of these conclusions could have been reached without the detailed analysis presented above. In particular, the equation (3.143) is precisely the equation which would be obtained without any effects of divergence or gravity waves. It is Rayleigh's equation for a monotonic PV profile. The difference is that, without a turning point and gravity waves in the far field, the boundary conditions for (3.143) would normally be that the eigenfunctions should be exponentially decaying for  $|z| \rightarrow \infty$  at all orders, and in particular there would be no exponentially growing imaginary term. That would force  $c_i < 0$ , which is a contradiction, since  $c_i$  was assumed to be greater than zero.

Now, since it is possible to prove Rayleigh's theorem without recourse to eigenmodes, we should know that any attempt to construct solutions to (3.143), which are exponentially decaying as  $|z| \rightarrow \infty$ , by introducing an infinitesimally small imaginary part to  $c$  must ultimately contradict itself, and this is exactly what has happened. Reversing the signs of the imaginary terms in  $v_r$  throughout the analysis leads to the same contradiction for any postulated temporally decaying modes with  $c_i < 0$ . There are no analytic solutions to (3.143) satisfying exponentially decaying boundary conditions, and Rayleigh's theorem holds.

It follows that, if the structure of the instability is to be retained, the Rossby wave critical layers at  $\sigma = 0$  must not introduce an imaginary part in the eigenfunction greater than that required for matching to the imaginary part of the radiating solution in  $r > 1$ . Since the amplitude of the imaginary part introduced by critical layers will depend linearly on the strength of the PV gradient at the critical layers, and since the radiating solution has only an exponentially small (in  $m$ ) imaginary component as  $r \rightarrow 1^+$ , it follows that the PV gradient must be exponentially weak in  $m$  at the locations of the critical layers. Consequently, a rapidly decaying profile for the PV gradient, such as  $\text{sech}^2\zeta$ , will require only a small enhancement of the peak PV gradient (in this case given by  $\epsilon^{-1} = O(m^{1/2})$ ), whereas a broader function, such as  $1/(1 + \zeta^2)$  for example, would require PV gradients exponentially large (in  $m$ ) at  $\zeta = 0$  in order that they will decay to exponentially small amplitudes for  $z$  of order 1 where the critical

layers occur. The order of the peak PV gradient required to retain the instability is thus very dependent on the profile of the potential vorticity chosen. The common feature is the order of the PV gradient at the critical layers of the flow, which must be exponentially small in  $m$ .

### 3.4 Relevance to the existence or non-existence of a slow manifold

Having shown that an axisymmetric shallow water vortex is unstable for all Froude and Rossby numbers, one may ask how this result relates to the question of existence or non-existence of a slow manifold for the  $f$ -plane shallow water equations.

As a preliminary, let us recall two general properties of the inviscid shallow water equations.

Firstly, suppose we have a solution of the shallow water equations  $\{(u_r^{(1)}, u_\theta^{(1)}), h^{(1)}\}$ :

$$u_r^{(1)} = \mathcal{U}_r(r, \theta, t; f); \quad u_\theta^{(1)} = \mathcal{U}_\theta(r, \theta, t; f); \quad h^{(1)} = \mathcal{H}(r, \theta, t; f), \quad (3.164)$$

where  $(u_r, u_\theta)$  are the radial and azimuthal components of the velocity field, and  $h$  the height field. Then another solution of the shallow water equations,  $\{(u_r^{(2)}, u_\theta^{(2)}), h^{(2)}\}$ , is given by

$$u_r^{(2)} = -\mathcal{U}_r(r, \theta, -t; -f); \quad u_\theta^{(2)} = -\mathcal{U}_\theta(r, \theta, -t; -f); \quad h^{(2)} = \mathcal{H}(r, \theta, -t; -f). \quad (3.165)$$

This is a general transformation property of the shallow water equations, which states that if all particle velocities are reversed, including the sense of the background rotation, then the flow evolution is reversed. The effect on the potential vorticity is to transform  $Q \rightarrow -Q$ . This we shall refer to as the particle symmetry of the equations.

Secondly, suppose again that we have a solution of the shallow water equations given by (3.164). Then another solution of the shallow water equations,  $\{(u_r^{(3)}, u_\theta^{(3)}), h^{(3)}\}$ , is given by

$$u_r^{(3)} = \mathcal{U}_r(r, -\theta, t; -f); \quad u_\theta^{(3)} = -\mathcal{U}_\theta(r, -\theta, t; -f); \quad h^{(3)} = \mathcal{H}(r, -\theta, t; -f). \quad (3.166)$$

This is also a general transformation property of the shallow water equations, which states that the motion is unchanged if the system is viewed in a mirror, with the radial coordinate unchanged, but with the sense of the azimuthal coordinate reversed. As in the case of (3.165), the effect on the potential vorticity is to transform  $Q \rightarrow -Q$ . However, unlike (3.165), time is not reversed under this transformation.

Now, in order to discuss the existence or non-existence of a slow manifold, we must say what properties we shall assume a slow manifold to possess. Such a set of properties, consistent with the notion of a slow manifold as it is usually understood, is the following:

- (a) The dimension of the slow manifold is one-third the dimension of the phase space of the shallow water equations.
- (b) The slow manifold is tangent to the quasigeostrophic manifold at zero Rossby number, so that flow on the slow manifold is identical to quasigeostrophic flow at the leading order in Rossby number.
- (c) Steady axisymmetric vortices and steady parallel flows are on the slow manifold.
- (d) Viewing the system in a mirror ( $f \rightarrow -f, u_r \rightarrow u_r, u_\theta \rightarrow -u_\theta, h \rightarrow h$ ) keeps the system on the same slow manifold as that which it was on when viewed in the original frame.
- (e) Reversing the absolute direction of motion of all particles ( $f \rightarrow -f, u_r \rightarrow -u_r, u_\theta \rightarrow -u_\theta, h \rightarrow h$ ) keeps the system on a slow manifold.
- (f) At any instant in time, the entire velocity field and the entire height field on the slow manifold can be determined uniquely from the potential vorticity distribution  $Q(x, y)$  at that instant in time.

Notice that (c), (d), (e) and (f) all follow from (a) and (b) in the small Rossby number limit. In particular, for quasigeostrophic flow, the potential vorticity field can be shown to determine all other dynamical fields uniquely. Notice also that (f) is a strong form of (a). Furthermore, notice the distinction between property (d), which states that, under the specified transformation, the system must remain on the same slow manifold, and property (e), which states that under a different transformation, the system must simply remain on a slow manifold. It seems reasonable to make this distinction, in that the transformation under consideration in (d) can be effected entirely by regarding the system under reflection in a mirror, and its evolution should therefore be identical to the original flow, whereas the transformation under consideration in (e) involves a change in the physical state of the system, and is therefore not directly connected to the original flow.

Since, on any slow manifold having property (f),  $Q$  and  $f$  are sufficient to determine the entire velocity field and the entire height field, it is natural to impose one further condition:

- (g) Under the transformation  $Q \rightarrow -Q; f \rightarrow -f$ , the implied flow on the manifold  $\{\mathbf{u}_s, h_s\}$ , will remain on the slow manifold, and be transformed according to  $-\mathbf{u}_s; h_s \rightarrow h_s$ .

This last property was termed “sign consistency” by McIntyre & Norton (1978). It is a property of all standard balanced models, such as the quasigeostrophic and shallow water equations. Property (g), where it applies, is a strong form of property (e), and is due to giving the same force to property (e) as that which was given to property (f). That under the relevant transformation, the slow manifold is not simply mapped onto another manifold, but it is mapped onto the same slow manifold. If  $\mathcal{M}$  were assumed to be invariant, then property (g) and property (e) would be equivalent.

It will now be shown that, for the shallow water equations at least, a slow manifold with properties (a) – (g) cannot exist. This is done by first supposing that there is a slow manifold,  $\mathcal{M}$ , say, and then deriving a contradiction.

Firstly, recall the vortex instability result. In an unbounded domain, it was shown that a vortex was temporally unstable for all Froude and Rossby numbers. Moreover, there is a unique temporally growing mode for each azimuthal mode number  $m$ , provided  $Ro$  is large, and the amplitude of the mode is assumed to be finite at infinity. It is also a unique temporally decaying mode for each such  $m$ , assuming that the amplitude is finite at infinity. We shall fix attention on a single such azimuthal mode number  $m$ , and denote the growing and decaying eigenmodes for that mode number by  $\phi_1(r)$  and  $\phi_2(r)$ . Here, the functions  $\phi_1(r)$  and  $\phi_2(r)$  are taken to represent the three-vector perturbation case. In the limit  $Ro \rightarrow 0$ ,  $\phi_1$  and  $\phi_2$  coincide, since the growth rate of the growing mode is small order in Rossby number.

Now, let us consider the nature of the evolution of the vortex with a perturbation under the assumption of linearized perturbations. The boundary of the vortex is a function on it, of small amplitude, and of fixed mode number  $m$ . On the slow manifold, from property (f) and linearization that, at any instant in time, the amplitude of the vortex boundary undulation are sufficient to determine the perturbation velocity fields everywhere. Since we are considering linearized perturbations, we can represent

location of the vortex boundary as a function  $r(\theta, t)$ , in the form

$$r(\theta, t) = \operatorname{Re} \left\{ 1 + a(t)e^{im\theta} \right\}, \quad (3.167)$$

for some complex function  $a(t)$ . Moreover, the assumption of linearized perturbations implies that the amplitude of the perturbations of the velocity and height fields depends linearly on the amplitude of the vortex boundary undulations, so we may represent the perturbation fields  $\varphi$  in the form

$$\varphi(r, \theta, t) = \operatorname{Re} \left\{ a(t)\Phi(r)e^{im\theta} \right\}, \quad (3.168)$$

where here, as before,  $\varphi$  represents the three-vector  $(u, v, h)$ . By substitution of (3.168) into the linearized shallow water equations for disturbances to an axisymmetric vortex, it can be shown using elementary techniques from the theory of solution of partial differential equations by separation of variables that

$$\frac{da}{dt} = \lambda a, \quad (3.169)$$

for some possibly complex constant  $\lambda$ , and therefore

$$\varphi(r, \theta, t) = \operatorname{Re} \left\{ A\Phi(r)e^{i(m\theta - \lambda t)} \right\} \quad (3.170)$$

for some complex constant  $A$ .

Now, we know from the shallow water vortex instability analysis that, in the unbounded domain, only two bounded solutions of form (3.170) exist, and that they are the temporally growing eigenmode,  $\phi_{\uparrow}$ , and the temporally decaying eigenmode,  $\phi_{\downarrow}$ . Therefore, in the limit of linearized perturbations of fixed mode number to the boundary of an axisymmetric vortex, the flow on the slow manifold  $\mathcal{M}$  consists of either the temporally growing mode alone, or the temporally decaying mode alone.

Suppose that the flow on the slow manifold consists of the temporally growing mode alone. Suppose also, without loss of generality, that  $f > 0$ . Then, under the transformation  $Q \rightarrow -Q; f \rightarrow -f$ , it follows, from property (g) and the time symmetry of the shallow water equations (3.164 & 3.165), that the temporally growing mode is mapped onto the temporally decaying mode. However, by property (d) and the reflectional symmetry of the shallow water equations (3.164 & 3.166), the transformation  $Q \rightarrow -Q; f \rightarrow -f$  must map the temporally growing mode onto the temporally growing mode. This implies that the flow on the slow manifold for

$\{-Q, -f\}$  consists simultaneously of the temporally growing mode alone and the temporally decaying mode alone, which is a contradiction.

Now let us suppose we relax the condition  $(g)$ , the condition of sign consistency, and ask whether there can exist a slow manifold satisfying only conditions  $(a) - (f)$ . The velocity field on such a slow manifold, which we shall denote by  $\mathbf{u}_s$ , can then be written as the sum of two components,  $\mathbf{u}_s = \mathbf{v} + \mathbf{w}$ , where, under the transformation  $Q \rightarrow -Q; f \rightarrow -f$ , the velocity fields  $\mathbf{v}$  and  $\mathbf{w}$  transform according to the transformation laws  $\mathbf{v} \rightarrow -\mathbf{v}$  and  $\mathbf{w} \rightarrow \mathbf{w}$ . One can regard  $\mathbf{v}$  as the sign-consistent part of the slow manifold flow, and  $\mathbf{w}$  as the sign-inconsistent part of the flow. The sign-inconsistent part,  $\mathbf{w}$ , is in general non-zero, and in particular it is non-zero, at arbitrarily small Froude and Rossby numbers, in the neighbourhood of an axisymmetric vortex. On the other hand, if  $\mathbf{v} + \mathbf{w}$  is the velocity field on a slow manifold for a given  $\{Q(x, y), f\}$  then, from the general transformation properties of the shallow water equations (3.164, 3.165),  $-\mathbf{v} - \mathbf{w}$  constitutes a velocity field for  $\{-Q(x, y), -f\}$ , which must also be on a slow manifold. Then, from the transformation properties assumed for  $\mathbf{v}$  and  $\mathbf{w}$ ,  $\mathbf{v} - \mathbf{w}$  constitutes the flow on a slow manifold for a potential vorticity distribution and Coriolis parameter  $\{Q(x, y), f\}$ . We have thus now arrived at a situation in which two flows,  $\mathbf{v} + \mathbf{w}$  and  $\mathbf{v} - \mathbf{w}$ , are both flows on a slow manifold corresponding to the same potential vorticity distribution  $Q(x, y)$  and Coriolis parameter  $f$ , and that  $\mathbf{w}$  is in general non-zero, even at arbitrarily small Rossby numbers. It follows at once that, if condition  $(g)$ , the condition of sign consistency, is not imposed, then a slow manifold, if one exists, is not uniquely defined by the potential vorticity distribution,  $Q(x, y)$ , even in the limit of arbitrarily small Rossby number.

We might now attempt to make the definition of the slow manifold unique by insisting that its gravity wave field satisfies a causality condition, and hence, in the case of the shallow water instability problem, that the temporally growing mode is taken for both  $f > 0$  and  $f < 0$ . This is feasible in the case of the vortex instability problem, because we can require that there are no gravity waves in the flow at  $t = -\infty$ . In this case, the limit  $t \rightarrow -\infty$  is well defined, and the flow approaches an axisymmetric balanced vortex in that limit. For a general shallow water flow, however, the limit  $t \rightarrow -\infty$  is not necessarily well defined, and imposing a causality condition will require the specification of an initial instant  $t_0$  (say), at which time the vortex flow was “turned on”, and before which time no gravity waves had been radiated. The choice of initial instant is clearly not unique, and yet in general we must expect the details of the

gravity waves generated, and their effect on the vortical flow, to depend on that initial instant. This point was made explicitly in analysis of the effect of gravity wave generation on a localized vortical disturbance at small Froude number, discussed in chapter 2. Each flow corresponding to a different choice of  $t_0$  can be thought of as a “slow manifold”, but with  $t_0$  required to select one of the infinite number of possible branches.

There can now be little doubt now that the original concept of the unique slow manifold, as defined by Leith (1980), and clarified by Lorenz (1986), cannot apply to the shallow water equations. The shallow water vortex instability analysis showed that, at sufficiently large mode number, an axisymmetric vortex is unstable at arbitrarily small Rossby number, from which it follows that a slow manifold cannot be sign consistent, and therefore cannot be unique. Furthermore, the eigenfunctions have a gravity wave-like tail, albeit an exponentially weak one. One might argue from a physical viewpoint that the clear appearance of gravity-wave like structures at arbitrarily small Rossby number is sufficient to show that no so-called slow manifold could be truly slow, even if an invariant manifold specified only by potential vorticity distributions did exist, since it would inevitably contain “fast” gravity wave-like structures. From a mathematical viewpoint we have seen that the appearance of these gravity wave-like structures at arbitrarily small Rossby number is indeed inextricably linked to our inability to define a sign-consistent slow manifold, and hence our inability to define a unique slow manifold.

### 3.5 Instability of a parallel jet

In this section, we consider the linear stability of a parallel jet. The potential vorticity in the jet is taken to be piecewise uniform, with a single discontinuity at  $y = 0$ . The discontinuity is sometimes referred to as a front.

We choose to work with a nondimensionalization that is different from the one used in the study of the axisymmetric vortex instability. Instead of nondimensionalizing such that the jump in potential vorticity across the interface is unity, we shall set the potential vorticity in the region  $y < 0$  to unity. There is no loss of generality here, since if we wish to have a layer of finite depth, with velocity decaying away from  $y = 0$ , the potential vorticity will have to be positive in both  $y < 0$  and  $y > 0$ . The timescale must then be set by the Coriolis parameter  $f$ , and not the potential vorticity jump. We take  $f = 1$ , and so the layer depth is unity in the

limit  $y \rightarrow -\infty$ . The Rossby deformation radius is effectively  $Q^{-1/2}$ , where  $Q$  is the potential vorticity. A result of these nondimensionalizations is therefore to set the deformation radius to unity in  $y < 0$ .

### 3.5.1 The basic state

With the nondimensionalizations introduced above, the equations for the basic state velocity  $U(y)$  and height  $H(y)$  are

$$U = -\frac{dH}{dy} \quad (3.171)$$

$$1 - \frac{dU}{dy} = QH. \quad (3.172)$$

It follows that

$$\frac{d^2H}{dy^2} - QH = -1. \quad (3.173)$$

Now we let  $Q$  take the form

$$Q(y) = \begin{cases} q & \text{for } y > 0 \\ 1 & \text{for } y < 0 \end{cases}, \quad (3.174)$$

then the equations for the basic state can be solved in terms of elementary functions. Imposing continuity of  $H$  and  $U$  at  $y = 0$  gives

$$H(y) = \begin{cases} \frac{1}{q} + \frac{\sqrt{q-1}}{q} e^{-\sqrt{q}y} & y > 0 \\ 1 - \frac{\sqrt{q-1}}{\sqrt{q}} e^y & y < 0 \end{cases}; \quad U(y) = \begin{cases} \frac{\sqrt{q-1}}{\sqrt{q}} e^{-\sqrt{q}y} & y > 0 \\ \frac{\sqrt{q-1}}{\sqrt{q}} e^y & y < 0 \end{cases}. \quad (3.175)$$

### 3.5.2 Ripa's theorem

Before proceeding to the linear instability calculations for the basic state given by (3.175), we shall discuss Ripa's theorems for the stability of parallel and axisymmetric shallow water flows, and show linear stability for the basic state (3.175) in the case  $q < 4$ .

The basic technique is to consider first and second variations to some linear combination of the conserved quantities of energy and momentum, plus a Casimir. The first variation of the sum is required to be zero, which sets the Casimir, and the second variation is required to be of definite sign. The requirement of sign definiteness gives conditions on the basic flow which are sufficient for linear stability.

For the shallow water equations, the energy is given by

$$E = \frac{1}{2} \iint (hu^2 + h^2) dx dy, \quad (3.176)$$

while the  $x$ -momentum is given by

$$M = \iint h(u - fy) dx dy. \quad (3.177)$$

General Casimirs are given by

$$C = \iint hF(Q) dx dy, \quad (3.178)$$

where  $F(Q)$  is an arbitrary function of the potential vorticity  $Q$ .

It follows that the combination

$$\mathcal{H} \equiv E + \alpha M + C \quad (3.179)$$

is a conserved quantity. Taking the first variation of  $\mathcal{H}$  gives

$$\delta\mathcal{H} = \iint \left[ h \left( u + \alpha + \frac{\partial}{\partial y} C'(Q) \right) (\delta u) - \frac{\partial}{\partial x} C'(Q) (\delta v) \right. \quad (3.180)$$

$$\left. + \left( \frac{1}{2} u^2 + h + \alpha(u - fy) + C(Q) - QC'(Q) \right) (\delta h) \right]. \quad (3.181)$$

For stability we require  $\delta\mathcal{H} = 0$ . This imposes conditions on the Casimir  $C$ , such that

$$C''(Q) = -\frac{h(u + \alpha)}{Q'(y)}. \quad (3.182)$$

For linear stability, we now require that the second variation  $\delta^2\mathcal{H}$  should be of definite sign.

The second variation of  $\mathcal{H}$  is given by

$$\delta^2\mathcal{H} = \iint \left[ h(\delta v)^2 + (\delta h + (u + \alpha)\delta u)^2 + \left( h - (u + \alpha)^2 \right) (\delta u)^2 - \frac{h^2(u + \alpha)}{Q'(y)} (\delta Q)^2 \right]. \quad (3.183)$$

If we impose the condition  $\delta^2\mathcal{H} > 0$ , we obtain

$$(u + \alpha)Q'(y) < 0 \quad \text{and} \quad (u + \alpha)^2 < h. \quad (3.184)$$

If we assume that  $Q'(y) > 0$  for all  $y$ , then the maximum value for  $\alpha$  which we may take to obtain stability by the first of these conditions is the peak jet velocity  $-u_{max}$ . This choice gives us the greatest stability information from the second of the conditions, so we have

$$Q'(y) > 0 \quad \text{and} \quad (u_{max} - u(y))^2 < h(y). \quad (3.185)$$

The condition is just the standard condition of monotonic PV required to ensure that the flow is not unstable to barotropic instability, with the further condition that the flow must be everywhere subsonic with respect to the peak jet velocity, since  $h(y)^{1/2}$  is just the nondimensionalized gravity wave phase speed. This condition is analogous to Arnol'd's first theorem.

From (3.175), we see that these conditions are satisfied when  $q < 4$ .

In passing we note that, by considering the subclass of variations in which  $\delta q = 0$  and  $\delta u = 0$ , the remaining terms are always positive definite, and hence it is not possible to impose the condition  $\delta^2\mathcal{H} < 0$ . Consequently there is no analogue of Arnol'd's second theorem for the shallow water equations <sup>1</sup>.

### 3.5.3 The disturbance equations

The disturbance equations for the parallel flow are very similar, except for geometrical factors, to those for axisymmetric flow.

Now we assume that perturbations are of the form  $f(y)e^{i(kx-\omega t)}$ . The wavenumber  $k$  is assumed real, and again the growth rate of any instability is represented by an imaginary part to  $\omega$ . The disturbance equations then become

$$\frac{du}{dy} = A(y)u + B(y)v \quad (3.186)$$

$$\frac{dv}{dy} = C(y)u + D(y)v, \quad (3.187)$$

where  $Q$  is the (piecewise uniform) potential vorticity of the background flow, and

$$A(y) = \frac{Q(-\omega + kU)}{k} \quad (3.188)$$

$$B(y) = i \left( k + \frac{Q^2 H}{k} \right) \quad (3.189)$$

$$C(y) = i \left( \frac{(-\omega + kU)^2}{Hk} - k \right) \quad (3.190)$$

$$D(y) = \left( \frac{U}{H} - \frac{(-\omega + kU)Q}{k} \right) \quad (3.191)$$

Continuity of  $v$  and  $h$  at  $y = 0$  reduce to

$$(-\omega + kU(0)) \left[ \frac{u}{v} \right] + iH(0)[Q] = 0. \quad (3.192)$$

---

<sup>1</sup>This observation arose in discussions with Prof. T. G. Shepherd and Dr. T. E. Dowling

### 3.5.4 Numerical technique

The equations (3.186-3.187) represent an eigenvalue problem for  $\omega$ . As for the axisymmetric problem, we use a shooting method based on an initial guess for  $\omega$ . In the far field the disturbances take the form  $e^{i(kx+ly-\omega t)}$ , where  $l$  is given by  $\omega^2 - 1 = Q^{-1}(k^2 + l^2)$ . Note that  $l$ , which takes different values as  $y \rightarrow \pm\infty$ , always has non-zero imaginary part  $l_i$ . The disturbance variables are therefore rescaled by  $e^{l_i y}$ , so that the computed variables remain of order one throughout the domain  $-\infty < y < \infty$ . Evanescence conditions at  $y = \pm\infty$  are used to impose the ratio of  $u/v$  to be taken at some large value of  $|y|$ , as in the axisymmetric vortex calculations. The equations are then integrated in to  $y = 0$  using a stiff integrator for ordinary differential equations from the NAG library, and the continuity condition (3.192) at  $y = 0$  is imposed.

#### Initialization for small $q$

Initial values for the eigenfrequencies supplied to the shooting method were taken, in the case of a small jump in potential vorticity, using a quasi-geostrophic analysis. The magnitude of the potential vorticity jump could then be increased, taking the eigenfrequency for one value of the potential vorticity jump as the initial guess for the eigenfrequency at the next.

The equation for the basic state streamfunction  $\psi$ :

$$\left(\frac{d^2}{dy^2} - 1\right)\psi = \begin{cases} q & \text{for } y > 0 \\ 1 & \text{for } y < 0 \end{cases} . \quad (3.193)$$

Continuity of  $\psi$  and  $\psi_y$  at  $y = 0$  lead to

$$\psi = \begin{cases} \frac{1}{2}(q-1)e^{-y} - q & y > 0 \\ -\frac{1}{2}(q-1)e^y - 1 & y < 0 \end{cases} . \quad (3.194)$$

If we now introduce a disturbance streamfunction  $\tilde{\psi}(y)e^{i(kx-\omega t)}$ , the equation for  $\tilde{\psi}$  is

$$\left(\frac{d^2}{dy^2} - k^2 - 1\right)\tilde{\psi} = 0. \quad (3.195)$$

At this point it is convenient to introduce

$$\gamma \equiv (1 + k^2)^{1/2}, \quad (3.196)$$

so that

$$\tilde{\psi} = \begin{cases} \tilde{a}e^{-\gamma y} & \text{for } y > 0 \\ \tilde{b}e^{+\gamma y} & \text{for } y < 0 \end{cases}. \quad (3.197)$$

We must also introduce a disturbance to the position of the interface between the two uniform potential vorticity regions, such that

$$y = \tilde{\eta}e^{i(kx - \omega t)}. \quad (3.198)$$

Imposing continuity of  $\psi$  and  $\psi_y$  leads to a kinematic condition on  $\tilde{\eta}$ , which can then be solved for  $\omega$ :

$$\omega = \frac{1}{2} \left( 1 - \frac{1}{\gamma} \right) (q - 1)k. \quad (3.199)$$

Note that this eigenfrequency is real, regardless of the magnitude of  $q - 1$ . It is valid in the low Rossby number limit  $q - 1 \ll 1$ , and is not valid for  $q - 1$  of order one. It therefore gives no information in the regime  $q > 4$ , in which we might expect instability to occur.

### 3.5.5 Results of the eigenvalue calculations

In the present study, the growth rate of any instability depends on two parameters: the potential vorticity  $q$  in the region  $y > 0$ ; and the wavenumber  $k$  of the instability.

In figure 3.30, the growth rate of the instability is shown as a function of wavenumber for  $q = 6, 10, 20$  and  $30$ . One can see that, at low wavenumbers, the flow is stable, whereas at higher wavenumbers the instability occurs. This is to be expected when we consider the nature of the instability mechanism. Far from the jet, the disturbances satisfy the linear gravity wave dispersion relation

$$\omega^2 - f^2 = c^2(k^2 + l^2). \quad (3.200)$$

Now, the instability exists due to coupling between the vortical wave on the potential vorticity jump, and a gravity wave at infinity. This implies that, in one of  $y < 0$  or  $y > 0$ , we will need  $l$  to be real at leading order in the wavenumber  $k$ . If we suppose that  $\omega \sim Uk$ , then the condition  $l^2 > 0$  is  $k^2(U^2 - c^2) - f^2 > 0$ . Thus, the larger the value of  $k$ , the less the disturbances are influenced by the Coriolis parameter, and the remaining condition is that the jet speed must exceed the gravity wave phase speed at infinity – exactly Ripa's condition. Hence, we should expect to see Rossby wave – gravity wave instabilities at large wavenumber.

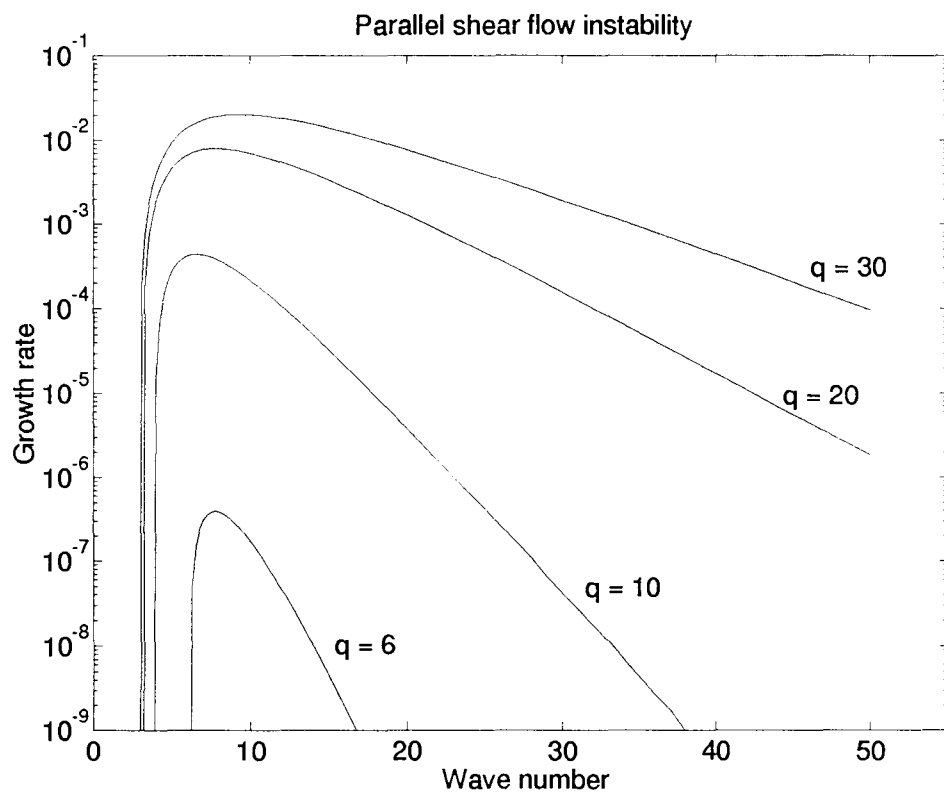


Figure 3.30: Growth rates of linear eigenmodes on a parallel shear flow with a single discontinuity in potential vorticity. Potential vorticity ratios of 6, 10, 20, 30 are shown, with growth rates of eigenmode wavenumbers  $k = 0$  to 50.

We shall therefore proceed to analyse the instability in the high wavenumber limit, as we did for the axisymmetric vortex at large mode number.

### 3.5.6 The limit of large wavenumber

The results of the eigenvalue calculations have shown that there is a tendency towards instability at high wavenumbers. Motivated by the success of the WKBJ analysis for the axisymmetric vortex instability, we shall now perform a WKBJ analysis for the parallel flows discussed in this section. In particular, we shall show that the range of stability found by Ripa's theorem is complete - all flows that do not satisfy Ripa's theorem are unstable.

The details of the parallel flow and axisymmetric vortex analyses are very similar, and only a summary will be given here. The principal difference is that we now impose an evanescence/radiation condition as  $y \rightarrow \pm\infty$ , and this will lead to zero, one or two turning points in the flow.

As in the analysis for the axisymmetric flow, we choose to work with a single second order ordinary differential equation with a single variable. In the interests of consistency with the axisymmetric analysis, we choose to work with the along-stream variable  $u$ .

Again, one works with a frequency  $c = \omega/k$ . After rearranging the disturbance equations (3.186, 3.187) one obtains

$$\frac{d^2u}{dy^2} + F(y)\frac{du}{dy} + G(y)u = 0. \quad (3.201)$$

The function  $F(y)$  is everywhere of order unity, and the function  $G(y)$  is given by

$$G(y) = \left[ \frac{(-c + U(y))^2}{H(y)} - 1 \right] k^2 + O(1). \quad (3.202)$$

Again, it is straightforward to see that the jump condition at  $y = 0$  can only be satisfied if  $c_0 = U(0)$ . This gives a condition for a turning point to occur:

$$(u(0) - U(y))^2/H(y) = 1, \quad (3.203)$$

which is precisely the same as the stability boundary predicted by Ripa's theorem.

Now  $U(0) = 1 - 1/\sqrt{q}$ , and  $U \rightarrow 0$  as  $y \rightarrow \pm\infty$ . If we consider first  $y > 0$ , then there will be a turning point if and only if

$$(U(0) - U(y))^2 > H(y). \quad (3.204)$$

Now  $H(y) > 1/q$ , and  $U(0) - U(y) < U(0)$ , and therefore a necessary condition for a turning point to exist is

$$U(0)^2 > 1/q; \quad \text{i.e. } q > 4. \quad (3.205)$$

Taking  $y = \infty$  in (3.203) ensures that (3.205) is also a sufficient condition.

If we now consider  $y < 0$ , then  $H(y) < H(0)$ . There

$$U(0) - U(y) = \frac{\sqrt{q} - 1}{\sqrt{q}}(1 - e^y) < 1, \quad (3.206)$$

and therefore  $H(y) - (U(0) - U(y)) = 1/\sqrt{q}$ , and hence

$$1 > H(y) > U(0) - U(y) > ((U(0) - U(y))^2), \quad (3.207)$$

and so there is no turning point in  $y < 0$ .

The situation is now very similar to that of the axisymmetric vortex, in which there is a single turning point and a single potential vorticity discontinuity.

The turning point at  $y = y_c$  means that the domain is split into four regions, and the analysis is given below. The four regions and the character of the solutions in them are:

$y < 0$  Exponential decay of solution away from  $y = 0$ .

$0 < y < y_c$  Exponential decay of real part of solution away from  $y = 0$ , with exponentially growing imaginary part, such that real and imaginary parts are of the same order of magnitude at  $y = y_c$ .

$y - y_c = O(k^{-2/3})$  Combination of Airy functions, appropriate for matching onto radiating wave solution in  $y > y_c$ .

$y > y_c$  Oscillatory functions, satisfying radiating boundary conditions as  $t \rightarrow \infty$ . Small imaginary part of eigenfrequency ensures exponential decay of eigenfunction at very large range.

Continuity conditions at  $y = 0$  are then used to obtain the eigenvalue. If we let the eigenvalue  $\omega$  be written as  $\omega = k(c_0 + k^{-1}c_1 + \dots)$ , then

$$c_0 = 1 - 1/\sqrt{q}; \quad c_1 = -\frac{q-1}{2\sqrt{q}}. \quad (3.208)$$

Then if we define

$$\Psi_0 = -\int_0^{y_c} \left( 1 - \frac{(\sqrt{q}-1)^2(1-e^{-y\sqrt{q}})}{1+(\sqrt{q}-1)e^{-y\sqrt{q}}} \right)^{1/2} dy \quad (3.209)$$

and

$$\Psi_1 = -\frac{q-1}{2\sqrt{q}} \int_0^{y_c} \frac{U(0)-U(y)}{\Psi_0' H(y)} dy \quad (3.210)$$

then the growth rate  $c_i$  is given by

$$c_i = \frac{q-1}{4\sqrt{q}} e^{2(k\Psi_0+\Psi_1)}. \quad (3.211)$$

### Comparison with numerical eigenvalue calculations

In figure 3.31, the growth rate curves shown in figure 3.30 are reproduced, together with their predictions from the WKBJ analysis, valid in the limit  $k \gg 1$ . On average, there seems to be reasonable agreement at large  $k$ , though at moderate  $k$  the agreement is not generally as good as it was for the WKBJ analysis of the axisymmetric vortex instability at moderate  $m$ .

#### 3.5.7 The limit $q \rightarrow \infty$

As discussed in the section 1, the instability of a potential vorticity jump has already been analysed in the limit  $q \rightarrow \infty$  by Paldor (1983), who showed that all eigenmodes are stable in that limit. However, one can show that, in the limit  $q \rightarrow \infty$ ,

$$\Psi_0 \sim -\frac{\pi}{4}q^{-3/4}; \quad \Psi_1 \sim -\frac{1}{2}, \quad (3.212)$$

and hence

$$c_i \sim \frac{1}{4}q^{1/2} e^{-(\frac{1}{2}k\pi q^{-3/4}+1)}, \quad (3.213)$$

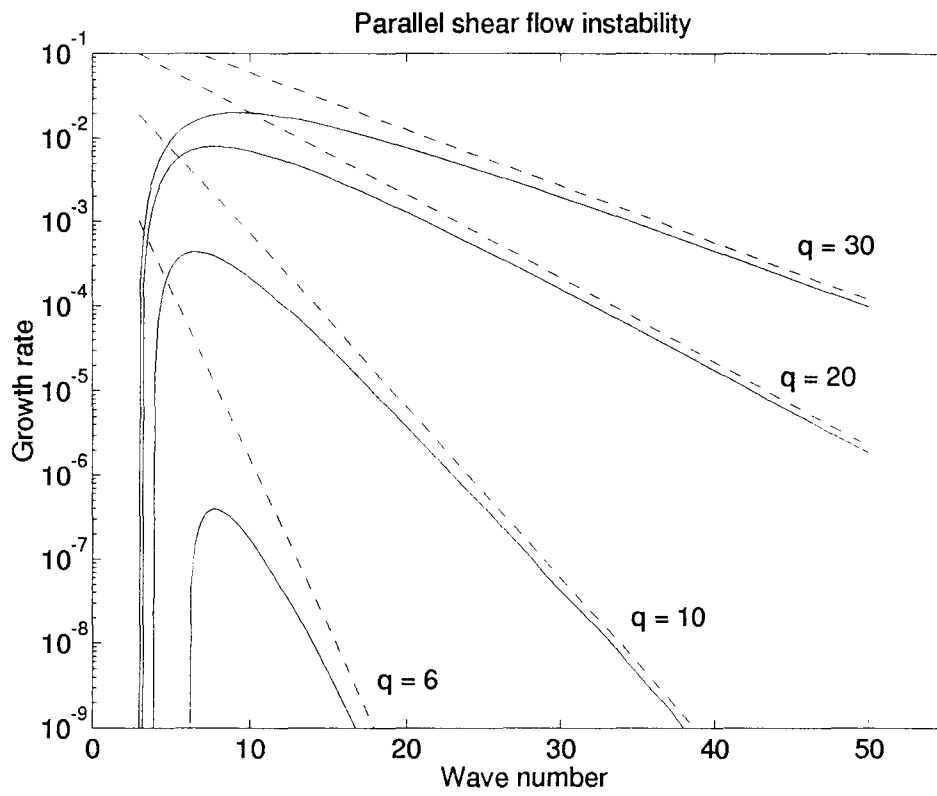


Figure 3.31: Solid lines as figure 3.30, and dashed lines are corresponding growth rate predictions obtained by the WKBJ analysis.

which becomes unbounded in the limit  $q \rightarrow \infty$ . The purpose of this section is to show that the limit  $q \rightarrow \infty$  is a singular limit. The point is that, at large fixed  $k$ , as  $q$  is increased, we will approach a limit in which the potential vorticity interface falls within the turning point region. The region  $0 < y < y_c$  effectively disappears, and we will be left with only three regions. The appropriate scaling in this limit is to take  $q = O(k^{4/3})$ .

### The scaling $q = O(k^{4/3})$

The aim here is to appreciate the origins of the scaling  $q = O(k^{4/3})$ . We are seeking to eliminate the inner region  $0 < y < y_c$ , and therefore we impose that the region including the turning point  $y = y_c$  should also include the potential vorticity interface  $y = 0$ . In the limit  $q \rightarrow \infty$ , the turning point and the interface coincide.

To derive the necessary scaling, we first note that

$$U(0) - U(y) = \left(1 - \frac{1}{\sqrt{q}}\right) \left(1 - e^{-\sqrt{q}y}\right). \quad (3.214)$$

Notice that  $1/\sqrt{q}$  is the natural length scale in the region  $y > 0$ , and in this analysis we seek to place the turning point at some  $y \ll 1/\sqrt{q}$ . Therefore,

$$U(0) - U(y) \sim -y\sqrt{q}. \quad (3.215)$$

At the turning point  $y = y_c$ , we will have  $(U(0) - U(y_c))^2 = H(y_c)$ . Now  $H(y) \sim 1/\sqrt{q}$  for small  $\sqrt{q}y$ , and therefore the turning point occurs at

$$y^2 q \sim 1/\sqrt{q}; \quad \text{i.e.} \quad y \sim q^{-3/4}. \quad (3.216)$$

On the other hand, the natural length scale for disturbances is  $k^{-1}$ , and hence the turning point will lie in the same asymptotic region as the interface if

$$\frac{1}{k} \sim y \sim q^{-3/4} \quad \text{i.e.} \quad q \sim k^{4/3}. \quad (3.217)$$

This scaling could have been predicted with reference to (3.213). The asymptotic analysis of the previous section assumed  $k\Psi_0 \gg \Psi_1$ , and it can clearly be seen that this assumption breaks down when  $q = O(k^{4/3})$ . Throughout the remainder of this chapter, we shall therefore replace  $q$  with  $k^{4/3}\mathfrak{q}$ , where  $\mathfrak{q}$  is to be taken to be of order unity.

### Equations in the region $y = O(k^{-1})$

With the scaling for the potential vorticity jump now fixed, we are able to write down an equation governing disturbances in the region  $y = O(k^{-1})$ . We introduce an inner length coordinate  $Y = ky$ , for which the interface is to be found at  $Y = 0$ , and the turning point at  $Y = \mathfrak{q}^{-3/4}$ .

We express the eigenfrequency  $\omega$  as

$$\omega = k(c_0 + k^{-1/3}\mathfrak{q}^{1/2}c_1 + \dots). \quad (3.218)$$

The leading order is satisfied by taking  $c_0 = U(0)$ . The factor of  $\mathfrak{q}^{1/2}$  is introduced to scale  $c_1$ , which is convenient for analysing the limits  $\mathfrak{q} \rightarrow 0$  and  $\mathfrak{q} \rightarrow \infty$ .

Then, after some routine algebra, we obtain an equation for  $u$  at leading order in  $k$ :

$$\frac{d^2u}{dY^2} + (\mathfrak{q}^{3/2}(Y + c_1)^2 - 1)u = 0. \quad (3.219)$$

The solution to (3.219) may be represented in terms of parabolic cylinder functions (see Abramowitz & Stegun, 1965, chapter 19).

In the limit  $Y \rightarrow \infty$ , we shall seek to match the solution of (3.219) onto a radiating wave form. We therefore take the solution

$$u(Y) = E(a, 2^{1/2}\mathfrak{q}^{3/8}(Y + c_1)), \quad (3.220)$$

where

$$a = \frac{1}{2}\mathfrak{q}^{-3/4}. \quad (3.221)$$

The function  $E(a, x)$  is related to the real parabolic cylinder function  $W(a, x)$  via

$$E(a, x) = \lambda^{-1/2}W(a, x) + i\lambda^{1/2}W(a, -x), \quad (3.222)$$

where

$$\lambda = \sqrt{1 + e^{2\pi a}} - e^{\pi a}; \quad \lambda^{-1} = \sqrt{1 + e^{2\pi a}} + e^{\pi a}. \quad (3.223)$$

In the limit  $Y \rightarrow \infty$ ,  $u(Y)$  then takes the form

$$u(Y) \sim \sqrt{2/Y} \exp\{i(\mu^2(Y + c_1)^2/4 - a \ln \mu Y + \arg(\Gamma(ia + 1/2)) + \pi/4)\}, \quad (3.224)$$

where

$$\mu = \sqrt{2}\mathfrak{q}^{3/8}. \quad (3.225)$$

If  $c_1$  has an imaginary part, one can see from (3.224) that  $u(Y)$  is exponentially decaying in the limit  $Y \rightarrow \infty$ .

The continuity equation at  $Y = 0$  becomes

$$c_1 \left( \frac{1}{(1 - c_1^2 \mathfrak{q}^{3/2})^{1/2}} - \frac{(1 + \mathfrak{q}^{3/2})E(a, \sqrt{2}\mathfrak{q}^{3/8}c_1)}{\sqrt{2}\mathfrak{q}^{3/8}E'(a, \sqrt{2}\mathfrak{q}^{3/8}c_1) + \mathfrak{q}^{3/2}c_1E(a, \sqrt{2}\mathfrak{q}^{3/8}c_1)} \right) = -1, \quad (3.226)$$

where the prime denotes differentiation with respect to the second argument. The second term in the bracket is the ratio of  $u/v$  at  $Y = 0^+$ . Recalling that  $du/dy = A(y)u + B(y)v$ , the complicated form of the denominator comes from the fact that, in this scaling,  $du/dy$ ,  $A(y)u$  and  $B(y)v$  are all of the same order of magnitude, whereas in the limit of large  $k$  and order one potential vorticity jumps,  $A(y)u$  may be neglected. The first term is the ratio of  $u/v$  at  $Y = 0^-$ . Notice that, unlike the previous analysis, it is not unity at leading order. Although there is no turning point in  $Y < 0$ , the expression

$$\Psi' = \left( 1 - \frac{(c - U(y))^2}{H(y)} \right)^{1/2} \quad (3.227)$$

becomes

$$\Psi' = (1 - c_1^2 \mathfrak{q}^{3/2}) \quad (3.228)$$

This explains the modification in the first term in (3.226).

The equation (3.226) is a nonlinear equation for the eigenvalue  $c_1$ , and it is in general difficult to prove results about the existence or uniqueness of its solutions. For the present analysis, we shall be concerned only with the development of the Rossby wave – gravity wave mode, already discussed in this section, in the limit as the potential vorticity jump is made very large.

### The limit $\mathfrak{q} \rightarrow 0$

We consider first the limit  $\mathfrak{q} \rightarrow 0$ . In this limit, we introduce a new variable  $z = \mathfrak{q}^{3/4}Y$ . In this variable, (3.219) becomes

$$\mathfrak{q}^{3/2} \frac{d^2 u}{dz^2} + \left( z^2 - 1 + 2c_1 \mathfrak{q}^{3/4} z + c_1^2 \mathfrak{q}^{3/2} \right) = 0. \quad (3.229)$$

Moreover,  $c_1$  is also expanded in powers of  $q^{3/4}$ :

$$c_1 = c_1^0 + q^{3/4}c_1^1 + \dots \quad (3.230)$$

For the present purposes, only  $c_1^0$  will be required to obtain the leading order expression for the growth rate of the instability.

The solution to (3.229) is then written in the form

$$u(z) = A(z)e^{q^{-3/4}\psi_0(z)+\psi_1(z)} + O(q^{3/4}). \quad (3.231)$$

Substituting (3.231) into (3.229), one obtains

$$\frac{d\psi_0}{dz} = (1 - z^2)^{1/2} \quad (3.232)$$

$$\frac{d\psi_1}{dz} = -\frac{c_1^0 z}{(1 - z^2)^{1/2}}. \quad (3.233)$$

The analysis from this point is very similar to the WKBJ analyses in the limit of large  $k$ . The turning point in the WKBJ analysis occurs at  $z = 1$ , and so we set  $\psi_0(1) = 0$  and  $\psi_1(1) = 0$ . Then the continuity equation (3.192) becomes

$$c_1^0 \left[ 1 + 1 + ie^{2(q^{-3/4}\psi_0(0)+\psi_1(0))} \right] = -1. \quad (3.234)$$

From this it follows that  $c_1^0 = -1/2$ , and hence

$$\psi_0(0) = -\frac{\pi}{4}; \quad \psi_1(0) = -\frac{1}{2}. \quad (3.235)$$

The growth rate of the instability is then given by

$$\text{Im}(c) \sim \frac{1}{4}e^{-(q^{-3/4}\pi/2+1)}. \quad (3.236)$$

This expression is in agreement with the expression (3.213) for the growth rate of the instability obtained by assuming  $q = O(1)$ , and then taking the limit  $q \rightarrow \infty$ .

### The limit $q \rightarrow \infty$

In the limit  $q \rightarrow \infty$ , the equation (3.226) is rather difficult to analyse. The principal difficulty comes from the fact that there may be roots with  $c_1 = O(q^{-3/8})$ , for which the second argument

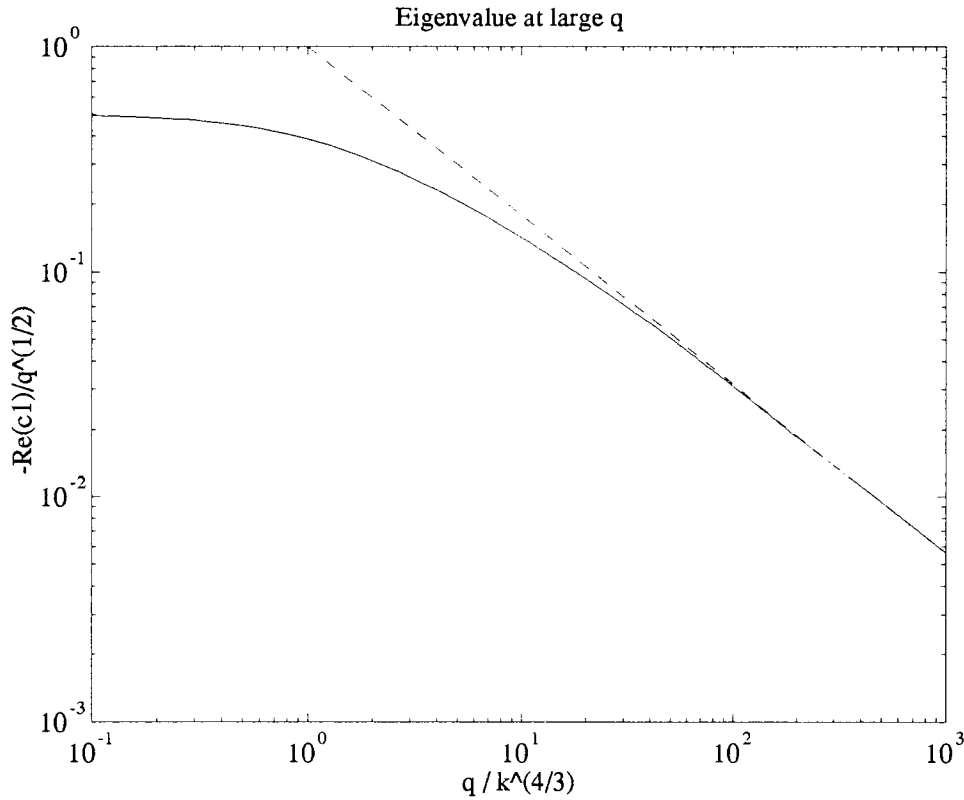


Figure 3.32: Real part of  $c_1$ , as a function of  $q$  (solid line), with  $\text{Re}c_1 = -q^{-3/4}$  (dashed line).

of the parabolic cylinder function is of order unity. However, we are concerned in this thesis with the character of the Rossby – gravity wave instability as  $q$  is varied, and we shall therefore concentrate on the eigenmode which reduces to the above in the limit  $q \rightarrow 0$ . In the limit  $q \rightarrow \infty$ , it will be seen that the appropriate root of (3.226) comes by taking

$$c_1 = q^{-3/4}c_1^1 + q^{-3/2}c_1^2 + \dots \quad (3.237)$$

There is a unique root under this scaling. It shall further turn out that  $c_1^1$  is real, whereas  $c_1^2$  is complex, and the growth rate of the eigenmode, which is  $k^{2/3}q^{1/2}c_1$ , thus tends to zero in the limit  $q \rightarrow \infty$ .

To see this first examine figure 3.32, which shows the real part of  $c_1$ , computed numerically by solution of (3.219). At large  $q$ , on the log-log scale, one can see that  $\text{Re}c_1 \rightarrow -q^{-3/4}$  as  $q \rightarrow \infty$ . The point about this is that then  $1 - c_1^2q^{3/2}$  is of small order, and hence the balance of terms in (3.226) may change. Expanding

$$c_1 = -q^{-3/4} + Cq^{-3/2} \quad (3.238)$$

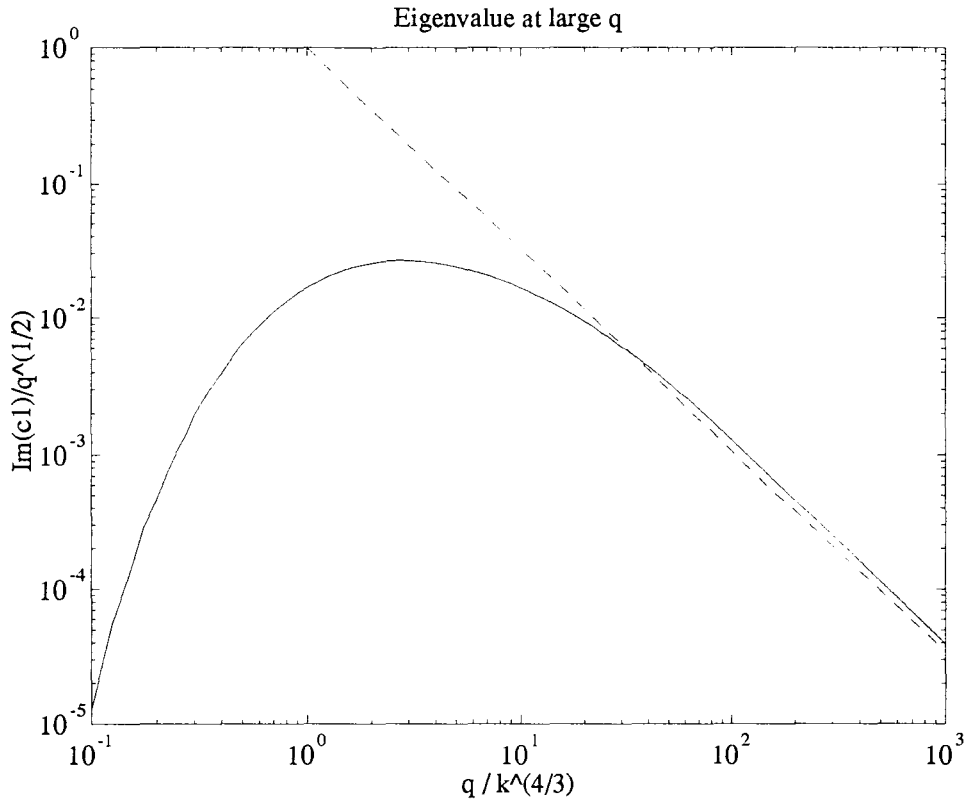


Figure 3.33: Imaginary part of  $c_1$ , as a function of  $q$  (solid line), with  $\text{Im}c_1 = \frac{1}{8}(\Gamma(1/4)/\Gamma(3/4))^2 q^{-3/2}$  (dashed line)

we obtain

$$\frac{1}{(2C)^{1/2}} + \sqrt{2} \frac{E'(0,0)}{E(0,0)} = 0 \tag{3.239}$$

for which the solution is

$$C = \frac{i}{8} \left( \frac{\Gamma(1/4)}{\Gamma(3/4)} \right)^2 \approx 1.09i. \tag{3.240}$$

The imaginary part of  $c_1$  is shown in figure 3.33, with the value given by (3.240) for comparison. In this case, quite large values of  $q$  seem to be required for the validity of (3.240).

Thus,  $c_1$  is imaginary at order  $q^{-3/2}$ , and hence  $\text{Im}(\omega) = O(q^{-1})$ . Therefore, this mode is stable in the limit  $q \rightarrow \infty$ , consistent with the analysis of Paldor (1983).

### 3.5.8 Eigenvalue calculations for large $q$

In figure 3.34, the growth rates of the instabilities are shown for potential vorticity jumps of  $10^2$ ,  $10^3$  and  $10^6$ . The ordinate is  $q^{-3/4}$ , or  $k/q^{3/4}$  in terms of the original problem. On the

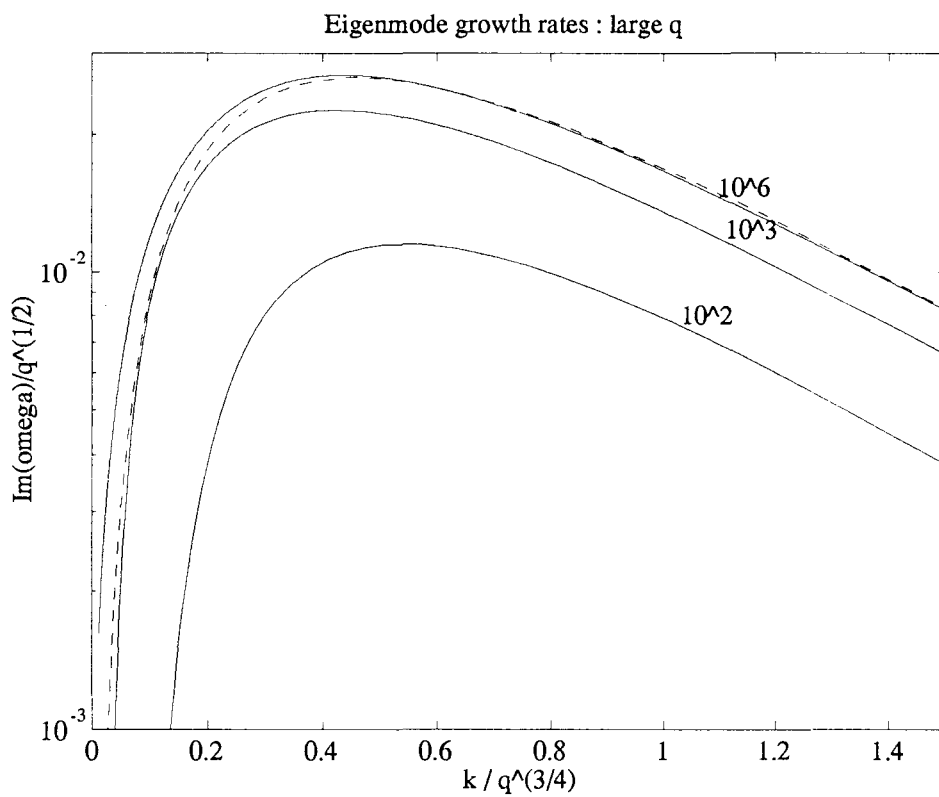


Figure 3.34: Solid lines are growth rates of linear eigenmodes for parallel flows with single potential vorticity jumps of  $10^2$ ,  $10^3$  and  $10^6$ . Dashed line is the growth rate predicted in the limit  $q \gg 1$ ,  $k \gg 1$ ,  $q \equiv q/k^{4/3} = O(1)$

abscissa is  $\text{Im}(\omega)/\sqrt{q}$ . In the limit of large  $q$ , with  $q$  of order unity, all the curves should fall on the dashed curve, which is obtained from the eigenvalue equation (3.226).

Comparison of the computed with the predicted growth rates shows that quite large values of  $q$  are required to obtain good agreement between computed growth rates and the large  $q$  limit. With  $q = 10^6$ , there is very good agreement for  $k/q^{3/4}$  between 0.5 and 1.0. Outside this range, agreement is less good. It would improve with a larger value of  $q$ . However, the differential equations that must be integrated to obtain the eigenvalue become very stiff, and there is some doubt as to whether the numerical eigenvalue finder is sufficiently accurate to proceed to values of  $q$  in excess of about  $10^6$ . However, calculation with  $q = 2 \times 10^7$  (not shown) did appear to show some improvement over  $q = 10^6$  for  $k/q^{3/4}$  down to around 0.2, apparently confirming that we can ultimately expect to see agreement between the computed and theoretical curves for all but the smallest values of  $k/q^{3/4}$ , for which the analysis, which assumes  $k \gg 1$ , can never be valid.

### 3.5.9 Remarks

The instability of a parallel shear flow with a single discontinuity of potential vorticity has been investigated numerically, and analytically in the limit of short wavelength instabilities. The instability at short wavelength is present whenever the stability criteria of Ripa (1983) fail.

In the limit of a large potential vorticity jump, the instability becomes very strong, with a growth rate of order  $k^{2/3}$  if the potential vorticity jump is of order  $k^{4/3}$ . However, as the jump is made large compared with  $k^{4/3}$ , the growth rate decays algebraically, and the limiting case of a surfacing front, investigated by Paldor (1983), is stable, as Paldor found.

## 3.6 Discussion

This chapter has furthered the study of vortex – gravity wave interactions in the shallow water equations by investigating instabilities which owe their existence to a coupling between Rossby waves and gravity waves.

First we investigated the stability of an axisymmetric vortex with a single radial discontinuity in potential vorticity. Numerical results showed that the presence of background rotation had a significant effect on the growth rates of any instabilities. This appeared to be due mainly

to differences in the character of the basic states. The sonic radius tended to be closer to the vortex boundary for values of the Coriolis parameter between 0 and -1. Asymptotic analysis for large azimuthal mode number showed that the vortex was always unstable, provided some rather weak assumptions were made about the basic state – assumptions which were always found to hold in practice. The growth rates are predicted to be exponentially small in the mode number for large mode number. There was good agreement between analysis and numerical eigenvalue calculations for quite moderate values of the mode number. The analysis was generalized to a limited class of flows with smooth potential vorticity profiles, and the connections between the current work and the study of Sozou (1987) were clarified.

The implications for the nature of a slow manifold for the shallow water equations were then discussed. Although there is no absolute proof that an invariant manifold of dimension  $1/3$  the dimension of the full phase space cannot be found, two things are clear. One is that any such invariant manifold is not unique. Another is that it is not truly slow, in that gravity wave - like features are bound to be present on it, albeit exponentially weakly at small Rossby number.

Finally, the stability of a parallel flow with a single discontinuity of potential vorticity was analysed. The numerical eigenvalue problem and large wavenumber limits are similar to those for the axisymmetric vortex. The problem was nondimensionalized somewhat differently from the axisymmetric vortex problem, and it allows a limit in which the potential vorticity on one side of the discontinuity becomes unbounded, corresponding to a vanishing layer depth. This limit has already been shown to be stable, and it turns out that a further asymptotic regime, in which the potential vorticity  $q$  in the shallow layer scales as  $k^{4/3}$ , where  $k$  is the wavenumber of the disturbance, is required to capture this limiting behaviour. Thus, although the maximum growth rate of the instability becomes unbounded as  $q \rightarrow \infty$ , it occurs at a wavenumber with a fixed value of  $k/q^{3/4}$ , with the growth rate tending to zero as  $k/q^{3/4}$  tends to infinity.

In conclusion, a number of Rossby wave – gravity wave instabilities have been investigated in this chapter. They are generally short wave instabilities, and are therefore ideally suited to analysis by the WKBJ technique. In all cases investigated, the growth rates of the instabilities tended to be rather small, with the possible exception of an axisymmetric vortex at fairly large Froude number, with potential vorticity of opposite sign to the background. Nonetheless, it was shown that the instability persists, albeit exponentially weakly, for arbitrarily small

Rossby number, and this has significant implications for the slow manifold hypothesis. It seems increasingly unlikely that a slow manifold exists for the shallow water equations. In this chapter, it has been shown that if one does exist it is not unique, and must contain structures on it which are definitely gravity wave - like. It is unlikely that the concept of a truly slow manifold is therefore a useful one.

## Chapter 4

# Nonlinear simulation of gravity wave generation

## 4.1 Introduction

Since the development of the theory of aerodynamic sound by Lighthill (1952), several attempts have been made to verify it, and to investigate the range of Mach numbers over which it is valid (see, for example, Lighthill, 1954; Lush, 1971; Bridges & Hussain, 1992). In this chapter, we shall be concerned with two questions:

- 1 Over what range of Froude and Rossby numbers does the Lighthill theory of aerodynamic sound generation, appropriately modified to incorporate the effects of background rotation, give a quantitatively accurate description of the gravity wave field radiated by vortical motions in the shallow water equations?
- 2 How does the gravity wave radiation depend on the Froude and Rossby numbers as the Froude number is increased beyond the regime in which the Lighthill theory is valid, and, specifically, what conditions must exist in the vortical flow to enable gravity waves with order-one fluxes to be generated?

A comparison of the theory with early experimental data was made by Lighthill (1954). In general, there was reasonable agreement between theory and experimental data. In accordance with equation (2.10), the power of the acoustic waves radiated from the jet scaled approximately as the eighth power of the jet speed, providing some support for the validity of the theory when applied to actual turbulent jet flows.

Subsequent experiments by Lush (1971) confirmed the  $U^8$  scaling law for the radiated power, where  $U$  is the speed of the jet, in somewhat more convincing detail than the earlier experiments discussed by Lighthill (1954), but also observed that when the acoustic waves passed through the jet for several wavelengths, they do not obey Lighthill's scaling law. This raises doubts about the claim, implicit in Lighthill's original formulation of his theory, that eddies in compressible jets will tend to be incoherent over a typical acoustic wavelength, and will not interfere with the radiated acoustic waves. Much of the literature on the aeroacoustics of jets over the last 20 years has been concerned with this point (see, for example, Moore, 1977; Mankbadi & Liu, 1984).

Recently, Bridges & Hussain (1992) have returned to the issue of the detailed verification of the Lighthill theory in a jet undergoing shear instability, in which the entire sound generation

region is acoustically compact with respect to all but the shortest wavelengths of the radiated acoustic wave field. They present a detailed analysis of the jet flow, identifying vorticity as the most robust measurable quantity from which to reconstruct velocities in the jet, under the assumption that the Mach number in the jet is sufficiently low that the velocity field can be approximated by the incompressible velocity field due to a given vorticity distribution, and hence to effective quadrupole source term for the radiated sound field. Comparisons between measurements of the acoustic field and its reconstruction from the Lighthill theory of aerodynamic sound generation are exceptionally good, thus verifying that the compact source assumption can be applied successfully to actual jet flows. If the vortical source of the radiated sound field is well modelled by a compact source approximation, one can show that for axisymmetric vortical flows, an extinction angle occurs at  $54^\circ$  to the axis of symmetry. In the experiments of Bridges & Hussain, the jet axis serves as the axis of symmetry, and the extinction angle is well captured in the experimental data. However, agreement between theory and observations is not perfect, since the theory also predicts a second extinction angle which is not observed in their experimental data. Bridges & Hussain suggest that noise associated with the nozzle from which the jet issues is the most likely cause of the discrepancy.

A set of experiments even more idealized than those of Bridges & Hussain, also designed to test the validity of the Lighthill aeroacoustic theory, has been carried out by Kambe & Minota (1983), and Minota & Kambe (1986), who investigate experimentally the sound generated by a pair of colliding vortex rings. These experiments allow an especially detailed investigation of the validity of the theory of sound generation, since the flows may be made localized and compact for sufficiently small Mach number, and there is somewhat more detailed knowledge of the velocity field than in the experiments of Bridges & Hussain (1992). Moreover, since the sound generation is most intense when the vortex rings are interacting, and the point of interaction is well separated from the position of the generation of the vortex rings, there is no difficulty equivalent to the “nozzle noise” problems encountered by Bridges & Hussain (1992). The radiated sound field is compared with that predicted by the analytical work of Kambe & Minota (1981). They find that there is good agreement between experiments and theory, provided viscosity is taken into account. This is clear from their plots of directivity, which are initially consistent with a compact quadrupolar source, but develop a strong isotropic component from an effective monopole, which is due to viscosity, as the experiments proceed

in time.

Although there has been much experimental work with three dimensional jet flows, there appears to have been comparatively little experimental study of gravity wave generation in two dimensional flows. The only study to have been reported in the literature was undertaken by Webster (1970), who verified that a jet in shallow water excites surface waves whose intensity scales with the seventh power of the jet speed for Froude numbers up to approximately 1.0, consistent with (2.11). The Froude number must also be large enough that the jet noise exceeds the noise generated by interaction between the fluid and the nozzle from which the jet is issued. This confirms that the Lighthill theory appears to work well for quite large Froude numbers in two dimensional flows, just as it works well for quite large Mach numbers in three dimensional flows – a fact which could not have been assumed *a priori*, since there is no reason to expect the domain of validity of a small Froude number approximation in two dimensions to be the same as the domain of validity of a small Mach number approximation in three dimensions

Recently, Lele & Ho (1993) have presented a numerical study of a compressible mixing layer in a two dimensional numerical model. The mixing layer is unstable, and the waves which grow on the edges of the mixing layer eventually develop into a train of coherent vortices. The simulations are performed in a domain which is periodic in the the direction of the initial flow, and has absorbing regions placed near the boundaries which are parallel to the initial flow. Since it can be shown that the Lighthill theory is formally valid in the limit of low Mach number, it might be asked whether the source term to be taken in the Lighthill theory should come directly from the velocity and density fields in the numerical simulation, or whether it should be constructed from the vorticity field, under the assumption of incompressible flow, as Bridges & Hussain did in their experimental study. Lele & Ho found that the agreement between the simulated radiated wave field and its reconstruction using the Lighthill theory was significantly better when actual velocity and density fields were used to compute the Lighthill source term than when the incompressible fields were used, and that the Lighthill reconstruction could work quite well at Mach numbers of up to about 0.6, at which they found errors in the acoustic pressure field predicted by the Lighthill theory of only about 10%. For Mach numbers up to 0.2, the errors were only about 1–2%. It seems that the the low Mach number approximation is violated in the source region at quite small Mach numbers, whereas the assumption that the source region is small compared with the scale of the acoustic waves generated, although

formally a low Mach number approximation itself, is valid over a much wider range of Mach numbers.

The basic conclusion from the studies discussed above is that, leaving aside subtleties associated with extensive jets and directivity of the radiated sound, all experiments to date have demonstrated good agreement with the Lighthill theory up to quite large values of the Mach number, with the intensity of the ‘sound’ scaling with the eighth power of the Mach number in three dimensions, and the seventh power in two dimensions. This implies that the sound radiated, although weak at low Mach numbers, will rise very sharply in intensity as the Mach number is increased. Moreover, when a complete knowledge of the source flow is available, as in the numerical experiments of Lele & Ho (1993), the acoustic sound field can be reconstructed with excellent accuracy for Mach numbers up to 0.6 from the Lighthill source term. They also found that the momentum flux in the acoustic wave region scaled as the sixth power of the Mach number, consistent with scaling arguments which can be derived for one dimensional wave radiation from a vortical source (see Ffowcs-Williams, 1969).

Although the Lighthill theory of aerodynamic sound generation is therefore apparently well established for simple flows and turbulent jet flows over a range of Mach numbers, there remains no numerical or experimental study of the corresponding gravity wave generation problem, for cases where the rotation of the reference frame should be taken into account.

Recently, McIntyre & Norton (1993) presented simulations of a forced polar vortex in a hemispherical shallow water model. The forcing is applied over a long time scale, so it does not generate gravity waves directly, but acts to disrupt the polar vortex, thereby generating gravity waves as a result of the subsequent vortical motions. They compared the shallow water simulations with simulations using balanced models of varying accuracy, and found that the amplitude of gravity waves generated appeared to be very low, even when the Froude number in the flow reached 0.7. Without further investigation, their results might appear to contradict the established body of literature on aerodynamic sound generation and the validity of the Lighthill (1952) theory, which predicts that the amplitude of gravity waves generated by vortical motions will increase rapidly with increasing Froude number.

The complexity of the flows simulated by McIntyre & Norton (1993) makes it difficult to analyse nature of the gravity wave generation process in detail for their simulations. In this chapter, we shall investigate only simple flows, in which the vortical field is comparatively well

understood. We shall use the shallow water equations on an  $f$ -plane. This way, large scale Rossby waves are avoided, and the potential vorticity will be non-uniform only in some finite region. A modified version of the Lighthill theory of aerodynamic sound generation can then be used to investigate the validity of the compact source approximation as the Froude number is increased.

The nature of gravity waves generated by vortical motions, and the domain of validity of the modified Lighthill theory, are not only of theoretical interest. Frequently, the passage of a jet streak at the level of the tropopause can give rise to a significant amount of gravity wave activity. Usually, the gravity waves generated will propagate vertically upwards into the stratosphere. Occasionally the tropospheric conditions can act as a wave guide, and a significant amount of the waves generated by the passage of the jet streak remain trapped in the troposphere.

Such an event was observed and analysed by Koch & Dorian (1988) using a mesoscale observing network. In addition to presenting an analysis of the gravity wave field, they investigated possible source mechanisms. After ruling out convection as a possible source, they concluded that the gravity waves were generated either as a result of stratified-shear-flow instability, or through nonlinear interaction with the unsteady vortical motions associated with the jet streak itself. They were unable to demonstrate conclusively which of these two possible mechanisms was responsible for the observed waves. However, if we can gain some more insight into how to apply and interpret the modified Lighthill theory, and have some knowledge of its domain of validity as the Froude number is increased, we may lay the foundations for the development of a test to determine whether the amplitude and form of the observed waves is consistent with their being generated by coupling with the vortex dynamics. Gravity waves of long wavelength and period, apparently generated by vortical motions, have also been observed in simulations of baroclinic lifecycles by D. J. O'Sullivan (personal communication).

Although we may bear in mind these applications as a motivation for the present study, I have chosen not to concentrate on any particular flow which might be observed in the atmosphere, but rather to concentrate on flows which can be analysed and interpreted readily. I have therefore required three things of the idealized experiments to be discussed in this chapter:

- 1 Any gravity waves present in the simulation must be unequivocally due to vortical motions, and should not be due to any forcing or initialization procedure.

- 2 The simulations should depend on the minimum number of adjustable parameters, which should be related to the Froude number and the Rossby number.
- 3 Whatever mechanism is used to generate the vortical flow should apply in the limit of low Froude number, so that in this limit the modified Lighthill theory of gravity wave generation may be tested.

Of these requirements, it is undoubtedly the first requirement which places the most severe restrictions on the nature of the initial flow whose subsequent evolution we may study. Suppose we wish to initialize our simulation with an arbitrary potential vorticity field. A small amount of gravity wave activity is inevitable, due to the non-existence of a true slow manifold for the shallow water equations, established in the previous chapter. How much gravity wave activity there is depends inevitably on which balanced model we choose. In any case, even if the very minimum of gravity waves are introduced by the initialization procedure, we will be in the position of having gravity waves present from the initial instant in our simulation, but no knowledge of the flow which is supposed to have generated them. This is a totally unsuitable situation for testing the validity of a modified Lighthill theory.

The only flows from which we can unambiguously eliminate gravity waves are the steady solutions of the shallow water equations – parallel flow and axisymmetric flow. Since these are steady flows, they will never develop gravity waves. However, if they are unstable, then an arbitrarily small disturbance may develop into a vigorous vortical motion from which gravity waves may be radiated. From the viewpoint of numerical simulation, it is simpler to work with initially parallel flow than initially axisymmetric flow, and that is the sole focus of the study presented here.

The most familiar form of parallel flow instability is the so-called “barotropic” shear flow instability, described, for example, in Hoskins *et al.* (1985). This instability can occur when there is a reversal in the sign of the potential vorticity gradient across the flow. This means that there are potential vorticity gradients of both signs in the flow. Physically, the direction of the potential vorticity gradient sets the direction of Rossby wave propagation, and therefore we can have counter-propagating Rossby waves in the flow, propagating on potential vorticity gradients of opposite sign. For some critical values of wavelength, these two counter-propagating waves can lock onto each other, and thereby cause each other to grow. For this reason, the instability

is sometimes referred to as “Rossby wave – Rossby wave” instability.

An extensive review of shear flow instability, including barotropic shear flow instability, was given by Ho & Huerre (1984). As the instability develops, the potential vorticity rolls up into a train of vortices, spatially periodic in the streamwise direction. Many previous studies have addressed the subsequent merging of adjacent vortices as subharmonics of the fundamental wavelength of the instability develop (see Ho & Huerre (*op. cit.*) and refs. therein). In this study, we are concerned with the degree to which the vortex motions, following the roll up of the primary instability, will excite gravity waves which radiate away from the shear layer. To enable a thorough investigation of the Froude and Rossby number parameter space, I have chosen to concentrate resources on simulating just one wavelength of the primary instability. It follows that subharmonics do not develop, and so the extent to which the vortex merging process excites gravity waves has not been investigated.

An alternative mechanism for parallel flow instability in the shallow water equations was presented in chapter 3, and can be regarded as a “Rossby wave – gravity wave” instability. However, there are three reasons for preferring to use barotropic instability for generating the vortical motions which will excite gravity waves in our experiments.

- 1 Typical growth rates of Rossby wave – gravity wave instability are very small, so the instability will take a long time to develop, and might saturate at low amplitude.
- 2 The Rossby number and Froude number are not independent parameters for an initial flow with a single discontinuity of or sharp jump in potential vorticity, so it is not possible to vary them independently in simulations initialized in this way
- 3 The Rossby wave – gravity wave instability is not present at arbitrarily small Froude number, so rendering a comparison with the modified Lighthill theory impossible in the small Froude number limit in which the theory is formally valid.

For these reasons, all the numerical simulations presented in this chapter are simulations of barotropically unstable parallel flows. Initially, the potential vorticity is everywhere uniform, equal to  $Q_0$ , say, except in some strip of finite width. The velocity tends to zero far from the strip, and the height tends to a uniform value. Inside the strip, the potential vorticity takes a different uniform value,  $Q_1$ . The potential vorticity jump is smoothed over at least 5 grid

points in the numerical model. The ratio of the difference between the strip and background potential vorticities,  $Q_1 - Q_0$ , to the background value,  $Q_0$ , defines an effective Rossby number  $Ro = Q_1/Q_0 - 1$  for the flow. As the strip width is increased, so the velocities in the strip increase, and hence the Froude number is governed by the width of the strip.

The rest of this chapter is organized as follows.

In §4.2 the Lighthill analysis for the shallow water equations is developed, as appropriate for periodic jets.

In §4.3 the pseudomomentum and pseudoenergy are introduced as possible diagnostic quantities for quantifying the intensity of gravity wave radiation, and it is shown that the pseudoenergy flux is the natural wave quantity to choose in this study.

In §4.4 the numerical model to be used for the nonlinear simulations is described, and an overview of the simulations performed with the model is presented in §4.5.

In §4.6, the gravity wave radiation from a train of vortices generated by the roll up of a cyclonic strip of potential vorticity is discussed. The strip has potential vorticity equal to six times the background value.

In §4.7, the effect of increasing the potential vorticity in the strip is investigated.

In §4.8, anticyclonic strips are investigated, with potential vorticity in the strips equal to 0.1 and 0.0 times the background value.

In §4.9, the effects of negative potential vorticity is investigated, with potential vorticities in the strip of -0.1, -1.0 and -19.0 times the background value.

Some conclusions are offered in §4.10.

## 4.2 A “Lighthill” theory of gravity wave generation for a periodic parallel flow

In this section the analysis necessary to investigate the quantitative accuracy of the Lighthill theory, applied to periodic flows in a rotating frame, is developed. In further sections the analysis will be used to investigate the degree to which the theory remains useful as the Froude number is increased and the compact source assumption becomes less valid.

Returning to equation (2.4), we recall that manipulation of the shallow water equations gives

$$\left(\frac{\partial^2}{\partial t^2} + f^2 - c_0^2 \nabla^2\right) \frac{\partial h}{\partial t} = \frac{\partial^2}{\partial x_i \partial x_j} T_{ij}, \quad (4.1)$$

where

$$T_{ij} = \frac{\partial}{\partial t}(h u_i u_j) + f \varepsilon_{ik} h u_j u_k + \frac{1}{2} g \frac{\partial}{\partial t}(h - h_0)^2 \delta_{ij}, \quad (4.2)$$

$h_0$  is the layer depth far from the region of vortical motion, and  $c_0 = (gh_0)^{1/2}$  is the gravity wave phase speed far from the region of vortical motion. These equations have formal solution

$$\frac{\partial h}{\partial t} = \frac{1}{4\pi c_0} \frac{\partial^2}{\partial x_i \partial x_j} \int_{t-t' > |\mathbf{x} - \mathbf{x}'|/c_0} \frac{T_{ij}(\mathbf{x}', t') \cos(f((t-t')^2 - |\mathbf{x} - \mathbf{x}'|^2/c_0^2)^{1/2})}{((t-t')^2 - |\mathbf{x} - \mathbf{x}'|^2/c_0^2)^{1/2}} d^2 \mathbf{x}' dt'. \quad (4.3)$$

The key point in Lighthill's theory is now to assume that the source term  $T_{ij}$  is only non-zero over a small enough region that it may be approximated by a quadrupole point source, so that we may write the solution as

$$\frac{\partial h}{\partial t} = \frac{1}{4\pi c_0} \frac{\partial^2}{\partial x_i \partial x_j} \int_{t-t' > |\mathbf{x}|/c_0} \frac{S_{ij}(t') \cos(f((t-t')^2 - |\mathbf{x}|^2/c_0^2)^{1/2})}{((t-t')^2 - |\mathbf{x}|^2/c_0^2)^{1/2}} dt', \quad (4.4)$$

where

$$S_{ij}(t') = \int_{\mathbb{R}^2} T_{ij}(\mathbf{x}', t') d^2 \mathbf{x}'. \quad (4.5)$$

In the classical problem of aerodynamic sound generation, this is the compact source approximation – that the length-scale of the source is small compared with the length-scale of the waves. Here we are imposing an additional condition – that the length-scale of the source is also small compared with a Rossby deformation radius.

If we now assume that we know the way in which the source term scales as the flow parameters are varied, then we may estimate how the amplitude of the wave field depends on parameters such as the Froude number and the Rossby number. Lighthill (1954) proposed that the theory could be applied to an extensive body of turbulence by assuming that each turbulent eddy was itself compact, and not correlated with other eddies.

It is clearly not possible to apply this analysis directly to a radiating vortex train, since the eddies in the train are highly correlated with each other. We must therefore develop a version of the theory specifically for the case where the source, and therefore the waves, are periodic in the  $x$  direction.

In comparing the gravity wave radiation with that which is predicted by the Lighthill theory, we shall concentrate on that component of the wave field which is independent of the streamwise coordinate  $x$ . In the asymptotic limit of small Froude number, it can be shown by the method of matched asymptotic expansions that all other components of the radiated wave field are exponentially small compared with the  $x$ -independent component, and so this seems the natural component on which to focus the analysis.

Now, let the  $x$ -average of a quantity  $a$  be denoted by  $\bar{a}^x$ . To derive the effective source for the  $x$ -independent component of the wave field, we must take the  $x$ -average of equation (4.1). The  $x$  derivatives, in both the wave operator and the quadrupole term, then vanish, and we are left with a one-dimensional Klein-Gordon equation, with a one-dimensional quadrupole source term:

$$\left( \frac{\partial^2}{\partial t^2} + f^2 - \frac{1}{c_0^2} \frac{\partial^2}{\partial y^2} \right) \frac{\partial \bar{h}^x}{\partial t} = \frac{\partial^2}{\partial y^2} \bar{T}_{22}^x. \quad (4.6)$$

To proceed, we need only assume that the source term  $\bar{T}_{22}^x$  is compact with respect to the cross stream direction  $y$ . Making that assumption, we obtain

$$\frac{\partial \bar{h}^x}{\partial t}(y, t) = \frac{1}{2c_0} \frac{d^2}{dy^2} \int_{-\infty}^{t-|y|/c_0} S(t') J_0(\sqrt{((t-t')^2 - y^2/c_0^2)}) dt', \quad (4.7)$$

where

$$S(t') = \int_{-\infty}^{\infty} \bar{T}_{22}^x(y', t') dy', \quad (4.8)$$

and  $J_0$  is the regular Bessel function of order zero (see Morse & Feshbach, 1953). The factor  $\frac{1}{2}$  arises from the fact that waves propagate in both positive and negative  $y$  directions away from the source at  $y = 0$ .

To reconstruct the wave field from a numerical simulation using equation (4.7), we now need only know the function  $S(t)$ , a single function of time, which is obtained for each time  $t$  during the simulation by evaluating the integral (4.8) over the entire flow.

We may readily proceed from here to show how  $\partial h / \partial t$  in the wave region scales with properties of the vortical flow in the vortex train. Taking the Fourier transform of (4.6) with respect to  $t$ , we have, making the compact source approximation,

$$i\omega \tilde{h} \sim \frac{\sqrt{\omega^2 - f^2}}{2c_0} e^{i\sqrt{\omega^2 - f^2}y/c_0} \int \bar{T}_{22}^x(y', \omega) dy', \quad (4.9)$$

where, as usual,  $\omega$  is the transform variable. Now, scale analysis of (4.2) gives a scaling for  $T_{22}$ :  $\overline{T_{22}^x}(y', \omega) \sim \omega u^2 \lambda \tilde{h}_0$ , where  $\lambda$  is the length scale of the vortical region, and hence, for  $\omega^2 > f^2$ ,

$$h' \sim h_0 \left( \frac{u}{c_0} \right)^2 \left( \frac{(\sqrt{\omega^2 - f^2}) \lambda}{c_0} \right). \quad (4.10)$$

### 4.3 Pseudoenergy and pseudomomentum for the shallow water equations

Since we are interested in the amplitude of gravity wave radiation over a wide range of Froude and Rossby numbers, it is desirable to take the flux of an appropriate wave quantity, such as pseudoenergy or pseudomomentum, as a measure of the strength of gravity wave radiation by the vortical flow.

In general, a wave activity density  $A$  is a field, second order in disturbance amplitude in the limit of small disturbances, for which there exists an associated wave flux  $\mathbf{F}$ , such that

$$\frac{\partial A}{\partial t} + \nabla \cdot \mathbf{F} = 0. \quad (4.11)$$

Definition of wave activities and their corresponding fluxes must be made with respect to some reference state. In this chapter, we shall take the initial parallel flow as the reference state for the definition of wave activities and their fluxes. Throughout this section,  $\mathbf{u}_0$ ,  $h_0$  and  $Q_0$  represent the velocity, height and potential vorticity of the basic state respectively, and  $\mathbf{u}'$  and  $h'$  represent departures of velocity and height from the basic state values. The basic state possesses symmetries with respect to  $x$ -translation and time translation, and therefore it is possible to define both pseudoenergy and  $x$ -pseudomomentum fluxes. For the present study, we are interested in developing a wave quantity which can be used to characterise the strength of gravity wave radiation. If we are to take a single quantity, such as a wave flux strength, to characterise gravity wave radiation, then that quantity should satisfy a monotonic radiation property – that is, all radiating waves should give rise to fluxes of the same sign, at least in the limit of linear waves. It turns out that this “monotonic radiation property” is not satisfied by the pseudomomentum, but is satisfied by the pseudoenergy.

The technique for obtaining wave activities and fluxes is now quite well established (McIntyre & Shepherd, 1987; Haynes, 1988), and the details of the calculations of the pseudoenergy and

pseudomomentum for the shallow water equations will not be reproduced here.

The pseudomomentum density for the shallow water equations is given by

$$A_m = h'u' + h \int_{y_0}^y (Q - Q_0(y')) h_0(y') dy' \quad (4.12)$$

and its flux is given by

$$\mathbf{F}_m = \mathbf{u}A_m + \left( \frac{1}{2}h_0(u'^2 - v'^2) + \frac{1}{2}gh'^2, u'v'h_0 \right), \quad (4.13)$$

so that

$$\frac{\partial A_m}{\partial t} + \nabla \cdot \mathbf{F}_m = 0. \quad (4.14)$$

The pseudoenergy density is

$$A_e = \frac{1}{2}h(u'^2 + v'^2) + u_0u'h' + \frac{1}{2}gh'^2 + h \int_{y_0}^y (Q - Q_0(y')) h_0(y') u_0(y') dy' \quad (4.15)$$

and its flux is

$$\mathbf{F}_e = \mathbf{u}A_e + h_0\mathbf{u}_0 \cdot \mathbf{u}'\mathbf{u}' - \frac{1}{2}h_0\mathbf{u}'^2\mathbf{u}_0 + \frac{1}{2}gh'^2\mathbf{u} + gh_0h'\mathbf{u}'. \quad (4.16)$$

In (4.12) and (4.15),  $y_0$  is the initial  $y$  location of the fluid in the reference state which is at location  $(x, y)$  at time  $t$  at which the wave activity or flux is to be evaluated. The integrals in (4.12) and (4.15) represent ‘‘Lagrangian information’’ about the motion of fluid particles. Notice, however, that they will be non-zero only if the potential vorticity in the basic state is non-uniform between  $y$  and  $y_0$ , implying that Rossby waves exist at the location  $y$ . In this chapter, we shall be concerned with gravity wave fluxes in a region of uniform potential vorticity. In computing the fluxes far from the vortical region, therefore, the contribution to (4.12) and (4.15) from the potential vorticity integrals will be identically zero.

To investigate the properties of the pseudoenergy and pseudomomentum fluxes in the far field, we consider the linearized shallow water momentum equations about a state of no motion. We assume that disturbances are wavelike, of the form  $e^{i(kx+ly-\omega t)}$ . The equations are

$$-i\omega u' - fv' + ikgh' = 0 \quad (4.17)$$

$$-i\omega v' + fu' + ilgh' = 0. \quad (4.18)$$

Considering the quadratic terms in the pseudoenergy flux in the limit where  $u_0 = 0$ , we see that the  $y$ -component of the pseudoenergy flux is dominated by the term  $h_0h'v'$ . To evaluate

$h'v'$  we eliminate  $u$  from (4.17-4.18). This gives

$$gh' = \frac{\omega^2 - f^2}{\omega^2 l^2 + f^2 k^2} (\omega l + ikf) v'. \quad (4.19)$$

Averaging over wave periods gives

$$\overline{gh'v'} = \frac{\omega^2 - f^2}{\omega^2 l^2 + f^2 k^2} \frac{\omega l}{2} |v'|^2. \quad (4.20)$$

For the pseudomomentum, we see that in the far field the  $y$ -component of the pseudomomentum flux is dominated by  $h_0 u' v'$ . So, to analyse the pseudomomentum flux in the far field, we eliminate  $h'$  from (4.17-4.18). This leads to

$$u' = \frac{(\omega^2 - f^2)kl + i\omega f(k^2 + l^2)}{\omega^2 l^2 + f^2 k^2} v'. \quad (4.21)$$

Averaging over wave periods here gives

$$\overline{u'v'} = \frac{\omega^2 - f^2}{\omega^2 l^2 + f^2 k^2} \frac{kl}{2} |v'|^2. \quad (4.22)$$

To check for radiation properties, we consider the dispersion relation for gravity waves

$$\omega^2 - f^2 = c_0^2(k^2 + l^2), \quad (4.23)$$

where  $c_0 = \sqrt{gh_0}$ .

We wish to impose a radiation condition with respect to the propagation in the  $y$  direction, so that

$$\frac{\partial \omega}{\partial l} \equiv c_0^2 \frac{l}{\omega} \begin{cases} > 0 & \text{for } y > 0 \\ < 0 & \text{for } y < 0 \end{cases}. \quad (4.24)$$

It follows that  $l$  and  $\omega$  should be of the same sign as  $y \rightarrow +\infty$ , but should be of opposite sign as  $y \rightarrow -\infty$ .

Now we want to select the wave flux such that  $\mathbf{F} \cdot \mathbf{n}$  is the same sign on the upper and lower  $y$ -boundaries, recalling that the normal is in the positive  $y$  direction for  $y > 0$ , and is in the negative  $y$  direction for  $y < 0$ . This forces us to choose the pseudoenergy flux, since  $h_0 \overline{h'v'}$  takes the same sign as  $\omega l$  provided  $\omega^2 > f^2$ , so that the waves are radiating. If  $\omega^2 < f^2$  then  $l$  is imaginary, the waves are evanescent, and there is no wave flux.

It follows that, with the present sign convention for pseudoenergy, there should be a net flux of pseudoenergy in time away from the jet due to gravity wave radiation, whereas there is no corresponding monotonic radiation property for the flux of pseudomomentum.

To see how the intensity of the pseudoenergy flux scales with the Froude number, we note that

$$F_e = h_0 g h' v' = \frac{g^2 h_0 \omega l}{\omega^2 - f^2} h'^2. \quad (4.25)$$

From (4.10), this implies

$$F_e \sim h_0 c_0^2 \left( \frac{u}{c_0} \right)^4 \lambda^2 \omega l. \quad (4.26)$$

From the dispersion relation (4.23), with  $k = 0$ , we therefore obtain

$$F_e \sim \begin{cases} h_0 c_0 \left( \frac{u}{c_0} \right)^4 \lambda^2 \omega \sqrt{\omega^2 - f^2} & \omega^2 > f^2 \\ 0 & \omega^2 < f^2 \end{cases}. \quad (4.27)$$

Thus if, at low Froude numbers, we assume that the velocity  $u$  scales as  $u \sim \omega \lambda$ , and the Froude number  $F \sim \omega \lambda / c_0$ , it follows that

$$F_e \sim \begin{cases} h_0 c_0^3 F^6 \sqrt{1 - f^2/\omega^2} & \omega^2 > f^2 \\ 0 & \omega^2 < f^2 \end{cases}. \quad (4.28)$$

Thus, if  $\omega$ ,  $c_0$  and  $h_0$  are held fixed, and the Froude number is increased by increasing  $\lambda$ , the scale of the vortical motions, the intensity of the pseudoenergy flux will increase as the sixth power of the Froude number, in agreement with the analysis of one-dimensional sound radiation by vortical motions presented by Ffowcs-Williams (1969). However, if the Froude number is increased by increasing the magnitude of the vorticity in the vortical region, and therefore increasing  $|\omega|$ , no such simple scaling law applies. In general, for a given Froude number, the intensity of wave fluxes will be greatest when  $\omega^2 \gg f^2$ , and the  $f^2/\omega^2$  term in (4.28) becomes insignificant.

## 4.4 The numerical model

The numerical model used in this chapter integrates the nonlinear  $f$ -plane shallow water equations in a channel geometry. The channel is periodic in the  $x$ -direction, and has solid boundaries at  $y = \pm Y$ , for some (usually large)  $Y$ . The shallow water equations are integrated in nondimensional form, viz:

$$\frac{\partial \mathbf{u}}{\partial t} + \mathbf{u} \cdot \nabla \mathbf{u} + \mathbf{k} \times \mathbf{u} + \nabla h = 0 \quad (4.29)$$

$$\frac{\partial h}{\partial t} + \nabla \cdot (h\mathbf{u}) = 0, \quad (4.30)$$

where  $\mathbf{u}$  is the two-dimensional velocity field,  $h$  is the layer depth, and  $\mathbf{k}$  is the unit vector normal to the plane. The nondimensionalization sets the length scales and time scales for the flow, such that the unit timescale is the inertial period  $f^{-1}$ , and the unit length scale is the Rossby deformation radius where the fluid is at rest  $\sqrt{gh_0}/f$ . In (4.29) and (4.30),  $h$  has been rescaled so that  $g$  may be set to unity. The potential vorticity away from the region of vortical motions will therefore be unity. In subsequent sections, all results of model integrations will be presented using this nondimensionalization of length and time scales.

Several numerical schemes for integrating the shallow water equations have been presented in the literature, of which the best known is that of Arakawa & Lamb (1981). A possible advantage of the Arakawa & Lamb scheme is that it can be shown to conserve energy and enstrophy exactly. The proof relies on an assumption that a regularly-spaced grid is used to discretize the equations. In this chapter, however, we are interested in flows which will generally consist of a highly nonlinear but highly localized region of vortical motion, from which low amplitude gravity waves are radiated, with a wavelength much longer than the scale of the vortical region. In the interests of computational efficiency, the model used in this chapter will therefore allow variable resolution in both the streamwise and cross-stream directions. There is therefore no particular reason to favour a scheme such as that of Arakawa & Lamb, and the model used here was developed so as to allow the fields with variable resolution to be represented in a convenient way, but not to possess any particular conservation properties.

The geometry is periodic in  $x$ , but of finite extent in  $y$ . Therefore, the equations were discretized using finite differences in the  $y$  direction, with fields at each value of  $y$  being represented as a sum of Fourier modes in  $x$ . The  $y$ -discretization is performed on a staggered grid, with  $u, v$  on physical grid levels, and  $h$  at intermediate levels. The model is a pseudo-spectral model, with streamwise derivatives being computed in spectral space, and nonlinear products computed in physical space.

The variable cross stream resolution was implemented using a coordinate transformation. The numerical model is written in terms of a cross-stream variable  $\eta$ . The grid positions are equally spaced in the model coordinate  $\eta$ , and the physical coordinate transformation is implemented by specifying a relationship between the model coordinate  $\eta$  and the physical

coordinate  $y$ . Cross-stream differencing is performed on the  $\eta$  grid, where centred differencing can be used. By a simple application of the chain rule, the centred differences are then multiplied by  $d\eta/dy$  to give the value of the derivative with respect to  $y$ . In the vortical region the value of  $d\eta/dy$  is unity, whereas in the wave region its value is generally less than unity. In the region of variable resolution, a self-similar transformation is employed, in which  $d\eta/dy = e^{-a(\eta-\eta_1)}$ , where  $\eta_1$  is the outer limit of the region of high resolution, and  $a$  is a constant which sets the size of the region of variable cross-stream resolution.

The variable streamwise resolution is implemented in a very simple way. The streamwise resolution is specified in the vortical region by specifying a maximum number of Fourier components which are to be used to represent the flow there. A full set of Fourier harmonics is retained throughout the vortical region, and in the region of varying cross-stream resolution. Beginning at the start of the region of low resolution, the number of Fourier components used to represent the solution is then reduced by a factor of two at every fifth cross-stream grid point, until a specified minimum number of streamwise components are left. This number of components is then used to represent the solution in the region of low resolution. In all simulations presented in this chapter, 64 Fourier coefficients in the  $x$  direction were used to resolve the vortical region.

Several shallow water models have been presented which use vorticity, divergence and height as prognostic variables (e.g. Bourke, 1972). They have the advantage of a flux formulation with only quadratic nonlinearity, ensuring that quadratic quantities are conserved (but not energy, which is cubic in the shallow water system) when integrated using the leapfrog timestepping scheme. However, these models require inversion of the Laplacian operator at each time step, and the velocity field at one location depends on the vorticity, divergence and height at all locations in the model. This seems an undesirable property for a model when a large domain, with regions of greatly differing character, is to be integrated. The present model uses the two components of velocity and height as the prognostic variables. Therefore, the model does not require inversion of elliptical operators to obtain the velocity and height fields and, although it is not a conservative scheme, there is no reason to expect it to be less accurate locally than a model which uses a flux formulation.

Some diffusion is required to remove fine scales, especially in the vortical region. This was implemented by applying a small amount of hyperdiffusion to the Fourier components in each

of the fields  $u$ ,  $v$  and  $h$ . The hyperdiffusion is proportional to  $k^6$ , where  $k$  is the wave number. Since the hyperdiffusion acts only in the  $x$ -direction, its anisotropic nature may make it appear to be a particularly unphysical type of hyperdiffusion. However, the rotational nature of vortical flow means that it should be sufficient to apply a diffusion in the  $x$ -direction only. Any fine scale structure which builds up in the cross-stream direction in the vortical flow will rotate into a streamwise orientation, where it will be removed by the hyperdiffusion. This type of hyperdiffusion was used in a model with streamwise spectral representation and cross stream grid-point representation in a numerical study of nonlinear critical layer evolution by Haynes (1989), and appears to control fine scale structure adequately for the present purposes. One advantage is that it is quite simple to implement, and in particular may be implemented in an implicit diffusion scheme using only division, and not tridiagonal matrix inversion, as would be required for an isotropic diffusion with a grid point discretization in the cross stream direction.

At the lateral boundaries, sponge layers may be placed over a variable number of grid levels. Rayleigh friction is applied there, which relaxes the flow back to the initial state. The value of the Rayleigh friction is small at the point where it is first encountered by waves propagating towards the boundary, and increases linearly towards the boundary. In the model, the number of grid levels over which the Rayleigh friction is applied, and its amplitude, are arbitrary. However, for all simulations presented here, it was found that applying Rayleigh friction over 30 grid levels, with a maximum value of 1.0 at the boundary, corresponding to an  $e$ -folding decay time of 1.0 for disturbances at the boundary, generally prevented any significant reflection from the boundary, and these values were used throughout.

The equations are integrated forward in time using an explicit leapfrog time step, but with the hyperdiffusion and Rayleigh friction being performed implicitly. The basic leapfrog method is unstable, however, and a time filter must be used to prevent the growth of a rapidly oscillating computational mode. In the present simulations, a Robert-Asselin time filter (Robert, 1966; Asselin, 1972) was used with a value of 0.02.

## 4.5 Overview of numerical simulations

Using the numerical model described in §4.4, gravity wave generation by vortical motions in the shallow water equations is now studied by numerical simulation of the nonlinear evolution

of a barotropically unstable strip of potential vorticity. The potential vorticity in the strip is  $Q_1$ , and the background value of the potential vorticity is unity. The Rossby number  $Ro$  can then be defined as  $Ro = Q_1 - 1$ . The only other significant parameter in the initial flow is the width of the strip,  $\Delta$ , which determines the Froude number of the flow.

In the following sections, simulations with a range of values of  $Q_1$  and  $\Delta$  are discussed. The simulations are labelled by letters **A** – **H**, with each letter corresponding to a different value of  $Q_1$ . Simulations with the same value of  $Q_1$  are distinguished by Roman numerals (e.g. **Ai**–**vi**), with the Roman numeral increasing with increasing initial strip width. Table 4.1a shows the values of  $Q_1$  and  $\Delta$  investigated, with their corresponding labels.

In all cases, the initial conditions for the numerical simulation consist of a strip of potential vorticity  $Q_1$  centred on  $y = 0$ . The model domain in the cross-stream direction extends from  $y = -Y$  to  $y = +Y$ , for some large  $Y$ , to accommodate several wavelengths of the radiating gravity waves within the computational domain. Only one wavelength of the fastest growing unstable linear eigenmode is simulated in all cases. The wavenumber of the fastest growing eigenmode is shown in table 4.1b, and a matrix method is used to obtain the eigenmode. In all cases except simulations **Ci**–**iv** and **Hi**–**iv**, a small amplitude disturbance of the form of the fastest growing eigenmode is added to the initial parallel flow at  $t = 0$ . If a large amplitude of the fastest growing eigenmode is added, then the flow will adjust, radiating gravity waves. The amplitude of the eigenmode added was therefore controlled such that any gravity waves generated by this initial adjustment had an amplitude of no more than 1–2% of the gravity waves subsequently generated by the vortical motions, when viewed in the  $\partial h/\partial t$  field. In cases **Ci**–**iv** and **Hi**–**iv**, the strips are very narrow compared with a deformation radius. Consequently, the eigenmode decays very slowly with distance away from the strip, when compared with the width of the strip. This presents very large memory requirements for the matrix method used to find the eigenmode, and in these cases the flow was disturbed by the addition of random noise. Again, the amplitude of the random noise added was chosen to be sufficiently small that any gravity wave radiation associated with it was of small amplitude compared with the gravity waves subsequently generated by the vortical motions.

In the nonlinear evolution of the flow, the strip of potential vorticity rolls up into a train of vortices, which then nutate, radiating gravity waves as they do so. In general, it was found that the maximum value of the Froude number, found in the vortical region, can increase by

(a)		$Ro$	Initial strip width					
Simulation			i	ii	iii	iv	v	vi
A	5	0.018	0.035	0.07	0.14	0.21	0.28	
B	8	0.018	0.035	0.07	0.21			
C	20	0.011	0.021	0.041	0.081			
D	-0.9	0.42	0.84	1.68	3.36	6.00	9.00	
E	-1.0	0.42	0.84	1.26	2.52	6.00		
F	-1.1	0.42	0.84	1.26	1.68	2.52	3.04	
G	-2	0.07	0.21	0.42	0.63			
H	-20	0.007	0.013	0.021	0.031			

(b)		$Ro$	Wavenumber of fastest growing mode					
Simulation			i	ii	iii	iv	v	vi
A	5	28.0	14.0	7.0	4.2	3.05	2.3	
B	8	28.0	13.75	6.6	2.6			
C	20	50.0	30.0	14.0	5.6			
D	-0.9	2.0	1.15	0.75	0.475	0.245	0.165	
E	-1.0	2.0	1.15	0.9	0.55	0.255		
F	-1.1	2.0	1.15	0.9	0.75	0.55	0.47	
G	-2	7.2	3.5	1.85	1.2			
H	-20	65.0	44.0	30.0	20.0			

(c)		$Ro$	Froude number					
Simulation			i	ii	iii	iv	v	vi
A	5	0.11	0.20	0.36	0.50	0.59	0.66	
B	8	0.17	0.32	0.53	0.84			
C	20	0.23	0.37	0.66	1.06			
D	-0.9	0.25	0.44	0.64	0.88	1.05	1.08	
E	-1.0	0.30	0.51	0.64	0.99	1.78		
F	-1.1	0.33	0.58	0.75	0.93	1.36	1.92	
G	-2	0.17	0.38	0.73	1.31			
H	-20	0.20	0.31	0.49	0.75			

Table 4.1: Initial strip widths, fastest growing wave numbers and Froude numbers for all simulations.

as much as 50% during the initial development of the instability, and then tends to fluctuate as the vortices nutate. In subsequent sections, we shall consider how the amplitude of the flux of the radiated gravity waves scales with the Froude number, with reference to the predictions made in §4.2, and in particular equation (4.28). Therefore, as a measure of the Froude number of the flow, we shall require a Froude number associated with the gravity wave generation phase of the flow, rather than the initial roll-up phase. For this reason, the maximum value of the Froude number over all times was taken to characterize the Froude number of the flow, and for each simulation this value is shown in table 4.1c.

With the values of  $Q_1$  and  $\Delta$  selected, the remaining parameter which must be adjusted is the hyperviscosity. Since it has no physical meaning, it was selected by experimentation with the simulation Aiii, with the aim of finding the minimum value which prevented an unacceptable build-up of noise on small scales in the potential vorticity field. On the other hand, it was important to ensure that the vortices did not become axisymmetric too quickly as a result of excessive hyperdiffusion, and thereby lose their ability to radiate gravity waves. It was found that 64 Fourier coefficients were required to represent the fields at each cross stream grid level if the required level of hyperdiffusion was not to be so great as to cause the vortices to become axisymmetric after one or two nutations. With the value of the hyperviscosity  $\nu$  selected, it was then adjusted between simulations so as keep  $\nu k_{\max}^6 \times (\delta Q)$  constant, where  $k_{\max}$  is the maximum wavenumber in the simulation, and  $(\delta Q)$  is the magnitude of the potential vorticity difference between the vortices and the surroundings, meaning that in all simulations it takes the same amount of time to damp out noise in the highest wave numbers on typical vortex dynamical timescales, set by the magnitude of the potential vorticity variations. For  $k = 1.0$  and  $(\delta Q) = 1.0$ , the value of  $\nu$  used is  $\nu = 6.4 \times 10^{-9}$ .

To accommodate the wide range of strip widths (see table 4.1a), the grid-point spacing in the cross-stream direction had to be changed between simulations. In all cases, the region of uniform potential vorticity in the strip was distributed over at least seven grid intervals, and the potential vorticity was adjusted to the background value over five grid intervals. Details of the cross-stream resolution for all simulations are given in table 4.2. For the streamwise resolution, the 64 Fourier coefficients which were used in the vortical region were frequently more than sufficient to resolve the flow in the wave region. Therefore, in addition to varying the cross-stream resolution, the streamwise resolution was also varied, as described in §4.4. The

Simulation		$(\Delta y)^i$	$Ny^i$	$(\Delta y)^e$	$Ny^t$	$Nx^e$	$\Delta t$
A	i	0.0025	150	0.0625	1000	8	0.000625
	ii	0.005	150	0.125	600	8	0.00125
	iii	0.01	350	0.2	1000	8	0.0025
	iv	0.01	350	0.2	1000	8	0.0025
	v	0.01	350	0.2	1000	8	0.0025
	vi	0.01	350	0.2	1000	8	0.0025
B	i	0.0025	150	0.0625	1000	8	0.000625
	ii	0.005	150	0.125	600	8	0.00125
	iii	0.01	350	0.2	1000	8	0.0025
	iv	0.01	350	0.2	1000	8	0.0025
C	i	0.001	350	0.02	1000	8	0.00025
	ii	0.001	350	0.02	1000	8	0.00025
	iii	0.001	350	0.02	1000	8	0.00025
	iv	0.004	350	0.04	1000	16	0.001
D	i	0.02	350	0.2	1000	8	0.005
	ii	0.04	350	0.2	1000	8	0.01
	iii	0.04	350	0.2	1000	16	0.01
	iv	0.04	500	0.2	1000	16	0.005
	v	0.2	600	0.2	600	64	0.025
	vi	0.2	600	0.2	600	64	0.025
E	i	0.02	350	0.2	1000	8	0.005
	ii	0.04	350	0.2	1000	8	0.01
	iii	0.04	350	0.2	1000	16	0.01
	iv	0.04	425	0.2	1000	16	0.005
	v	0.2	600	0.2	600	64	0.0125
F	i	0.02	350	0.2	1000	8	0.005
	ii	0.04	350	0.2	1000	8	0.01
	iii	0.04	350	0.2	1000	16	0.01
	iv	0.04	350	0.2	1000	16	0.005
	v	0.04	2000	0.04	2000	64	0.005
	vi	0.04	1000	0.04	1000	64	0.0025
G	i	0.01	350	0.2	1000	8	0.0025
	ii	0.01	350	0.2	1000	8	0.0025
	iii	0.02	350	0.2	1000	8	0.005
	iv	0.03	2000	0.03	2000	64	0.005
H	i	0.001	350	0.025	1000	8	0.00025
	ii	0.001	350	0.02	1000	8	0.00025
	iii	0.001	350	0.02	1000	8	0.00025
	iv	0.001	350	0.02	1000	16	0.000125

Table 4.2: Details of numerical resolution used in all experiments.  $(\Delta y)^i$  is the cross-stream grid spacing in the vortical region;  $Ny^i$  is the number of cross-stream gridpoints in the vortical region;  $(\Delta y)^e$  is the cross-stream grid spacing in the wave region;  $Ny^t$  is the total number of cross-stream gridpoints;  $Nx^e$  is the number of Fourier coefficients in the streamwise direction used to resolve the wave region;  $\Delta t$  is the timestep.

number of Fourier coefficients used in the wave region are given in table 4.2.

## 4.6 Jets with moderate Rossby number and variable Froude number

In the first set of numerical experiments, to be described in this section, the Rossby number is fixed, and the effect of varying the Froude number is investigated. In all cases to be described in this section, therefore, the model is initialized with a strip in which the potential vorticity is equal to six times the background value. This can be regarded as fixing the Rossby number at 5. The Froude number then is varied by varying the width of the strip.

Six simulations were performed with the potential vorticity in the strip equal to six times the background value. Initial strip widths of 0.018, 0.035, 0.07, 0.14, 0.21, and 0.28 were used. The corresponding Froude numbers found in the subsequent evolution varied from 0.11 to 0.67, increasing monotonically as the initial strip width increased.

Figure 4.1 shows the potential vorticity field during the initial development and saturation of the instability in the simulation Ai. All potential vorticity plots are shown with an aspect ratio of unity, and consequently they show only a small portion of the domain in the cross-stream direction. While the model domain accommodates only one wavelength of the primary instability in the streamwise direction, in figure 4.1, and in all subsequent figures shown, two periods of the model domain are displayed.

In figure 4.1, one can see that, as the instability develops, waves develop on the edges of the potential vorticity strip, which can be seen clearly in figures 4.1b and 4.1c. Nonlinear saturation of the instability is shown in figure 4.1d, where the strip has rolled up into a train of coherent vortices, connected by thin filaments.

Figure 4.2 shows the potential vorticity field at four subsequent equally spaced time intervals until the end of the simulation. Although a small amount of hyperdiffusion is applied in the  $x$ -direction to prevent an accumulation of noise on the grid scale of the numerical model, it seems that the inviscid character of the vortical flow has been well simulated in this experiment. The vortices appear to nutate between almost axisymmetric and substantially elliptical shapes, whereas if the hyperviscosity is increased significantly they become axisymmetric after only two or three rotations. It is possible that the presence of background shear in the experiment is

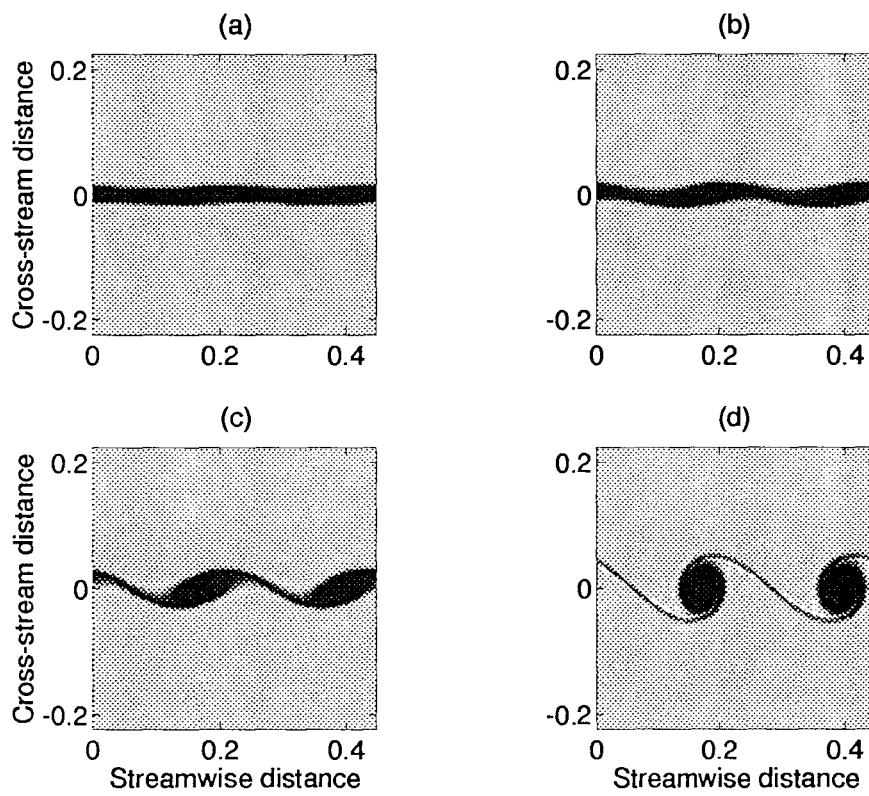


Figure 4.1: Early stages of potential vorticity evolution, simulation Ai. Figures a,b,c,d correspond to times 1.56, 2.81, 4.06 and 5.31 respectively. Two periods of the model domain are shown.

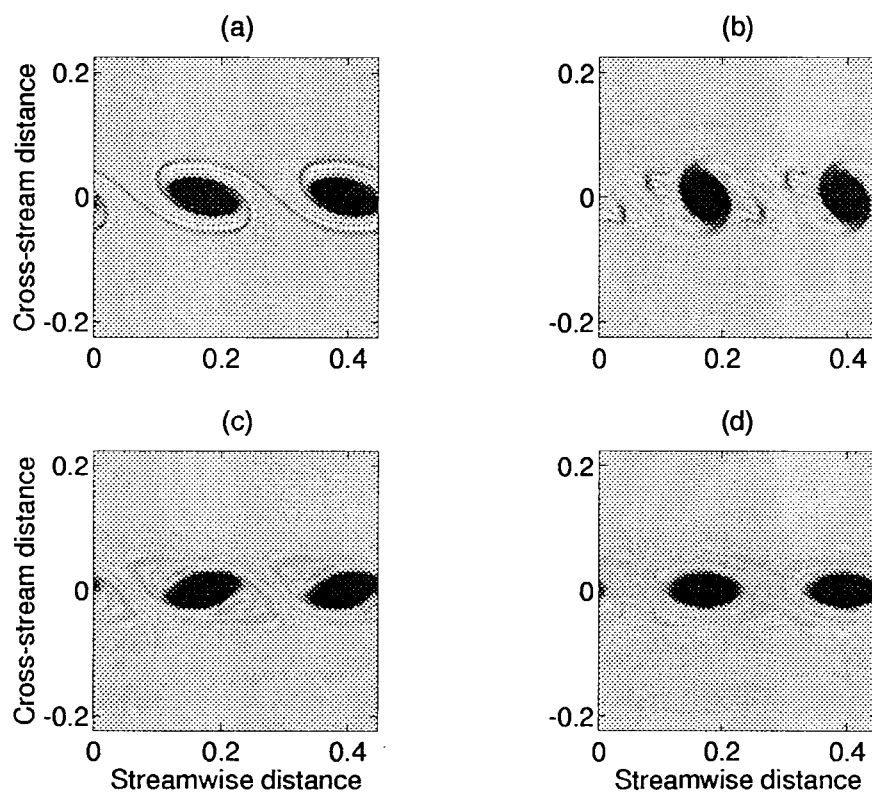


Figure 4.2: Nonlinear evolution of potential vorticity field, simulation Ai. Figures a,b,c,d correspond to times 6.56, 12.2, 17.8 and 23.4 respectively. Two periods of the model domain are shown.

responsible for this nutating behaviour, as proposed by Kida (1981). The filamentary structure appears to have been almost completely smeared out after one rotation of the vortices.

Linear gravity waves have zero potential vorticity perturbation, and so they are not observed in the potential vorticity plots shown in figures 4.1 and 4.2. However, we recall from (4.6) that, in the absence of nonlinearity, the Eulerian time derivative of the height field,  $\partial h/\partial t$ , satisfies the linear wave equation for gravity waves, i.e.

$$\left( \frac{\partial^2}{\partial t^2} + f^2 - c_0^2 \nabla^2 \right) \frac{\partial h}{\partial t} = \text{nonlinear terms.} \quad (4.31)$$

It is therefore natural to use  $\partial h/\partial t$  to investigate gravity waves radiated by the shear instability. For each of the times shown in figure 4.2, the corresponding  $\partial h/\partial t$  field is shown in figure 4.3. Only the region  $y > 0$  is shown, since all simulations are symmetric about  $y = 0$ . The entire computational domain for  $y > 0$  is shown in all plots of  $\partial h/\partial t$ . In figure 4.3, to show the entire computational domain requires that the cross-stream direction be compressed compared with the streamwise direction. As in the case of the potential vorticity field, two periods of the model domain in the streamwise direction are shown in all plots of  $\partial h/\partial t$ . The colourmap is chosen to saturate at the peak amplitudes in the wave region, even though typical values of  $\partial h/\partial t$  in the vortical region may be more than 10 times greater than those found in the wave region. No quantitative information should be inferred from the the greyscale plots of  $\partial h/\partial t$  shown in this chapter. We shall address the quantitative aspects of the gravity wave radiation when we compare the waves generated with those predicted by the Lighthill theory, and discuss the way in which the amplitude of the radiating wave fluxes depend on the Froude and Rossby numbers of the vortical flow.

In the greyscale figure 4.3, however, two features of the radiated gravity wave field are nonetheless particularly striking. Firstly, the wavelength of the gravity waves is much longer than the cross-stream scale of the vortical motions. Secondly, the radiated gravity wave field is almost independent of the streamwise coordinate  $x$ . This means that we should expect the reconstruction of the gravity wave field from the Lighthill source term to be quite good for this simulation.

Figure 4.4 shows the source function  $S(t)$  for simulation Ai, computed from (4.8). During the growth phase of the instability,  $S(t)$  remains almost zero, and only becomes significant during the subsequent rotation of the vortices in the train.

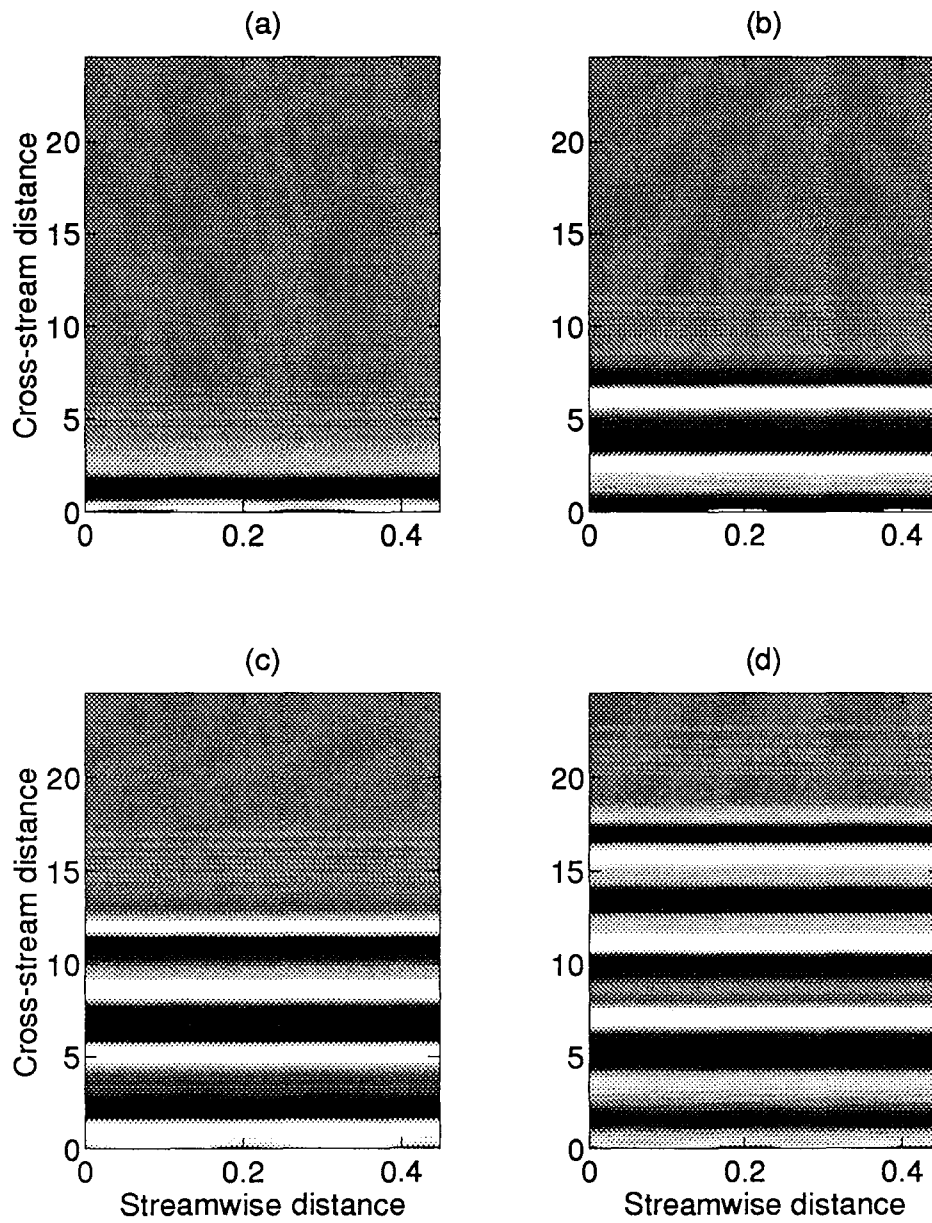


Figure 4.3: Development of gravity wave radiation, simulation Ai. Figures a,b,c,d correspond to times 6.56, 12.2, 17.8 and 23.4 respectively. Two periods of the model domain are shown.

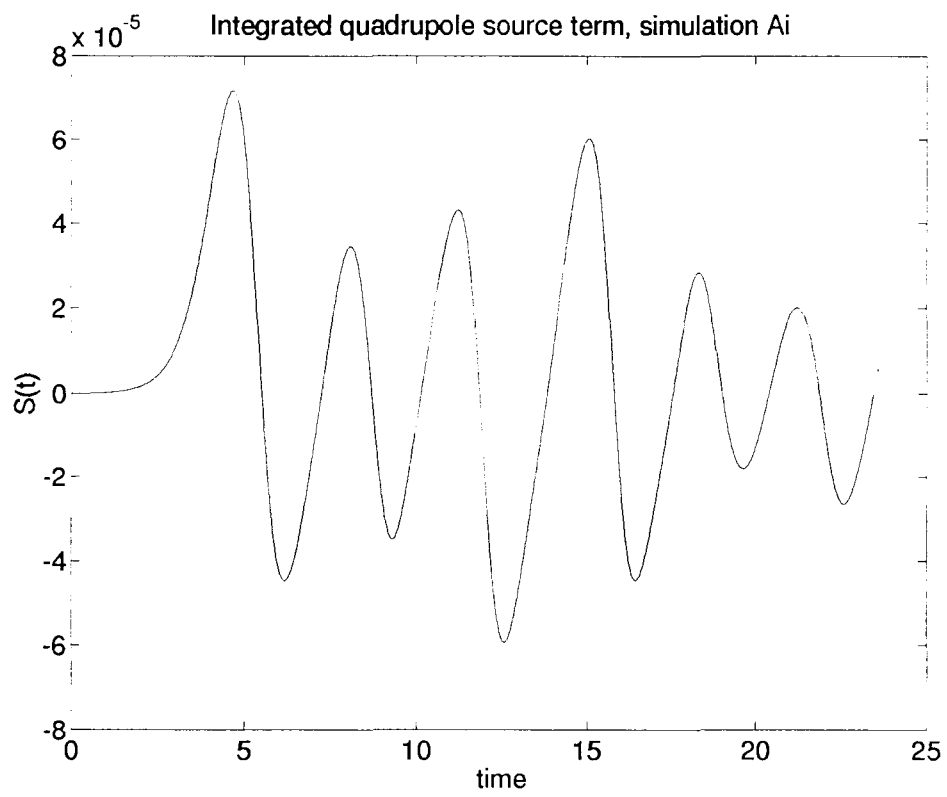


Figure 4.4: Integrated quadrupole source term,  $S(t)$ , for simulation Ai

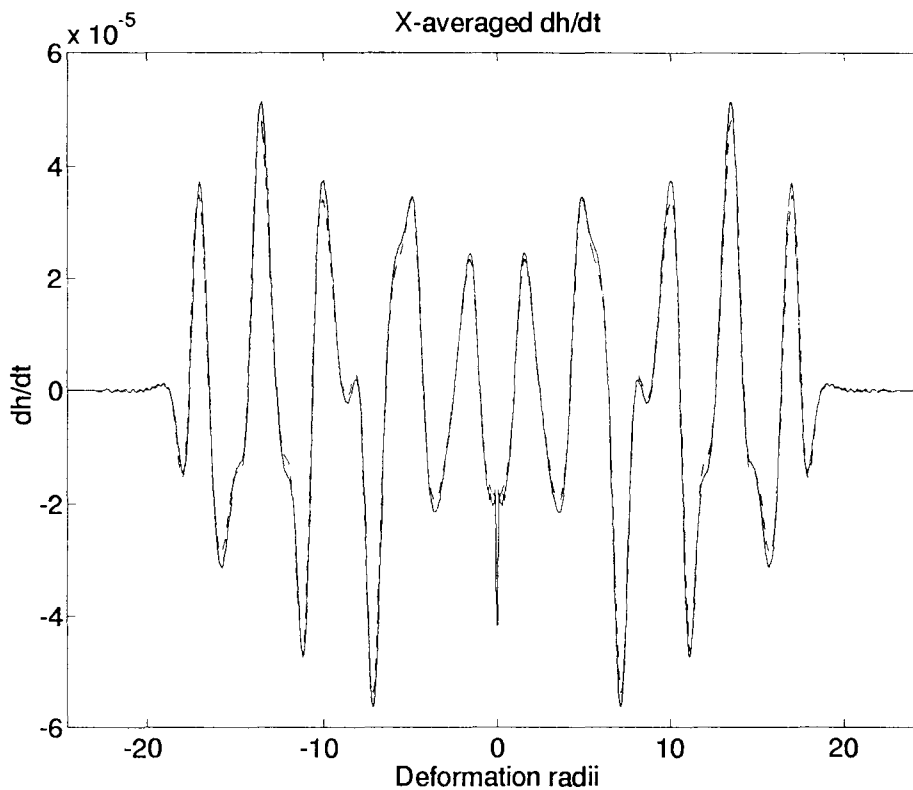


Figure 4.5: Comparison of  $x$ -averaged  $\partial h/\partial t$  field at termination of simulation Ai: solid line is from nonlinear simulation, dashed line is reconstruction from Lighthill convolution integral

In figure 4.5, the  $x$ -averaged  $\partial h/\partial t$  field is shown at the termination of simulation Ai. The solid line in figure 4.5 is the  $x$ -average of the height field obtained directly from the nonlinear simulation. The dashed line in figure 4.5 is the result of using the source term  $S(t)$ , shown in figure 4.4, in (4.7), and is therefore the wave field predicted by this modified form of the Lighthill theory, using the actual velocity and height fields from the simulation to evaluate the source term. For this simulation, the agreement between the full simulation and the Lighthill reconstruction seems very good. This is reassuring, partly because the Froude number is quite small, and the compact source approximation should be reasonably accurate for this flow; and partly because it means that the numerical model is performing sufficiently well to capture the Lighthill mechanism, and that the resolution employed is adequate to reconstruct the Lighthill source term for the convolution integral (4.7).

Figures 4.6 and 4.7 show the potential vorticity and  $\partial h/\partial t$  respectively from simulation Aii at four equally spaced time intervals during the simulation, and figures 4.8 and 4.9 show the

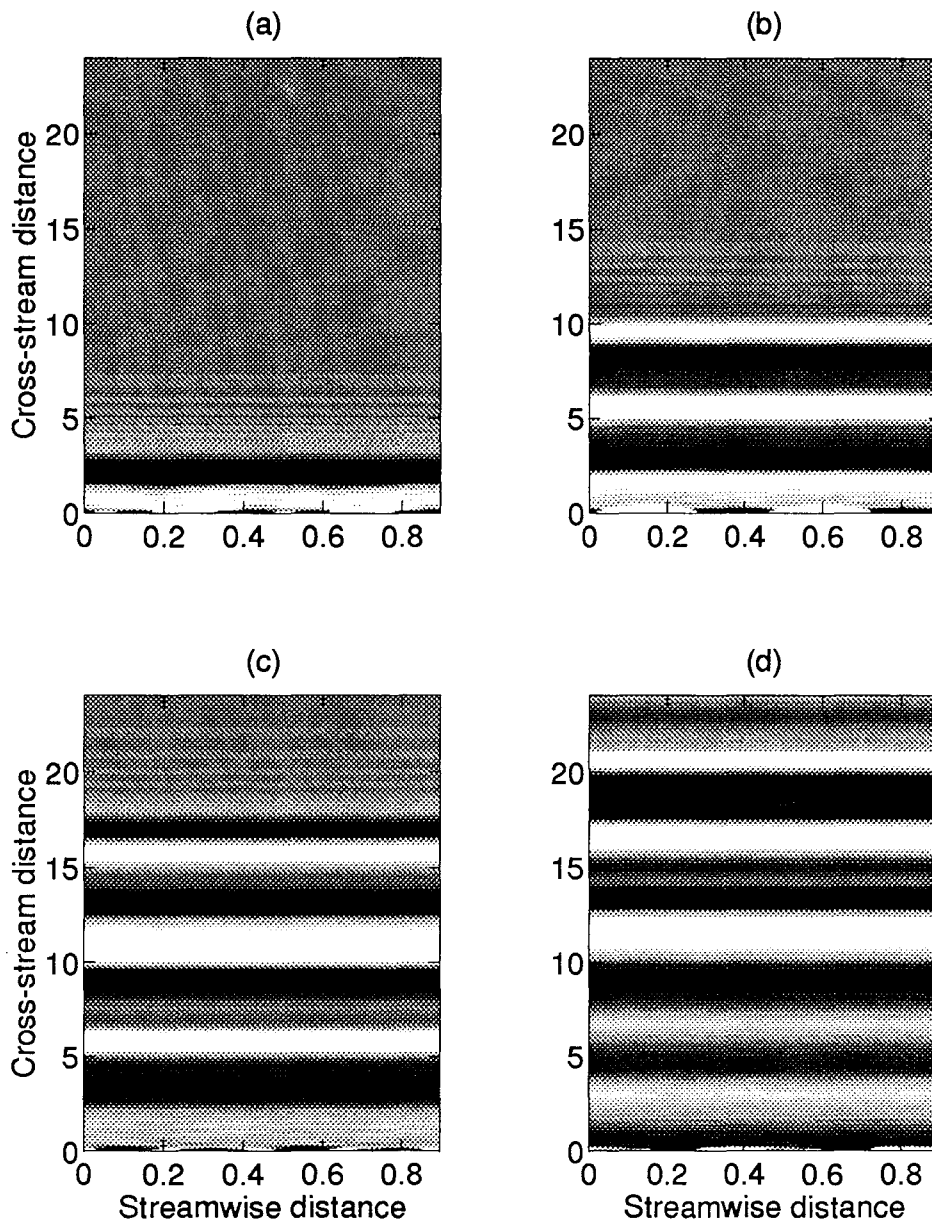


Figure 4.7: Development of gravity wave radiation, simulation Aii. Figures a,b,c,d correspond to times 6.9, 15.0, 23.1 and 31.2 respectively. Two periods of the model domain are shown.



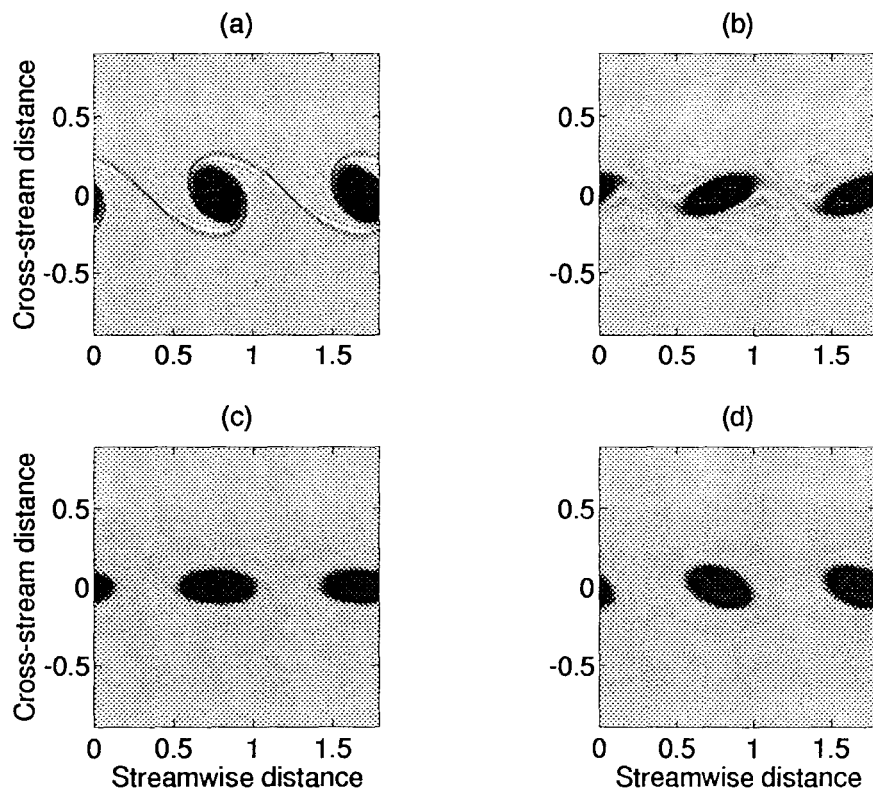


Figure 4.8: Nonlinear evolution of potential vorticity field, simulation Aiii. Figures a,b,c,d correspond to times 8.13, 26.3, 44.4 and 62.5 respectively. Two periods of the model domain are shown.

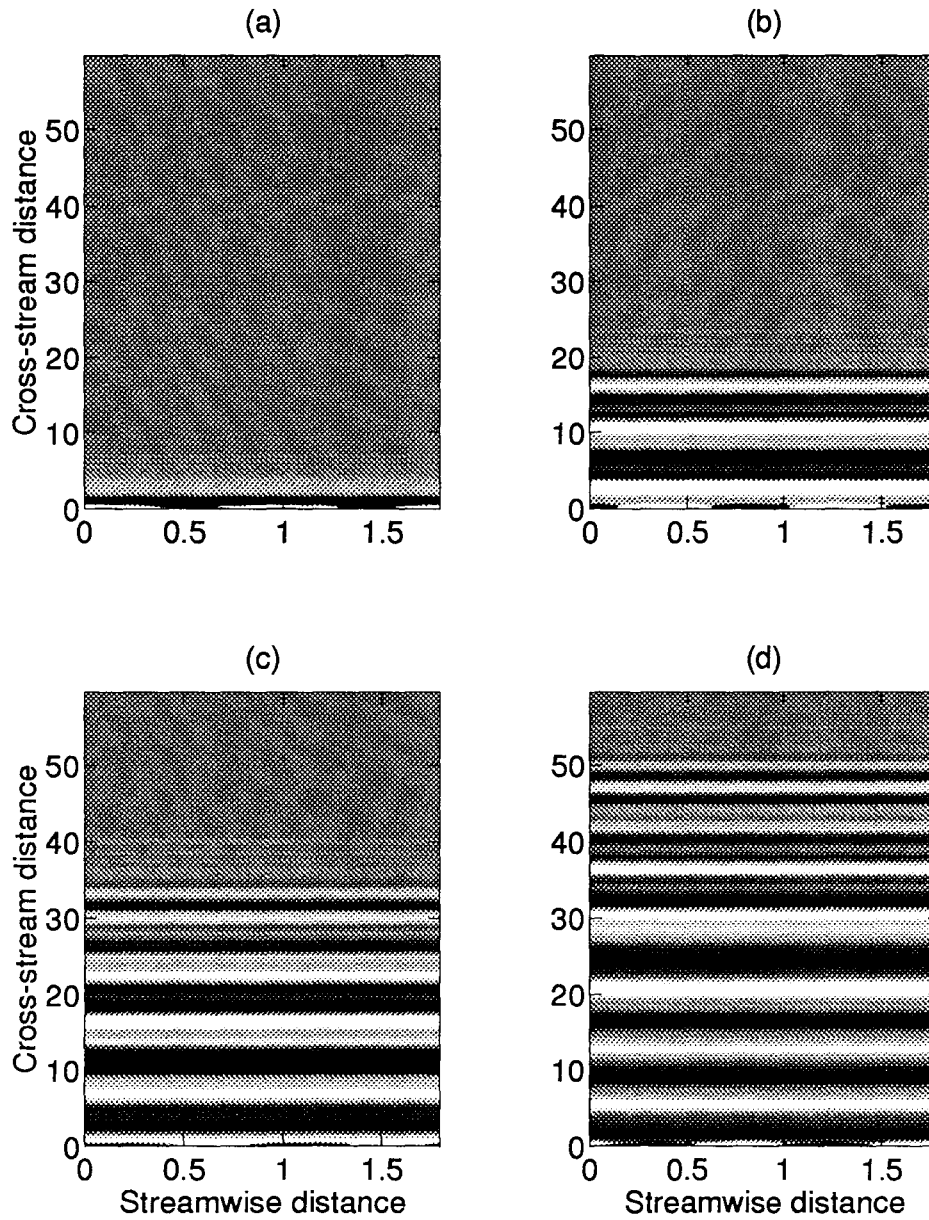


Figure 4.9: Development of gravity wave radiation, simulation Aiii. Figures a,b,c,d correspond to times 8.13, 26.3, 44.4 and 62.5 respectively. Two periods of the model domain are shown.

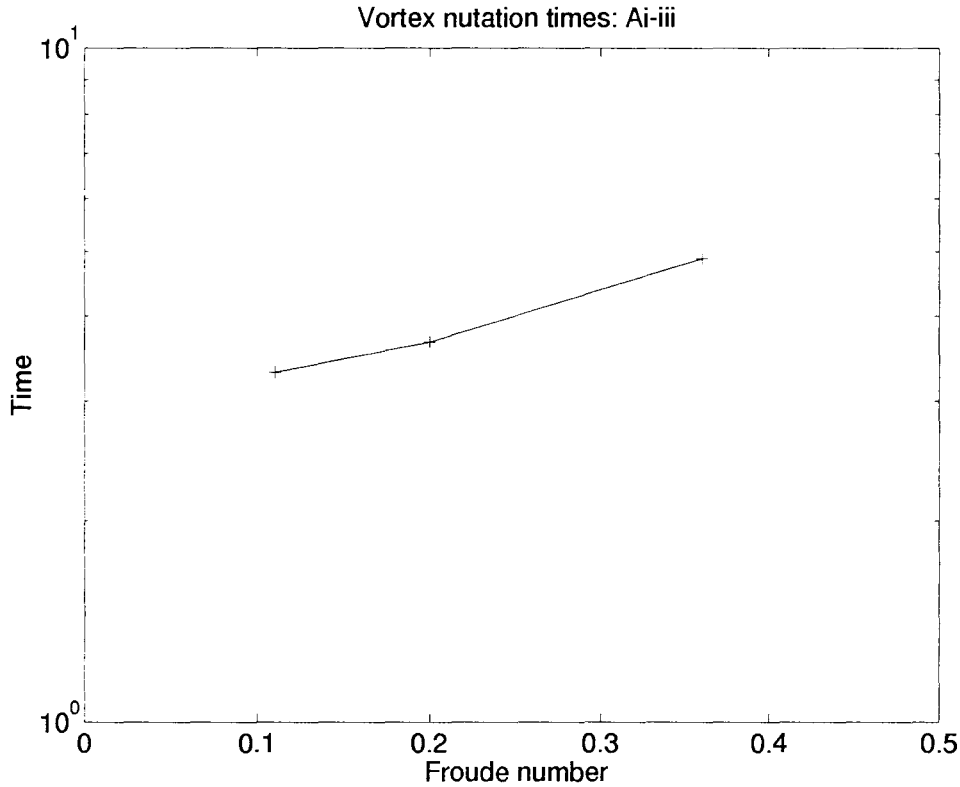


Figure 4.10: Vortex nutation times: simulations Ai-iii

same fields respectively for simulation Aiii.

On visual inspection, there appears to be little difference in the vortical aspects of the dynamics between each of the three simulations Ai-iii. In each case, the strip of high potential vorticity rolls up into a periodic train of vortices, which subsequently nutate. The only perceptible difference is in the nutation time, shown in figure 4.10, which increases from 3.44 inertial periods (simulation Ai) to 4.88 inertial periods (simulation Aiii). The vortex nutation times are a significant feature of the flow, in that they are a broad measure of the degree of unsteadiness of the vortical flow compared with the unit inertial period.

Considering now the gravity wave aspects of the flows Aii and Aiii, we see from figures (4.7) and (4.9) that the form of the radiated gravity waves remains similar in these two cases to those observed in simulation Ai. In figure 4.11, the  $x$ -averaged  $\partial h/\partial t$  field at the end point of each of the numerical simulation is represented by the solid lines, and its reconstruction using the compact source approximations is shown by the dotted lines. The agreement seems to be

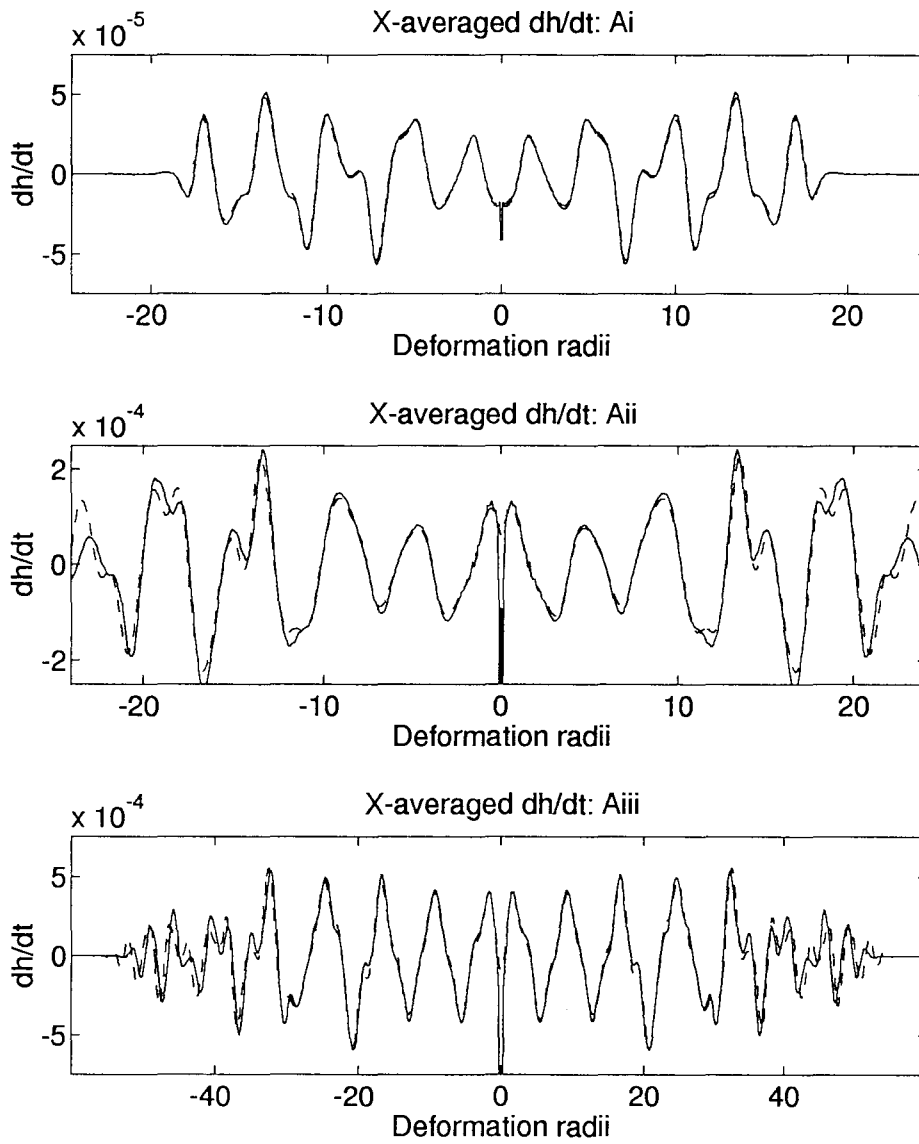


Figure 4.11: The  $x$ -averaged  $\partial h/\partial t$  field at the termination of simulations Ai-iii. Solid lines are from the nonlinear simulation, and dashed lines are from the Lighthill convolution integral

quite good in each case.

From figure 4.11, we can also see that the amplitude of the radiated gravity waves increases by a factor of about 12 between **Ai** and **Aiii**. The maximum Froude number found in the evolution increases from 0.11 (**Ai**) to 0.36 (**Aiii**) (see table 4.1c). However, we should recall from (4.10) that, as the Froude number is increased, we expect the amplitude of the radiated gravity waves to increase as the third power of the Froude number. Thus, on the basis of the low Froude number asymptotic analysis, we should expect the gravity wave amplitude to change by a factor of 35. Evidently, the increase in gravity wave amplitude as a function of Froude number over this range is not as large as one might expect on the basis of the Lighthill theory. Two assumptions were made to predict that the amplitude of the radiated waves would scale with the third power of the Froude number – the point source assumption, and the scaling assumption  $u \sim \omega l$ . The fact that the wave amplitudes do not increase as rapidly as the theory predicts is thus not necessarily an indication that the point source approximation will fail for these simulations.

Three further simulations (**Aiv** – **Avi**) were then performed, with strip widths of 0.14, 0.21, and 0.28. The vortical aspects of the flow remained qualitatively unchanged as the width of the strip, and hence the Froude number, was increased. In each case, the strip initially rolled up into a periodic train of vortices, which were allowed to rotate several times before the simulation was terminated. The most significant quantitative difference in the vortical aspects of the flow between these three cases is in the nutation rate of the vortices in the train, shown in figure 4.12, which increase super-exponentially with increasing Froude number.

Figure 4.13 shows the  $\partial h/\partial t$  field at the termination of the simulations **Aiii**–**Avi**. The main point is that, as the Froude number is increased, the radiated gravity waves develop more  $x$ -dependent structure. The gravity wave field is expected to be  $x$ -independent at low Froude numbers, and it is reasonable to expect more  $x$ -dependence in the field as the Froude number is increased, as the lengthscale separation between the vortices and the gravity waves diminishes.

Figure 4.14 shows the  $x$ -averaged  $\partial h/\partial t$  field at the termination of simulations **Aiii**–**vi**, and its reconstruction from the Lighthill source term. The most striking feature of the sequence of figures is that, in contrast to the rapid increase in wave amplitude with Froude number predicted by Lighthill's scaling argument, the radiated wave amplitudes actually decrease. This clearly differs from the scaling arguments presented by numerous authors on aeroacoustics, which were

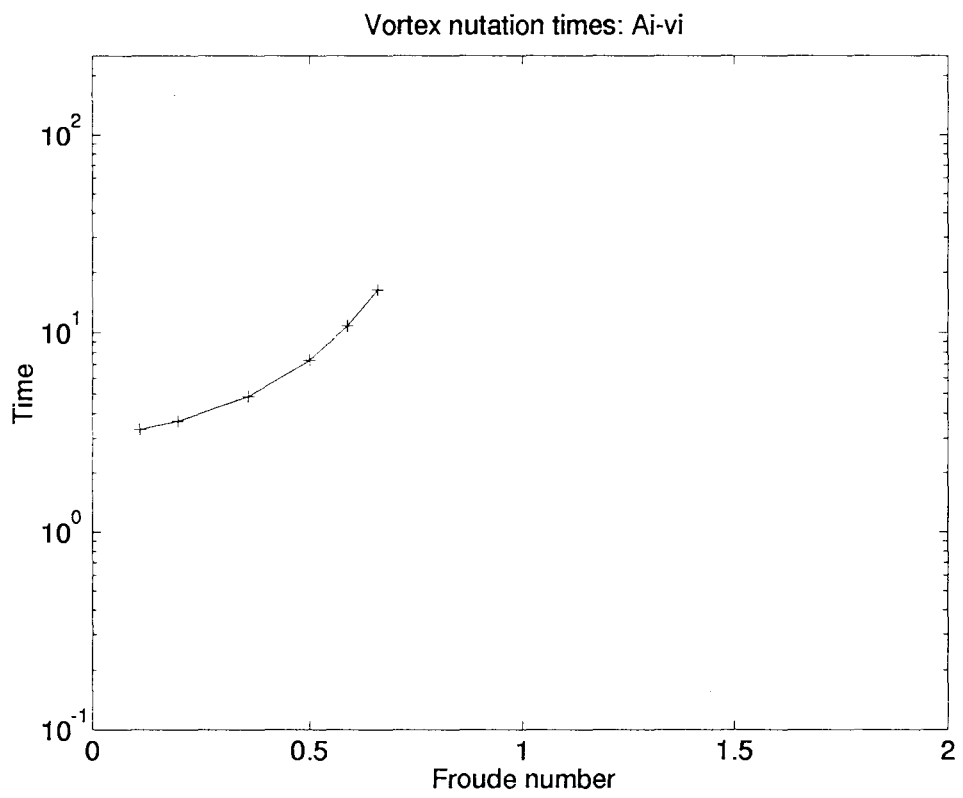


Figure 4.12: Vortex nutation times: simulations Ai-vi

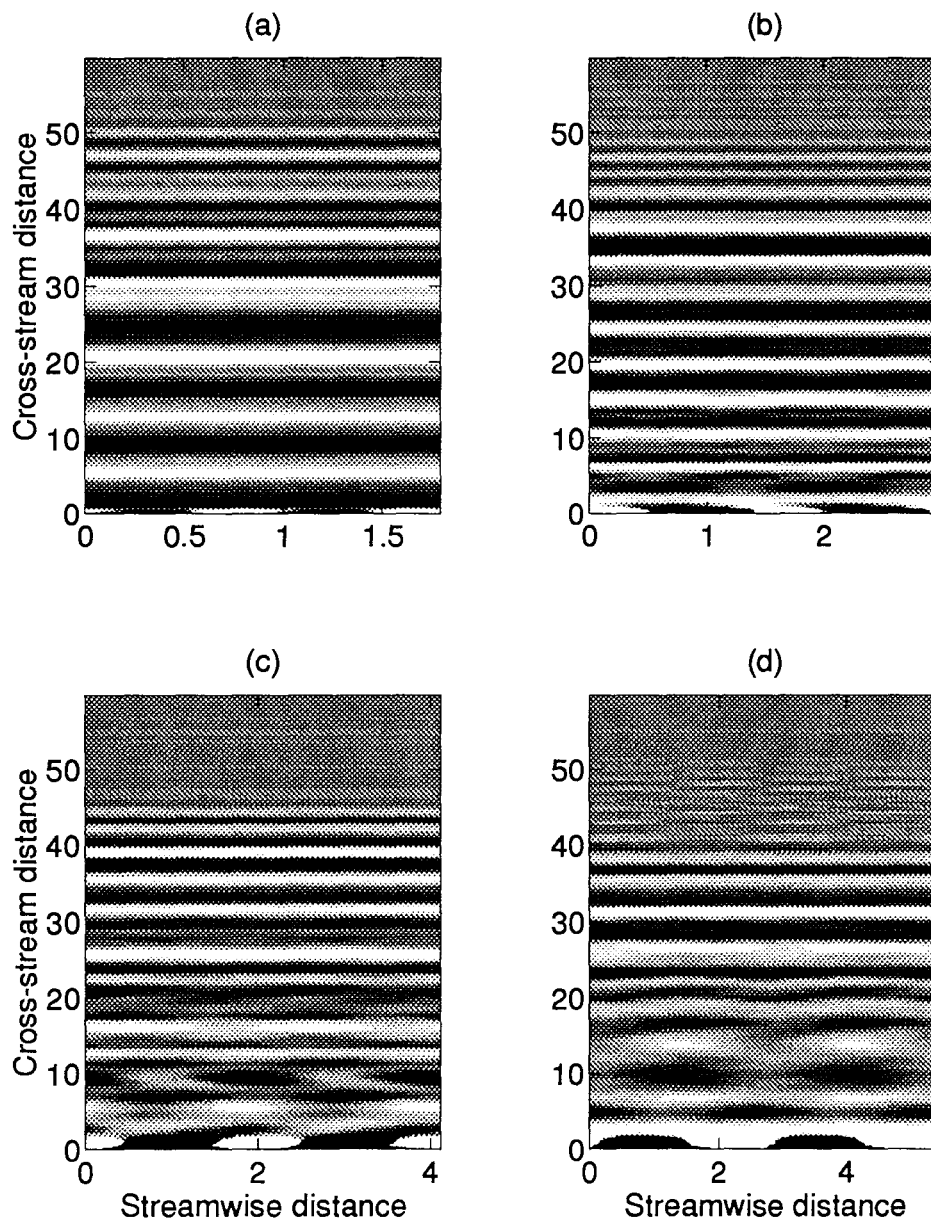


Figure 4.13: The  $\partial h/\partial t$  field at the termination of simulations Aiii-vi (time 62.5). Two periods of the model domain are shown.

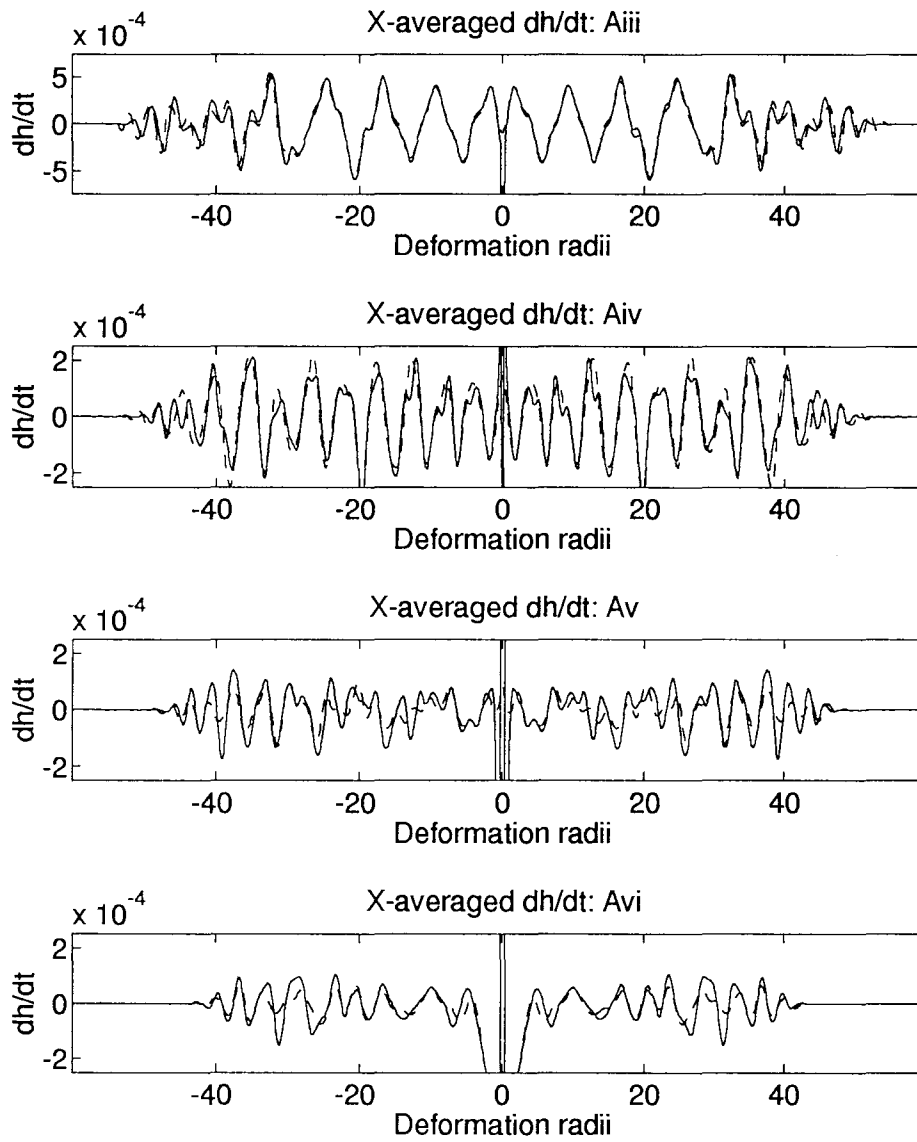


Figure 4.14: The  $x$ -averaged  $\partial h / \partial t$  field at the end of simulations Aiii-vi

discussed at the beginning of this section, and from the mass of experimental data that confirm the Lighthill scaling in practice.

Since the only new effect in the present study is the inclusion of background rotation, it follows that background rotation must be responsible for decreasing the wave amplitude as the Froude number is increased. Moreover, since the reconstruction of the wave field from the Lighthill source term effectively captures the decrease in wave amplitude, it must be explicable within the framework of the Lighthill theory.

There are two possibilities. One is that the quadrupole source strength decreases, rather than increases, as the Froude number is increased. However, we should bear in mind that in order for the quadrupole source to excite propagating waves, it must have a significant component of its frequency above the inertial frequency. Therefore, it is possible that, although the magnitude of the source terms might actually increase as the Froude number is increased, their frequency component above the inertial frequency might decrease.

Figure 4.15 shows the integrated source term for each of the simulations Ai–vi. In general, the amplitude of the source term increases with increasing Froude number, but with frequency decreasing very rapidly with increasing Froude number. It seems, therefore, that the effect of the inertial cut-off, inhibiting gravity wave radiation at frequencies below the inertial frequency, is now dominant over the increased magnitude of the source term, leading to reduced wave amplitudes as the Froude number is further increased.

We may conclude that, although the potential vorticity in the strip was chosen to be six times the background value, both the vortical flow and the wave generation process are significantly affected by the presence of background rotation. For very small Froude numbers (between 0.11 and 0.35), the amplitude of the radiated gravity waves increases with Froude number, although not quite as rapidly as  $F^3$ , as found in the asymptotic limit  $F \ll 1$ . When the Froude number exceeds 0.35, however, the radiated gravity wave amplitudes are found to decrease with increasing Froude number, even though the typical amplitudes of  $S(t)$  are generally increasing. This behaviour has never been found in numerical or laboratory experiments in a non-rotating frame. The presence of background rotation thus severely inhibits gravity wave radiation at moderate Rossby numbers, and there seems little doubt that the present study has investigated a case in which the effect of background rotation is quite strong, despite a notional Rossby number of 5. Therefore, in the next section, we investigate the effect of increasing the potential

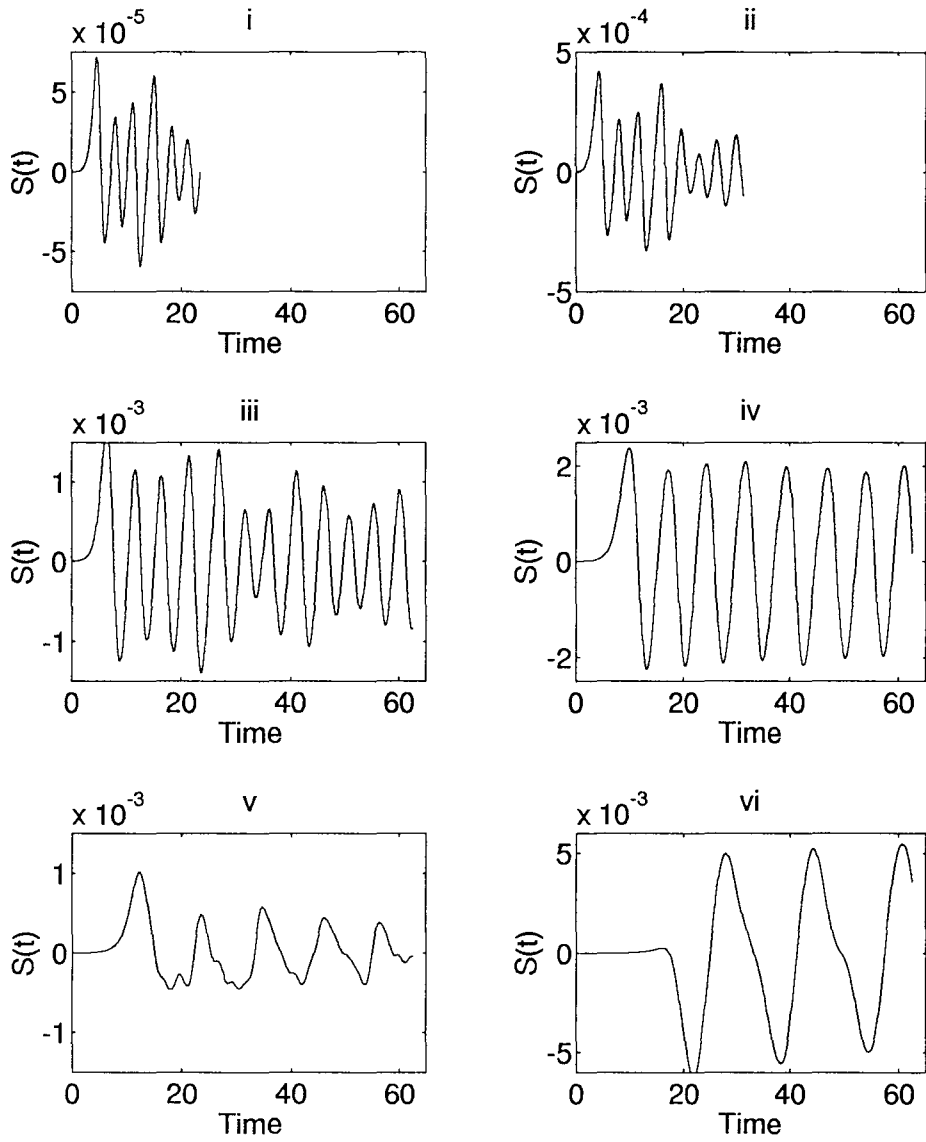


Figure 4.15: The source term  $S(t)$  for simulation Ai-vi. Note the differing scales on the  $S(t)$  axes.

vorticity in the strip. The strip remains cyclonic, but the effect of background rotation should decrease as the potential vorticity in the strip increases.

## 4.7 Cyclonic strips at large Rossby number

In this section the results of simulations with strip potential vorticities of 9 and 21 are presented. There are four simulations with strip potential vorticity of 9, and four with strip potential vorticity of 21. The simulations with strip potential vorticity of 9 are labelled **Bi-iv**, and those with strip potential vorticity of 21 are labelled **Ci-iv**. In neither set of simulations should we expect to observe any qualitative difference from the simulations with potential vorticity of 6 in the strip. Quantitatively, we should expect to see more rapid vortical motions, and consequently a larger pseudoenergy flux in the radiated wave field.

In simulations **Bi-iv**, the initial strip widths are 0.018, 0.035, 0.07 and 0.21, resulting in Froude numbers of 0.17, 0.32, 0.53 and 0.84 respectively. In each case, the strip rolled up into a periodic train of vortices, which then nutated, radiating gravity waves. The vortical flow appeared very similar to that observed in experiments **Ai-vi**, and potential vorticity plots are not shown here. The nutation periods for these vortices are shorter than for the corresponding simulations in sequence **A**, but still appear to increase super-exponentially with Froude number (figure 4.16), in common with sequence **A**.

In figure 4.17, the  $\partial h/\partial t$  field is shown for the end of each simulation **Bi-iv**. The wave field follows broadly the same pattern as in the lower Rossby number simulations **Ai-vi**. At small Froude numbers, the wave field is almost independent of  $x$ , and as the Froude number is increased, amplitudes of the  $x$ -dependent modes increase.

In figure 4.18, the  $x$ -independent wave field is shown at the end of each simulation (solid line), and compared with its reconstruction from the Lighthill theory (dashed line). Overall, there is good agreement between the Lighthill theory and the numerical simulations, as there was in the lower Rossby number simulations **Ai-vi**. As before, the agreement is best when the Froude numbers are lowest. The radiated wave amplitudes are seen to increase with increasing Froude number for simulations **Bi-iii**, but then decrease between **Biii** and **Biv**. The corresponding pseudoenergy fluxes are shown in figure 4.19, and the maximum pseudoenergy flux in the radiated wave field for simulations **A** and **B** is shown in figure 4.20. Notice in figure 4.19 that

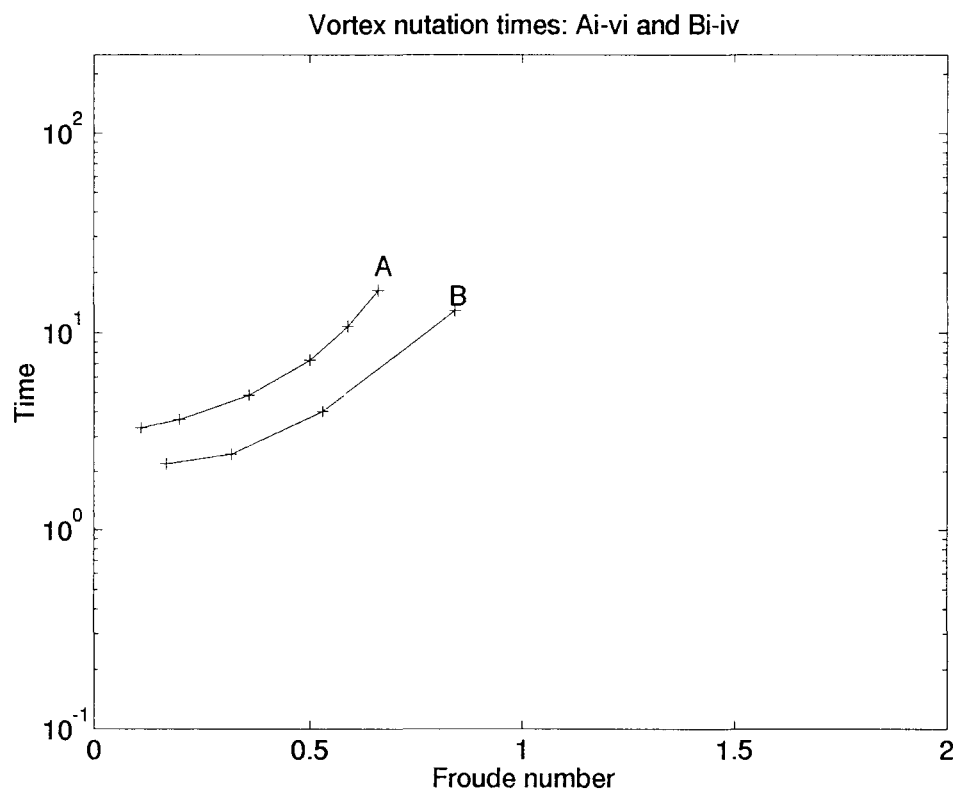


Figure 4.16: Vortex nutation times: simulations Bi-iv

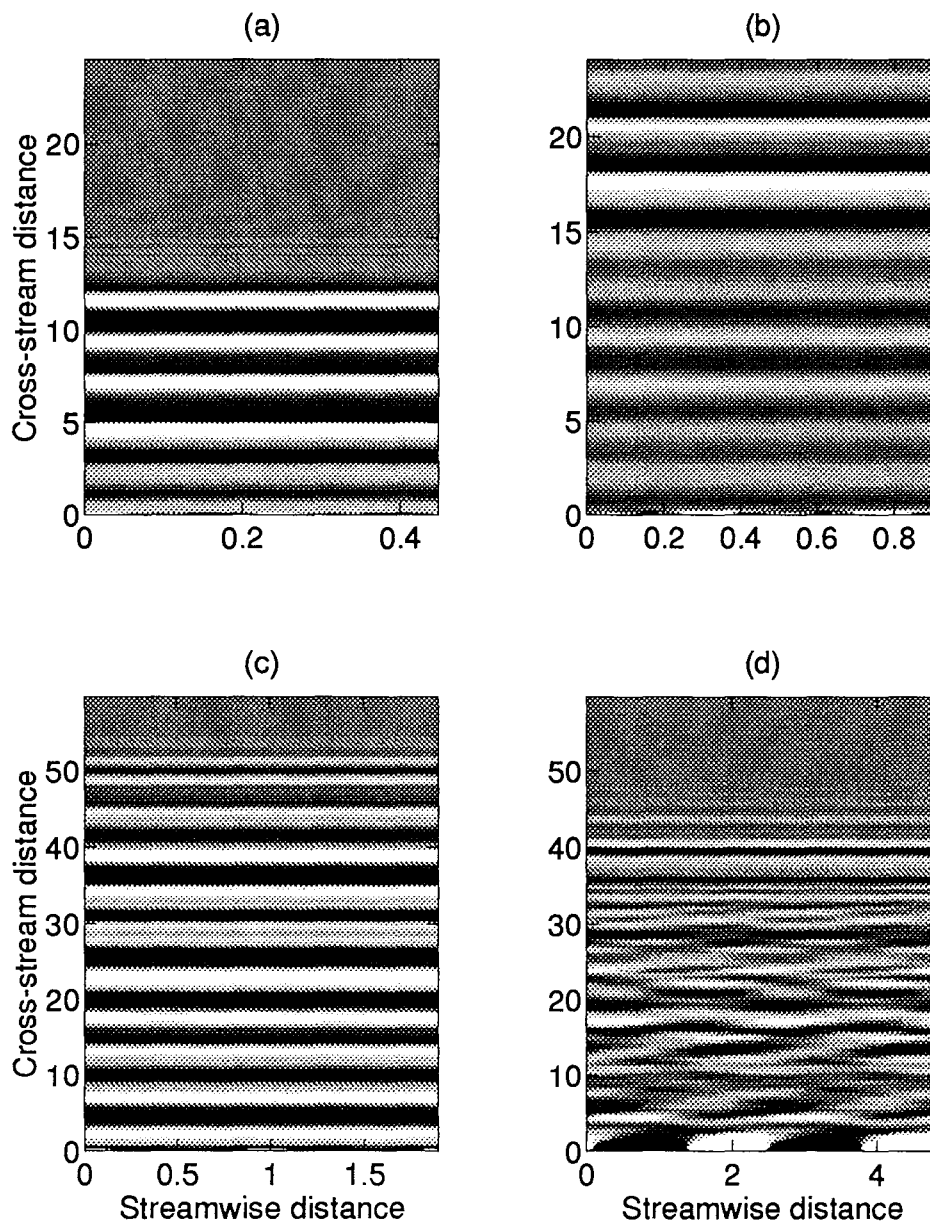


Figure 4.17: The field  $\partial h/\partial t$  at the termination of simulations Gi-iv. Two periods of the model domain are shown.

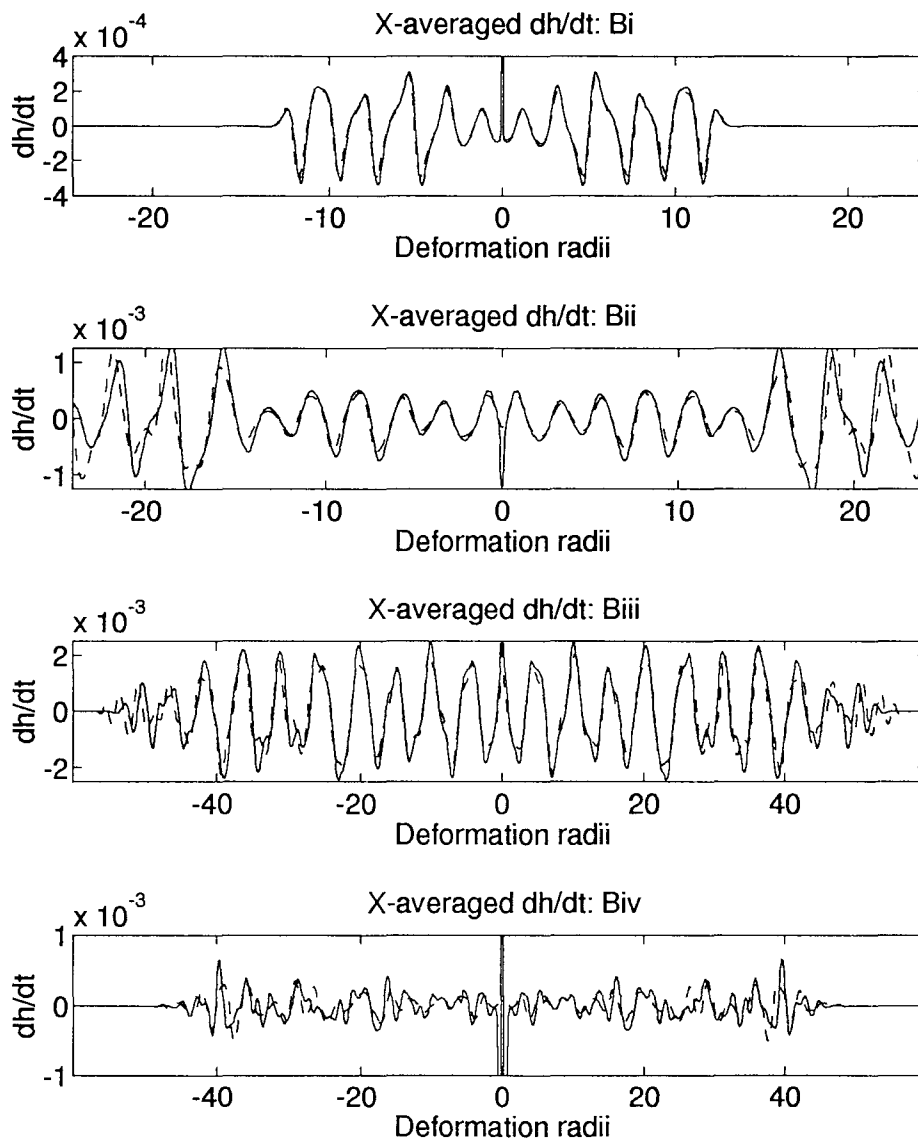


Figure 4.18: The  $x$ -averaged  $\partial h/\partial t$  field at the termination of simulations **Bi-iv**. Solid lines are from the nonlinear simulation, and dashed lines are from the Lighthill convolution integral

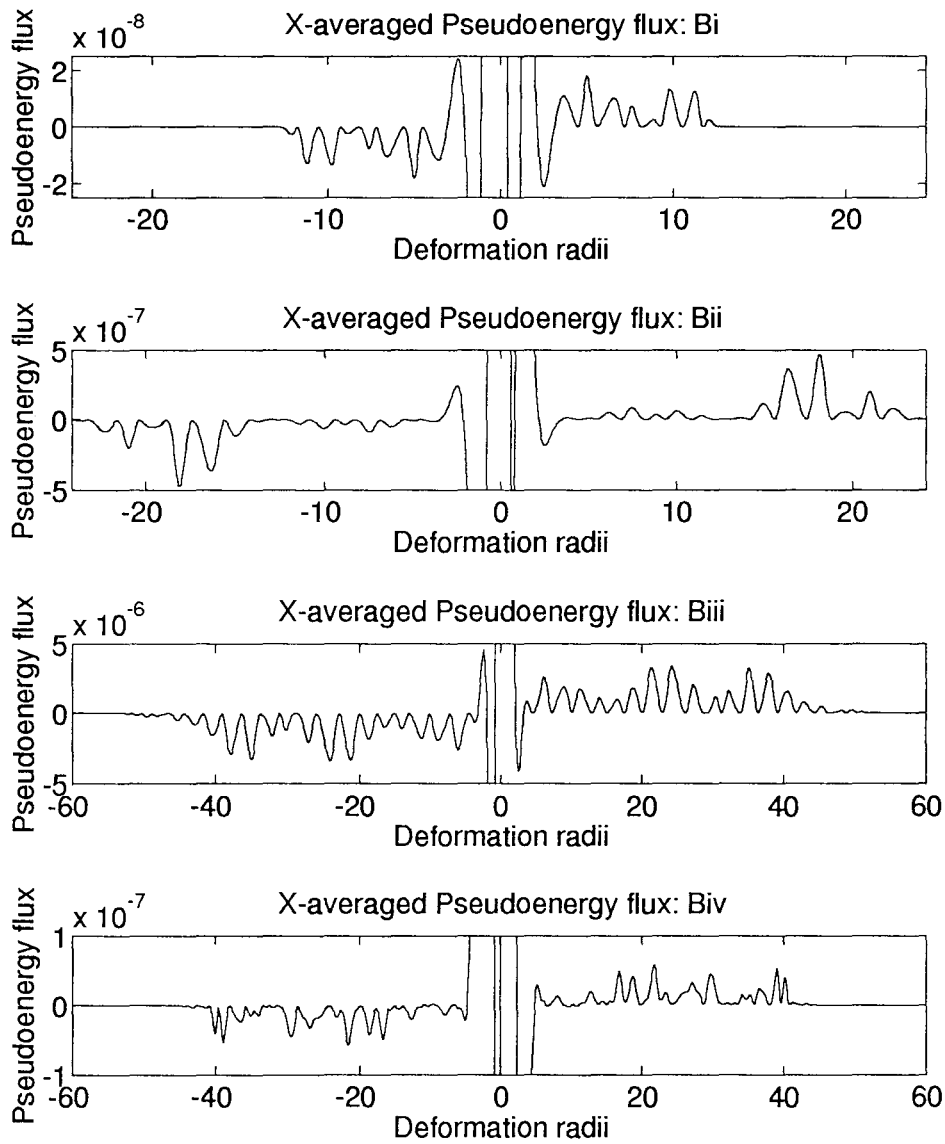


Figure 4.19: The  $x$ -averaged pseudoenergy flux at termination of simulations Bi-iv

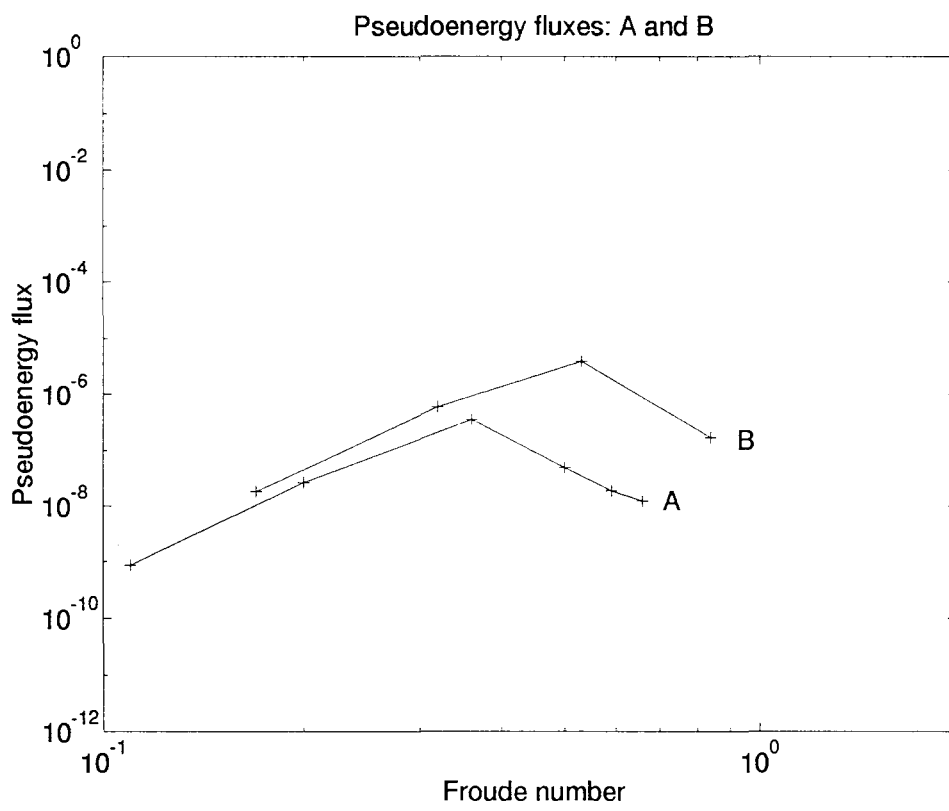


Figure 4.20: The peak pseudoenergy flux due to gravity wave radiation throughout simulations A and B

the pseudoenergy fluxes are negative for  $y < 0$ , and positive for  $y > 0$ , confirming that the flux of pseudoenergy away from the vortical flow at  $y = 0$  is single-signed, as demonstrated by the analysis of §4.3.

The Froude number at which the maximum pseudoenergy flux occurs is greater in case **B** than in case **A**, but the strip width at which the transition from increasing to decreasing pseudoenergy fluxes appears to be about the same, at around 0.1.

Overall, increasing the potential vorticity in the strip from 6 to 9 has the effect of increasing the amplitude of radiated gravity waves. However, in both cases, there exists a Froude number (or equivalently a strip width) which is in some sense optimal for gravity wave radiation. The amplitude of the  $x$ -averaged flux of radiated gravity waves increases with increasing Froude number up to this critical Froude number, but then decreases as the Froude number is increased further. This property appears to be specific to flows in a rotating frame, and is due to the reduced unsteadiness of the vortical flow at larger Froude numbers, manifested in the rapidly increasing nutation times at larger Froude numbers, combined with the inhibiting effect of the inertial cut-off frequency on gravity wave radiation. It has not been observed in non-rotating aeroacoustic experiments or simulations.

Four further experiments were then performed with a strip potential vorticity of 21. The experiments are labelled **Ci**–**iv**. These correspond to initial strip widths of 0.011, 0.021, 0.041 and 0.081 respectively. Once again, in each case the strip rolls up into a periodic train of vortices, which then nutate several times before the simulation is terminated. The dependence of the nutation time upon the Froude number is shown in figure 4.21, and is consistent with the behaviour found in experiments **A** and **B** – i.e., it appears to be increasing super-exponentially with Froude number.

The  $\partial h/\partial t$  field at the end of each simulation is shown in figure 4.22, and again has similar properties to those for simulations **A** and **B**, although at the largest Froude number simulated smaller scale features seem to appear in the  $\partial h/\partial t$  field. The comparison of the  $x$ -averaged  $\partial h/\partial t$  field with its reconstruction by the Lighthill theory is shown in figure 4.23, and again good agreement is generally obtained. Indeed, it seems that the agreement improves as the Rossby number is increased, when compared with simulations **Ai**–**vi** and **Bi**–**iv**. Even in simulation **Civ**, in which the Froude number exceeds unity in the vortical region, the general form of the radiated wave field is captured by the Lighthill theory, although the fine details are not captured

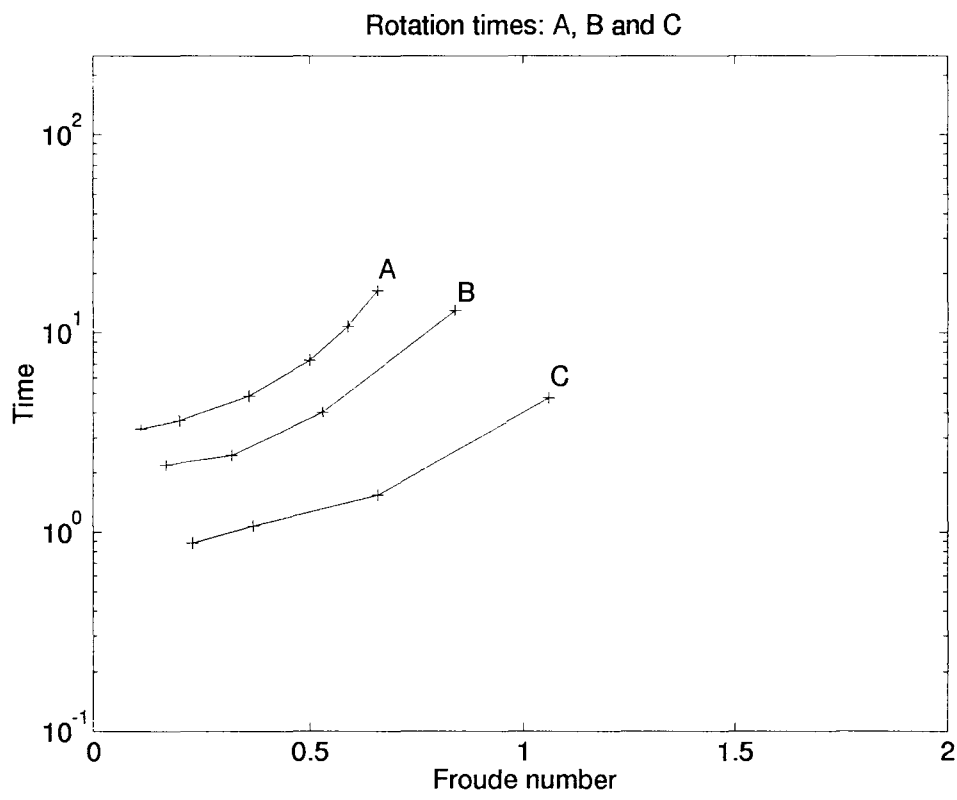


Figure 4.21: Vortex nutation times for simulations Ci-iv

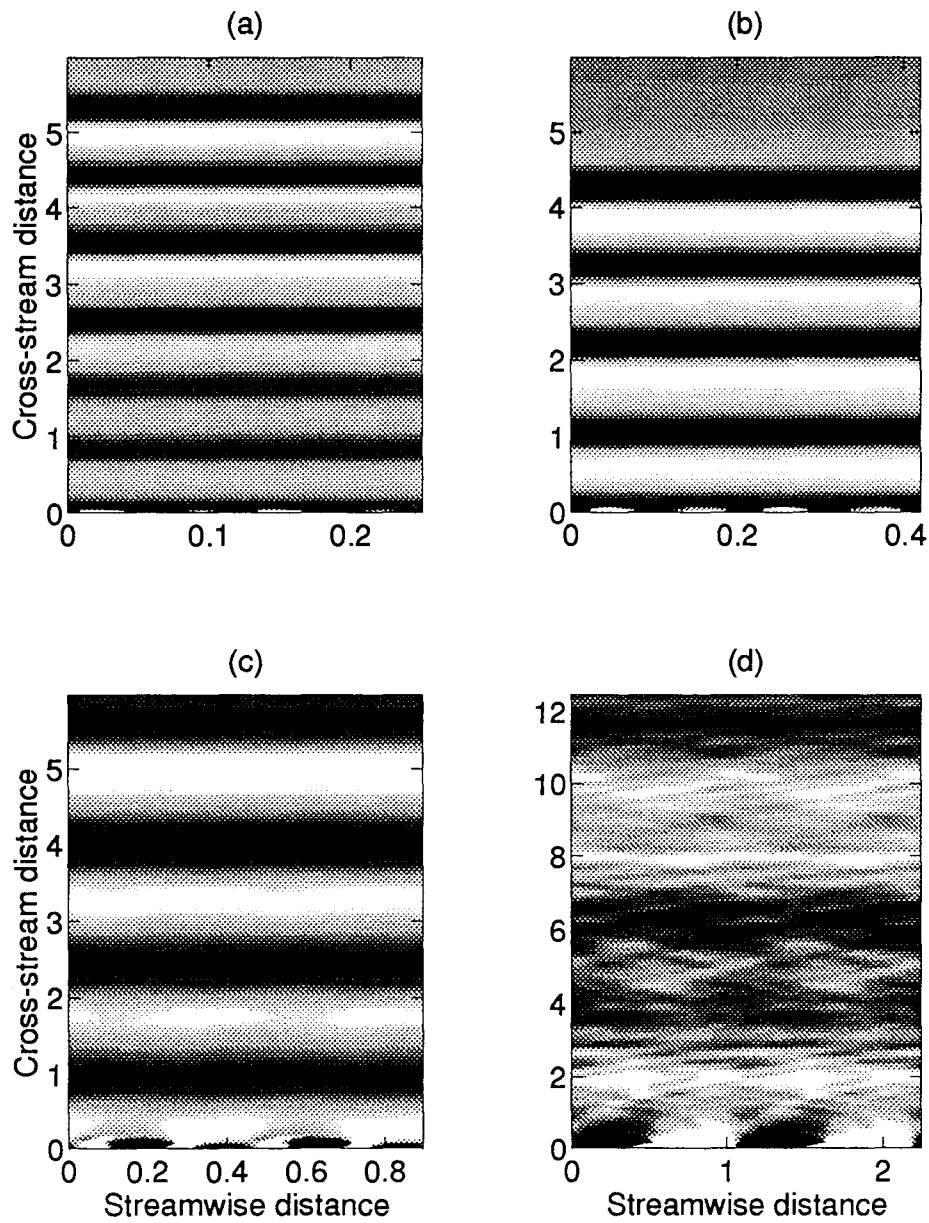


Figure 4.22: The field  $\partial h/\partial t$  at the termination of the simulations Ci-iv. Two periods of the model domain are shown.

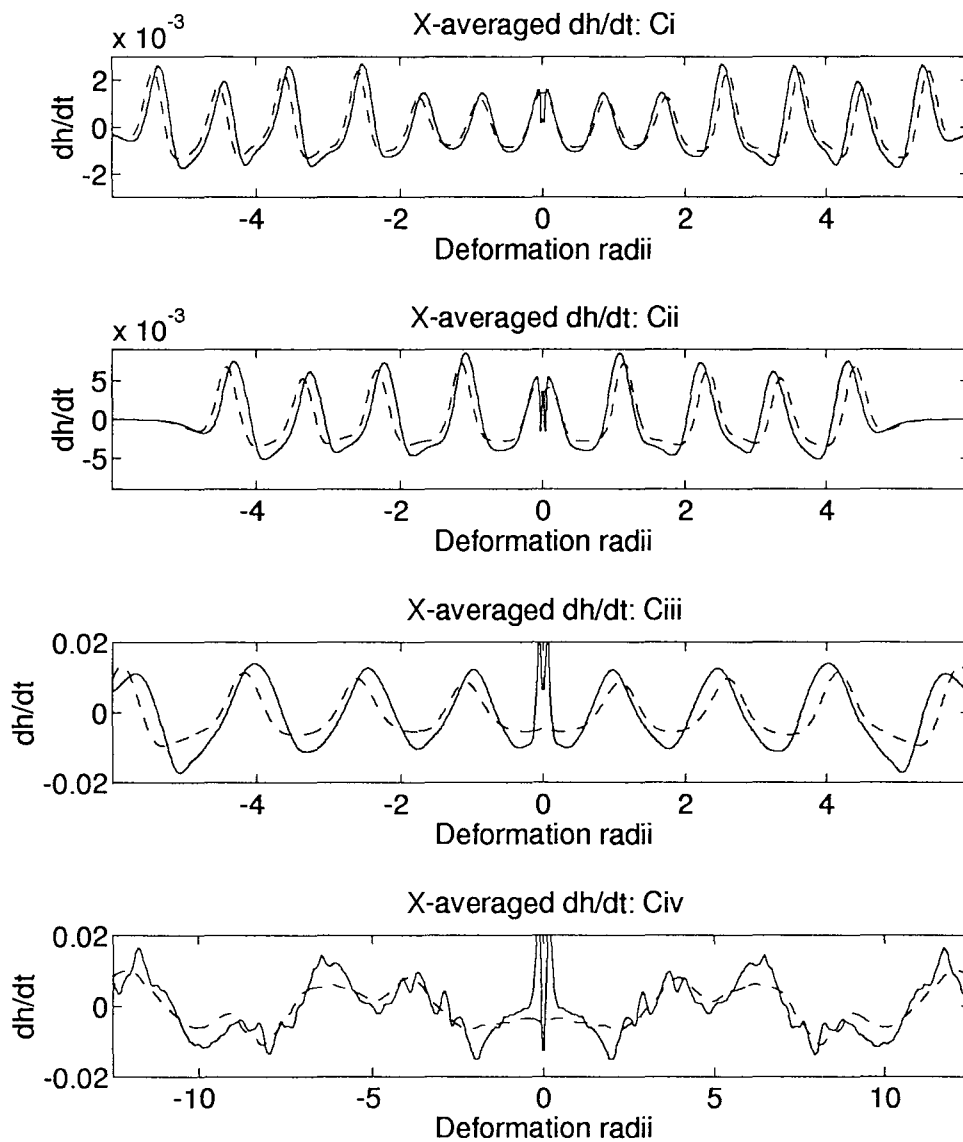


Figure 4.23: The  $x$ -averaged  $\partial h / \partial t$  field at the termination of simulations Ci-iv (solid lines), and its reconstruction from the Lighthill convolution integral (dashed lines)

by the Lighthill theory.

The pseudoenergy flux at the end of each simulation is shown in figure 4.24. In this case, the pseudoenergy flux appears to be increasing as the Froude number is increased, unlike simulations **A** and **B**, where it decreased as the Froude number was increased beyond a certain critical value. It is interesting to note that in simulation **C**iv the  $x$ -averaged pseudoenergy flux appears to be a smoother measure of wave radiation than the  $x$ -averaged  $\partial h/\partial t$  field, shown in figure 4.23.

In figure 4.25 the maximum  $x$ -average pseudoenergy flux over all time in the wave region for each simulation is plotted against Froude number, for the sequences of simulations **A**i–vi, **B**i–iv and **C**i–iv. The dashed line is a line of gradient 6 on the log-log scale, which would be predicted by the compact source asymptotics (equation 4.28). In all cases the pseudoenergy flux increases as the sixth power of the Froude number at small Froude number but, as the Froude number is increased, the pseudoenergy flux increases less rapidly with increasing Froude number. It seems plausible from figure 4.25 that the very large Rossby number simulations **C** will exhibit an optimal Froude number for gravity wave radiation, in the same manner as simulations **A** and **B**, but that it exceeds the values of Froude number investigated by the nonlinear simulations.

From this section, we may conclude that several of the features exhibited by the strips with a potential vorticity of 6 are robust features of cyclonic strip roll-up, subsequent nutation and gravity wave radiation. In particular, the nutation time increases super-exponentially with increasing Froude number. In general the pseudoenergy flux associated with the radiating gravity waves increases with the sixth power of the Froude number at small Froude number, but ultimately decreases as the Froude number is made very large, due to the increased nutation times, and consequently reduced fraction of the effective gravity wave source spectrum lying above the inertial frequency.

It is important to realize at this point that thus far only cyclonic strips have been investigated in this study. All cyclonic strips appear to exhibit similar behaviour, in respect of their vortex nutation times and pseudoenergy flux dependences upon the Froude number. In the remainder of this chapter, we shall investigate gravity wave generation by anticyclonic vortex trains, and compare it with that found for the cyclonic cases. The anticyclonic parameter space is divided into three parts: strips with positive potential vorticity, strips with negative potential vorticity, and the single case of a strip with a potential vorticity of zero. In the next section, §4.8, we

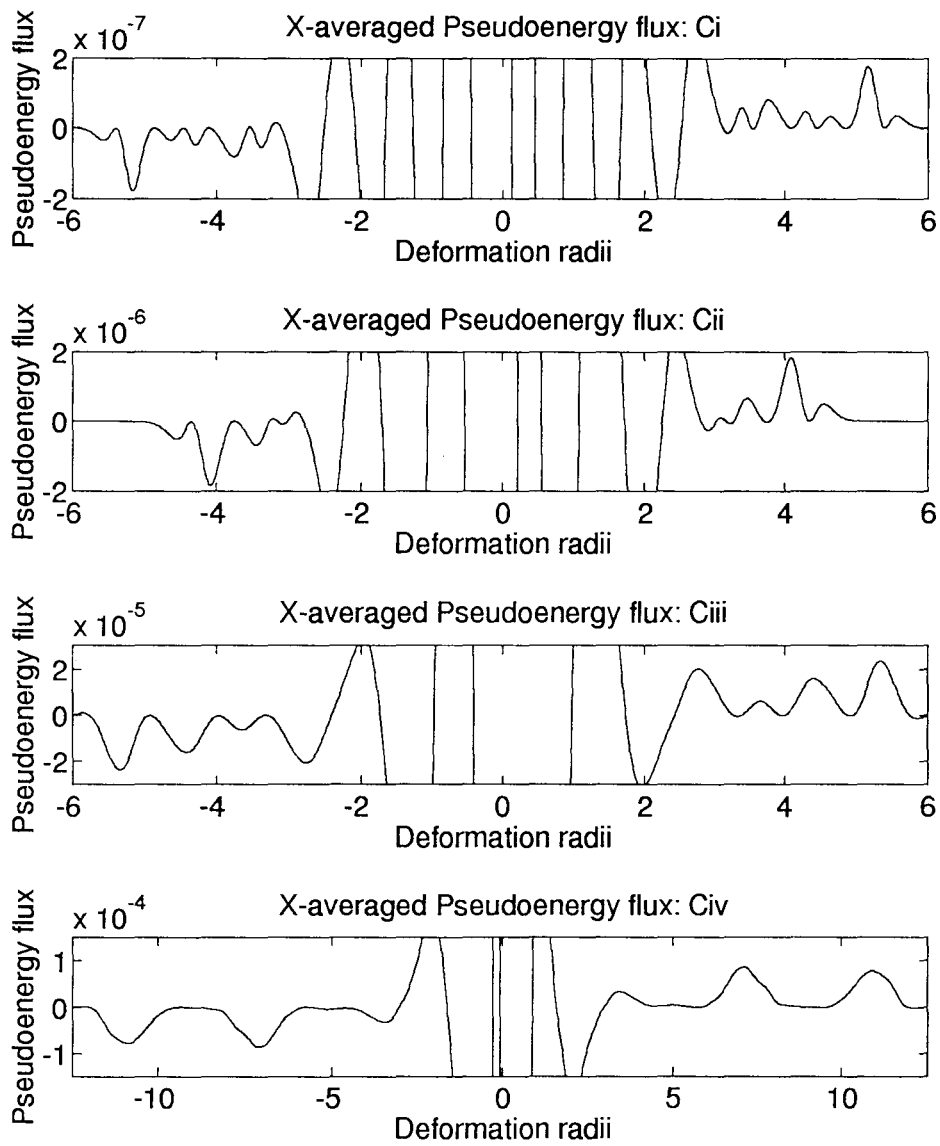


Figure 4.24: The pseudoenergy flux at the termination of simulations Ci-iv

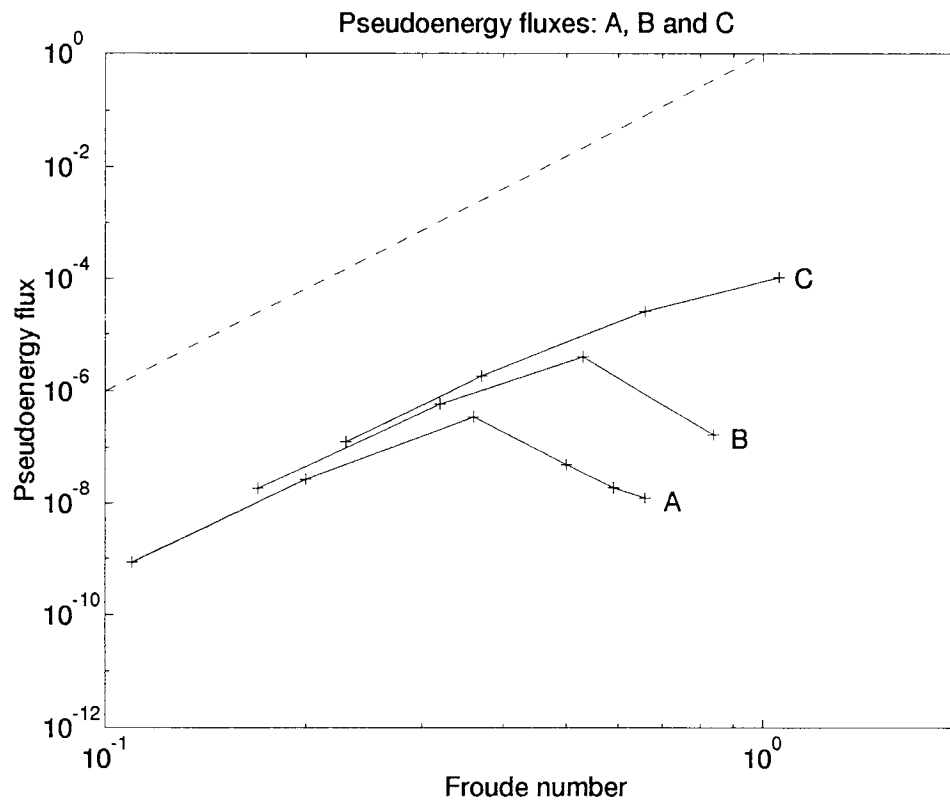


Figure 4.25: The peak pseudoenergy flux due to gravity wave radiation throughout simulations A, B and C

consider strips with non-negative potential vorticity, and then proceed in the following section, §4.9, to consider strips with negative potential vorticity.

## 4.8 Anticyclonic strips with non-negative potential vorticity

In this section, two sets of simulations are presented, with strip potential vorticity values of 0.1 and 0.0, to be labelled **D** and **E** respectively.

Now, at low Froude number, the vortical flow is identical for all Rossby numbers, except that the timescale is set by the magnitude of the potential vorticity jump, with strips with small jumps evolving more slowly than those with larger jumps. However, we know from simulations **A** – **C** that a potential vorticity jump of at least 5 is required if the pseudoenergy flux is to exceed  $10^{-6}$  at a Froude number of 0.1. In this section we are concerned with anticyclonic but positive potential vorticity in the strip. We are therefore restricted to strip potential vorticity values between 1 and 0, and hence potential vorticity jumps between 0 and 1. It follows that we must expect very weak gravity wave radiation at low Froude numbers when the potential vorticity in the strip is between 0 and 1. Consequently, it was decided to concentrate on a strip potential vorticity value of 0.1, which is quite small (i.e.  $\delta Q$  is quite large for anticyclonic potential vorticity of the same sign as the background), and hence the flow will give rise to reasonably large radiated gravity wave amplitudes, without the strip potential vorticity being so close to zero that very large Froude numbers would be required to establish any significant differences between the two cases **D** and **E**.

Six simulations were performed with a strip potential vorticity of 0.1, with initial strip widths of 0.42, 0.84, 1.68, 3.36, 6.00 and 9.00, labelled **Di**–**vi** respectively. The vortical aspects of the dynamics in these simulations are similar to those found for simulations **A** – **C**. Figure 4.26 shows the dependence of the nutation time on the Froude number for experiments **A**, **B**, **C** and **D**. In common with the strips with cyclonic potential vorticity, the nutation times for experiments **Di**–**vi** increase super-exponentially with increasing Froude number.

However, agreement with the Lighthill theory is not found to be very good, even in the case **Di**, with a Froude number of only 0.2. Figure 4.27 shown the  $x$ -averaged  $\partial h/\partial t$  field during simulations **Di** and **Dii**. Although the Lighthill reconstruction is capturing the essential features, on the whole it is performing rather poorly, when compared with cyclonic experiments

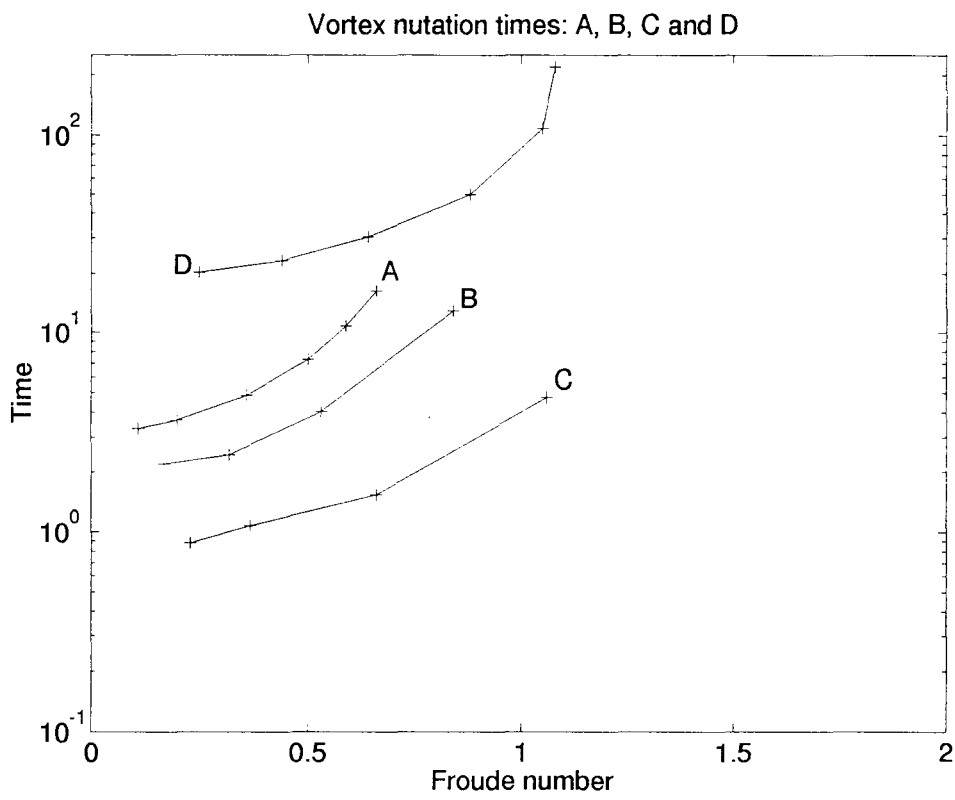


Figure 4.26: Vortex nutation times for simulations Di-vi

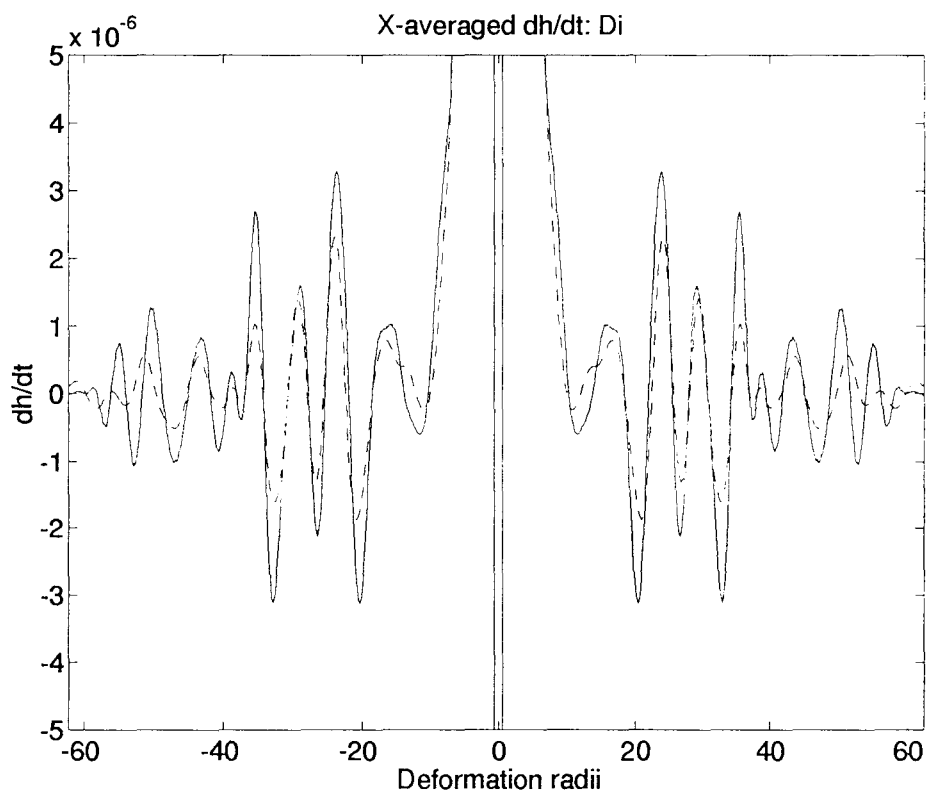


Figure 4.27: The  $x$ -averaged  $\partial h/\partial t$  field at the termination of simulation **Di** (solid line), and its reconstruction using the Lighthill convolution integral (dashed line)

at similar Froude numbers.

Now, in classical aeroacoustics, only two length scales are present in the flow: the scale of the vortical motions, and the scale of the aeroacoustic waves which they generate. In the problem of gravity wave generation by vortical motions in a rotating frame, however, the Rossby deformation radius is an additional length scale, which is unity in the nondimensionalization used here. The Lighthill theory assumes that the quadrupole source may be concentrated at a single point. If this is to be a good approximation, the scale of the vortical flow must be small with respect to the wavelength of the waves it generates, which is the usual low Froude number assumption, and must also be small compared with a Rossby deformation radius. It seems likely that the reason for the rather poor agreement in figure 4.27 is that, although the Froude number is low, the vortices are not very small compared to a Rossby deformation radius, the initial width of the strip being 0.42.

In figure 4.28, the  $\partial h/\partial t$  field is shown, at the time of most intense gravity wave emission, for simulations **Di-iv**. As the Froude number increases, the nature of the gravity wave generation appears to change. At low Froude numbers, the generation appears to be a rather long range effect, with gravity waves generated being of much longer wavelength than the scale of the vortical motions. At higher Froude numbers, however, the generation mechanism appears to be a rather more local effect, with gravity waves apparently being “launched” off the edges of the vortices as they rotate. Figure 4.29 shows a sequence of four frames from simulation **Div**, during the period of generation of its most intense gravity waves, in which this process is illustrated, and figure 4.30 shows the potential vorticity field at the same times.

As the Froude number is increased still further, the gravity waves radiated by the vortex train lose their coherent  $x$ -independent structure. Figure 4.31 shows the gravity wave field during simulations **Dv** and **Dvi**. In comparison with simulations **Diii** and **Div**, these gravity wave fields appear to be more arc-like, resembling radiation from point sources, rather than  $x$ -independent radiation from a line source exhibited at lower Froude numbers.

Figure 4.32 shows the dependence of the gravity wave pseudoenergy flux on the Froude number for experiments **A – D**. As in the case of experiments **A – C**, experiments **Di-vi** exhibit an optimal Froude number, above which the gravity wave pseudoenergy flux decreases as the Froude number is further increased. The existence of an optimal Froude number is almost certainly due to the fact that the vortex rotation times are increasing very rapidly with Froude

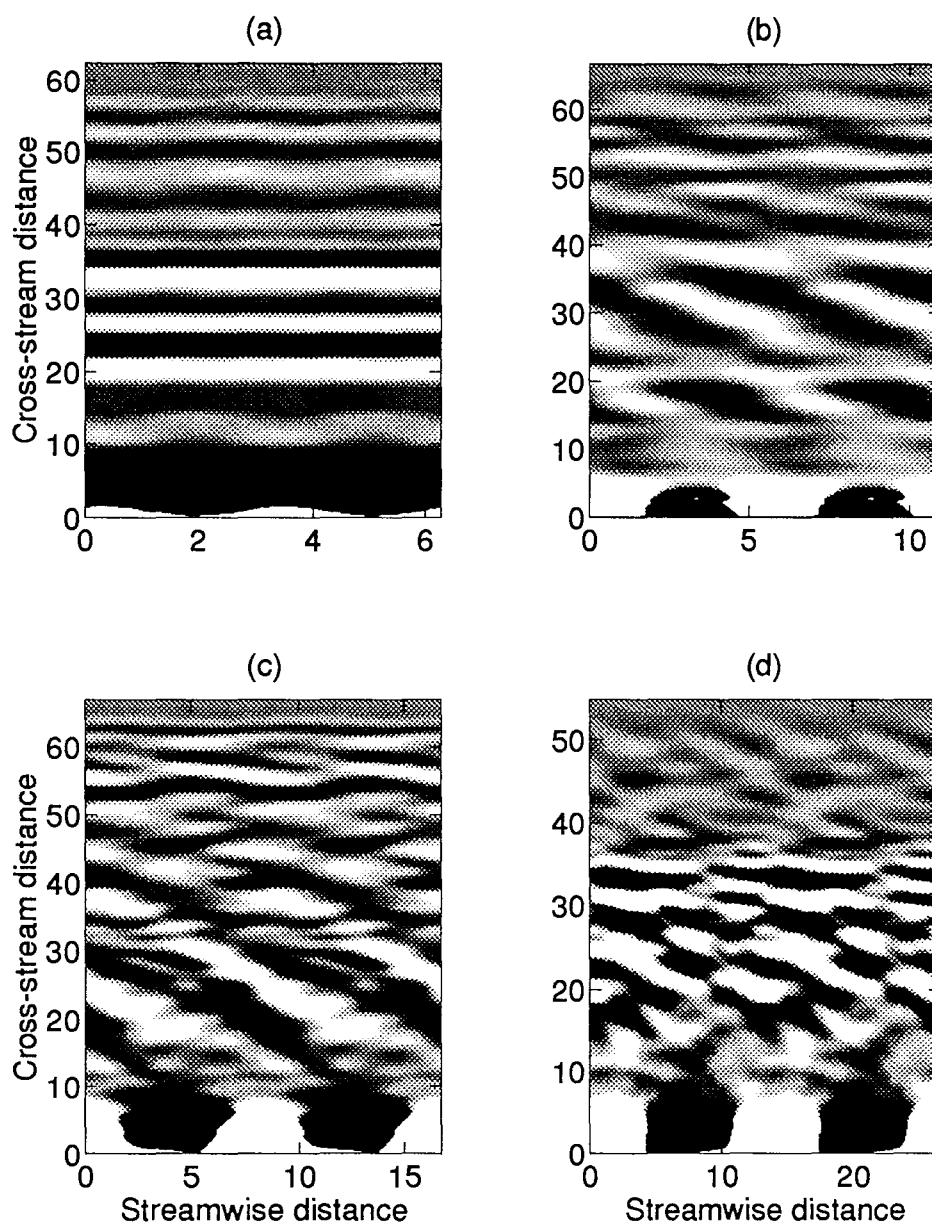


Figure 4.28: The  $\partial h / \partial t$  field during the most active phase of gravity wave generation in simulations Di-iv. Two periods of the model domain are shown.

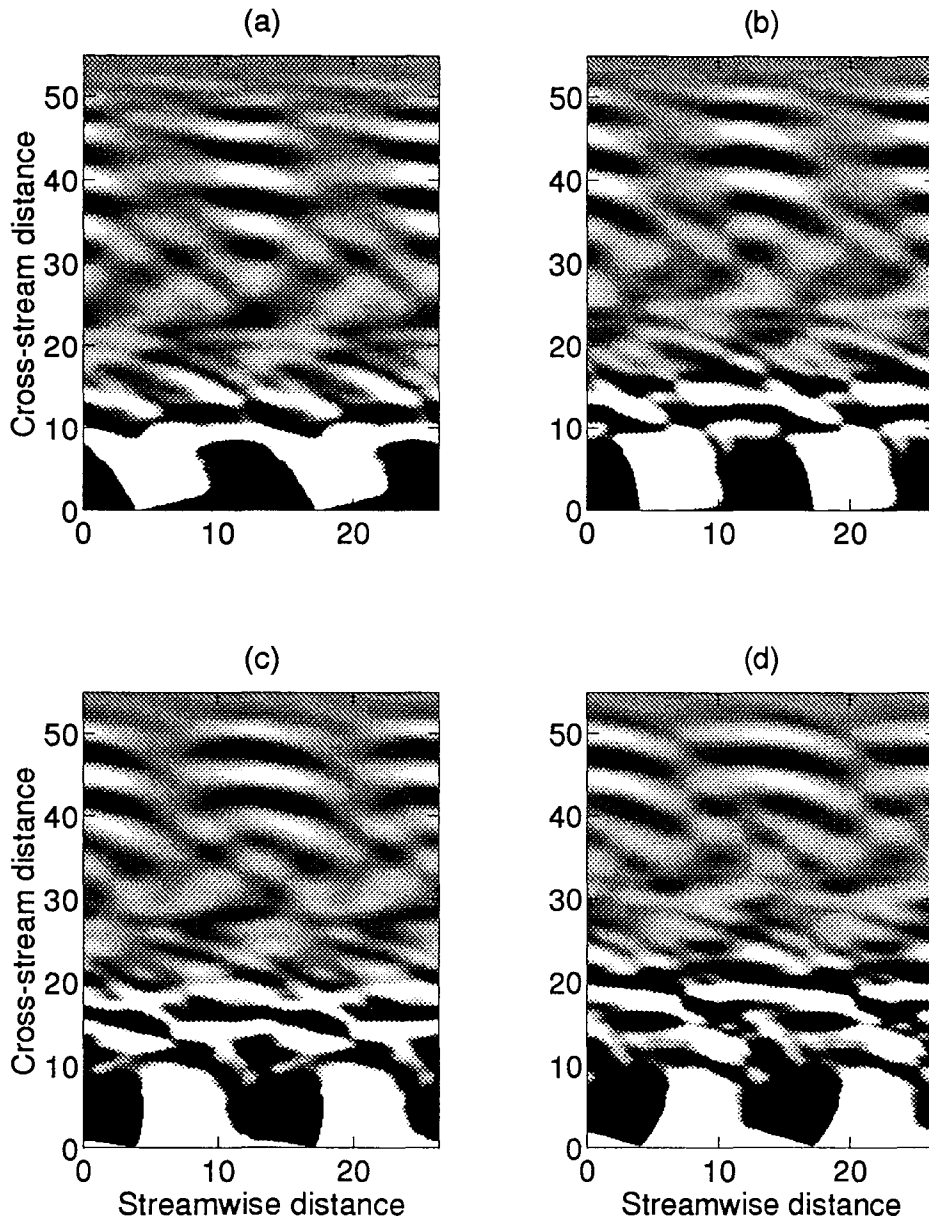


Figure 4.29: The stages of gravity wave emission during simulation Div. Figures a,b,c,d correspond to times 140, 143.75, 147.5 and 151.25 respectively. Two periods of the model domain are shown.

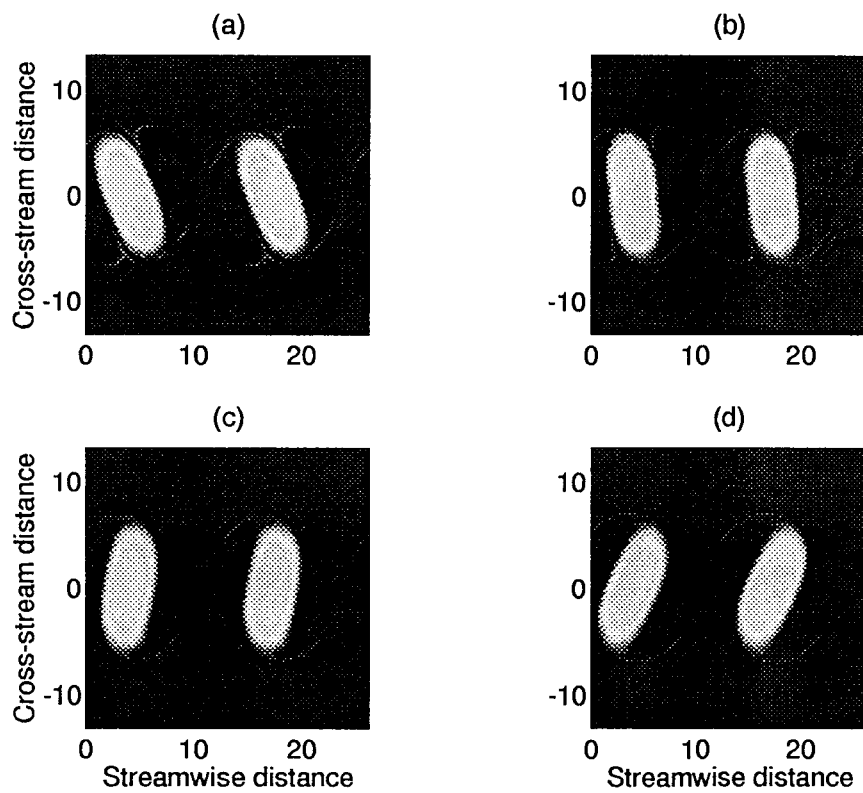


Figure 4.30: The potential vorticity field during the stages of gravity wave emission during simulation **Div**. Figures a,b,c,d correspond to times 140, 143.75, 147.5 and 151.25 respectively. Two periods of the model domain are shown.

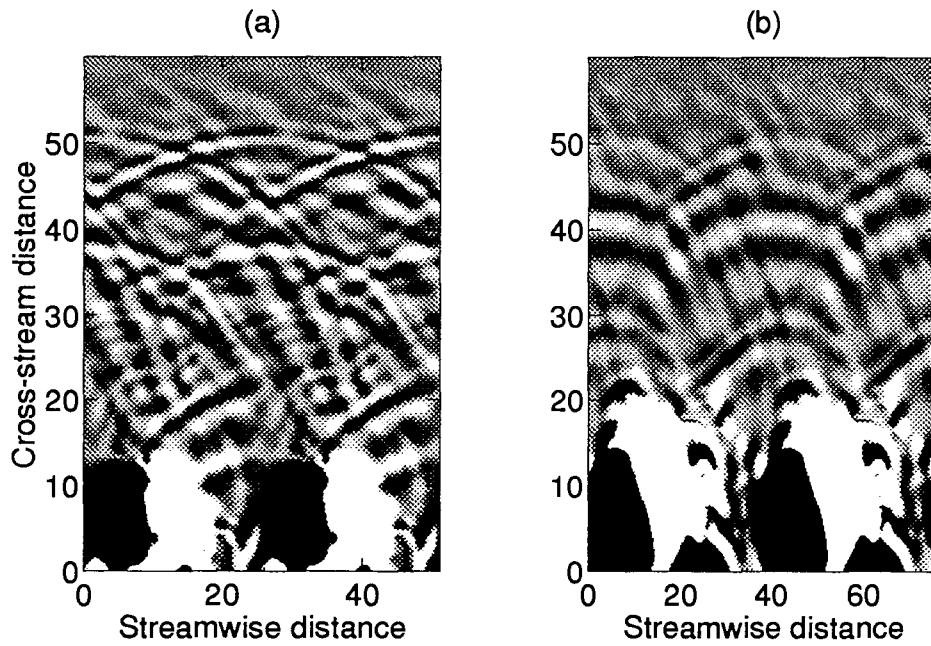


Figure 4.31: The  $\partial h/\partial t$  field during simulations **Dv** and **Dvi**. Two periods of the model domain are shown.

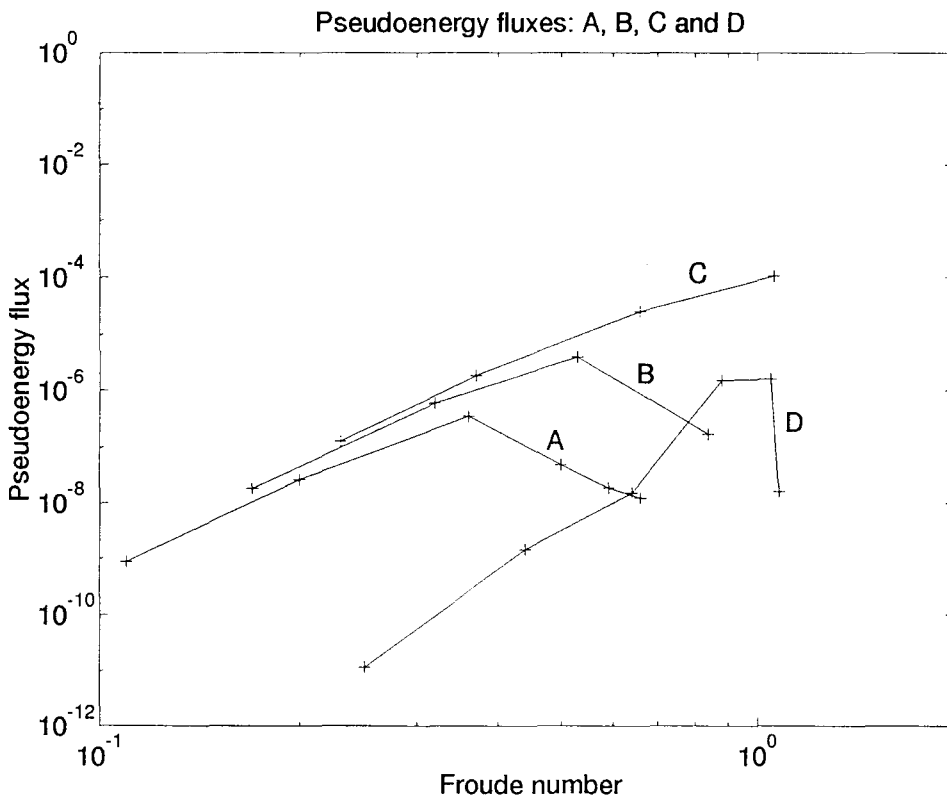


Figure 4.32: The maximum pseudoenergy flux plotted against Froude number for simulations **Di-vi**

number, and hence the gravity waves are severely inhibited by the presence of background rotation.

It seems clear that the nature of the gravity wave radiation, and its ultimate limitation, is somewhat different in simulations **D**i–vi from that found in simulations **A** – **C**. The gravity wave pseudoenergy flux appears to increase more rapidly with Froude number, at moderate Froude numbers, and the transition from increasing gravity wave amplitudes to decreasing amplitudes as the Froude number is increased is much more abrupt than is found for cases **A** – **C**, with cyclonic potential vorticity in the strip. However, analysis in this case is difficult because, unlike the cyclonic simulations **A** – **C**, the vortices are very much larger, when compared with a Rossby deformation radius, at the critical Froude number at which the transition from increasing to decreasing pseudoenergy fluxes occurs. This means that the Lighthill theory is inapplicable in this limit, and an alternative analytical description of the flow has not been attempted.

The experiments with small positive potential vorticity in the strip are to be contrasted with experiments in which the potential vorticity in the strip is exactly zero. Five experiments were conducted with a strip potential vorticity of zero, with initial strip widths of 0.42, 0.84, 1.26, 2.52 and 6.00. The experiments are labelled **E**i–v respectively.

Figure 4.33 shows the dependence of the vortex nutation times on the Froude number for experiments **E**i–v, with those for experiments **A** – **D** for comparison. Although there appears to be a very gradual increase in vortex nutation times with Froude number in this case, the behaviour is to be contrasted sharply with that found for a strip potential vorticity of just 0.1. A very significant difference in the nature of the vortical flows is thus observed between simulations **D** and **E**, although the general nature of the flow remains broadly similar: the strip rolls up into a periodic chain of vortices which proceed to nutate, albeit at markedly different rates between simulations **D** and **E**, without significant change of form.

The  $\partial h/\partial t$  field during simulations **E**ii–v is shown in figure 4.34. At lower Froude numbers, it appears to behave in a similar way to the wave field in simulations **D**, with the gravity waves being launched from the edges of the vortices as they rotate. However, as the Froude number is increased, the radiated wave field does not become less coherent, but rather the wave crests of the launched waves become progressively sharper, almost resembling shock waves in the highest Froude number simulation **E**v.

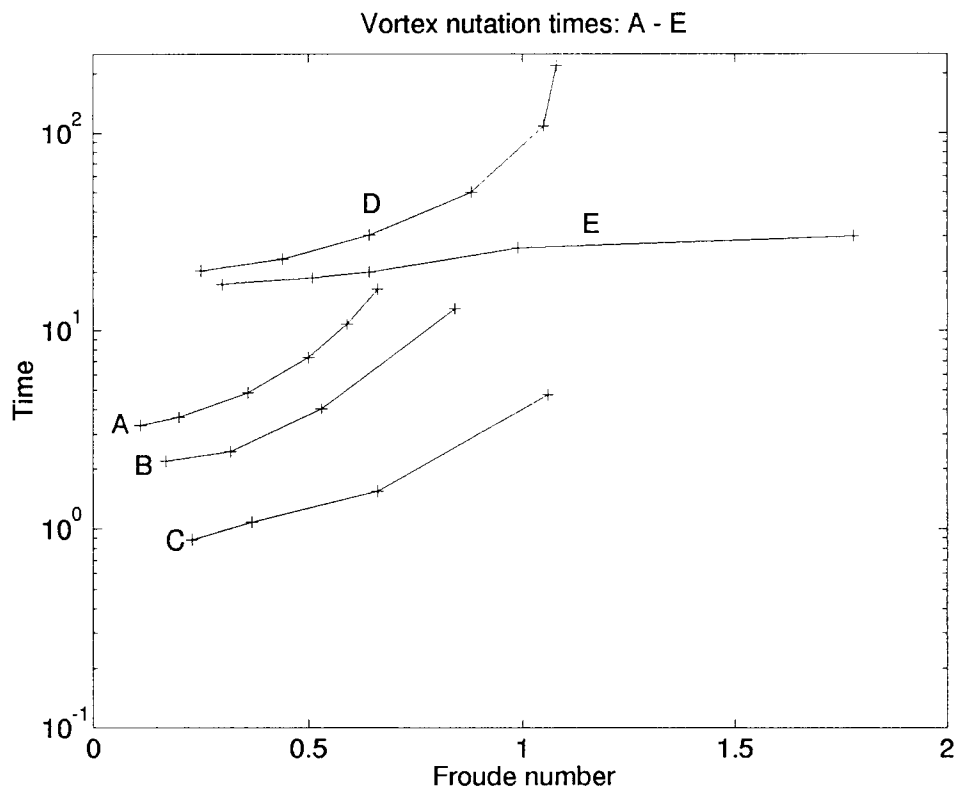


Figure 4.33: Vortex nutation times for simulations Ei-v

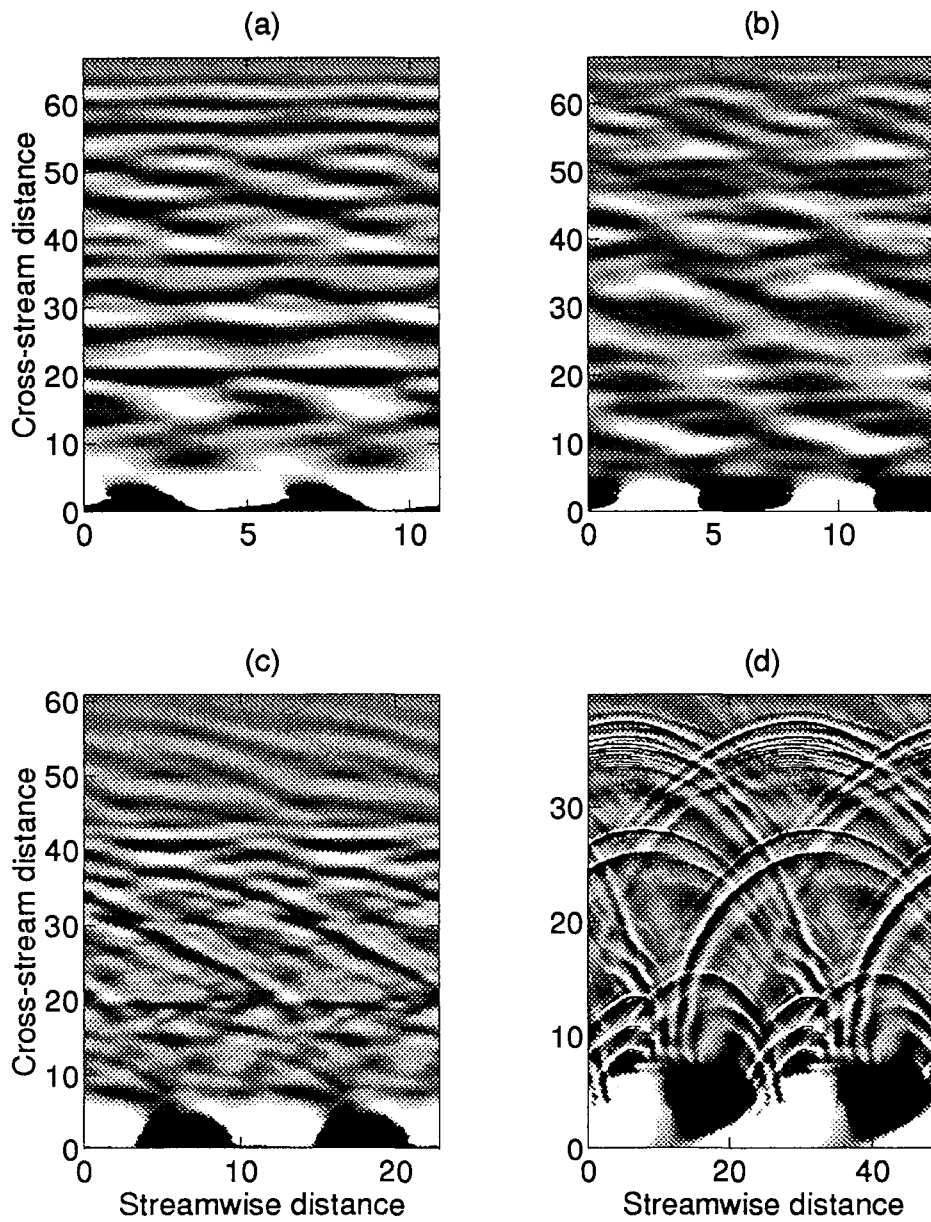


Figure 4.34: The  $\partial h/\partial t$  field during simulations Eii-v. Two periods of the model domain are shown.

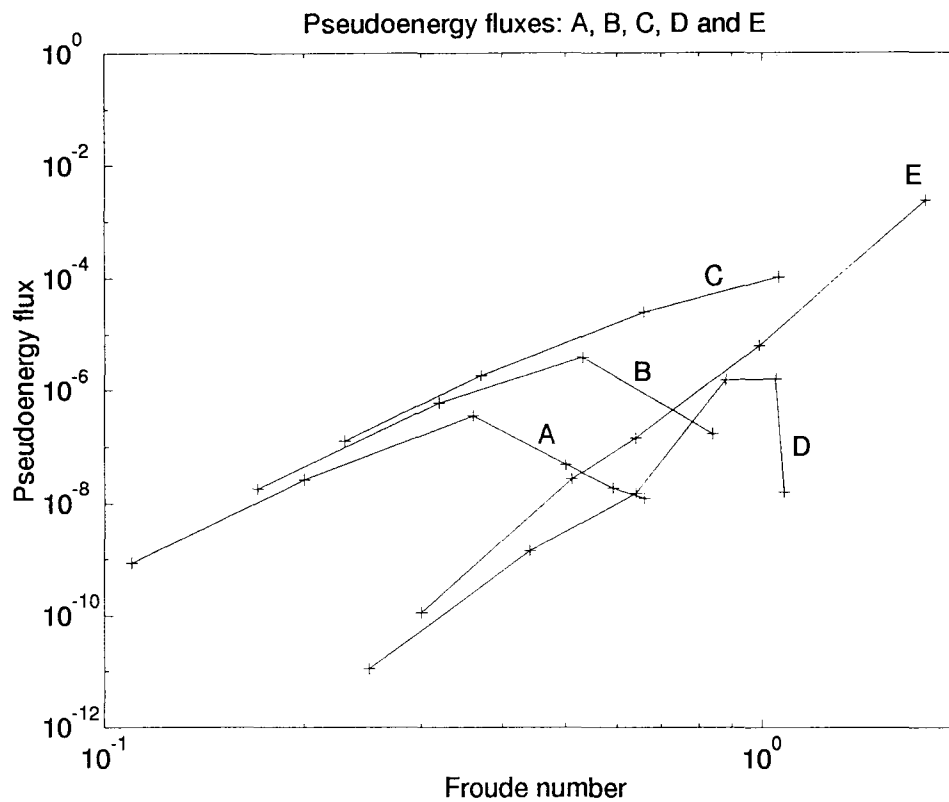


Figure 4.35: Maximum pseudoenergy flux plotted against Froude number for simulations *Ei-v*

The maximum pseudoenergy flux found in the gravity wave field in simulations *Ei-v* is shown in figure 4.35, with that found for experiments *A – D* for comparison. At moderate Froude numbers the pseudoenergy flux increases strongly with Froude number, in parallel with that observed for simulations *Di-iv*. However, in case *E* the pseudoenergy flux increases with increasing Froude number apparently without bound, with the gravity wave field apparently becoming highly nonlinear, and somewhat shock-like, at the largest Froude numbers.

#### 4.9 Anticyclonic strips with negative potential vorticity

Having now classified the behaviour of the flows with non-negative potential vorticity, three further sets of simulations were undertaken to investigate gravity wave generation by vortex trains with negative potential vorticity. Strip potential vorticity values of -0.1, -1.0 and -19.0 were investigated, with a range of strip widths in each case.

The experiments with a strip potential vorticity of -0.1 were performed for comparison

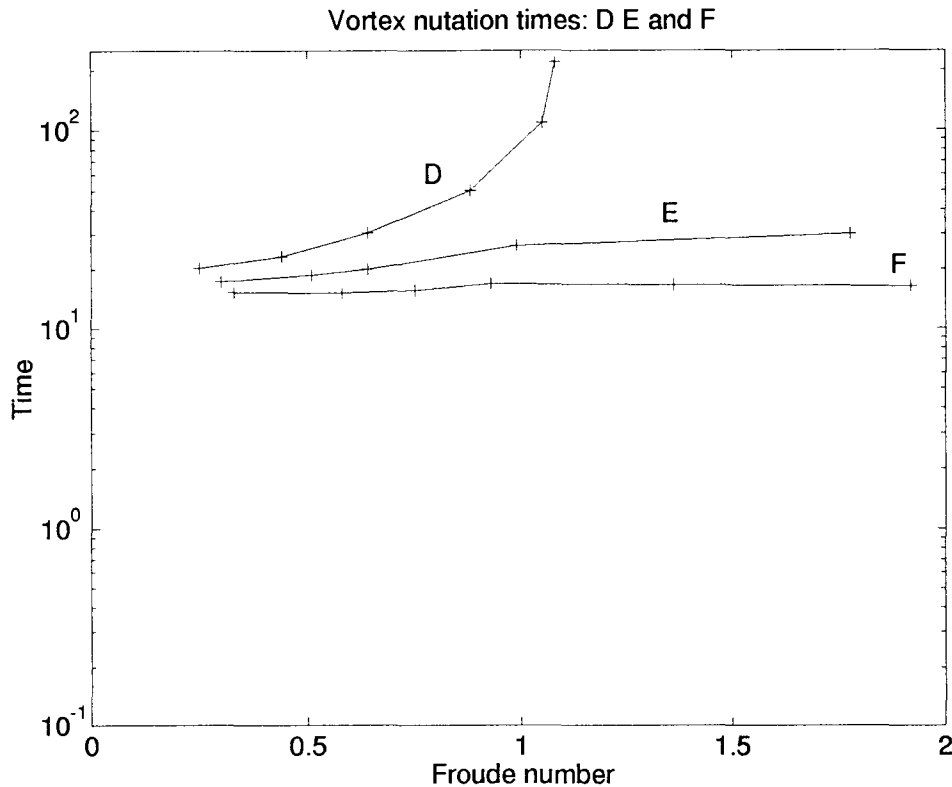


Figure 4.36: Vortex nutation times for simulations **F**i-v

with experiments **E**i-v, in which the strip potential vorticity was zero, to investigate whether any additional effects occurred when slightly negative potential vorticity was present in the simulations. Six simulations were performed with a strip potential vorticity of -0.1. Initial strip widths taken were 0.42, 0.84, 1.26, 1.68, 2.52 and 3.04. Figure 4.36 shows the vortex nutation times for simulations **D**, **E** and **F**. One can see that although there is a substantial difference between a strip potential vorticity of 0.1 and 0.0, there appears to be comparatively little difference between strip potential vorticity of 0.0 and -0.1.

In figure 4.37 the gravity wave pseudoenergy fluxes are shown for simulations **D**, **E** and **F**. Again, although there is a substantial difference between simulations **D** and **E**, there is almost no qualitative difference between simulations **E** and **F**.

The  $\partial h/\partial t$  field for simulations **F**iii-vi is shown in figure 4.38. One can readily see that, at large Froude number, both sets of simulations **E** and **F** are tending to produce shock waves, and neither appears to be exhibiting any tendency for the pseudoenergy flux to stop increasing

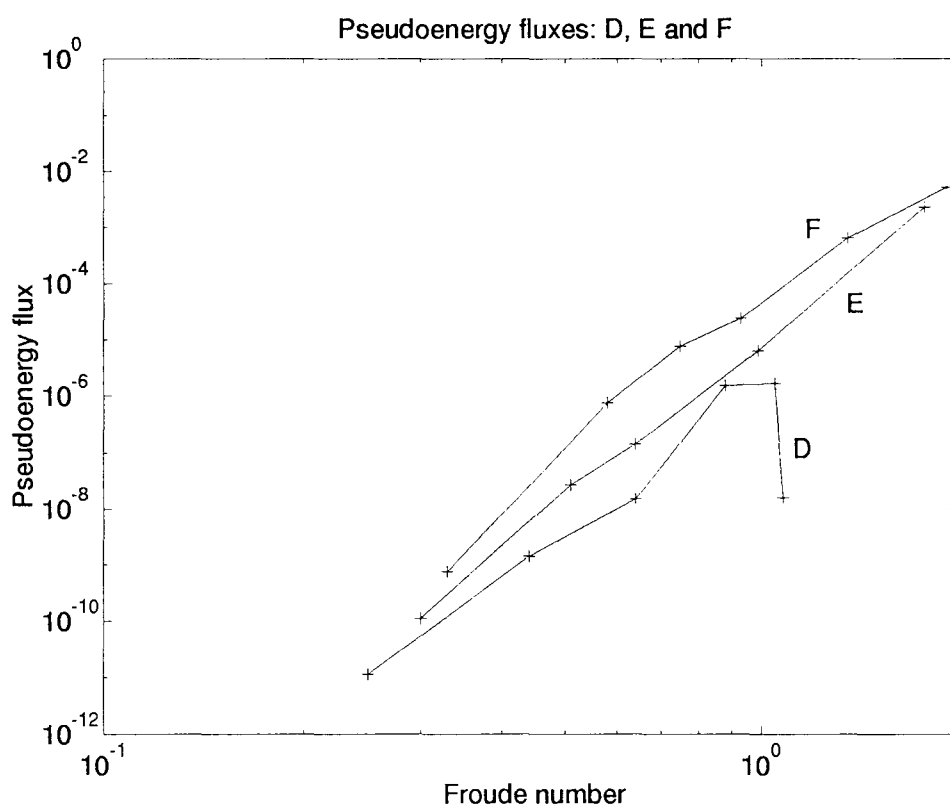


Figure 4.37: Maximum pseudoenergy flux against Froude numbers for simulation sets **D**, **E** and **F**

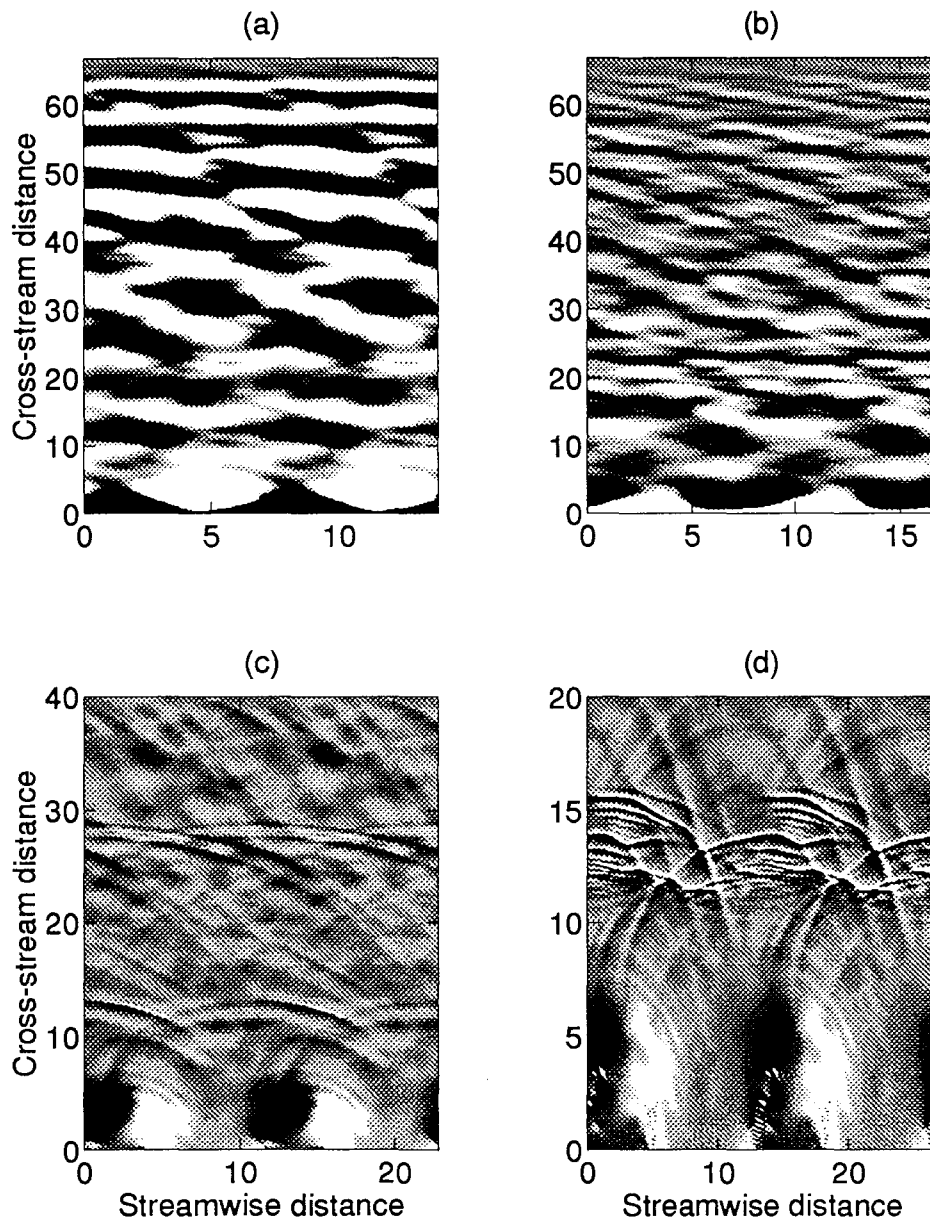


Figure 4.38: The  $\partial h / \partial t$  field during simulations Fiii-vi. Two periods of the model domain are shown.

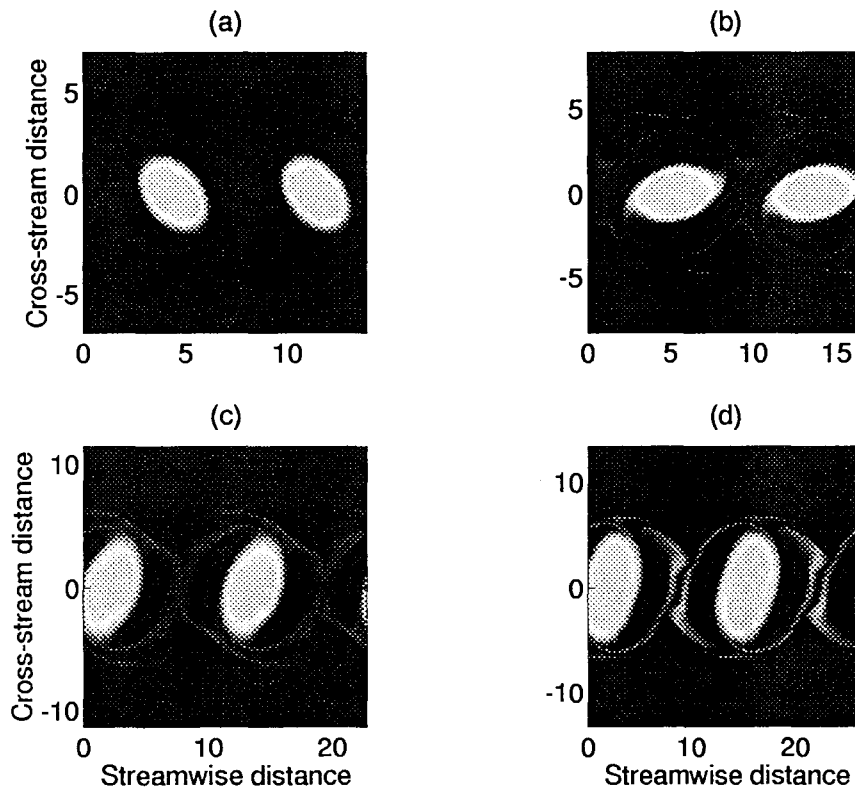


Figure 4.39: The potential vorticity field during simulations **Fiii-vi**

with increasing Froude number. It seems reasonable to conclude that there is no appreciable difference between strips with zero potential vorticity, and strips with slightly negative potential vorticity.

The potential vorticity field corresponding to figures 4.38a–d is shown in figures 4.39a–d respectively. In simulation **Fvi**, one can see in figure 4.38d that there is some small-scale noise in the  $\partial h/\partial t$  field, in the vortical region, and hence the flow may be under-resolved. However, the potential vorticity in figure 4.39d does not exhibit significant small-scale noise, and so we can have some confidence that the performance of the model is at least reasonably good, even in this extreme case with a Froude number of almost 2.0.

Four simulations were then performed with a strip potential vorticity of -1.0. The strips had initial strip widths of 0.07, 0.21, 0.42 and 0.63, and are labelled **Gi-iv**. The vortex nutation times do not appear to change significantly with Froude number, and are shown in figure 4.40, with those for simulations **D – F** for comparison.

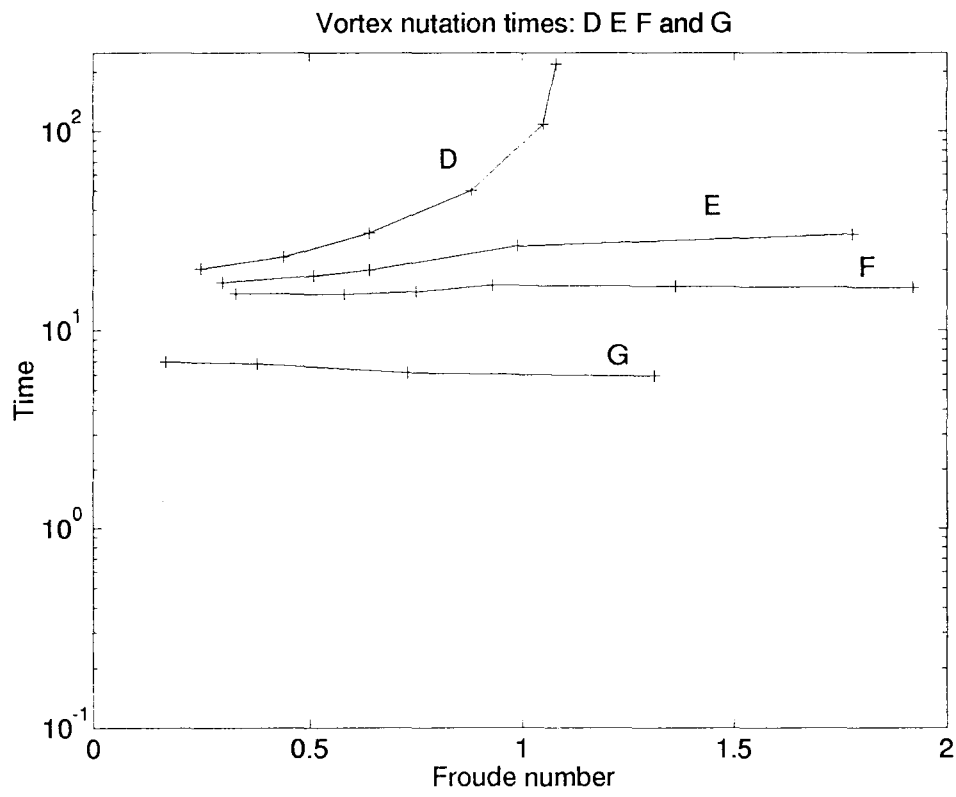


Figure 4.40: Vortex nutation times for simulations Gi-iv

The size of the vortices compared to a Rossby deformation radius is now much smaller than was the case in simulations **D**, **E** and **F**, with the largest initial strip width being 0.63, only 50% wider than the smallest initial strip with in simulations **D**, **E** and **F**. Consequently, the Lighthill theory is significantly more successful at reconstructing the wave field. The  $x$ -averaged  $\partial h/\partial t$  field, and its reconstruction from the Lighthill source term, is shown for simulations **Gi-iii** in figure 4.41, and good agreement is obtained for initial strip widths of 0.07 and 0.21.

However, in line with experiments **E** and **F**, the character of the wave field does depart significantly from that of linear waves as the Froude number is increased. In figure 4.42, the  $\partial h/\partial t$  field is shown at the end of each simulation for the cases **Gi-iv**. In the first three cases the wave field appears to be well described by linear waves. At low Froude numbers the wave field is dominated by  $x$ -independent waves, with  $x$ -dependence increasing with increasing Froude number in simulations **Gi-iii**. Indeed, linear wave-like motions in the gravity wave field are a pre-requisite for good agreement with the Lighthill theory, observed in figures 4.41a&b, which assumes a linear radiating wave field. In simulation **Giv**, however, the character of the wave field differs markedly from linear wave-like motions, with shock waves appearing in the radiating gravity wave field. In common with simulations **Ev** and **Fv**, the shocks in simulation **Giv** also appear to originate in the vortical region itself, although they appear to be somewhat sharper in this case.

At this point it should be recognised that the discretization scheme is not designed to capture shocks, and any quantitative discussion of differences between shocks is inappropriate. However, it seems unlikely that a more sophisticated numerical scheme would significantly affect the existence of sharp shock structures in these high Froude number strongly anticyclonic simulations.

The maximum  $x$ -averaged pseudoenergy flux is shown against the Froude number in figure 4.43, with the flux for simulations **D – F** for comparison. At low Froude numbers, the pseudoenergy flux is increasing as the sixth power of the Froude number. The increase then appears to become more rapid as the Froude number increases, in common with with other anticyclonic simulations **D – F**, in which it appeared that the pseudoenergy flux was increasing more rapidly than the sixth power of the Froude number. These do, of course, differ from the cyclonic simulations, in which the pseudoenergy flux never increased more rapidly than the sixth power of the Froude number.

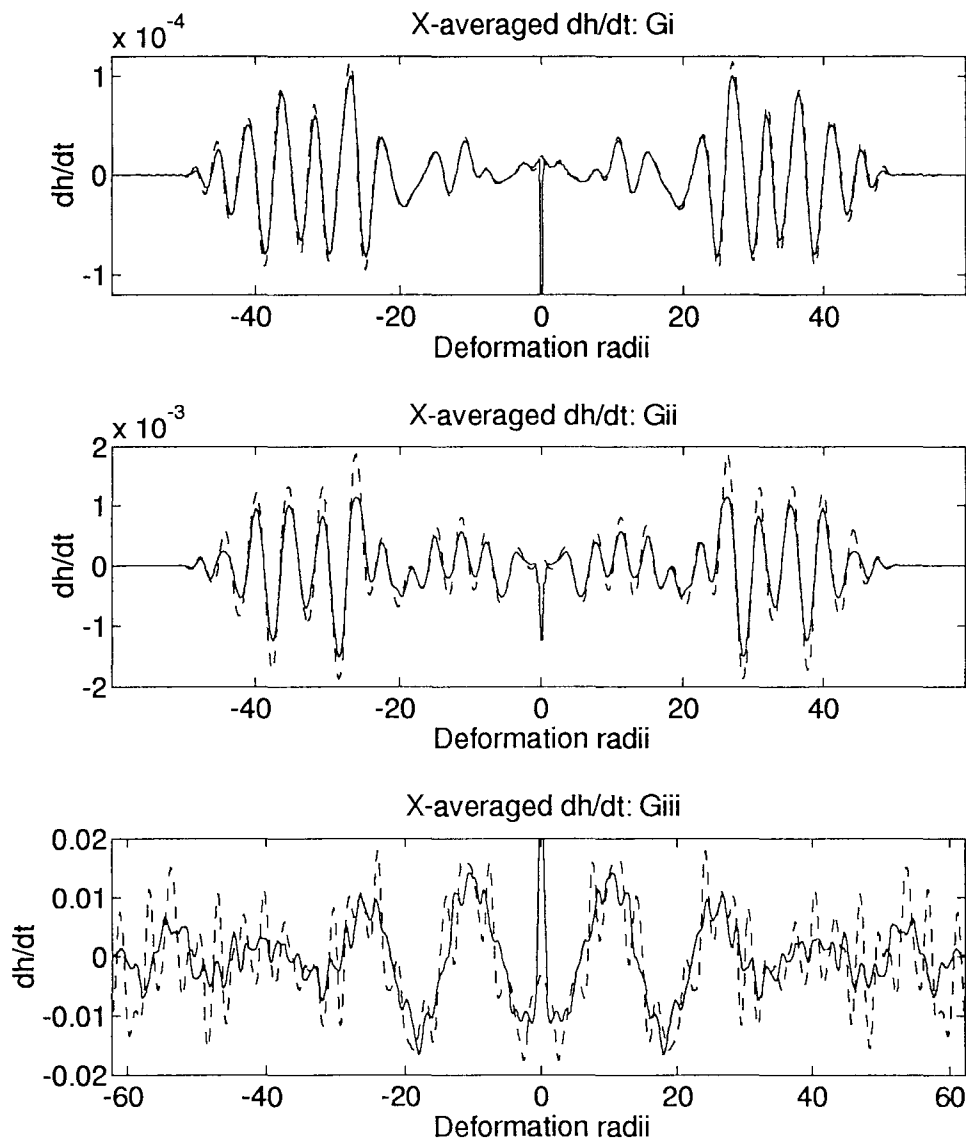


Figure 4.41: The  $x$ -averaged  $\partial h/\partial t$  field at the termination of simulations **Gi-iii** (solid line), and its reconstruction from the Lighthill convolution integral (dashed line)

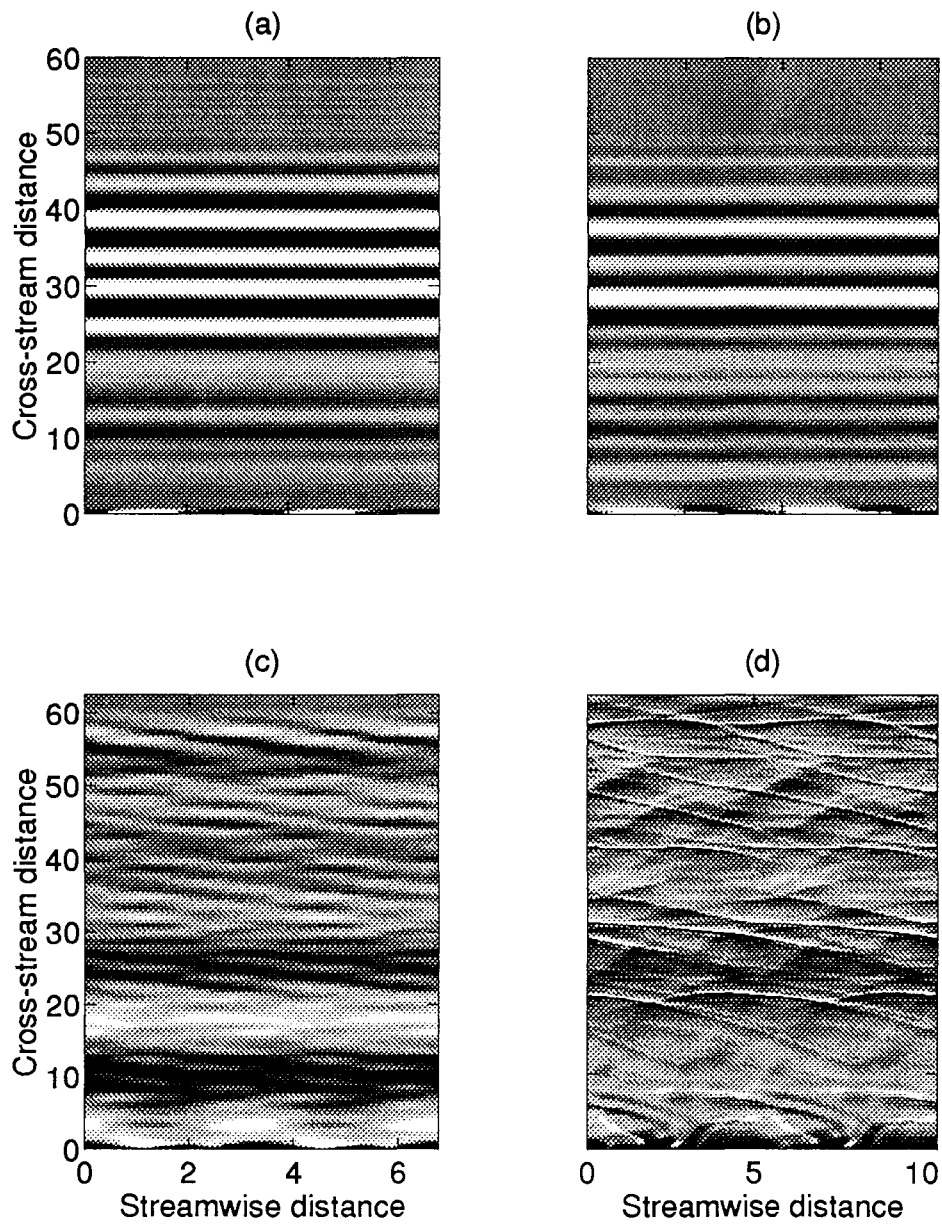


Figure 4.42: The  $\partial h/\partial t$  field during the simulations **Gi-iv**. Two periods of the model domain are shown.

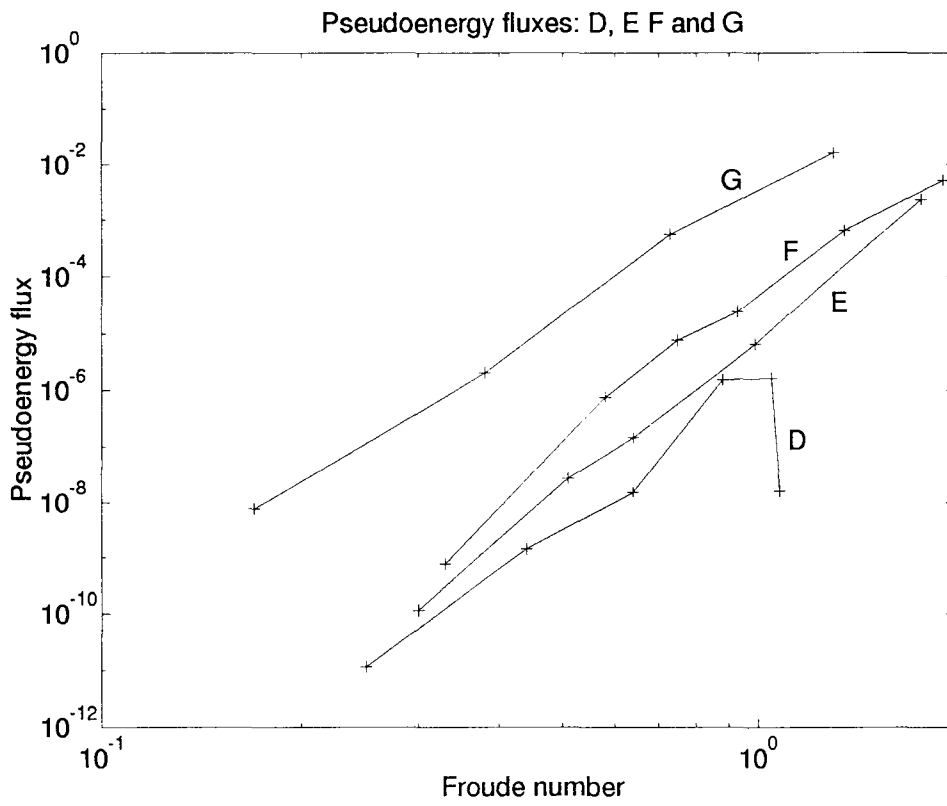


Figure 4.43: The maximum pseudoenergy flux against Froude number for simulations Gi-iv

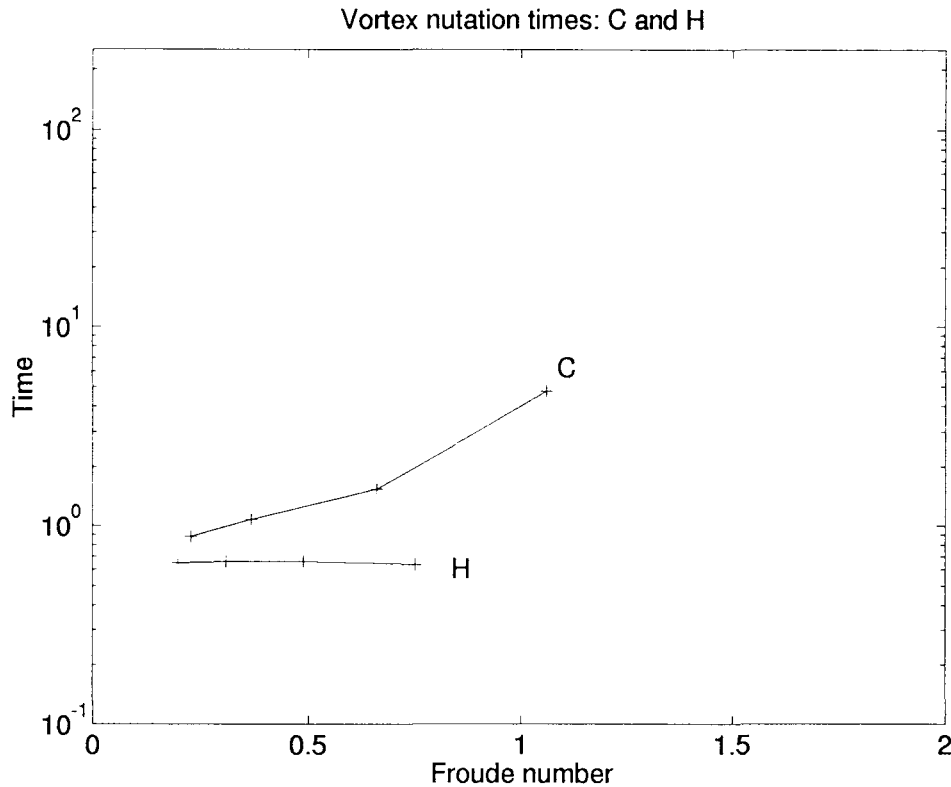


Figure 4.44: Vortex nutation times for simulations **Hi-iv**

Finally, four simulations were performed with a strip potential vorticity of  $-19.0$ . These simulations were performed for comparison with simulations **Ci-iv**, in which the strip potential vorticity was taken to be  $21.0$ . Consequently, at low Froude numbers, the dynamics of the strips should be identical in the two cases, with the magnitude of the potential vorticity jump being equal to  $20$  in both cases. Strip widths of  $0.007$ ,  $0.013$ ,  $0.021$  and  $0.031$  were taken, and the simulations are labelled **Hi-iv** respectively.

Figure 4.44 shows the vortex nutation times for simulations **C** and **H** as a function of Froude number. It can clearly be seen that when there is negative potential vorticity in the strip the nutation times remain almost constant as the Froude number is increased, whereas in the case of positive potential vorticity in the strip the nutation times increase superexponentially.

In figure 4.45 the  $\partial h/\partial t$  field is shown at the termination of simulations **Hi-iv**, and in figure 4.46 the comparison with the Lighthill theory is shown. The agreement seems quite good at low Froude numbers, but not as good as in simulations **Ci-iv**, even though the waves remain

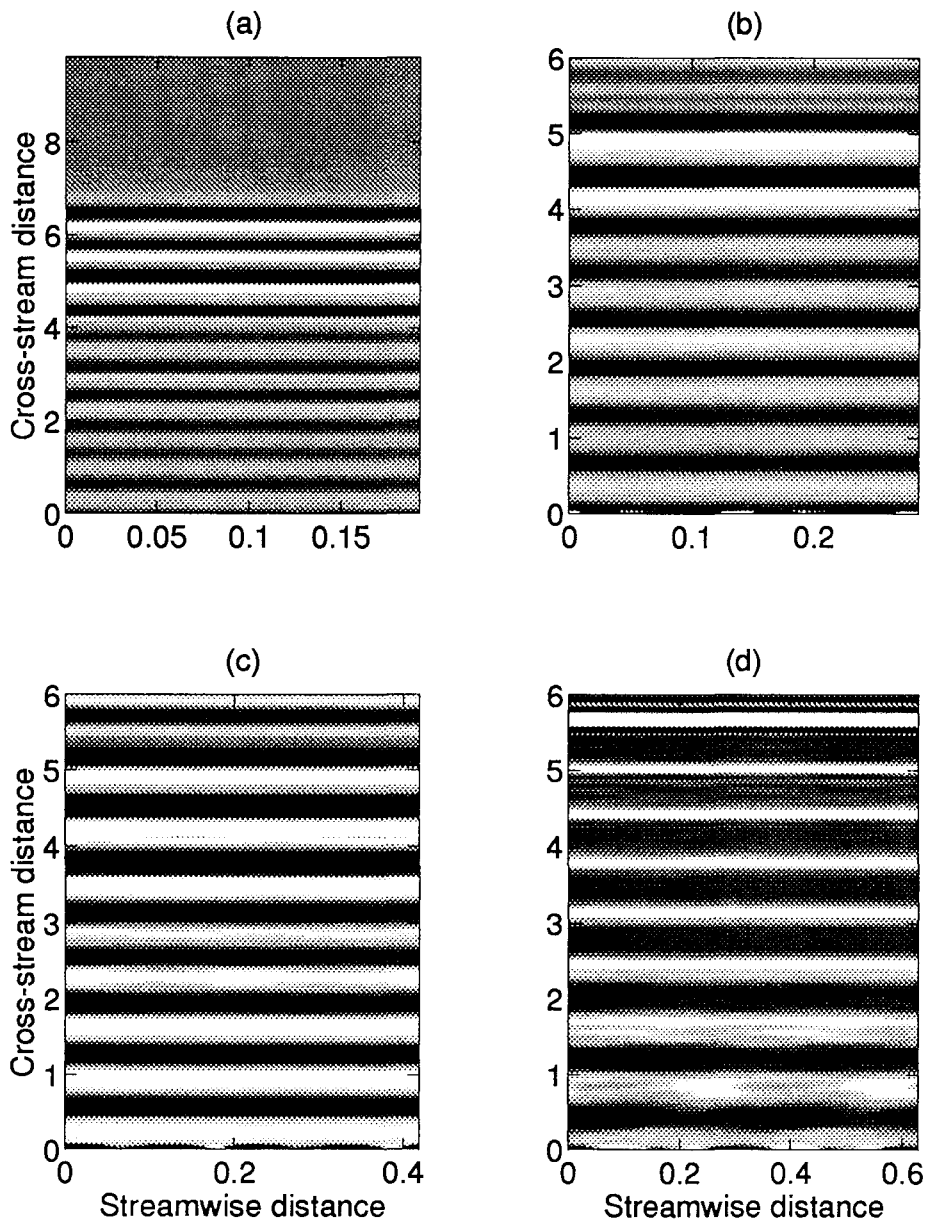


Figure 4.45: The  $\partial h / \partial t$  field at the termination of simulations **Hi-iv**. Two periods of the model domain are shown.

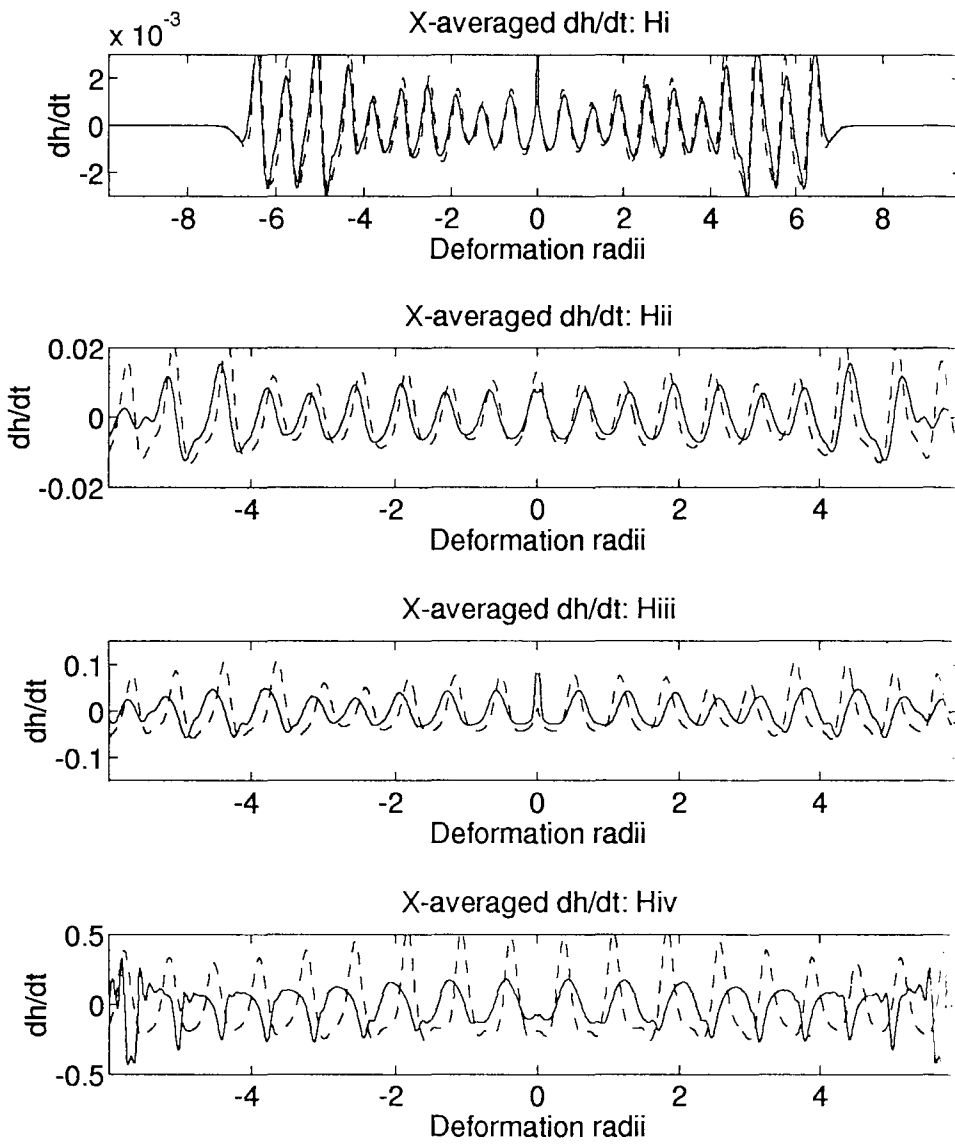


Figure 4.46: The  $x$ -averaged  $\partial h/\partial t$  field at the termination of simulations  $H_i$  and its reconstruction from the Lighthill convolution integral (dashed lines)

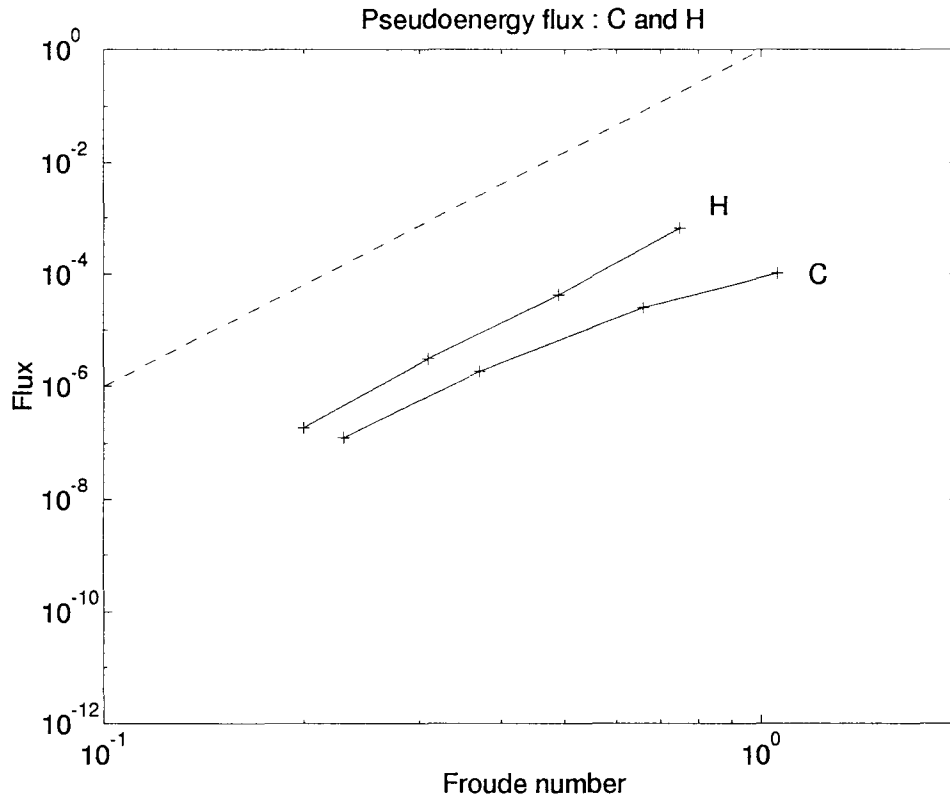


Figure 4.47: Maximum pseudoenergy flux plotted against Froude number for simulations **Hi-iv** nearly independent of  $x$ .

The peak pseudoenergy flux in the gravity wave far field is shown against Froude number for simulations **Ci-iv** and **Hi-iv** in figure 4.47. One can see that, although both sets of simulations are initially quite similar, as the Froude number is increased the simulations **Hi-iv**, with negative potential vorticity in the strip, radiate gravity waves much more strongly than the corresponding cyclonic simulations with the same magnitude of potential vorticity difference between the strip and the background.

When comparing the  $x$ -averaged  $\partial h/\partial t$  field with its reconstruction from the Lighthill convolution integral (4.7), it is of interest to note that, while in most cases the maxima of the actual and reconstructed field co-incide, in simulations **C** and **H**, shown in figures 4.23 and 4.47 respectively, the maxima appear to be offset. In figure 4.23, the maxima of the field obtained by reconstruction from (4.7) appear to lead those obtained by direct numerical simulation, whereas in 4.47, they tend to lag those obtained by direct numerical simulation. The reason is that the

Lighthill theory assumes that the wave phase speed  $c_0$  is constant everywhere. However, the vortical flow adjusts to rest over the scale of a Rossby deformation radius. In most cases, the radiated waves are of long wavelength compared with a Rossby deformation radius. However, as the potential vorticity in the strip increases, so the frequency of the vortical motion increases, and hence the wavelength of the radiated waves decreases. In cases **C** and **H**, the wavelength of the radiated waves is of the order of a deformation radius, and therefore they may be significantly affected during their propagation through the region over which the flow relaxes adjusts to rest. In the cyclonic case **C**, the layer depth is less near the strip than at infinity, and the waves will tend to propagate more slowly there. Hence, the waves predicted by (4.7) will tend to lead those obtained by direct numerical simulation. Conversely, in the anticyclonic case **H**, the layer depth is greater near the strip than at infinity, and the waves will propagate more quickly there. Hence, the waves predicted by (4.7) will tend to lag those obtained by direct numerical simulation, in agreement with what is found in figures 4.23 and 4.47.

## 4.10 Discussion

Gravity wave radiation by a train of vortices in shallow water has been studied by direct numerical simulation. The dependence of the gravity waves radiated upon the Froude and Rossby numbers was investigated.

Arguably the most surprising result is that, for cyclonic vortices at moderate Rossby number, increasing the Froude number above 0.35 can lead to a decrease in the amplitude of the gravity waves radiated by the vortex train. This is in contrast to laboratory experiments, and the numerical experiments of Lele & Ho (1993) for a non-rotating gas, in which the acoustic wave amplitudes scaled according to the Lighthill theory for Mach numbers of up to 0.6 or so.

A summary of the results, showing the dependence of the radiated pseudoenergy flux on the Froude number for various Rossby numbers is shown in figure 4.48.

One can see that, in general, whereas positive potential vorticity trains tended to exhibit an “optimal” Froude number for gravity wave generation, the amplitude of gravity waves radiated by negative potential vorticity trains increase apparently without bound as the Froude number increases.

Typical vortex nutation times for all experiments are shown in figure 4.49. One can see

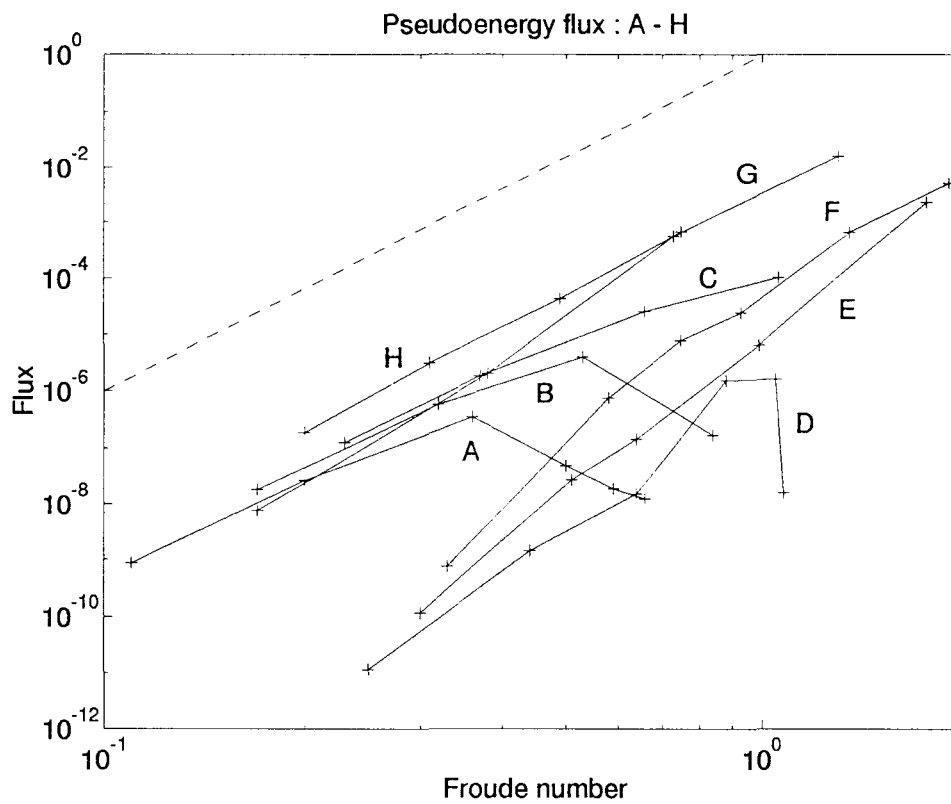


Figure 4.48: Pseudoenergy flux against Froude number for all simulations (solid lines). The gradient of the dashed line corresponds to pseudoenergy increasing as the sixth power of the Froude number

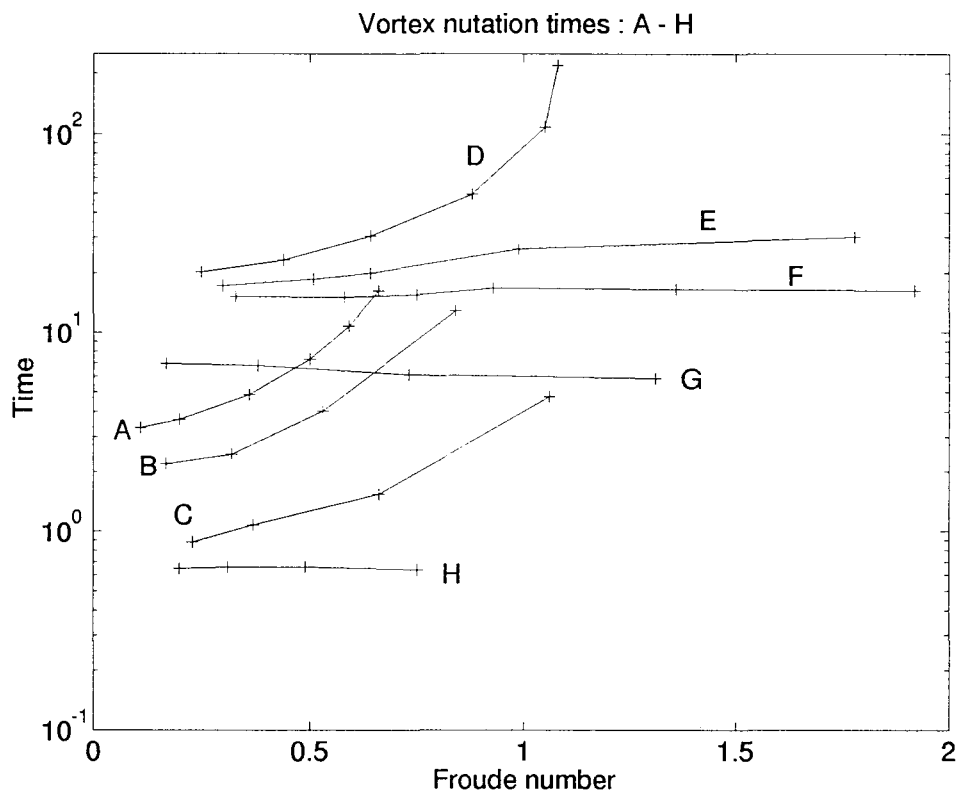


Figure 4.49: Vortex nutation times for all experiments, A - H

that nutation times increase super-exponentially with Froude number for all cyclonic vortex simulations, **A** – **C**, and also for anticyclonic simulations, when the potential vorticity in the strip is strictly positive. As a result, the intensity of the radiated gravity waves never exceeds about  $10^{-4}$  in simulations **A** – **D**, as the inhibiting effect of the inertial frequency becomes increasingly significant as the nutation times increase. However, when the potential vorticity in the strip is zero or negative, there does not appear to be any significant dependence of the nutation time upon the Froude number, and the radiated gravity wave fluxes apparently increase without bound.

It might be suggested that symmetric instability might account for this difference. Symmetric instability, with wavenumber zero, will exist in parallel flow when  $f(f - U_y)$  is negative in some part of the domain (Hoskins, 1974). Although his analysis is for a continuously stratified fluid, it can be readily extended to the shallow water equations (R. T. Pierrehumbert, personal communication). The condition  $f(f - U_y) < 0$ , which is both necessary and sufficient for symmetric instability, is met, at the initial instant, by flows **Fi-vi**, but not by flows **Ei-vi**.

However, there seems very little difference between simulations **E** and **F**, even though the initial states of **F** have an additional instability mechanism available to them, not present in the initial states of **E**. Therefore, it would appear that symmetric instability does not play a significant role in these simulations.

It should be noted, however, that all flows were initialized with an eigenmode at finite wavelength, corresponding to the fastest growing barotropic, or “Rossby wave–Rossby wave”, instability mode. It may be of interest to repeat some of the experiments **F**, **G** and **H**, initializing with a symmetric instability mode of zero wavelength, or perhaps with a combination of the symmetric and barotropic instability modes, to investigate the characteristics of the gravity wave field which develops under their subsequent nonlinear evolution.

Some asymmetry between cyclones and anticyclones at Rossby and Froude numbers of order unity has been observed in numerical simulations by L. M. Polvani (personal communication). In his simulations, the geometry of the flow is doubly-periodic, and the initial vorticity field is random. The flow is balanced using the nonlinear balance equations (McWilliams, 1985). In time, large coherent vortices develop, and at small Froude number, there is symmetry between cyclonic and anticyclonic vortices. At larger Froude numbers, however, the flow is dominated by large coherent anticyclones, with much of the cyclonic potential vorticity smeared out into thin

filaments. In some simulations, shock waves have been observed, emanating from the anticyclones. Polvani's simulations thus broadly confirm the results presented here, that anticyclones are more vigorous features than cyclones in shallow water dynamics at order-one Froude numbers, capable of generating shock waves in the gravity wave field at sufficiently large Froude number.

Finally, we recall that this study was motivated, in part, by the observation by McIntyre & Norton (1993) that gravity waves of large amplitude were generally not generated by the vortical motions in their disturbed polar vortex simulations. Now, in polar vortex simulations, the majority of the vortical motions are cyclonic, and the potential vorticity is all of one sign throughout the hemispherical domain. Consequently, they are not able to access the regime of zero and negative potential vorticity, which has been demonstrated in this chapter to be the regime in which the strongest gravity wave generation might be expected. The results presented therefore support their findings, and offer some explanation for them.

# Chapter 5

# Discussion

## 5.1 Review of aims and objectives of this thesis

In the introduction to this thesis, it was stated that the aims of the thesis were:

- To investigate the generation of gravity waves in the shallow water system, and the dependence of their amplitudes and character on the Froude and Rossby numbers of the basic flow;
- To quantify the effect of the generation of gravity waves in the shallow water system on the potential vorticity distributions which generate them;
- To establish whether, without additional regard to flow geometry, there can or can not exist a slow manifold for the shallow water equations in any region of Froude and Rossby number space.

To be fair, it can not be said that these aims have been neatly divided up, with successive chapters each dealing with one particular aim. The investigation of gravity waves generated by vortical flows in the shallow water system has been an overall objective of the thesis, and each of the three substantive chapters of the thesis has made a significant contribution to it.

The general nature of gravity waves generated by vortical motions was investigated in chapter 2. The Lighthill theory, as extended to the rotating frame by Norton, was confirmed by a matched asymptotic analysis. The analysis enabled an expression to be derived for the effect of gravity wave radiation on the vortical flow. This expression would not be available through a “classical” application of the Lighthill theory, which would predict the amplitude and character of the gravity waves generated, but not their effect on the vortical flow which generates them.

The nature of the back reaction of the gravity waves on the vortical motions which generate them was then analysed with reference to balanced models. The back reaction takes the form of a large scale straining field, whose amplitude depends on time, and is given by a convolution integral involving the entire past history of the vortical flow. Hence it was shown that, without reference to an initial instant of time, the correction to the balanced dynamics which was required to account for the gravity wave radiation at low Froude number could not be regarded as an instantaneous function of the potential vorticity distribution, and could not therefore be regarded as part of the balanced dynamics.

The issue of the existence or non-existence of a slow manifold for the shallow water equations was pursued further in chapter 3, by analysing the character of the instability of an axisymmetric vortex with a potential vorticity which had a single discontinuity at  $r = 1$ . It was shown that the vortex was unstable to high wave number disturbances at arbitrary Froude and Rossby numbers. The instability is a coupled Rossby wave – gravity wave instability, and can not be part of a slow manifold which does not contain any gravity wave-like features. If a slow manifold were permitted to contain gravity wave-like features, it would then follow from the vortex instability analysis that it could not be unique. Thus, although the existence of a slow manifold can not be entirely ruled out, the notion of a unique slow manifold, entirely devoid of gravity wave activity, certainly can be.

Finally, nonlinear simulations of the shallow water equations were performed to investigate the nature of gravity wave generation by vortical flows at Froude and Rossby numbers of order unity. It was found that cyclonic vortices will tend to become progressively less unsteady as the Froude number is increased. This means that they become progressively less able to generate gravity waves, as typical frequencies in the vortical dynamics become smaller and smaller with respect to the inertial frequency. The result was that cyclonic vortices exhibited an optimal Froude number, above which the radiated gravity wave pseudoenergy flux actually decreased as the Froude number was further increased. It turned out that even for potential vorticity of nine times the background value, the optimal Froude number occurred at about 0.6, and the pseudoenergy flux did not exceed  $10^{-6}$ .

Anticyclonic vortices appeared to behave somewhat differently at moderate Froude number, with the pseudoenergy flux increasing more rapidly than in the cyclonic cases. However, if the potential vorticity was strictly positive, their nutation times also increased super-exponentially with increasing Froude number, thus inhibiting gravity wave radiation. The maximum pseudoenergy flux from anticyclonic vortices with positive potential vorticity did not exceed  $10^{-6}$ , and the Froude number at which the strongest gravity wave fluxes were observed was almost 1.0.

Vortices with zero and negative potential vorticity were not found to become significantly less unsteady as the Froude number increased. At large Froude numbers, it was found that such vortices tended to generate shock waves, which could then propagate through the fluid. The pseudoenergy flux continues to increase with increasing Froude number, at least as rapidly

as the sixth power of the Froude number, up to Froude number of order unity.

In the moderate Froude number regime, the gravity wave field generated was compared with that predicted by a suitably modified version of the Lighthill theory. In general, there seemed good agreement over a range of Froude numbers, provided the vortices were small compared with a deformation radius.

## 5.2 Suggestions for further research

This thesis has concentrated on specific features of flows which cannot be balanced, and there remains much work to be done in understanding and quantifying these phenomena.

In chapter 2, after the general theory was introduced, the response of an elliptical patch to radiating gravity waves was examined in some detail. The analysis supported the notion of “generalized adjustment” – i.e. the flow adjusts to a state where its gravity wave emission diminishes. This flow is, however, only one of many flows, and it would be of interest to investigate the nonlinear evolution of other vortical structures analytically, using the matched asymptotic expansions approach. A starting point for the study could be the flows classified by Abrashkin & Yakubovich (1984).

The nonlinear numerical experiments of chapter 4 illustrated a substantial difference between cyclonic and anticyclonic vortex motions, particularly when negative potential vorticity was present in the vortices. This phenomenon does not appear to have been studied in such extreme limits, and it would appear that there is much to be done in gaining a fully quantitative understanding of it.

One significant motivation for the numerical work in chapter 4 was to determine the range of validity of the Lighthill theory of aerodynamic sound generation, as applied to gravity wave generation in a rotating frame. The work presented in this thesis is that simple numerical models, at moderate resolution, can be expected to generate a radiated gravity wave field which is in good quantitative agreement with the wave field predicted by the Lighthill theory.

However, only a limited class of flows has been investigated. One serious omission is that there is no mean jet in the flow. Although not conceptually difficult, there is likely to be some technical difficulty in incorporating a mean jet into a modified version of the Lighthill theory.

The point is that, if there is to be a mean jet in rotating shallow water, the fluid will tend to different uniform heights on either side of the jet, far away from it. The Lighthill theory, as presented here, assumes that the background is homogeneous, and some work will be required to incorporate non-uniformity of the background into the theory. Only when this is done, however, will it be possible to test the Lighthill theory in flows with a mean jet in the quantitative way in which it was tested for flows without a mean jet in chapter 4.

Another development which will be required is the incorporation of vertical structure, so that the gravity waves generated by numerical simulations of baroclinic lifecycles can be analysed within the framework of the Lighthill theory.

Ultimately, we may wish to use the Lighthill theory as a quantitative tool to predict the intensity of gravity wave emission by jet streaks. To achieve this, we must first develop the theory to such a level that it can be applied to flows of practical meteorological interest. This aim, to be achieved through further analytical work with the shallow water and hydrostatic continuously stratified equations, is now of primary importance in furthering this work, and is being actively pursued. When complete, it should provide an excellent tool for analysing the performance of numerical models in which gravity wave generation is observed, and for assessing the significance of gravity waves generated by vortical motions in the global angular momentum budget, whose significance was first identified by Lindzen (1981).

## Chapter 6

## References

- Abramowitz M. and Stegun I.A., 1965: *Handbook of mathematical functions*. Dover, 1046pp.
- Abrashkin A.A. and Yakubovich E.I., 1984: Planar rotational flows for an ideal fluid. *Sov. Phys. Dokl.*, **29**, 370-371.
- Allen, J. S., Barth, J. A. and Newberger, P. A., 1990: On intermediate models for barotropic continental shelf and slope flow fields. Part I: Formulation and comparison of exact solutions. *J. Phys. Oceanog.*, **20**, 1017-1042.
- Allen, J. S., Barth, J. A. and Newberger, P. A., 1990: On intermediate models for barotropic continental shelf and slope flow fields. Part III: Comparison of numerical model solutions in periodic channels. *J. Phys. Oceanog.*, **20**, 1949-1973.
- Arakawa A. and Lamb V.R., 1981: A potential enstrophy and energy conserving scheme for the shallow water equations *Mon. Wea. Rev.*, **109**, 18-36.
- Asselin R., 1972: Frequency filter for time integrations. *Mon. Wea. Rev.*, **100**, 487-490.
- Baer, F. and Tribbia, J. J., 1977: On complete filtering of gravity modes through nonlinear initialization. *Mon. Wea. Rev.*, **105**, 1536-1539.
- Barsony-Nagy A., Er-El J. and Yungster S. 1987: Compressible flow past a contour and stationary vortices. *J Fluid Mech.*, **178**, 367-378.
- Barth, J. A., Allen, J. S. and Newberger, P. A., 1990: On intermediate models for barotropic continental shelf and slope flow fields. Part II: Comparison of numerical model solutions in doubly periodic domains. *J. Phys. Oceanog.*, **20**, 1044-1076.
- Batchelor G.K., 1967: *An introduction to fluid dynamics*, Cambridge University Press, 615pp.
- Bourke W., 1972: An efficient, one-level, primitive-equation spectral model. *Mon. Wea. Rev.*, **100**, 683-689.
- Bridges J., and Hussain A.K.M.F., 1992: Direct evaluation of aeroacoustic theory in a jet. *J. Fluid Mech.*, **240**, 469-501.

- Broadbent E.G. and Moore D.W., 1979: Acoustic destabilisation of vortices. *Phil. Trans. Roy. Soc. Lond.*, **A 290**, 353-371.
- Chan W.M., Shariff K. and Pulliam T.H., 1993: Instabilities of two-dimensional inviscid compressible vortices. *J. Fluid Mech.*, **253**, 173-209.
- Charney J.G., 1947: The dynamics of long waves in a baroclinic westerly current. *J. Meteor.*, **4**, 135-162.
- Charney J.G., 1948: On the scale of atmospheric motions. *Geof. Publ.*, **17, 2**, 17pp.
- Charney J.G., 1949: On a physical basis for numerical prediction of large-scale motions in the atmosphere. *J. Atmos. Sci.*, **6**, 371-385.
- Charney J.G., 1951: Dynamic forecasting by numerical process. In *Compendium of Meteorology*, T. Malone, ed., American Meteorological Society, 1334pp.
- Charney, J. G., 1955: The use of the primitive equations of motion in numerical prediction. *Tellus*, **7**, 22-26.
- Crighton D.G., 1972a: Radiation from vortex filament motion near a half plane. *J. Fluid Mech.*, **51**, 357-362.
- Crighton D.G., 1972b: Radiation properties of the semi-infinite vortex sheet. *Proc. Roy. Soc.*, **A 330**, 185-198.
- Crighton D.G., 1975: Basic principles of aerodynamic noise generation. *Prog. Aerospace Sci.*, **16**, 31-96.
- Crighton D.G. and Leppington F.G., 1974: Radiation properties of the semi-infinite vortex sheet - the initial value problem. *J. Fluid Mech.*, **64**, 393-414.
- Crow S.C., 1970: Aerodynamic sound generation as a singular perturbation problem. *Stud. Appl. Math.*, **49**, 21-44.

- Deem G.S. and Zabusky N.J., 1978: Stationary V-states: interactions recurrence and breaking. *Phys. Rev. Lett.*, **40**, 859.
- Dritschel, D. G., 1989: Contour dynamics and contour surgery: numerical algorithms for extended, high-resolution modelling of vortex dynamics in two-dimensional, inviscid, incompressible flows. *Computer Phys. Rep.*, **10**, 77–146.
- Dritschel, D. G., 1993: A fast contour dynamics method for many-vortex calculations in two-dimensional flows. *Phys. Fluids, A* **5**, 173–186.
- Dritschel D.G. and Legras B., 1991: The elliptical model of two-dimensional vortex dynamics. II: Disturbance equations. *Phys. Fluids, A* **3**, 855–869.
- Dritschel, D.G. and Saravanan, R., 1993: Three-dimensional quasi-geostrophic contour dynamics, with an application to stratospheric vortex dynamics. *Q. J. Roy. Met. Soc.*, submitted.
- Errico, R. M., 1982: Normal mode initialization and the generation of gravity waves by quasi-geostrophic forcing. *J. Atmos. Sci.*, **39**, 573–586.
- Ertel, H., 1942: Ein Neuer hydrodynamischer Wirbelsatz. *Met. Z.*, **59**, 271–281.
- Ffowcs-Williams J.E., 1969: Hydrodynamic noise. *Ann. Rev. Fluid Mech.*, **1**, 197–222.
- Gent, P.R. and McWilliams, J.C., 1983a: Consistent balanced models in bounded and periodic domains. *Dyn. Atmos. Ocean.*, **7**, 67–93.
- Gent, P.R., and McWilliams, J.C., 1983b: The equatorial waves balanced models. *J. Phys. Oceanog.*, **13**, 1179–1192.
- Gill, A.E., 1982: *Atmosphere-Ocean Dynamics*, Academic Press, 602pp.
- Griffiths R.W., Killworth P.D. and Stern M.E., 1982: Ageostrophic instability of ocean currents. *J. Fluid Mech.*, **117**, 343–377.

- Gryanik V.M., 1983: Emission of sound by linear vortical filaments. *Izv. Atm. Oc. Phys.*, **19**, 150-152.
- Haynes P.H., 1988: Forced, dissipative generalizations of finite-amplitude wave-activity conservation relations for zonal and non-zonal basic flows. *J. Atmos. Sci.*, **45**, 2352-2362.
- Haynes P.H., 1989: The effect of barotropic instability on the nonlinear evolution of a Rossby wave critical layer. *J. Fluid Mech.*, **207**, 231-266.
- Ho C.-M. and Huerre P., 1984: Perturbed free shear layers. *Ann. Rev. Fluid Mech.*, **16**, 365-424.
- Howe M.S., 1975: Contributions to the theory of aerodynamic sound, with application to excess jet noise and the theory of the flute. *J. Fluid Mech.*, **71**, 625-673.
- Hoskins B.J., 1974: The role of potential vorticity in symmetric stability and instability. *Q. J. Roy. Met. Soc.*, **100**, 480-482.
- Hoskins, B. J., McIntyre, M. E. and Robertson, A. W., 1985: On the use and significance of isentropic potential-vorticity maps. *Q. J. Roy. Meteorol. Soc.*, **111**, 877-946.
- Hayashi Y. and Young W.R., 1987: Stable and unstable shear modes on rotating parallel flows in shallow water. *J. Fluid Mech.*, **184**, 477-504.
- Jacobs, S. J., 1991: Existence of a slow manifold in a model system of equations. *J. Atmos. Sci.*, **48**, 893-901.
- Kambe T., 1986: Acoustic emissions by vortex motions. *J. Fluid Mech.*, **173**, 643-666.
- Kambe T. and Minota T., 1981: Sound radiation from vortex systems. *J. Sound Vib.*, **74**, 61-72.
- Kambe T. and Minota T., 1983: Acoustic wave radiated by head-on collision of two vortex rings. *Proc. Roy. Soc., A* **386**, 277-308.

- Lord Kelvin, 1880: On the oscillations of a columnar vortex. *Phil. Mag.*, **10**, 155-168.
- Kida S., 1981: Motion of an elliptic vortex in a uniform shear flow. *J. Phys. Soc. Japan*, **50**, 3517-3520
- Killworth P.D. and Stern M.E., 1982: Instabilities on density-driven boundary currents and fronts. *Geophys. Astrophys. Fluid Dyn.*, **22**, 1-28.
- Kimura Y., 1989: Transport properties of waves on a vortex filament. *Physica D*, **37**, 485-489.
- Kleinschmidt, E., 1950: Über Aufbau und Entstehung von Zyklonen (1 Teil). *Met. Rund.*, **3**, 1-6.
- Kleinschmidt, E., 1950: Über Aufbau und Entstehung von Zyklonen (2 Teil). *Met. Rund.*, **3**, 54-61.
- Kleinschmidt, E., 1951: Über Aufbau und Entstehung von Zyklonen (3 Teil). *Met. Rund.*, **4**, 89-96.
- Kleinschmidt, E., 1955: Die Entstehung einer Höhenzyklone über Nordamerika. *Tellus*, **7**, 96-110.
- Kleinschmidt, E., 1957: In "dynamic meteorology", by Eliassen, A., and Kleinschmidt, E., Handbuck der Physik, 48, 1-154.
- Klyatskin V.I., 1966: Sound radiation by a system of vortices. *Fluid Dyn.*, **1 6**, 54-57.
- Knessl, C. and Keller, J. B., 1992: Stability of rotating shear flows in shallow water. *J. Fluid Mech.*, **244**, 605-614.
- Koch S.E. and Dorian P.B., 1988: A mesoscale gravity wave event observed during CCOPE. Part III: Wave environment and possible source mechanisms. *Mon. Wea. Rev.*, **116**, 2570-2592.
- Kop'ev V.F. and Leont'ev E.A., 1983: Acoustic instability of an axial vortex. *Sov. Phys.*

*Acoustics*, **29**, 111-115.

Kop'ev V.F. and Leont'ev E.A., 1985: Energy aspects of the acoustic instability of certain steady-state vortices. *Sov. Phys. Acoustics*, **31**, 205-207.

Kop'ev V.F. and Leont'ev E.A., 1986: Some remarks on Lighthill's theory in connection with sound radiation by compact vortices. *Sov. Phys. Acoustics*, **32**, 109-112.

Kubokawa A., 1986: Instability caused by the coalescence of two modes of a one-layer coastal current with a surface front. *J. Oceanogr. Soc. Japan*, **42**, 373-380.

Lamb, H.H., 1932: *Hydrodynamics*, Dover, New York.

Lauvstad, 1968: On non-uniform Mach number expansion of the Navier-Stokes equations and its relation to aerodynamically generated sound. *J. Sound Vib.*, **7**, 90-105.

Leith, C.E., 1980: Non-linear normal mode initialization and quasi-geostrophic theory. *J. Atmos Sci.*, **37**, 958-968.

Legras B. and Dritschel D.G., 1991: The elliptical model of two-dimensional vortex dynamics. I: The basic state. *Phys. Fluids*, **A 3**, 845-854.

Legras B. and Zeitlin V., 1992: Conformal dynamics for vortex motions. *Phys. Lett.*, **A 167**, 265-271.

Lele S.K. and Ho C.-M., 1993: Acoustic radiation from temporally evolving free shear layers. *J. Fluid Mech.*, submitted.

Lighthill M.J., 1952: On sound generated aerodynamically, I. General theory. *Proc. Roy. Soc.*, **A 211**, 564-587.

Lighthill M.J., 1954: On sound generated aerodynamically, II. Turbulence as a source of sound. *Proc. Roy. Soc. Lond.*, **A 222**, 1-32.

Lighthill M.J., 1958: *An introduction to Fourier analysis and generalized functions*. Cambridge

University Press, 79pp.

Lindzen, R. S., 1981: Turbulence and stress owing to gravity wave and tidal breakdown. *J. Geophys. Res.*, **86**, 9707–9714.

Lorenz, E.N., 1960: Energy and numerical weather prediction. *Tellus*, **12**, 364–373.

Lorenz, E. N., 1986: On the existence of a slow manifold. *J. Atmos. Sci.*, **43**, 1547–1557.

Lorenz, E. N., 1992: The slow manifold – what is it? *J. Atmos. Sci.*, **49**, 2449–2451.

Lorenz, E. N., Krishnamurthy, V., 1987: On the nonexistence of a slow manifold. *J. Atmos. Sci.*, **44**, 2940–2950.

Love, A.E.H., 1893: On the stability of certain vortex motions *Proc. Lond. Math. Soc.*, **25**, 18–34.

Lush P.A., 1971: Measurements of subsonic jet noise and comparison with theory. *J. Fluid Mech.*, **46**, 477–500.

Machenhauer, B., 1977: On the dynamics of gravity oscillations in a shallow water equation model with applications to normal mode initialization. *Contrib. Atmos. Phys.*, **50**, 253–271.

Mankbadi R. and Liu J. T. C., 1984: Sound generated aerodynamically revisited: large-scale structures in a turbulent jet as a source of sound. *Phil. Trans. Roy. Soc. Lond.*, **A 311**, 183–217.

McIntyre, M.E. and Norton, W.A., 1993: Potential vorticity inversion on a hemisphere. *J. Atmos. Sci.*, submitted.

McIntyre M.E. and Shepherd T.G., 1987: An exact local conservation theorem for finite amplitude disturbances to non-parallel shear flows, with remarks on Hamiltonian structure and Arnol'd's stability theorems. *J. Fluid Mech.*, **181**, 527–565.

McWilliams, J.C., 1985: A uniformly valid model spanning the regimes of geostrophic and

- isotropic, stratified turbulence: balanced turbulence. *J. Atmos. Sci.*, **42**, 1773-1774.
- McWilliams, J.C., Gent, P.R. and Norton, N.J., 1986: The evolution of balanced, low-mode vortices on the  $\beta$ -plane. *J. Phys. Oceanog.*, **16**, 838-855.
- Margules M., 1904: Uber die Beziehung zwischen Barometerschwankungen und Kontinuitatsgleichung. *Festschrift Ludwig Boltzmann* pp. 585-589, Leipzig, J. A. Barth, 930pp.
- Minota T. and Kambe T., 1986: Observations of acoustic emission from head-on collision of two vortex rings. *J. Sound Vib.*, **111**, 51-59.
- Moore C.J., 1977: The role of shear-layer instability waves in jet exhaust noise. *J. Fluid Mech.*, **80**, 321-367.
- Moore D.W. and Pullin D.I., 1987: The compressible vortex pair. *J. Fluid Mech.*, **185**, 171-204.
- Morse P.M. and Feshbach H., 1953: *Methods of mathematical physics* II, McGraw - Hill, 997pp.
- Norton, W.A., 1988: *Balance and potential vorticity inversion in atmospheric dynamics*. Ph.D. thesis, University of Cambridge. 167pp.
- Norton, N.J., McWilliams, J.C. and Gent, P.R., 1986: A numerical model of the balance equations in a periodic domain and an example of balanced turbulence. *J. Comp. Phys.*, **67**, 439-471.
- Obermeier F., 1967: Berechnung aerodynamisch erzeugter Schallfelder mittels der Method der "Matched Asymptotic Expansions". *Acustica*, **18**, 238-240.
- Paldor N., 1983: Linear stability and stable modes of geostrophic modes. *Geophys. Astrophys. Fluid Dyn.*, **24**, 299-326.
- Platzman G.W., 1967: A retrospective view of Richardson's book on weather prediction. *Bull. Amer. Met. Soc.*, **48**, 514-550.
- Platzman G.W., 1968: Richardson's weather prediction. *Bull. Amer. Met. Soc.*, **49**, 496-500.

- Polvani L.M., Zabusky N.J. and Flierl G.R., 1989: Two-layer geostrophic vortex dynamics. Part I. Upper-layer V-states and merger. *J. Fluid Mech.*, **205**, 215-242.
- Rahman S., 1971: Berechnung der Schallerzeugung beim frontalen Zusammenstoss zweier Wirbelpaare. *Acustica*, **24**, 50-54.
- Richardson L.F., 1922: *Weather prediction by numerical processes*. Cambridge University Press, 236pp.
- Ripa P., 1983: General stability conditions for zonal flows in a one-layer model on the beta-plane or the sphere. *J. Fluid Mech.*, **126**, 463-489.
- Ripa P., 1987: On the stability of elliptical vortex solutions of the shallow water equations. *J. Fluid Mech.*, **183**, 343-363.
- Pullin, D.I., 1992: Contour Dynamics Methods. *Ann. Rev. Fluid Mech.*, **24**, 89-115.
- Robert A.J., 1966: The integration of a low order spectral form of the primitive meteorological equations. *J. Meteor. Soc. Japan*, **44**, 237-245.
- Robinson, A.R. and Stommel, H.M., 1959: The oceanic thermocline and the associated thermocline circulation. *Tellus*, **3**, 295-308.
- Rossby C.G., 1936: Dynamics of steady ocean currents in the light of experimental fluid mechanics. *Papers in physical oceanography and meteorology*, **5** 1, 43pp.
- Rossby C.G. et al., 1939: Relation between variations in the intensity of the zonal circulation of the atmosphere and the displacements of the semi-permanent centers of action. *J. Mar. Res.*, **2**, 38-55.
- Sakai S., 1989: Rossby-Kelvin instability: a new type of ageostrophic instability caused by resonance between Rossby waves and gravity waves. *J. Fluid Mech.*, **202**, 149-176.
- Salmon, R., 1985: New equations for nearly geostrophic flow. *J. Fluid Mech.*, **153**, 461-477.

- Salmon, R., 1988a: Semigeostrophic theory as a Dirac-bracket projection. *J. Fluid Mech.*, **196**, 345-358.
- Salmon, R., 1988b: Hamiltonian fluid mechanics. *Ann. Rev. Fluid Mech.*, **20**, 225-256.
- Satomura T., 1981: An investigation of shear instability in a shallow water. *J. Met. Soc. Japan*, **59**, 148-167.
- Sozou C., 1987: New solutions representing adiabatic transverse waves in a Rankine vortex. *Proc. Roy. Soc. Lond.*, **A 413**, 225-234.
- Spall, M.A. and McWilliams, J.C., 1992: Rotational and gravitational influences on the degree of balance in the shallow water equations. *Geophys. Astrophys. Fluid Dyn.*, **64**, 1-29.
- Stuber B., 1970: Schallabstrahlung und Körperschallanregung durch Wirbel. *Acustica*, **23**, 82-92.
- Tribbia, J. J., 1984: A simple scheme for high-order nonlinear normal mode initialization. *Mon. Wea. Rev.*, **112**, 278-284.
- Vallis, G. K., 1992: Mechanisms and parameterizations of geostrophic adjustment and a variational approach to balanced flow. *J. Atmos. Sci.*, **49**, 1144-1160.
- Vautard, R. and Legras, B., 1986: Invariant manifolds, quasi-geostrophy and initialization. *J. Atmos. Sci.*, **43**, 565-584.
- Warn, T. and Ménard, R., 1986: Nonlinear balance and gravity-inertial wave saturation in a simple atmospheric model. *Tellus*, **38A**, 285-294.
- Webster, R. B., 1970: Jet noise simulation on shallow water. *J. Fluid Mech.*, **40**, 423-432.
- Williams J. S., 1992: *Nonlinear problems in vortex sound*. PhD Thesis, University of Leeds.
- Zeitlin V., 1988: Acoustic radiation from distributed vortex structures. *Sov. Phys. Acoustics*, **34**, 188-191.

- Zietlin V., 1991: On the backreaction of acoustic radiation for two-dimensional vortex structures.  
*Phys. Fluids*, **A 3**, 1677-1680.